8-2022

Confirming New Suns and Searching for New Planets in IC 2602 and IC 2391

Azmain Nisak

CONFIRMING NEW SUNS AND SEARCHING FOR NEW PLANETS IN IC 2602 AND IC 2391

by

AZMAIN H. NISAK

Under the Direction of Russel White, Ph.D.

ABSTRACT

The open clusters IC 2602 and IC 2391 are important benchmarks for testing early star and planet evolution theories, both structural and dynamical, because they are the nearest open clusters with ages of ∼50 Myr. Because accurate membership lists are vital to age-determination of clusters and placing observational constraints on theories, we refine membership lists for these clusters. We identify 529 new candidate members (801 in total, including known members) using *Gaia* DR2 data and we confirm membership for 26 of these based on spectra obtained with the CHIRON spectrograph. We identify new binaries, measure signatures of youth (lithium, Hα), and determine effective temperatures, metallicities, surface gravities, as well as radial velocities and $v \sin i$ values for these new members.

A major challenge to detecting planets via radial velocity (RV) measurements in these clusters is stellar jitter that can mask or even mimic planetary RVs. However, the amplitude of stellar jitter in the age range of 10-100 Myr remains largely unknown. To address this, we monitor the radial velocity of 29 slower rotating ($v \sin i < 30$ km/s), Sun-like (FGK), *bona-fide* members of IC 2602, IC 2391, and the ∼45 Myr moving group Tucana-Horologium (Tuc-Hor). By fitting possible orbits, we find two stars that show RV variations similar to that expected for hot Jupiter companions. However, line bisector analyses reveal that the observed RV variations are most likely caused by stellar jitter. We measure the dispersion of

RVs for 29 stars to be 168 m/s for IC 2602, 225 m/s for IC 2391, and 311 m/s for Tuc-Hor. Overall, the stellar jitter at ∼50 Myr is 237 m/s. This is similar to the semi-amplitude produced by a 2 Jupiter-mass planet on a 3-day orbit or a 3 Jupiter-mass planet on a 10-day orbit. Our survey complements NASA's *TESS* and *Kepler K2* missions by helping to confirm or reject candidate planets in RV follow-up. Our survey also complements field studies in older open clusters, helping us to map out the evolution of stellar jitter and planetary systems as a function of age and strongly constraining competing theories of planet formation and migration.

INDEX WORDS: Star Clusters, Exoplanets, Stellar Jitter

CONFIRMING NEW SUNS AND SEARCHING FOR NEW PLANETS IN IC 2602 AND IC 2391

by

AZMAIN H. NISAK

A Dissertation Submitted in Partial Fulfillment of the Requirements of

Doctor of Philosophy

in the College of Arts and Sciences

Georgia State University

2022

CONFIRMING NEW SUNS AND SEARCHING FOR NEW PLANETS IN IC 2602 AND IC 2391

by

AZMAIN H. NISAK

Committee Chair:	Russel White
Committee:	Todd Henry
	Sebastien Lepine
	Debra Fischer

Electronic Version Approved:

Office of Graduate Studies

College of Arts and Sciences

Georgia State University

August 2022

DEDICATION

I dedicate this dissertation to my wife, who inspires me to be my best, my sister, who believed in me no matter what, my parents who helped make me who I am, and my advisor who supported me in every part of my PhD.

ACKNOWLEDGEMENTS

We are indebted to members of the SMARTS Consortium and NSF's National Optical-Infrared Astronomy Research Laboratory, especially the staff at CTIO, for efforts to keep the SMARTS/CTIO 1.5-m telescope and CHIRON spectrograph in operation. This research has used data from the CTIO/SMARTS 1.5m telescope, which is operated as part of the SMARTS Consortium by RECONS (www.recons.org) members Todd Henry, Hodari James, Wei-Chun Jao, Leonardo Paredes, and Azmain Nisak. At the telescope, observations were carried out by Roberto Aviles and Rodrigo Hinojosa. This research has made use of the SIMBAD database, operated at CDS, Strasbourg, France. This research has made use of the VizieR catalogue access tool, CDS, Strasbourg, France (DOI : 10.26093/cds/vizier). The original description of the VizieR service was published in 2000, A&AS 143, 23. This work has made use of data from the European Space Agency (ESA) mission *Gaia* (`https://www.cosmos.esa.int/gaia`), processed by the *Gaia* Data Processing and Analysis Consortium (DPAC, `https://www.cosmos.esa.int/web/gaia/dpac/consortium`). Funding for the DPAC has been provided by national institutions, in particular the institutions participating in the *Gaia* Multilateral Agreement.

TABLE OF CONTENTS

LIST OF TABLES

LIST OF FIGURES

CHAPTER 1

INTRODUCTION AND MOTIVATIONS

1.1 The Value of Planets with Known Ages

The last three decades of exoplanet science have revealed a dizzying array of planetary systems whose properties vary considerably from our own. These discoveries have raised profound questions about how gas giant planets form and how some of them migrate to small separations from their host stars. Competing theories of giant planet formation include core accretion, in which the formation of a solid 10 Earth-mass core precedes a runaway process of gas accretion (Perri & Cameron 1974; Pollack et al. 1996; Chabrier et al. 2014; Fortney, Dawson, & Komacek 2021), and disk instability, in which gravitational instabilities cause the protoplanetary disk to collapse into fragments (Boss 1997; Durisen et al. 2007; Mercer & Stamatellos 2020). Competing models of planet migration include disk interactions (Lin, Bodenheimer, & Richardson 1996), in which migration is driven by angular momentum transfer between young planets and their disks, dynamical instability (Rasio & Ford 1996; Weidenschilling & Marzari 1996), where collisions and ejections from gravitational interactions between planets drive migration, and secular interactions (Kozai 1962; Lidov 1962; Eggleton, Kiseleva, & Hut 1998; Wu & Murray 2003; Fabrycky & Tremaine 2007; Wu & Lithwick 2011; Naoz 2016), in which migration is driven by gravitational interactions between planets and distant companion(s) (Winn & Fabrycky 2015).

Fortunately, these competing theories can be distinguished because they predict different gas giant properties. For example, core accretion predicts cooler, smaller, and denser planets

than disk instability because it's a slower process of planet formation, which allows for dissipation of energy and entropy (Spiegel & Burrows 2012). These differences are predicted to persist for up to 1 Gyr (Fortney et al. 2008). Moreover, whereas migration via disk interactions (Bae et al. 2019) should occur within 10 Myr, before circumstellar disks have dissipated (Carpenter et al. 2006; Fujii & Hori 2019), migration via dynamical scattering or secular interactions can take many hundreds of millions of years (Jurić & Tremaine 2008; Marzari & Nagasawa 2020). In order to distinguish between these competing models of planet formation and migration, we need to determine the structural and orbital properties of giant exoplanets with known ages. Placing observational constraints on theories has been notoriously difficult because most planets do not have host stars with well-constrained ages (Bailey et al. 2016; Baruteau et al. 2016) and the overwhelming majority are adolescent age or older.

Open clusters, associations of stars that form from the same molecular cloud in a single burst of star formation and thus have similar ages and chemical properties (Lada & Lada 2003), are therefore fantastic laboratories for testing planet formation and migration theories (e.g. Quinn et al. 2014; Quinn & White 2016; Mann et al. 2017; Gaidos et al. 2017; Ragusa et al. 2018), as well as placing constraints on the early evolution of exoplanet atmospheres (Livingston et al. 2018). Ever since the first open cluster planet, a hot Jupiter identified from radial velocity (RV) measurements, was discovered nearly a decade ago (Quinn et al. 2012; Meibom et al. 2013), it has been clear that discoveries of giant planets in open clusters can strongly constrain theories. For example, the distinctly nonzero eccentricity of a planetary system discovered in the Hyades has implied that dynamical scattering has played a large role in its later evolution (Quinn et al. 2014; Shara, Hurley, & Mardling 2016, Mann et al. 2017; Vincke & Pfalzner 2018).

1.2 The Challenge of Young Planet Detection

One of the biggest challenges for detecting and confirming candidate planets at young ages via the RV method is stellar jitter ($\sigma_\star$), the noise in RV measurements induced by chromospheric activity, star spots, and flares, that can mask or even mimic planetary RVs if unknown or unaccounted for (Queloz et al. 2001; Desort et al. 2007; Moulds et al. 2013; Bailey et al. 2016; Donati et al. 2017). While previous work has shown that stellar jitter does not inhibit the discovery of giant planets at ages of a few 100 Myr ($\sigma_\star \sim$ 10-20 m/s at optical wavelengths; Paulson et al. 2004; Quinn et al. 2012), it will clearly mask most planets at ages less than 10 Myr ($\sigma_\star >$ 1,000 m/s; Crockett et al. 2012, Johns-Krull et al. 2016; Donati et al. 2017). Despite initial efforts to quantify the stellar jitter via multi-epoch RV observations of stars in nearby young (< 200 Myr) moving groups (Paulson & Yelda 2006; Lagrange et al. 2013), which confirm the expectation that stellar jitter is higher at younger ages due to increase in stellar rotation and chromospheric activity ($\sigma_\star \sim$ tens to hundreds of m/s), the magnitude and age dependence of stellar jitter in the critical age range of 10-100 Myr remains largely unknown. A summary of the known stellar jitter values available for young stellar populations are presented in Figure 1.1. The names of the clusters that will be investigated in this dissertation are colored red.

Despite these challenges to RV surveys, several dozens of planets have now been identified in open clusters based on space-based transit missions. NASA's Transiting Exoplanet Survey Satellite (*TESS*; Ricker et al. 2014) has identified over 1,600 planet candidates since its launch in 2018 in its survey of southern hemisphere stars down to V=16, including those in open clusters. Collectively, alongside NASA's repurposed *Kepler* mission, *K2* (Howell et al. 2014), these missions have identified over two dozen Earth- and Neptune-size planets in star-forming regions, moving groups, and open clusters (David et al. 2016a, b, 2019; Libralato et al. 2016; Mann et al. 2016a, b, 2017; Pepper et al. 2017; Livingston et al. 2018a, 2019; Newton et al. 2019; Barragán et al. 2019; Thao et al. 2020; Anger et al. 2020).

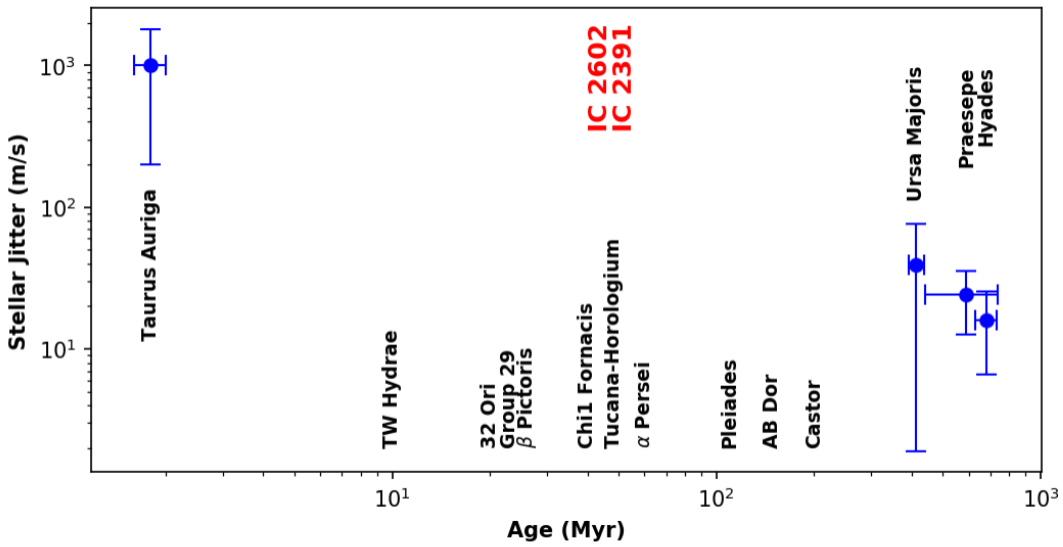

Figure 1.1 Stellar jitter measurements for nearby clusters and moving groups are shown. Despite initial efforts (Paulson & Yelda 2006), the range of 10-100 Myr is not well-sampled for stellar jitter measurements.

Critical to confirming these candidates are follow-up RV measurements to determine planet mass and orbital properties. However, confirming young *TESS* planets will be difficult if the stellar jitter, astrophysical RV noise associated with rapid rotation and enhanced magnetic activity, is not accounted for (Moulds et al. 2013). This has the potential to inhibit planet detection at young ages. Therefore, determining the magnitude and age dependence of stellar jitter in the critical age range of 10-100 Myr, which is largely unknown, is of great interest to NASA's *TESS* mission when establishing planet detection limits, as well as for resolving difficulties in RV follow-up work to confirm the planetary status of potential young planets.

A summary of planet detection results to-date are shown for the nearest open clusters in Figure 1.2. No planets have been discovered in open clusters younger than 100 Myr except for the transit planet in IC 2602. Planets with RV confirmation currently exist only for clusters older than 500 Myr.

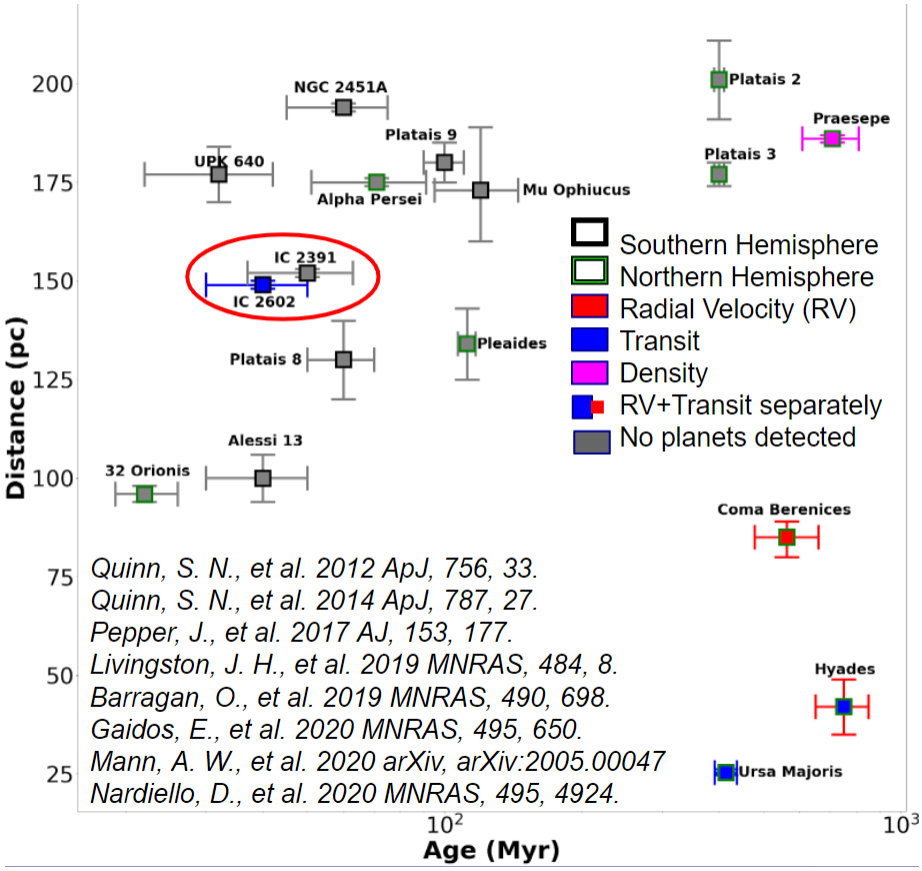

Figure 1.2 Distances to open clusters within 200 pc are shown as a function of cluster age. The outline of a marker is black if the cluster is in the southern hemisphere and green if the cluster is in the northern hemisphere. A marker is colored red if the cluster only has planet detections via the radial-velocity method, blue if the the cluster only has planet detections via the transit method, purple if detected planets have density measurements, blue with red error bars if detected planets have either radial velocity or transit detections but not both at the same time, and gray if no planets have been detected yet.

1.3 The Young Open Clusters IC 2602 and IC 2391

IC 2602 and IC 2391 (see Figure 1.3) are nearby (∼150 pc; Bravi et al. 2018) open clusters located in the Carina and Vela constellations respectively. Despite being spatially close on the sky (within 30 degrees), the clusters differ in their space motions and likely do not share a common origin; the mean radial velocities of IC 2602 and IC 2391 are estimated to be 17.4±1.0 km/s (Marsden et al. 2009) and 14.8±0.7 km/s (Platais et al. 2007) respectively. It is believed that IC 2602 formed in conjunction with the Local association, otherwise known

as the Pleaides supercluster (Eggen 1975, 1983a,b), while IC 2391 formed alongside the Argus association (Torres et al. 2008, De Silva et al. 2013) as part of the IC 2391 supercluster (Eggen 1991). IC 2602 and IC 2391 experience minimal reddening with estimated E(B-V) values of 0.068±0.025 and 0.088±0.027 respectively.

Figure 1.3 IC 2391 (left) & IC 2602 (right) in the Vela & Carina constellations *Credit:* Celestial Image Co.

Spectra of their main-sequence FGK stars reveal that IC 2602 and IC 2391 have near-solar metallicities of 0.00±0.01 and 0.06±0.06 respectively (Randich et al. 2001, 2002; Platais et al. 2007; D'Orazi & Randich 2009; Marsden et al. 2009; Boudreault & Bailer-Jones 2009; Spina et al. 2017). Age estimates for IC 2602 and IC 2391 are determined to be $43.7^{+4.3}_{-3.9}$ and $51.3^{+5.0}_{-4.5}$ Myr respectively, which are inferred by modeling the lithium depletion boundary and chasm (Barrado y Navascués et al. 2004; Dobbie et al. 2010; Bravi et al. 2018). The age estimates are consistent with those determined from the main sequence turnoff (∼30-50 Myr), which is potentially plagued by rapid rotation and gravity darkening (Jones et al. 2015; Brandt & Huang 2015; Cummings et al. 2017; Randich et al. 2018).

Given their close proximity and age, IC 2602 and IC 2391 are important benchmark clusters because they are the closest rich clusters with ages intermediate between that of star

forming regions (< 10 Myr) and that of well-studied open clusters (> 100 Myr; Lada & Lada 2003). At these transitional ages, low mass stars are still gravitationally settling towards the main sequence (Baraffe et al. 2015) and planetary systems are in the process of dynamically evolving (Quinn & White 2016; Mann et al. 2017; Gaidos et al. 2017; Ragusa et al. 2018). While these clusters have not been targeted in previous RV searches for planets, two planets were recently found to transit in IC 2602 as part of the NASA's *TESS* mission (Nardiello et al. 2020; Bouma et al. 2020). The planets are estimated to have orbital periods of 8.3 and 2.9 days, as well as radii of 0.6 and 0.3 times that of Jupiter, respectively.

1.4 The Young Moving Group Tucana-Horologium

More widely dispersed on the sky than the open clusters IC 2602 and IC 2391, the moving group Tucana-Horologium is one of the largest young stellar populations within 100 pc; the average distance of known members is ∼40 pc (Kraus et al. 2014). Members of this stellar association were initially identified separately as the Tucana association and Horologium association (Torres et al. 2000; Zuckerman & Webb 2000) but were later recognized to be part of a single comoving population with an age of ∼30 Myr (e.g. Torres et al. 2008; Zuckerman & Song 2004). Age estimates for Tucana-Horologium are determined to be 40±3 Myr based on the lithium depletion boundary (Kraus et al. 2014), which is consistent with the derived isochronal age of 45±4 Myr (Bell et al. 2015). Spectra of known members are used to infer a near-solar metallicity of -0.03±0.05 (Almeida et al. 2009). Recently, a transiting planet intermediate in size between Neptune and Saturn was discovered here (Newton et al. 2019; Montet et al. 2020; Zhou et al. 2020).

1.5 Overview of the Chapters in This Dissertation

In this dissertation, we discuss two projects we undertake to deepen our understanding of the stellar populations at the critical transitional age of ∼ 50 Myr. In the first project, we utilize the database of *Gaia* DR2 (Gaia Collaboration et al. 2018), which provides kinematic

and distance information for over 1 billion stars, to identify potential candidate members of IC 2602 and IC 2391 (Chapter 2). We obtain high-dispersion optical spectra for all newly identified candidate members of IC 2602 and IC 2391 brighter than G=13 magnitude (Chapter 3). We use the spectra to measure youth diagnostics, radial and projected rotational velocities, as well as determine stellar properties for each star. These measurements allow us to identify new candidate binaries, assess cluster membership, and characterize ensemble cluster properties (Chapter 4).

In the second project, we obtain high-dispersion optical spectra for 29 slowly rotating Sun-like stars in IC 2602, IC 2391, and Tucana-Horologium. We use the spectra to measure radial and projected rotational velocities, line bisectors, as well as determine stellar properties for each star (Chapter 5). These measurements allow us to identify candidate hot Jupiters, fit preliminary orbits, and determine stellar jitter at $\sim$50 Myr (Chapter 6). We then present our conclusions for both projects (Chapter 7).

CHAPTER 2

IDENTIFYING NEW CANDIDATE MEMBERS OF IC 2602 AND IC 2391

2.1 Open Cluster Census and Membership in the *Gaia* era

Progress in the charting of our galaxy, the Milky Way, and its star clusters was slow and painstaking until the launch of the European Space Agency's (ESA) *Gaia* mission (Gaia Collaboration et al. 2016, 2018, 2022). Dreyer (1888) listed ≈ 700 objects we now know to be open clusters in the New General Catalogue (NGC), the most comprehensive catalogue of its time. A century later, the catalogue of Mermilliod (1995) had only increased to 1200 open clusters, not even doubling the census. Furthermore, despite the large strides in astronomical instrumentation and data analysis taken in the 20th century, astronomers of the early 1990s knew the accurate positions of only about 8,000 stars (Hunt & Reffert 2021). The space-based astrometric survey of the *Hipparcos* satellite (Høg et al. 2000), which charted the positions of over 100,000 stars, in conjunction with wide-field infrared surveys, revealed many new clusters in studies such as those of Platais et al. (1988), Chereul et al. (1999), Dutra & Bica (2001), and Froebrich et al. (2007). Kharchenko et al. (2013) lists nearly 2,400 open clusters in the Milky Way Star Clusters Catalog (MWSC), greatly increasing the census from the figure of Mermilliod (1995) just two decades prior. With improvements in digital technology during the early 2000s, the field was ripe for ESA's *Gaia* satellite to revolutionize our capacity to recognize, characterize, and significantly refine membership lists of Galactic open clusters (Gaia Collaboration et al. 2016, 2018, 2022; Cantat-Gaudin et al. 2018; Lodieu et al. 2019; Zuckerman et al. 2019).

Since its launch in 2013, the *Gaia* mission has been creating the most comprehensive map of the Milky Way to-date by measuring the precise positions, proper motions, and parallaxes of about 2 billion of the brightest stars in the sky (Cantat-Gaudin 2022). Located at Lagrange Point 2, about 1.5 million km away from Earth, the *Gaia* satellite orbits the Sun in sync with our planet and scans the entire sky every two months, shielded from the Sun's glare by Earth and free from the distorting effects of Earth's atmosphere that plague ground-based observations. The flying-saucer-like spacecraft, as shown in Figure 2.1, is attached to a circular sunshield and fitted with two telescopes that project the light they capture onto a 1-billion-pixel camera. The blue and red photometers onboard provide visual photometry and colors in the satellite's own G, BP, and RP photometric bands, while the radial velocity spectrometer measures spectroscopic line-of-sight velocities for a small sample of bright stars. Data obtained from these instruments are used to derive temperatures, masses, ages, and chemical compositions of stars in the Galaxy. Thus far, *Gaia* has released four batches of data with increasingly precise measurements, including Data Release 1 (DR1; 2016), Data Release 2 (DR2; 2018), Early Data Release 3 (EDR3; 2020), and Data Release 3 (DR3; 2022). Compared with *Hipparcos*, *Gaia* has an order of magnitude more precision in astrometric parameters for 10,000 times as many stars, resulting in a groundbreaking dataset with full astrometric solutions and photometry for 1.3 billion stars as of *Gaia* DR2, 7 million of which also have radial velocities.

The unprecedented database, which generates an average of five papers per day, is greatly improving the quantity and quality of the open cluster census (Hunt & Reffert 2021; Cantat-Gaudin 2022). Works such as those of Castro-Ginard et al. (2018, 2019, 2020), Liu & Pang (2019), Sim et al. (2019), and Cantat-Gaudin et al. (2019) have reported hundreds of new candidate open clusters by applying clustering algorithms to *Gaia* data. Cantat-Gaudin et al. (2018) derive membership lists and parameters for 1,229 open clusters, which is expanded upon with newly detected clusters in Cantat-Gaudin & Anders (2020). Moreover, while distances to open clusters would traditionally be estimated by fitting model-dependent stellar

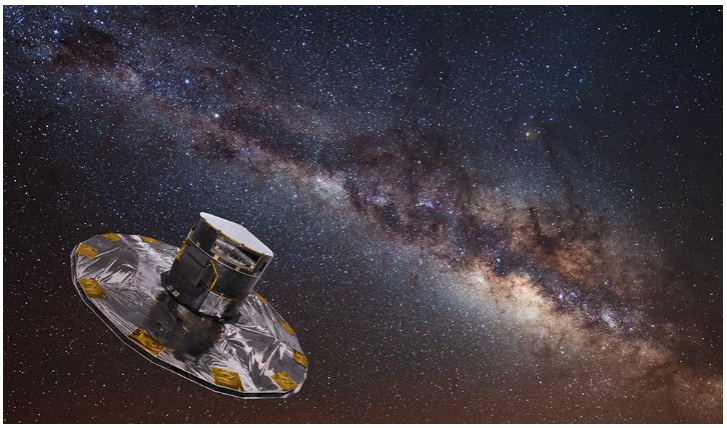

Figure 2.1 The European Space Agency's (ESA) *Gaia* spacecraft, shown here in an artist's concept, is creating the most comprehensive map of our Galaxy, the Milky Way *Credit:* ESA-D. Ducros, 2013

isochrones to their color-magnitude diagrams, *Gaia* parallaxes now provide an unbiased and model-independent distance estimator, allowing open cluster parameters to be determined more precisely (Cantat-Gaudin et al. 2020). The greatly improved quality and quantity of the census is allowing astronomers to map the age distribution of open clusters across the Galaxy (Yen et al. 2018), study their chemical composition (Baratella et al. 2020; Donor et al. 2020), observe them collide (Yep et al. 2022), and even investigate planet formation in clusters and their implications for the distribution of the wider exoplanet census (Fuji & Hori 2019).

Gaia Collaboration et al. (2017, 2018) infer membership for hundreds of candidate cluster members in nine nearby open clusters within 250 pc using an iterative analysis method that determines the location and space velocity vector of the cluster center based on the relative parallax of stars within a 15 pc radius about the assumed center. However, while the *Gaia* Collaboration's prescription is largely successful in identifying candidate cluster members (Gaia Collaboration et al. 2018), the prescription is still known to miss *bona-fide* members in some instances (Zuckerman et al. 2019). Furthermore, stars identified based on *Gaia* measurements are still only candidate members until confirmed with spectra because even the best samples are affected by contamination from field stars (Briceno et al. 2018). In

the current work, we utilize the second data release (*Gaia* DR2; Gaia Collaboration et al. 2018), which provides kinematic and distance information for over 1 billion stars, to identify potential candidate members of IC 2602 and IC 2391; the results in this chapter remain unchanged from the recent introduction of DR3.

2.2 Using *Gaia* DR2 data to identify candidate cluster members

We query the *Gaia* DR2 archive for candidate cluster members with right-ascension (RA) and declination (DEC) boundaries centered about the average SIMBAD coordinates of *bona-fide* members, reported by Wu et al. (2009) to be 160°, -65° for IC 2602 and 130°, -53° for IC 2391. Portions of these boundaries are shown in Figure 2.2, which extend 25° in DEC and 1.7 hr in RA or 65 pc and 67 pc in physical extent, respectively. Within these regions, we identify candidate cluster members using the constraints listed in Table 2.1 on parallax, proper motion, and measurement uncertainties. To derive these constraints, we first plot stellar positions and proper motions as shown in Figure 2.3. We then gradually adjust the constraints on stellar astrometric parameters until the over-density of the cluster can be distinguished from the field. We apply a less strict parallax uncertainty constraint for stars brighter than G = 8 mag (0.5 vs. 0.35 mas), based on the recommendations of Drimmel et al. (2019); brighter stars have parallaxes with larger systematic errors.

This prescription identifies 451 candidate members of IC 2602, with G magnitudes spanning from 4.7 to 19.5. Likewise, it identifies 350 candidate members of IC 2391 with G magnitudes spanning from 3.5 to 19.6. These stars are plotted on color-magnitude diagrams in Figure 2.4. Known cluster members from the literature and newly identified candidate members are distinguished as per the discussion in Section 2.3. The start of each spectral type sequence is indicated for corresponding *Gaia* colors based on the relation between effective temperature and luminosity given by Pecaut & Mamajek (2013). The G = 8 magnitude is indicated with a dashed line to show the limit above which a more lenient parallax constraint is applied. The G = 13 magnitude is indicated with a dashed line as well to show the magnitude limit of

the spectroscopic survey for confirming new candidate members; this is discussed in more detail in Chapter 3.

Considering candidate members with G $<$ 14, our membership lists agree with those identified by the *Gaia* collaboration (Gaia Collaboration et al. 2018) to 90% (96 stars) and 95% (78 stars) for IC 2602 and IC 2391, respectively. Over the full magnitude range, our prescription yields 46 and 54 candidate members of IC 2602 and IC 2391, respectively, that are not present in the *Gaia* Collaboration's membership lists. For G $<$ 14, 13 and 4 candidate members of IC 2602 and IC 2391, respectively, are identified by the *Gaia* Collaboration, but not by the prescription used in this work. These stars are also indicated as gold stars in Figure 2.4. Because we identify candidate cluster members based on astrometric parameters of stars and do not impose photometric cuts, such as those on color or magnitude, our new list of candidate members is less biased, except at the faintest end where measurement uncertainties become larger.

2.3 Comparison with pre-*Gaia* membership lists

To determine which of our candidate members are known members of these clusters independent of those proposed by the *Gaia* Collaboration, we conduct a cross-match with SIMBAD (Wenger et al. 2000) through Vizier's X-Match (Ochsenbein et al. 2000) within a 1 arc-second radius of the *Gaia* DR2 coordinates. A candidate member is considered to be a known member if (1) the star is present in SIMBAD and (2) the star has been previously classified as a candidate member of the cluster. We compare our membership lists for IC 2602 and IC 2391 with all of the major pre-*Gaia* DR2 membership lists known from the literature, as discussed in Chapter 1. These include the seminal works of Whiteoak et al. (1961), Feinstein et al. (1961), Braes et al. (1962), Lynga et al. (1962), Buscombe et al. (1965), Abt & Morgan (1972), Levato et al. (1974, 1988), Stauffer et al. (1989, 1997), Foster et al. (1997), Rolleston et al. (1997), Simon & Patten (1998), Barnes et al. (1999), James et al. (2000), Tschape et al. (2001), Pizzolato et al. (2003), Marino et al. (2003), Barrado y Navascues et al. (1999,

Table 2.1. Search Criteria to Identify Candidate Cluster Members

Cluster	**Property**	**Constraint**
IC 2602	RA (hr)	$10 \leq \text{RA} \leq 11.3$
	DEC (deg)	$-67.5 \leq \text{DEC} \leq -61$
	ϖ (mas)	$6.2 \leq \varpi \leq 7.0$
	$\mu_\alpha \cos\delta$ (mas/yr)	$-25 \leq \mu_\alpha \cos\delta \leq -10$
	μ_δ (mas/yr)	$6 \leq \mu_\delta \leq 17$
	ϵ_ϖ (mas)	$\epsilon_\varpi \leq 0.5$ (if G ≤ 8)
		$\epsilon_\varpi \leq 0.35$ (if G > 8)
	$\epsilon_{\mu_\alpha \cos\delta}$ (mas/yr)	$\epsilon_{\mu_\alpha \cos\delta} \leq 0.8$
	ϵ_{μ_δ} (mas/yr)	$\epsilon_{\mu_\delta} \leq 0.8$
IC 2391	RA (hr)	$8.3 \leq \text{RA} \leq 9$
	DEC (deg)	$-60 \leq \text{DEC} \leq -45$
	ϖ (mas)	$6.2 \leq \varpi \leq 7.4$
	$\mu_\alpha \cos\delta$ (mas/yr)	$-31 \leq \mu_\alpha \cos\delta \leq -19$
	μ_δ (mas/yr)	$15 \leq \mu_\delta \leq 28$
	ϵ_ϖ (mas)	$\epsilon_\varpi \leq 0.5$ (if G ≤ 8)
		$\epsilon_\varpi \leq 0.35$ (if G > 8)
	$\epsilon_{\mu_\alpha \cos\delta}$ (mas/yr)	$\epsilon_{\mu_\alpha \cos\delta} \leq 0.8$
	ϵ_{μ_δ} (mas/yr)	$\epsilon_{\mu_\delta} \leq 0.8$

Note. — Candidate cluster members are identified based on right-ascension (RA), declination (DEC), parallax (ϖ), proper motion in right ascension ($\mu_\alpha \cos\delta$), and proper motion in declination (μ_δ), as well as uncertainties of parallax (ϵ_ϖ) and proper motion ($\epsilon_{\mu_\alpha \cos\delta, \mu_\delta}$).

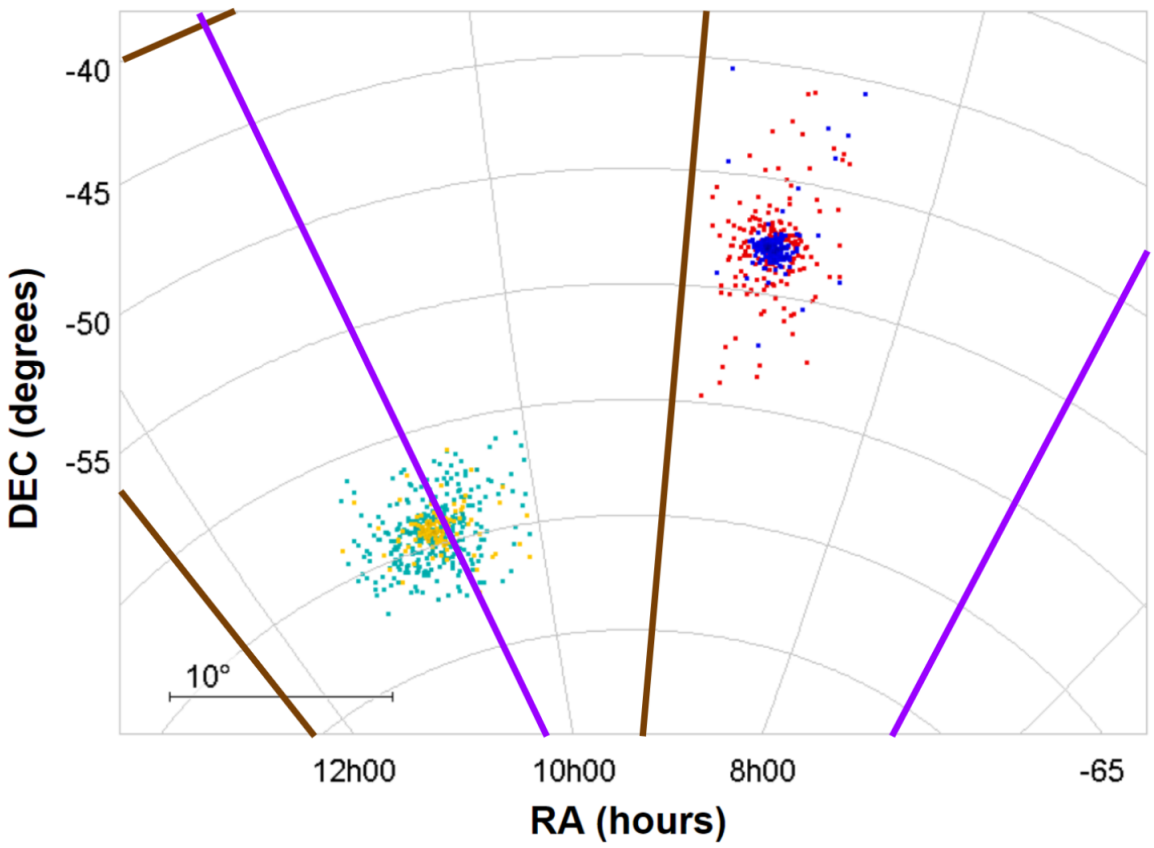

Figure 2.2 Sky positions for IC 2602 and IC 2391 candidate cluster members identified using the prescription in Section 2.2. The RA and DEC ranges of search regions are shown and extend off the plot (brown for IC 2602 and purple for IC 2391). New and known IC 2391 candidate members are represented by red and blue points, respectively. New and known IC 2602 candidate members are represented by cyan and yellow points, respectively.

2001, 2004), Dodd et al. (2004), Paulson & Yelda (2006), Platais et al. (2007), Marsden et al. (2004, 2005, 2009), Boudreault et al. (2009), Mermilliod et al. (2009), Dobbie et al. (2010), Messina et al. (2001, 2003, 2011), Smiljanic et al. (2011), De Silva et al. (2013), Merle et al. (2017), D' Orazi et al. (2017), Gagne et al. (2018), and Randich et al. (1997, 2001, 2002, 2005, 2018).

From this prescription, we determine that our membership lists contain 120 known members and 331 new candidate members for IC 2602, and 152 known members and 198 new candidate members for IC 2391 (see Figure 2.2 and 2.4). If these new candidate members are

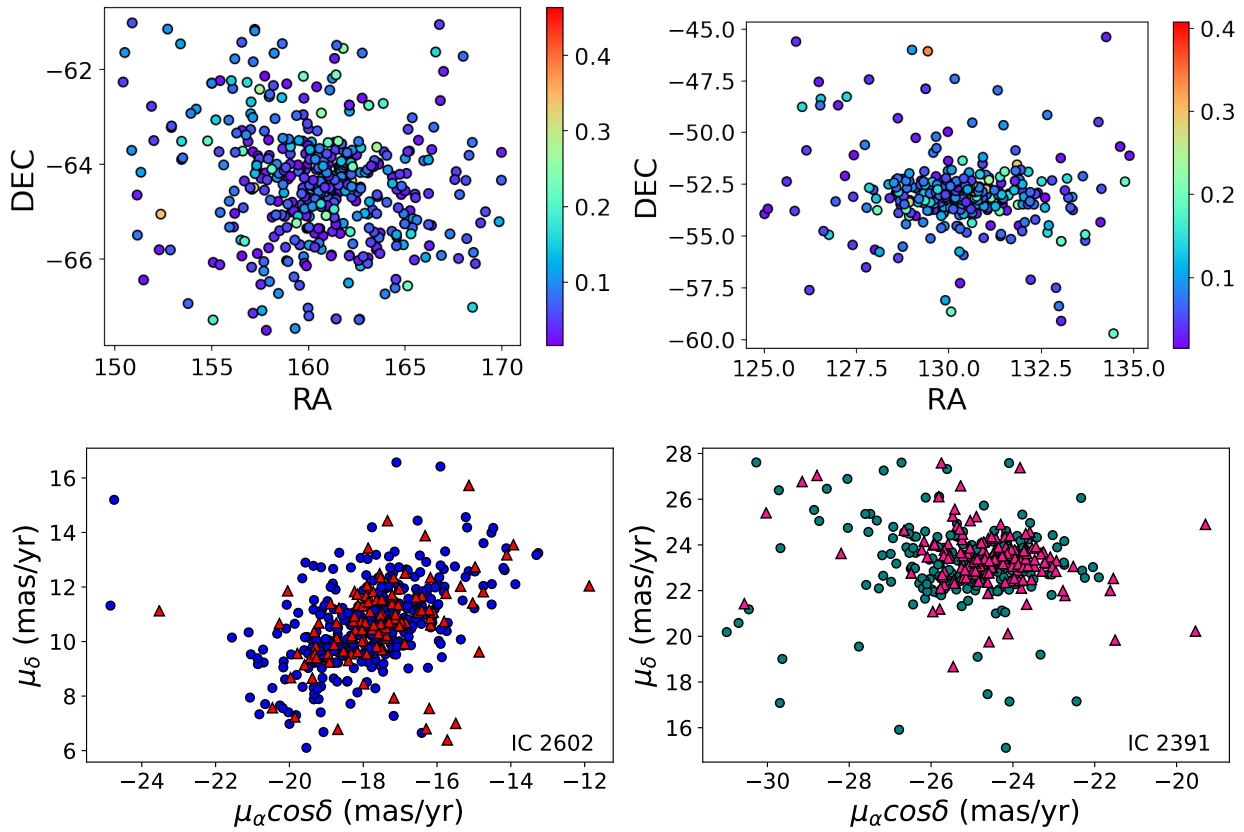

Figure 2.3 Plots of right-ascension and declination are shown for open clusters IC 2602 (upper left panel) and IC 2391 (upper right panel) using *Gaia* DR2 data as described in Section 2.2. The points are color coded based on parallax error. Proper motion in declination is plotted against proper motion in right-ascension for IC 2602 (lower left panel) and IC 2391 (lower right panel) as well. For IC 2602, known members are red triangles and new candidates are blue circles. For IC 2391, known members are pink triangles and new candidates are teal circles. Candidate cluster members can be identified from plots of astrometric parameters based on similar positions and space motions.

confirmed, the known stellar populations of these clusters will increase by 275% and 130%, respectively.

Renormalized unit weight error (RUWE) values, which are quantitative measures of the astrometric errors in *Gaia* DR2 observations (Lindegren et al. 2018), are used in some papers to assess membership of candidate cluster members (Esplin & Luhman 2019; Luhman & Esplin 2020). While more recent surveys, such as those of Penoyre et al. (2022) and Andrew et al. (2022), identify candidate binaries based on RUWE values > 1.6, other works, such as those of Esplin & Luhman (2019) and Luhman & Esplin (2020), apply similar

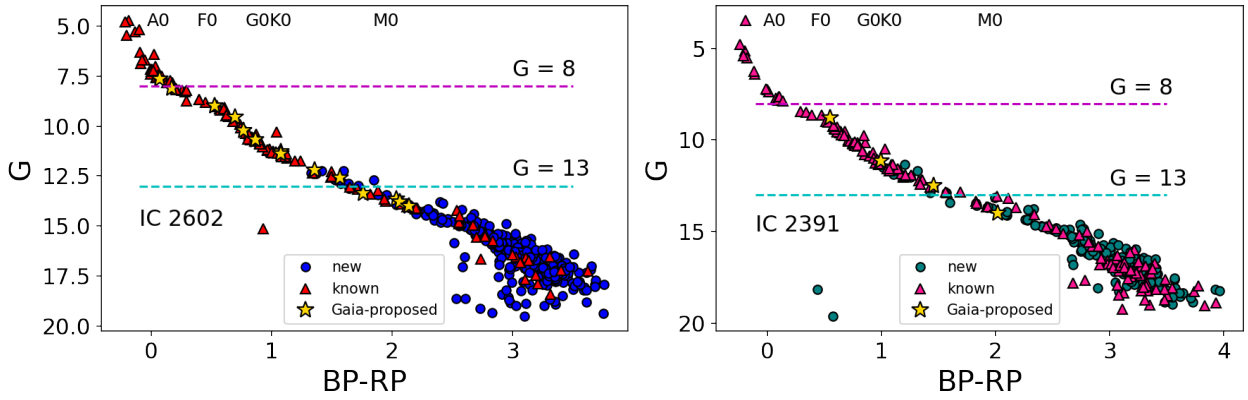

Figure 2.4 *Gaia* apparent G magnitude versus *Gaia* BP-RP color for 451 candidate members of IC 2602 (*left panel*) and 350 candidate members of IC 2391 (*right panel*); the 14 candidate members without *Gaia* colors (4 in IC 2391 and 10 in IC 2602) are not plotted. For IC 2602, 331 are new (blue circles) while 120 are known (red triangles). For IC 2391, 198 are new (teal circles) while 152 are known (pink triangles). Objects brighter than G=14 in the *Gaia* DR2 membership lists that are absent from ours are indicated by golden stars. The magenta line shows the brightness (G=8) above which a more lenient parallax constraint is applied in identifying membership (see Section 2.2). Estimated spectral types are shown at their corresponding *Gaia* colors (Pecaut & Mamajek 2013). We obtain optical spectra for all 26 new candidate members brighter than G=13 (see Chapter 3).

constraints to identify low-mass single-star members of the Taurus and Upper Scorpius associations. The degeneracy between single-star cluster members with poor astrometric fits and binaries with astrometric parameters that differ from single-star observations is difficult to untangle. Moreover, as Luhman & Esplin (2020) describe, many stars with RUWE values that significantly differ from zero still show signs of membership, such as lithium absorption, to young stellar associations. We do not use RUWE constraints because bright stars and photometric binaries are preferentially excluded. Bright stars are lost because they have large systematic errors in *Gaia* DR2 astrometry (Drimmel et al. 2019) while photometric binaries are lost because the astrometric χ^2 relies on a single-star model.

Our new refined membership lists can be found in Appendix tables A.1 (for IC 2391) and A.2 (for IC 2602). The lists are sorted by *Gaia* BP-RP color, which is a tracer of stellar mass, from bluer to redder colors. The colors range from -0.24 to 3.96 in IC 2391 and from -0.22

to 3.76 in IC 2602. For some stars (4 in IC 2391 and 10 in IC 2602), BP-RP color was not available in *Gaia* DR2.

Furthermore, the 3 stars shown in Figure 2.4, 1 of which is in IC 2602 and 2 of which are in IC 2391, with BP-RP < 1 and G > 13 appear to be well below the main sequence and near the white dwarf cooling curves. The star in IC 2602 is a known chemically peculiar single-star noted in the literature by works such as those of Megessier et al. (1983), Maitzen et al. (1988), Pohnl et al. (2003), Hubrig et al. (2008), and Naze et al. (2008). The two newly identified candidate IC 2391 stars appear to have temperatures of 7000-8000 K based on their *Gaia* magnitudes (G $\sim$ 18) and colors (BP-RP $\sim$ 0.5) according to Figure 3 of Bergeron et al. (2019). For these white dwarf temperatures, the cooling time is expected to be 450 Myr to 3 Gyr for 0.2 to 1.3 solar masses, as determined from the cooling models[1] provided by Montreal White Dwarf Database[2] (MWDD; Carrasco et al. 2014; Dufour et al. 2017). Given that these cooling times are of much larger than the estimated 52 Myr age for the open cluster IC 2391, we conclude these stars are not white dwarfs associated with the cluster. If the *Gaia* photometry is actually correct for these, follow-up spectroscopy may confirm them to be background giants (Richer et al. 2021). Because these stars show similar distance and space motion as per our prescription, we still consider them to be candidate members.

2.4 New Candidate Photometric Binaries

Unresolved multiple star systems in which the companions are of comparable brightness are expected to be positioned above the single star main sequence. To identify candidate photometric binaries, we use 8th-order polynomials to iteratively fit the main sequences of the open clusters IC 2602 and IC 2391. While the single-star main sequences are well-defined for these populations overall, they broaden for G > 15 due to larger distance errors; median

[1] `https://www.astro.umontreal.ca/~bergeron/CoolingModels/`
[2] `https://www.montrealwhitedwarfdatabase.org/`

parallax uncertainties for both clusters are 0.03 mas (G<15), 0.07 mas (15<G<17), and 0.12 mas (17<G; Gaia Collaboration et al. 2018). Given that uncertainties on derived parameters in the *Gaia* DR2 database depend strongly on the brightness of sources, most studies adopt a cut on datasets to ignore uninformative stars and improve the signal-to-noise ratio of open clusters in the *Gaia* data (Hunt & Reffert 2021).

For the purposes of this study, we fit the main-sequences of these clusters for stars brighter than G = 18 magnitude in these clusters. This is same magnitude cut applied by Cantat-Gaudin et al. (2018) and Liu & Pang (2019), although Castro-Ginard et al. (2020) adopts a brighter cut at G = 17. We classify candidate binary stars as those that sit above the fit by at least 0.6 magnitudes, as shown in Figures 2.5 and 2.6; this is roughly 0.2 standard deviations above the best-fit main sequences. While we can be confident this prescription works down to G $\sim$ 14 because the main-sequences are well-defined and *Gaia* DR2 astrometric uncertainties are low, the prescription fails at dimmer magnitudes due to the spread in the main sequence. Considering only candidate members with G < 14, we identify 18 candidate photometric binaries. We find that 14 of these are previously known cluster members (7 in IC 2602 and 7 in IC 2391) while 4 are new (2 in IC 2602 and 2 in IC 2391). Candidate photometric binaries are marked in Tables 3.4 and 3.5.

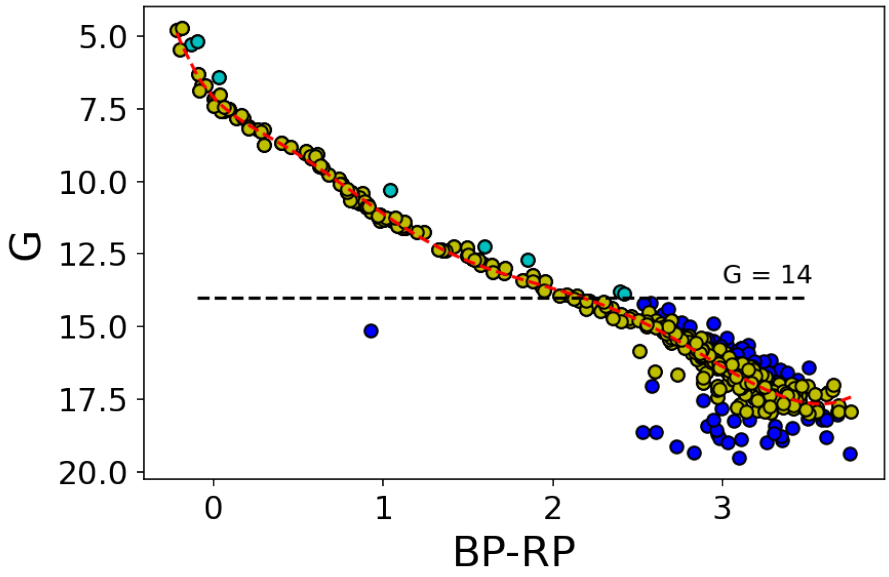

Figure 2.5 Candidate photometric binaries are identified in IC 2602 by an iterative fit to the main-sequence (down to G<18). Stars retained in the fit are shown as yellow circles. For stars brighter than G=14, any star more than 0.6 magnitudes above the fit are considered candidate binaries (cyan circles). For stars fainter than G=14 (blue circles), we do not identify binaries because of the broader main sequence.

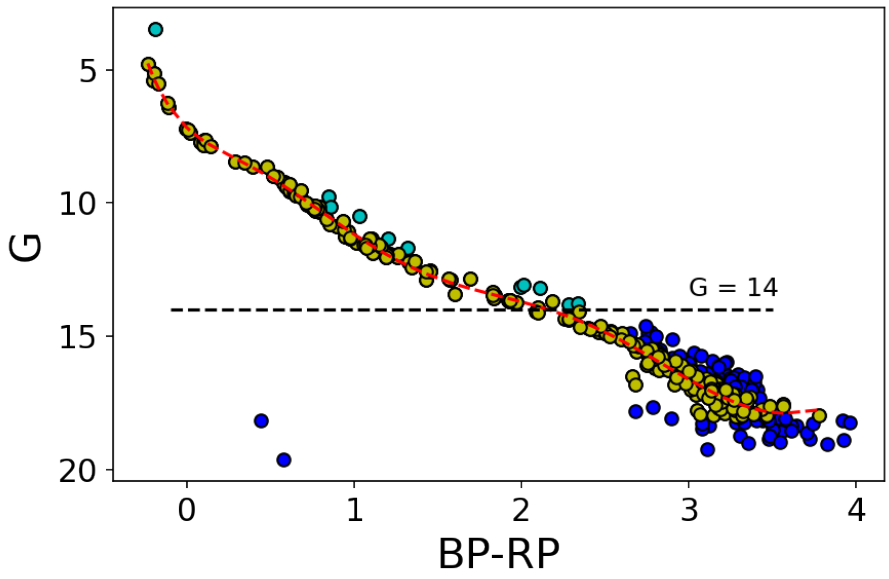

Figure 2.6 Candidate photometric binaries are identified in IC 2391 by an iterative fit to the main-sequence (down to G<18). Stars retained in the fit are shown as yellow circles. For stars brighter than G=14, any star more than 0.6 magnitudes above the fit are considered candidate binaries (cyan circles). For stars fainter than G=14 (blue circles), we do not identify binaries because of the broader main sequence.

CHAPTER 3

CONFIRMING NEW CANDIDATE MEMBERS OF IC 2602 AND IC 2391

3.1 Spectroscopic Observations of Candidate Cluster Members

To confirm the membership of the candidate members of the clusters IC 2602 and IC 2391 identified in Chapter 2, we initiate a spectroscopic survey to acquire high resolution spectra using the CHIRON instrument described in section 3.1.1. More specifically, we obtain spectra for all 26 bright ($G < 13$) candidate members newly identified in this study. We also observe 12 previously known cluster members (also with $G < 13$) to check the reliability of our analysis techniques.

3.1.1 The CHIRON Spectrograph

CHIRON is designed to be a highly stable, high-resolution, cross-dispersed echelle spectrograph on the 1.5-m Small and Moderate Aperture Research Telescope System (SMARTS) telescope, located at Cerro Tololo Inter-American Observatory (CTIO), Chile (Tokovinin et al. 2013; Paredes et al. 2021). This optical spectrometer is fed via a fiber bundle and provides a wavelength coverage of 4100-8900 Å. Four instrumental setups are available, including fiber, slicer, slit, and narrow modes. The specific binning (Horiz. $\times$ Vert.), spectral resolution, relative efficiency, velocity resolution per pixel, and number of echelle orders are displayed in Table 3.1. While Slit and Narrow modes are sometimes used for bright stars, most programs use Fiber or Slicer mode, which are the most efficient and appropriate for stars with $V \sim 6$ to 15 (see Figure 10 in Tokovinin et al. 2013).

Table 3.1. Resolution Modes of CHIRON

Mode	Binning	Resolving Power	Rel. Efficiency	Velocity Resolution	# orders
Fiber	4×4	27,400	1.0	10.9 km/s	62
Slicer	3×1	79,000	0.82	3.8 km/s	59
Slit	3×1	95,000	0.25	3.2 km/s	62
Narrow	3×1	136,000	0.11	2.2 km/s	62

The main elements of the CHIRON instrument are shown in the image and schematic of Figure 3.1. The path of starlight is directed towards the fiber module (FEM) by a diagonal mirror located in the telescope guiding-and-acquisition module (GAM). While the image of the star is focused on a mirror with a hole, most of the light goes into the fiber and the remaining light is reflected towards the acquisition or guiding camera. A small prism can be placed behind the mirror to feed calibration light from quartz or Th-Ar cathode ray lamps to the spectrometer. The beam of light emerging from the fiber can be re-shaped into a slit-like image by the image slicer to increase spectral resolution to $R \sim 79{,}000$ with minimal light loss and a fast CCD readout of 14 s per image. By moving the slicer out of the way, one can obtain the bare fiber image with $R \sim 27{,}400$ and a normal CCD readout of 4 s per image, or mask the fiber by slits to increase the resolution at the expense of light loss. The CCD detector is a CCD231-84 device manufactured by Teledyne e2v and has dimensions 4096 (horiz.) $\times$ 4112 (vert.), with square pixels 15 µm in size.

3.1.2 The Spectroscopic Sample

The sample of stars observed is listed in Table 3.2. For stars brighter than G = 13 ($\sim$ V = 13.5, based on the conversion from Gaia Collaboration et al. 2018), we obtain at least one optical spectrum in fiber mode at 1200 s integration time for each of the 14 new candidate members of IC 2602, 12 new candidate members of IC 2391, and 6 known members from each cluster. New candidate members are designated with the internal identifiers ALN if they are

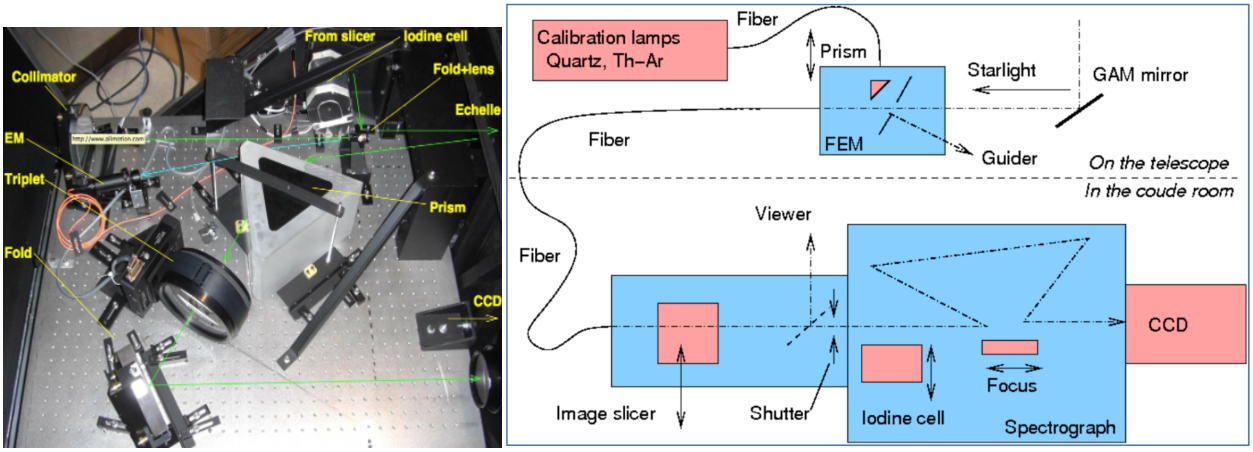

Figure 3.1 The CHIRON instrument and its internal components are shown in the left image as a photograph and in the right image as a schematic. For further details, please kindly consult the text of Section 3.1.1. The images are from Tokovinin et al. (2013).

in IC 2602 and NTC if they are in IC 2391. We also obtain a thorium-argon lamp spectrum with a 4 s exposure before each object spectrum for wavelength calibration. With remaining CHIRON time on-hand, we observed additional epochs for ALN 5, NTC 3, NTC 6, and NTC 8, until the closure of CHIRON from March 18, 2020 due to the global COVID-19 outbreak, in hopes of potentially identifying radial velocity variations suggestive of companions or stellar activity.

All of the stars observed in Table 3.2 were observed in fiber mode, with a caveat to be made for the IC 2391 star, L37, for which slicer spectra were obtained in addition to fiber spectra. While 5 of the 6 observations shown for L37 are taken in slicer mode, only the date of the fiber spectrum is reported in Table 3.2. We had initially monitored L37 for companions in October 2018 using slicer mode given the bright V=10.0 magnitude, Sun-like G spectral type, and single-star classification suggested by *Spitzer* observations in Siegler et al. 2007. However, upon monitoring this star, we quickly identified that L37 is a binary (as noted in Platais et al. 2007 and Marsden et al. 2009) and we confirm that this star is a double-lined spectroscopic binary in Section 3.3. For the 38 stars we observe in this program, 47 spectra were obtained in fiber mode between December 6, 2019 and February 12, 2020.

Table 3.2: Observations in Fiber Mode for IC 2602 and IC 2391

Name	RA (h:m:s)	DEC (h:m:s)	V (mag)	# Obs	Dates	Exposure (s)	Standards
New IC 2602							
ALN 1	10:42:03.62	-65:20:42.2	11.5	1	20-02-08	1200	41Ar,HD26965,H100623
ALN 2	10:42:26.17	-62:28:38.4	11.8	1	20-01-26	1200	12Oph,HD22049,HD16160
ALN 3	10:41:58.41	-65:33:07.9	12.6	1	20-01-06	1200	epsInd,HD191849
ALN 4	10:39:31.94	-63:36:58.3	12.7	1	20-01-26	1200	HD50281,HD131977,HD36003
ALN 5	10:39:36.45	-63:03:43.3	12.7	2	20-01-03	1200	HD36003,HD217357,HD191849
					20-01-04		
ALN 6	10:59:59.17	-64:44:35.5	12.7	1	20-01-12	1200	HD50281,HD131977,HD36003
ALN 7	10:32:29.49	-65:06:25.5	12.7	1	20-02-08	1200	HD50281,HD131977,HD36003
ALN 8	10:49:09.56	-66:01:08.1	13.1	1	20-01-27	1200	epsInd,HD36003,HD217357
ALN 9	10:20:00.14	-62:17:38.5	13.1	1	20-02-08	1200	epsInd,HD36003,HD217357
ALN 10	10:28:42.40	-63:22:15.1	13.2	1	20-01-07	1200	HD36003,HD217357,HD191849
ALN 11	10:52:19.33	-65:58:05.2	13.3	1	20-02-08	1200	HD36003,HD217357,HD191849
ALN 12	10:53:01.73	-65:09:12.3	13.3	1	20-01-28	1200	HD36003,HD217357
ALN 13	10:35:31.77	-62:18:40.5	13.3	1	20-02-09	1200	HD36003,HD217357,HD191849

Table 3.2: Observations in Fiber Mode for IC 2602 and IC 2391

Name	RA (h:m:s)	DEC (h:m:s)	V (mag)	# Obs	Dates	Exposure (s)	Standards
ALN 14	10:31:54.83	-62:34:35.6	13.4	1	20-02-09	1200	HD36003,HD217357,HD191849
New IC 2391							
NTC 1	08:20:27.96	-53:40:18.2	12.3	1	19-12-19	1200	HD22049,HD50281,HD16160
NTC 2	08:32:03.44	-55:38:50.9	12.9	1	19-12-19	1200	HD131977,epsInd,HD36003
NTC 3	08:37:32.93	-52:23:49.3	13.3	5	20-01-03	1200	HD131977,epsInd,HD36003
					20-01-05		
					20-01-06		
					20-01-13		
					20-01-14		
NTC 4	08:37:25.31	-52:54:21.7	13.3	1	20-02-09	1200	HD36003,HD217357,HD191849
NTC 5	08:38:37.50	-52:06:53.9	12.9	1	20-02-09	1200	HD131977,epsInd,HD36003
NTC 6	08:43:40.81	-51:30:13.0	11.7	3	19-12-16	1200	HD100623,12Oph,HD22049
					20-01-13		
					20-01-14		
NTC 7	08:43:41.30	-51:30:14.1	12.3	1	19-12-17	1200	HD50281,HD32147,HD131977

Table 3.2: Observations in Fiber Mode for IC 2602 and IC 2391

Name	RA (h:m:s)	DEC (h:m:s)	V (mag)	# Obs	Dates	Exposure (s)	Standards
NTC 8	08:44:36.97	-52:55:10.0	11.8	3	19-12-18	1200	12Oph,HD22049,HD16160
					20-01-13		
					20-01-15		
NTC 9	08:47:40.37	-52:16:23.5	12.0	1	20-02-09	1200	HD50281,HD131977,HD36003
NTC 10	08:58:33.57	-50:40:14.6	12.0	1	19-12-18	1200	12Oph,HD22049,HD16160
NTC 11	08:58:33.83	-50:40:51.5	11.6	1	20-02-09	1200	HD22049,HD50281,HD16160
NTC 12	08:59:34.60	-51:06:30.8	12.1	1	19-12-18	1200	12Oph,HD22049,HD16160
Known IC 2602							
W79	10:42:08.59	-64:46:07.5	11.6	1	20-02-10	1200	HD10700,epsFor,41Ar
R1	10:28:32.68	-63:44:15.3	11.6	1	20-02-10	1200	HD115617,HD10700,epsFor
R10	10:32:31.35	-65:06:43.2	12.8	1	20-02-11	1200	HD22049,HD50281,HD16160
R66	10:44:08.52	-63:59:35.3	11.1	1	20-02-10	1200	HD59967,HD114613,HD90156
R70	10:44:24.61	-64:15:32.4	10.9	1	20-02-11	1200	HD34721,HD9562,HD38858
SR3	10:43:17.17	-64:23:52.3	10.8	1	20-02-10	1200	HD9562,HD38858,HD4391
Known IC 2391							

Table 3.2: Observations in Fiber Mode for IC 2602 and IC 2391

Name	RA (h:m:s)	DEC (h:m:s)	V (mag)	# Obs	Dates	Exposure (s)	Standards
VXR16A	08:40:18.04	-52:56:44.0	11.8	1	20-02-12	1200	HD10700,epsFor,41Ar
VXR22A	08:40:50.93	-53:38:01.4	11.1	1	20-02-12	1200	HD21019,HD90156,HD115617
VXR70	08:44:07.30	-52:53:34.9	10.8	1	20-02-12	1200	HD4391,HD59967,HD114613
PMM4362	08:38:23.60	-52:56:58.4	11.0	1	20-02-11	1200	HD21019,HD90156,HD111031
SHJM6	08:39:54.98	-52:58:11.4	11.9	1	20-02-12	1200	41Ar,HD26965,H100623
L37	08:39:39.58	-53:10:18.7	10.0	6	20-02-11	1200	HD9562,HD38858,HD4391

Note. — For additional discussion regarding the star L37, please consult the text in Section 3.1.1. For additional information regarding the choice of standards for determining radial velocities and $v \sin i$ values in Section 3.2, please refer to the text in Section 3.1.3 and data in Table 3.3.

3.1.3 Data Reduction and Preparing Spectra for Analyses

The REsearch Consortium on Nearby Stars (RECONS) team at Georgia State University processes the observed echelle spectra from CHIRON to provide calibrated spectra, consisting of 59 spectral orders for Slicer mode and 62 otherwise. The stellar spectra are extracted using a customized data reduction pipeline written in IDL, as described by Tokovinin et al. (2013) and Paredes et al. (2021). This official CHIRON pipeline makes use of two sets of calibration frames, taken at the beginning and end of the night, that are integral to the data reduction process and included with each night's observations. Using the quartz lamp calibrations, each spectrum is first bias-corrected and then flat-fielded to remove electronic readout noise and correct for individual pixel sensitivities. Next, cosmic rays are removed from the spectrum and profile order extraction is performed using an extraction algorithm based on the REDUCE package by Piskunov & Valenti (2002). Finally, each spectrum with extracted orders is matched with its closest Th-Ar calibration frame to obtain the sampled wavelength solution.

While additional processing of spectra is not necessary for measuring equivalent widths as we do in Section 3.2.1, analyses for determining stellar properties work best with normalized and flattened spectra as we do in Sections 3.2.2 and 3.2.3. Figure 3.2 shows an example of a spectrum before and after we process it using a Python script we have independently written. We begin by iteratively fitting the blaze function of a reduced spectrum with a 5th order polynomial, excluding points in the spectrum more than 0.5 standard deviations below or more than 1.0 standard deviations above the fit, until no additional points can be dropped and the best fit for the blaze function is achieved. We then normalize the spectrum by dividing the original spectrum by this final polynomial fit to the blaze function, and then subtract 1 from the spectrum so that the continuum flux is normalized to zero. Finally, we flatten the spectrum, eliminating cosmic rays and hot pixels missed by the reduction pipeline, by excluding points in the spectrum more than 1 standard deviation above the local mean.

For the cross-correlation analyses in Section 3.2.2, we use a catalogue of 81 spectral standard stars with well-determined radial and projected rotational velocities. The high-quality fiber-mode CHIRON spectra of these stars are assembled by Yep et al. (2021) and publicly available to all CHIRON users[1]. While these bright, slowly-rotating CHIRON standards were observed following an identical spectral setup to that described in Section 3.1.1, exposure times were adjusted to achieve signal-to-noise (SNR) ratios ≥ 100.

In order to prepare the spectra of observed cluster stars described in Section 3.1.1 for entering the Python pipeline we have independently written that determines the radial and projected rotational velocities discussed in Section 3.2.2, we estimate the approximate spectral types of the stars by first using the relation between *Gaia* BP-RP color and dwarf spectral type given by the main-sequence grid of Pecaut & Mamajek (2013),[2] and then by visual comparison to the catalogue of CHIRON standards. Once every star observed in our survey is assigned an estimated spectral type, each is matched with 3 CHIRON standards, as listed in Table 3.2, whose spectral types most closely match that estimate. Observation details for the standards used in this survey are presented in Table 3.3.

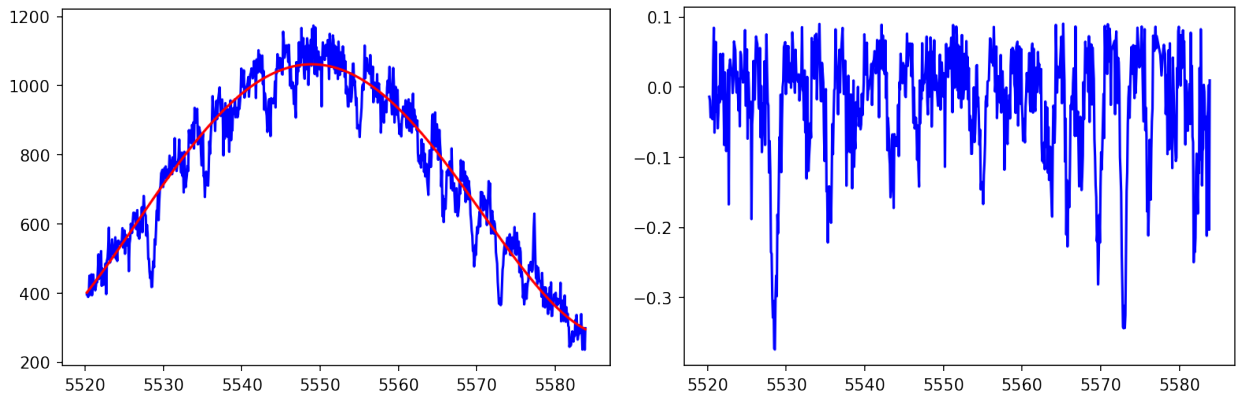

Figure 3.2 The 23rd echelle order of ALN 2, a newly identified candidate cluster member of IC 2602 observed on January 26, 2020, is shown. The original reduced CHIRON spectrum of this star (left panel) is processed to produce a normalized and flattened spectrum (right panel) as described in Section 3.1.3. The final polynomial fit to the blaze function is shown as a red line.

[1] https://github.com/alexandrayep/CHIRON$_$Standards

[2] https://www.pas.rochester.edu/~emamajek/EEM_dwarf_UBVIJHK_colors_Teff.txt

Table 3.3: CHIRON Fiber Standards for IC 2602 and IC 2391

Spectral Type	Name	RA (h:m:s)	DEC (h:m:s)	V (mag)	RV (km/s)	vsini (km/s)	Date Observed	Exposure Time (s)
G0V	HD34721	05:18:52.63	-18:07:48.2	5.96	40.448(N02)	4.4(A12)	19-10-29	400
G1V	HD9562	01:33:43.64	-07:01:29.4	5.76	-14.989(N02)	4.2(M14)	19-10-29	300
G2V	HD38858	05:48:36.76	-04:05:44.6	5.97	31.543(N02)	4.2(S09)	19-10-29	400
G3V	HD4391	00:45:48.54	-47:33:21.9	5.80	-11.01(G18)	5(S09)	18-11-01	300
G3V	HD59967	07:30:42.69	-37:20:18.9	6.64	9.37(G18)	3.4(S18)	20-02-08	800
G3V	HD114613	13:12:05.07	-37:48:19.6	5.55	-12.85(G18)	2.381(S18)	19-08-01	119
G5.5V	HD21019	03:23:19.65	-07:47:39.3	6.20	41.63(N02)	2.502(S18)	19-22-03	500
G5V	HD90156	10:23:56.42	-29:38:47.9	6.92	26.934(N02)	0.73(S18)	20-02-07	1000
G5V	HD111031	12:46:31.88	-11:48:49.0	6.87	-20.458(N02)	1.728(S18)	20-02-14	1000
G6.5V	HD115617	13:18:24.73	-18:19:16.7	4.74	-7.85(N02)	3.9(A12)	19-08-27	120
G8V	HD10700	01:44:02.88	-15:55:58.1	3.50	-16.619(N02)	3.26(M10)	18-07-28	60
G9V	epsFor	03:01:39.93	-28:05:17.4	5.85	38.36(Y21)	4.2(S09)	19-10-30	400
K0V	41Ar	17:19:06.15	-46:38:18.5	5.48	26.005(Y21)	4.5(S09)	19-07-01	139
K0V	HD26965	04:15:14.13	-07:40:25.9	4.43	-42.331(N02)	0.5(M14)	20-02-07	70
K0V	HD100623	11:35:29.48	-32:56:16.4	5.98	-21.959(N02)	6.79(M10)	20-02-04	300

Table 3.3: CHIRON Fiber Standards for IC 2602 and IC 2391

Spectral Type	Name	RA (h:m:s)	DEC (h:m:s)	V (mag)	RV (km/s)	vsini (km/s)	Date Observed	Exposure Time (s)
K1V	12Oph	16:36:23.10	-02:19:38.9	5.77	-12.857(N02)	2.2(M14)	19-07-01	300
K2V	HD22049	03:32:58.12	-09:27:22.9	3.73	16.332(N02)	2.4(M14)	18-10-22	19
K3.5V	HD50281	06:52:18.15	-05:10:28.5	6.57	-7.082(N02)	3.9(S09)	20-02-06	600
K3V	HD16160	02:36:10.08	06:53:57.8	5.83	24.37(Y21)	2.9(M14)	18-11-06	120
K3V	HD32147	05:01:48.54	-05:44:01.3	6.21	21.552(N02)	1.7(M14)	20-01-14	500
K4V	HD131977	14:57:33.92	-21:25:47.9	5.72	26.961(N02)	3.9(S09)	19-06-16	175
K5V	epsInd	22:03:31.39	-56:47:57.7	4.69	-40.038(Y21)	2.493(S18)	19-07-01	60
K5V	HD36003	05:28:26.89	-03:30:21.3	7.64	-55.527(N02)	3.35(M10)	20-02-07	1200
K7V	HD217357	23:00:15.99	-22:31:31.3	7.87	16.42(N02)	3.21(M10)	19-08-05	1028
M0V	HD191849	20:13:57.79	-45:09:23.1	7.97	-33.46(G18)	1(T06)	19-04-07	1200

Note. — CHIRON Fiber Standards (Yep et al. 2021) used to determine radial and projected rotational velocities are shown. The references are as follows: N02 = Nidever et al. 2002, A12 = Ammler-Von Eiff et al. 2012, M14 = Marsden et al. 2014, S09 = Schroder et al. 2009, G18 = Gaia Collaboration 2018, S18 = Soto et al. 2018, M10 = Martinez-Arnaiz et al. 2010, Y21 = Yep et al. 2021, T06 = Torres et al. 2006.

3.2 Spectroscopic Properties of Candidate Cluster Members

3.2.1 Li I *λ6708 Å* & *Hα Equivalent Widths*

We use the well-known spectroscopic indicators of stellar youth, lithium (^7Li) absorption and Hα emission, to distinguish cluster members of IC 2602 and IC 2391 from non-member field stars. Lithium absorption is a diagnostic of stellar youth (Soderblom et al. 2010; Zhou et al. 2021) because the element lithium is destroyed in the cores of Sun-like stars over a period of 200 Myr, due to proton-helium collisions that begin when stellar interiors reach 2.5 million Kelvins (Bodenheimer 1965; Skumanich et al. 1972; Bildsten et al. 1997) and subsequent convective mixing processes (White et al. 2007; Lopez-Santiago et al. 2010; Binks & Jeffries 2014; Baraffe et al. 2017). Thus, while the youngest late-type open cluster stars exhibit strong atmospheric lithium absorption, older stars such as the Sun are lithium-poor (Brault & Muller 1975; White & Hillenbrand 2005; Soderblom et al. 2014). Moreover, lithium depletion is spectral-type dependent; cooler dwarf stars burn through their primordial lithium abundances ($\sim$3.2 on a logarithmic scale where H = 12; Sestito & Randich 2005) more quickly thanks to their deeper convection zones, as shown in Figure 3.3 (Randich et al. 1997; Jeffries et al. 2014; Cummings et al. 2017; Riedel et al. 2017; Gutierrez et al. 2020; Constantino et al. 2021). Examples of CHIRON spectra with lithium absorption for new candidate members of IC 2602 and IC 2391 are shown in Figure 3.4.

Another commonly adopted diagnostic of stellar youth in solar-type stars is Hα emission (Herbig 1985; Lyra & Porto de Mello 2005), which may be observed from at least five sources: chromospheric activity from the magnetic dynamo and stellar wind mass loss of rapidly rotating young stars (Ebbets 1982; Noyes et al. 1984; Leitherer 1988; Lamers & Leitherer 1993; Puls et al. 1996; Barnes et al. 2007; Zhou et al. 2021), gas infall during accretion from a rapidly rotating T Tauri star's circumstellar disk (Conti & Leep 1974; White & Basri 2003), a corotating circumstellar structure (Stahl et al. 1996), a gas stream due to Roche lobe overflow or colliding winds in a close binary system (Thaller et al. 1997). While the first and

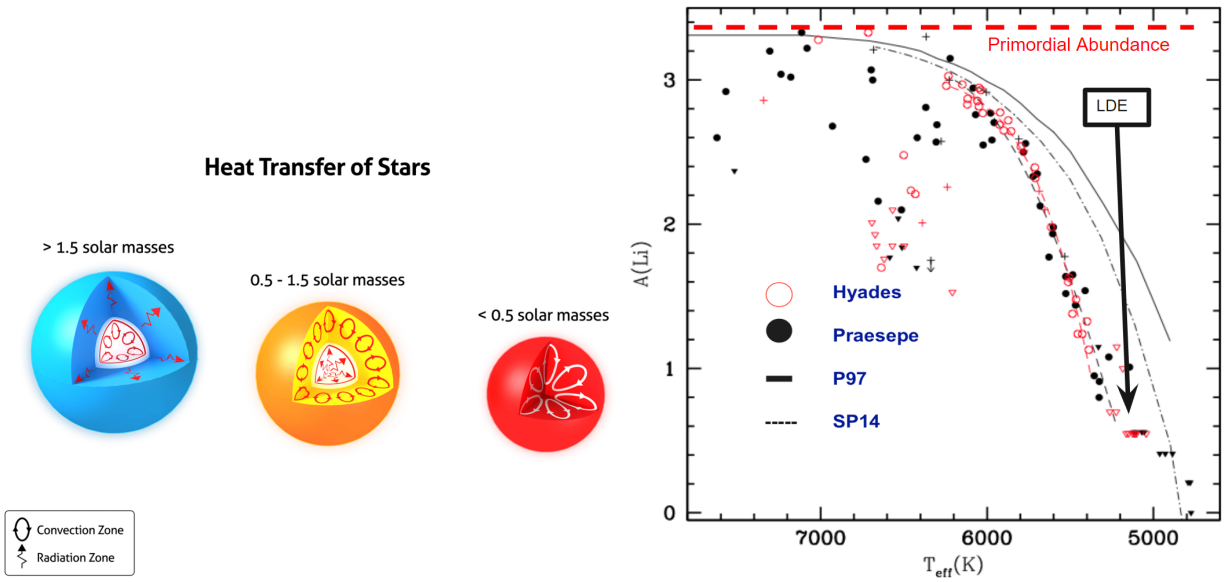

Figure 3.3 Convection and radiation zones for stars of different masses are shown in the left panel *Credit:* Sun.org. Cooler, lower-mass dwarf stars have deeper convective envelopes, which allow for more rapid depletion of atmospheric lithium by convective mixing as described in Section 3.2.1. The plot of lithium abundance versus effective temperature from Cummings et al. (2017) for stars in the Hyades and Praesepe open clusters is shown in the right panel. As the P97 (Pinsonneault 1997) and SP14 (Somers & Pinsonneault 2014) models indicate, lithium is destroyed over time in Sun-like stars and cooler stars burn lithium more quickly. We have indicated the primordial lithium abundance and lithium depletion edge (LDE), which are used to age-date young stellar clusters.

second of these can be distinguished if the Hα emission is narrow or broad, respectively, and main-sequence close binaries rarely display Hα emission (Thaller et al. 1997), the strength of the feature is known to vary by at least a factor of 2 over short timescales (Pettersson 1987; Kim et al. 2005; Chen et al. 2008; Yep et al. 2021). Examples of CHIRON spectra with Hα emission for new candidate cluster members of IC 2602 and IC 2391 are shown in Figure 3.5.

As a first assessment of stellar youth, we measure equivalent widths of the lithium doublet at 6708 Å and the Hα feature at 6563 Å using IRAF's Gaussian-fitting *splot* package, as shown in the example in Figure 3.6. We then determine the signal-to-noise (SNR) ratio per pixel using the flux per pixel F in analog-to-digital units (ADU), the gain G in units of electrons/ADU, the number of binned pixels across the order K (2.5 for fiber mode), and the CCD readout noise in electrons R, based on the method described by Tokovinin et al. (2013):

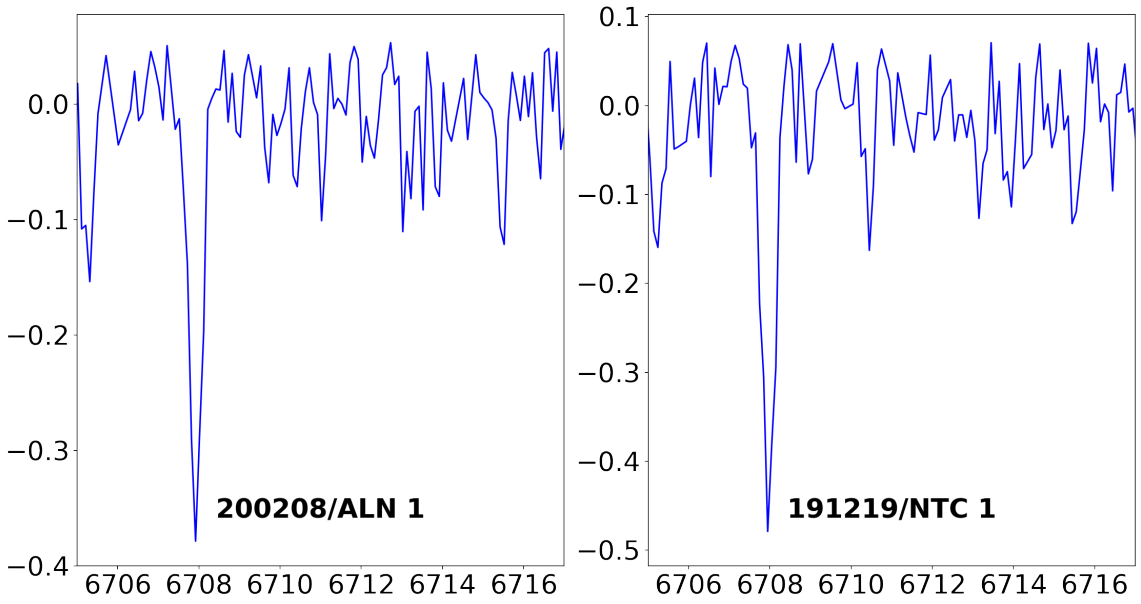

Figure 3.4 Flux versus wavelength is shown for the 40th echelle order in CHIRON fiber-mode spectra of ALN 1 (left panel) and NTC 1 (right panel), new candidate members of IC 2602 and IC 2391 respectively, to highlight the strong lithium absorption feature at 6708 Å .

$$SNR \simeq \frac{FG}{\sqrt{FG + KR^2}} \tag{3.1}$$

Next, we estimate equivalent width uncertainties using the spectrograph pixel-wavelength scale p (0.097 Å at Hα; 0.100 Å at lithium), the measured Gaussian full-width at half maximum f of the spectral line, and the SNR per pixel, following the prescription of Cayrel (1988) and Deliyannis et al. (1993, 2019):

$$\Delta EW \simeq 1.5 \frac{\sqrt{fp}}{SNR} \tag{3.2}$$

When reporting equivalent widths, we adopt the standard convention of assigning negative values for emission lines and positive values for absorption. Upper limits are assigned when the spectral line cannot be distinguished from the noise of the continuum. For the candidate double-lined spectroscopic binaries discussed in Section 3.3, equivalent widths are diminished due to the companion's continuum.

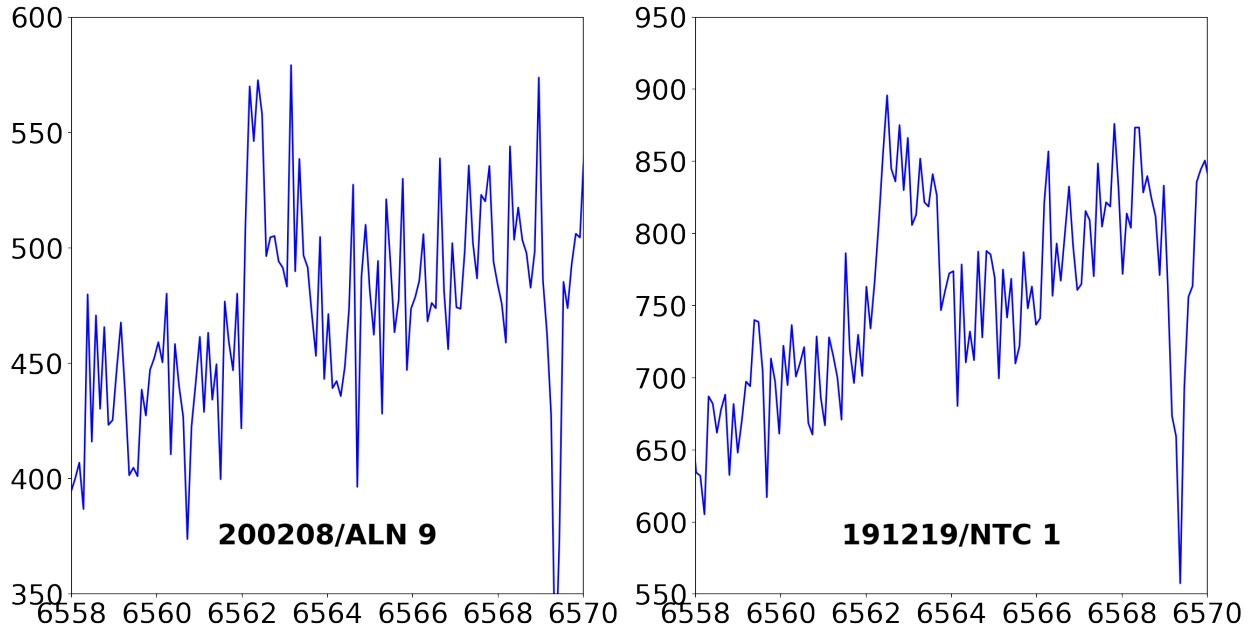

Figure 3.5 Flux versus wavelength is shown for the 38th echelle order in CHIRON fiber-mode spectra of ALN 9 (left panel) and NTC 1 (right panel), new candidate members of IC 2602 and IC 2391 respectively, to highlight the Hα emission feature at 6563 Å .

The measured equivalent widths of lithium absorption are plotted as a function of effective temperature in Figure 3.7. The distributions of values are consistent with measurements in clusters with similar age (30-50 Myr based on their main-sequence turnoffs) from Gutiérrez Albarrán et al. (2020). We also plot equivalent widths for Hα against lithium and find that, according to Figure 9 of James et al. (2022), most stars in our sample are likely young (see Figure 3.8). Compared with literature values of previously known members (as reported by Randich et al. 1997, 2001; Platais et al. 2007), our measured values agree within measurement uncertainties ($\sim$0.02 Å). This also suggests and confirms that the uncertainties associated with continuum choice are small compared with those determined from the equivalent width formula. Equivalent width values are listed in Tables 3.4 and 3.5. The results are used to assign cluster membership for observed stars in Section 3.4.

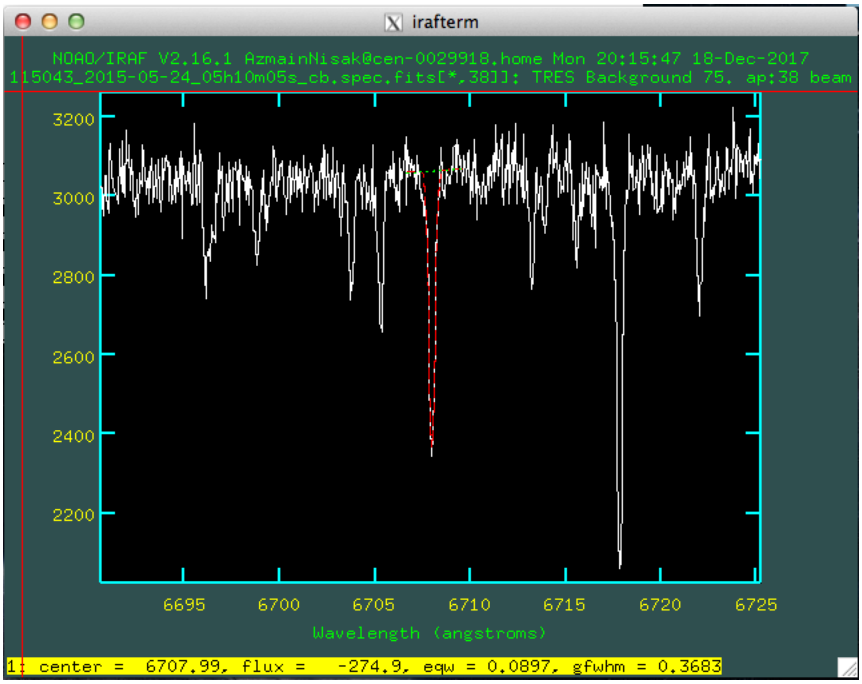

Figure 3.6 The Tillinghast Reflector Echelle Spectrograph (TRES) spectrum of the Ursa Major Moving Group star, HD 115043, is displayed in IRAF's *splot* program, which fits a Gaussian to the lithium feature. Based on the fit, the program provides the equivalent width (eqw) of the spectral line by integrating its flux with respect to the continuum, as well as the gaussian full-width at half maximum (gfwhm). This star is not part of our membership survey.

3.2.2 Radial & Projected Rotational Velocities

To measure the radial velocities (RV) and projected rotational velocities ($v \sin i$) of target stars, we perform normalized cross-correlation with PyAstronomy's *crosscorrRV* function in Doppler mode for 12 spectral orders (see Figure 3.9 for an example) covering a wavelength range of 4890-6330 Å between the target and three spectral standards of similar *Gaia* BP-RP color from the catalogue of CHIRON standards discussed in Section 3.1.3. We avoid orders with telluric absorption (e.g. O_2 A-band, B-band), chromospheric emission (e.g. Hα), and pressure-sensitive lines (e.g. Na I Doublet) that may bias the $v \sin i$ results.

A radial velocity is determined from each spectral order by fitting the peak of the cross-correlation function (CCF) with a Gaussian. The radial velocity uncertainty for each spectral order is estimated based on the equation from Butler et al. (1996). The intrinsic Doppler

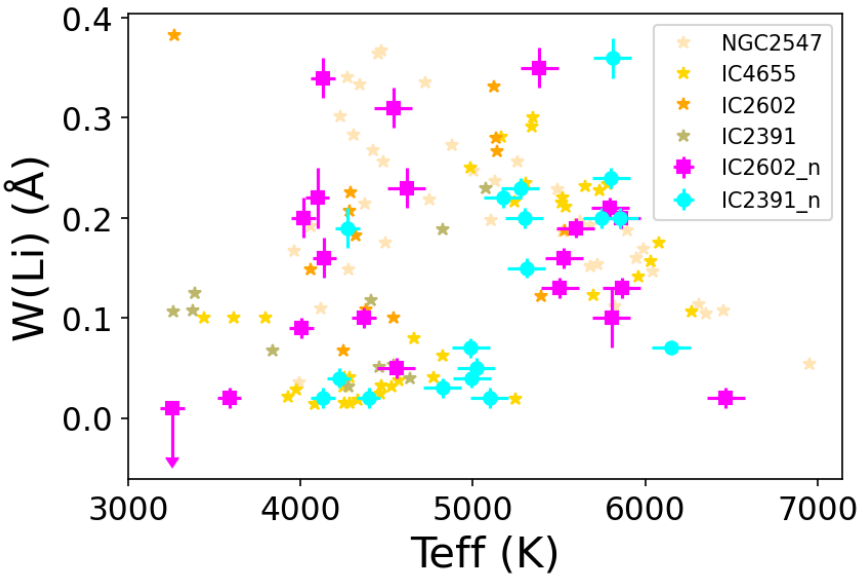

Figure 3.7 Equivalent widths of lithium at 6708 Å are plotted against effective temperatures (see Section 3.2.3) for all observed stars in this study for IC 2602 (magenta squares; IC2602_n) and IC 2391 (cyan circles; IC2391_n). Upper limits are indicated with arrows. Here, we show that our lithium measurements for IC 2602 and IC 2391 are consistent with those for other clusters of similar age from Gutiérrez Albarrán et al. (2020).

error for each spectral order σ_V, which is lowest for orders with the most spectral features, is determined using the SNR per pixel, the wavelength w and flux f at each pixel, the speed of light c, and the numerical derivative df/dw of the spectrum that represents the slope observed by the spectrometer, including smearing from instrumental and astrophysical origins. The sum is taken over all pixels in the portion of spectrum being used:

$$\sigma_V \simeq \frac{1}{\sqrt{\sum(\frac{df}{dw} \times \frac{w}{c} \times SNR)^2}} \tag{3.3}$$

By weighting the relative radial velocities determined for each spectral order of each observed star by their corresponding Doppler uncertainties (~ 0.5 km/s), a weighted mean relative radial velocity is calculated. This Doppler-error-weighted mean relative radial velocity is converted to a radial velocity relative to the center of mass of the Solar System by subtracting the radial velocity contributions of the CHIRON standards and the barycentric corrections due to Earth's rotation, Earth's orbit around the Earth-moon barycenter, and the

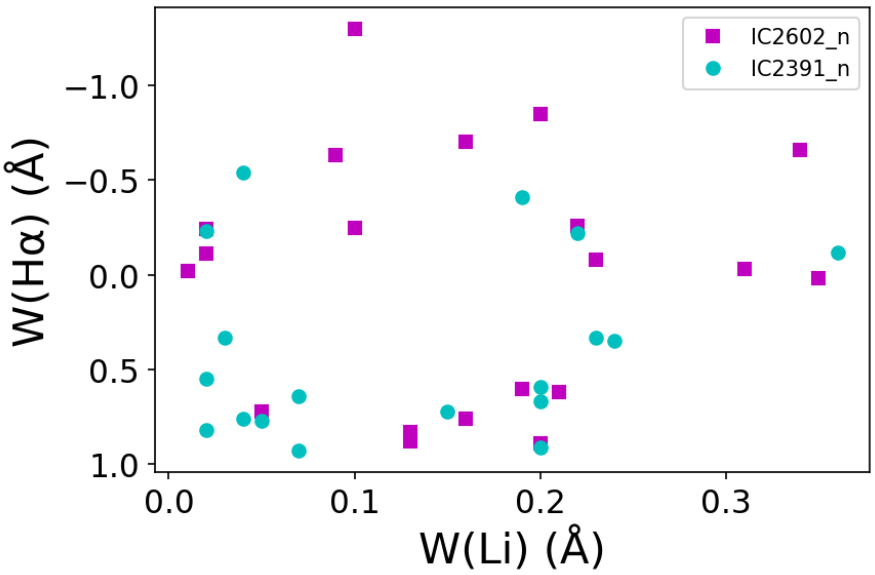

Figure 3.8 Equivalent widths of Hα at 6563 Å are plotted against equivalent widths of lithium at 6708 Å for all observed stars in this study for IC 2602 (magenta squares; IC2602_n) and IC 2391 (cyan circles; IC2391_n).

Earth-moon barycenter's orbit around the Sun. Barycentric velocities are determined using EXOFAST's (Eastman et al. 2013) barycentric correction algorithm (Wright & Eastman 2014) and PyAstronomy's *helcorr* function, which are accurate to $\sim$ 1 m/s if applied correctly (Czesla et al. 2019). Final radial velocities and uncertainties (typically $\sim$ 0.1 km/s) are determined by taking the average and standard deviation respectively for the three CHIRON standards used.

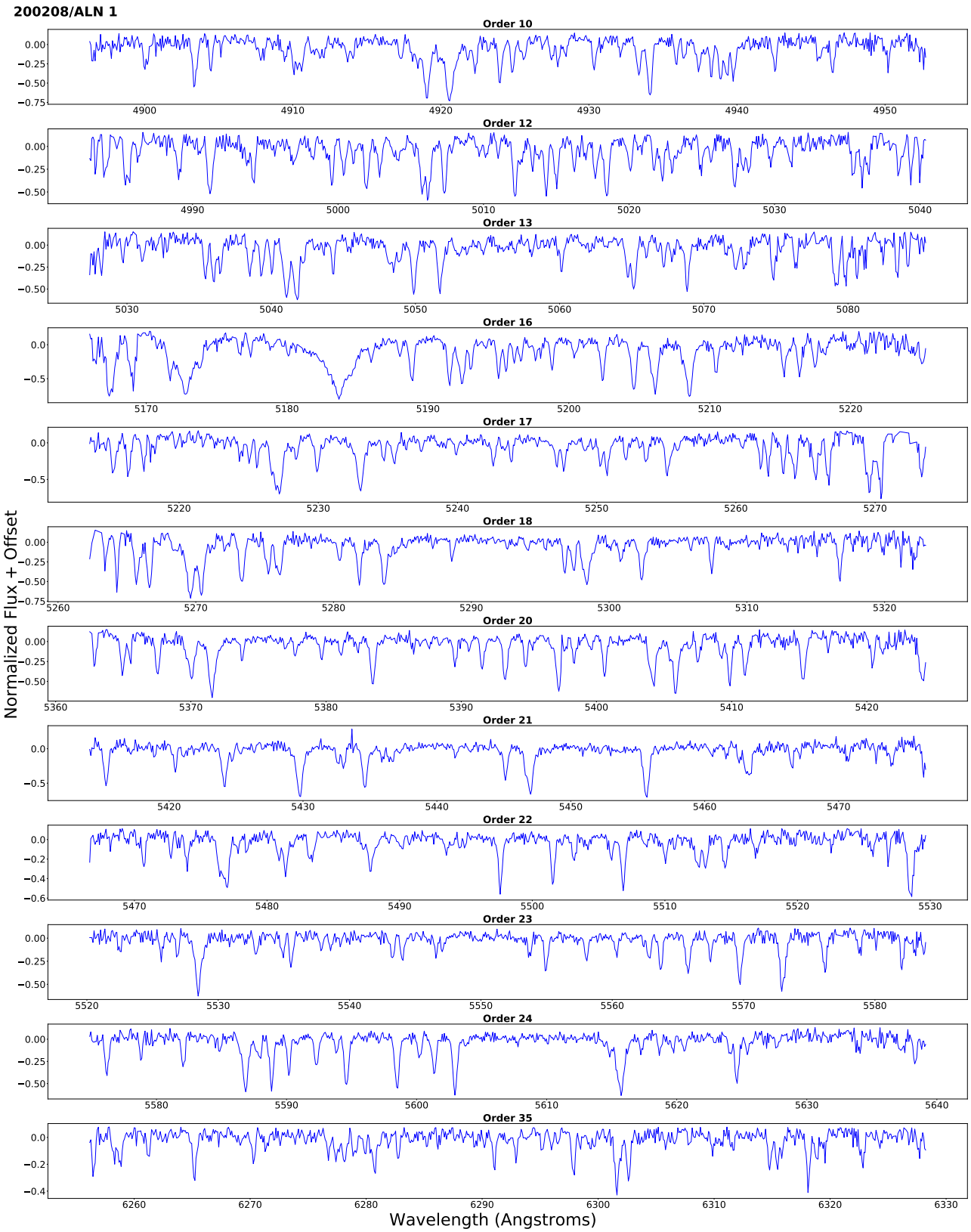

Figure 3.9 The 12 spectral orders of a CHIRON fiber-mode spectrum used for cross-correlation analyses are shown for the new candidate IC 2602 cluster member, ALN 1.

While the positions of cross-correlation peaks are used to determine radial velocities, cross-correlation widths are used to infer projected rotational velocities relative to comparison standards. First, each spectral order of a comparison standard spectrum is artificially broadened using PyAstronomy's *rotBroad* function (Gray 1976, 1992; White et al. 2007), with the limb-darkening coefficient set to $\epsilon = 0.6$ for optical wavelengths. For each spectral order, the Gaussian full width at half maximum is then measured from the autocorrelation function of the original spectrum of the comparison standard with rotationally broadened, synthetically generated versions of that standard spectrum for various $v \sin i$ values. These measurements allow us to derive an empirical relation between the Gaussian widths of the autocorrelation functions and associated $v \sin i$ values as shown in Figure 3.10. Next, $v \sin i$ values are determined by interpolating this relationship using the width measured from the cross-correlation function between the spectral order of an observed star with that of its comparison standard. A $v \sin i$ estimate for a star relative to its comparison standard is obtained by averaging the $v \sin i$ measurements for all 12 orders, taking the standard deviation of these as the uncertainty. Final projected rotational velocities and uncertainties (typically $\sim$ 1-6 km/s) are determined by taking the average and standard deviation respectively for the three CHIRON standards used.

To test the accuracy of our prescriptions, we compare our measured radial and projected rotational velocities for known cluster members of IC 2602 and IC 2391 with values from Stauffer et al. (1997), Randich et al. (2001), Platais et al. (2007), Marsden et al. (2009), Mermilliod et al. (2009), De Silva et al. (2013), and Randich et al. (2018). We find that our measurements agree within 2 standard deviations of published literature values. All values of radial and projected rotational velocities we measure and report from the literature are listed in Tables 3.4 and 3.5.

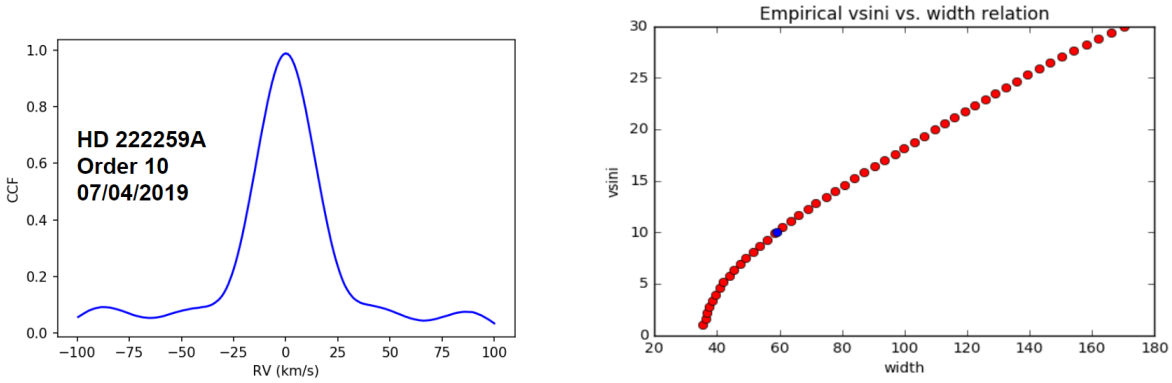

Figure 3.10 The left panel shows a cross-correlation function for the 10th echelle order in the CHIRON spectrum of the Tucana-Horologium star, HD 222259A. While the peak of this function can be used to determine a radial velocity, the Gaussian width can be used to determine a projected rotational velocity. The right panel shows an empirical relationship between $v \sin i$ values and autocorrelation widths for a CHIRON standard star as red dots. The blue dot represents a width measured from the cross-correlation function of a star and its standard, allowing us to determine the $v \sin i$ for the star by interpolation.

3.2.3 Stellar Fundamental Parameters

In addition to radial and projected rotational velocities, we also determine effective temperature (Teff), surface gravity (log(g)), and metallicity ([Fe/H]) values for the 38 observed stars using the Python algorithm, Empirical SpecMatch (Yee et al. 2017). This spectral characterization code extracts bulk stellar parameters of an input optical spectrum by comparing it to a dense library of high-resolution (R $\sim$ 55,000), high signal-to-noise (SNR $>$ 100) spectra for 404 calibrator stars. These stars were observed with the High Resolution Echelle Spectrometer (HIRES) spectrograph on the 10-m Keck telescope in Hawaii as part of the California Planet Search (CPS; Howard et al. 2010). These touchstone stars have well-determined parameters derived from a variety of independent methods, including interferometry, optical and near-infrared (NIR) photometry, asteroseismology, and local thermal equilibrium (LTE) analysis of high-resolution optical spectra. These parameters range from 3000 to 7000 K in Teff, 0.1 to 16 solar radii in radius, -0.6 to +0.6 dex in [Fe/H], and F1 to M5 in spectral type. Because the code relies on an "empirical library", it performs particularly well for mid- to late-K and M stars that are difficult to fit with synthetic spectra, given numerous atomic

and molecular lines with poorly known properties. Consequently, Empirical SpecMatch is frequently used to characterize exoplanet host stars in recent works (Persson et al. 2018; Nielsen et al. 2019; Carmichael et al. 2020; Furlan & Howell 2020).

To determine stellar parameters, the code first accounts for the line-of-sight velocity of the target star by shifting its spectrum onto the library wavelength scale using a bootstrapping approach in the Mgb triplet region (5100-5340 Å). Several useful line diagnostics are present in this spectral region, including ratios of weak metal lines for Teff, the Mg I b triplet for log(g), and various iron lines for [Fe/H] (e.g. Gray 1994, 1996; Sousa et al. 2010). The code accomplishes its first step by initially shifting the target spectrum in that region to the allowed references and comparing the heights of cross-correlation peaks, using the reference with the highest median peak as the template to shift the entire spectrum. Next, the code runs a pairwise match between the target spectrum and each library spectrum, fitting for $v \sin i$ line broadening and a cubic spline to the continuum level to account for differences in continuum normalization. The code extracts the final derived parameters by interpolating between library spectra and using a weighted linear combination of the five best-matching spectra. When obtaining the best-matching library spectra and generating the best-matching linear combination of library spectra to determine stellar properties, the code employs nonlinear least-squares minimization (Newville et al. 2014) to minimize the unnormalized χ^2 statistic, as shown in Figures 3.11 and 3.12. The uncertainties returned by Empirical SpecMatch are set by the scatter of the differences between the stellar parameters derived by the code for the library stars and their library values. These are typically 70-100 K in effective temperature, 0.12 dex in log(g), and 0.09 dex in [Fe/H].

Figure 3.13 illustrates the best fit metallicities versus effective temperatures of candidate cluster members, along with the values of the comparison standards from which these values were determined. Stellar properties for the candidate double-lined spectroscopic binaries (including the two stars with [Fe/H]<-0.5) marked in Tables 3.4 and 3.5 are unreliable due to contamination of spectra by companions. As Figure 3.13 reveals, the grid of standard spectra

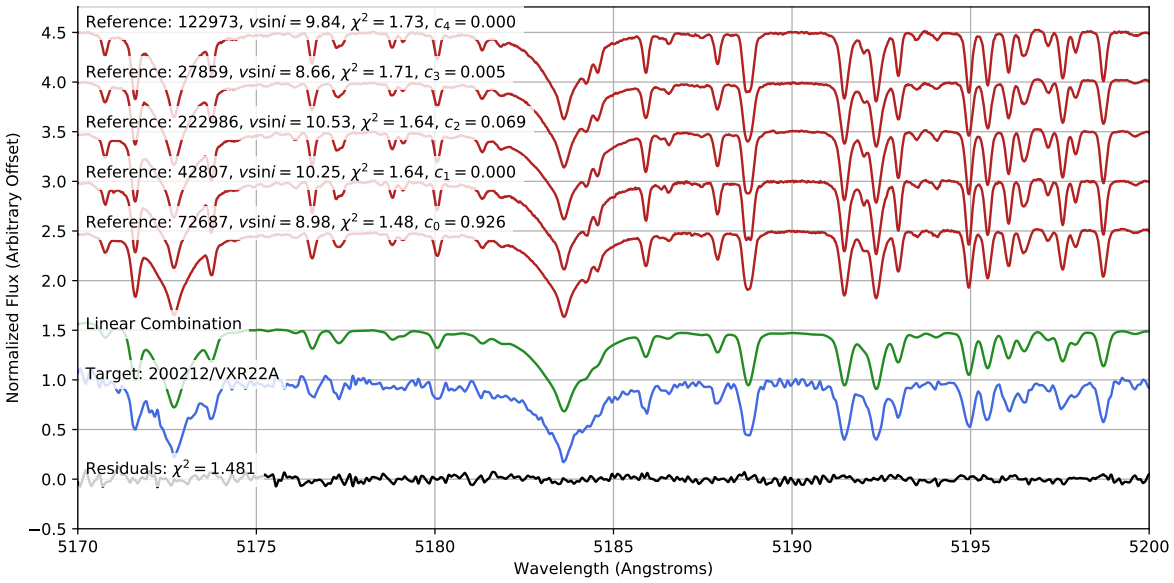

Figure 3.11 Using Empirical SpecMatch, 5 library spectra (in red) and their linear combination (in green) are matched with the spectrum for the IC 2391 star, VXR 22A (in blue), to derive stellar parameters. As indicated by residuals (in black), the fit is good. Derived properties (e.g. Teff, log(g), [Fe/H]) for this known cluster member agree well with those derived using the spectral synthesis code MOOG (De Silva et al. 2013).

available is non-uniform across stellar parameters, which biases results in some instances. For example, there is a paucity of stars with an effective temperature of $\sim$ 4500 Å and a wide range of [Fe/H].

Using previously known cluster members of IC 2602 and IC 2391 to test Empirical SpecMatch, we find that our derived properties for single star members are consistent to within the uncertainties of published literature values reported by Marsden et al. (2009), De Silva et al. (2013), and Randich et al. (2018). Best fit effective temperatures, surface gravities, and metallicities for new and known members are listed in Tables 3.4 and 3.5, respectively. For stars with multi-epoch spectra, we determine stellar properties using the epoch with the highest signal-to-noise ratio.

3.3 New Candidate Spectroscopic Binaries

Cluster members with RVs significantly different from the mean RVs of cluster stars may be spectroscopic binaries (Platais et al. 2007). To identify such candidate spectroscopic binaries, we determined the mean RVs of the clusters by iteratively excluding stars that were 3 standard deviations from the mean. To obtain the best fit, as shown in Figure 3.14, we regard as candidate spectroscopic binaries those stars with RVs different from the resulting means of the ensembles by more than 3 km/s ($\sim$ 1 standard deviation). Given that the internal radial velocity dispersions of these clusters is expected to be less than 1 km/s (Stauffer et al. 1997), we have applied a more stringent constraint for our 43-52 Myr clusters than the prescription used by Hayes & Friel (2014) for 1-3 Gyr clusters (3 km/s vs. 5 km/s).

This prescription identifies 11 new candidate spectroscopic binaries, including 5 in IC 2602 and 6 in IC 2391. We also find that 5 of the new candidate spectroscopic binaries are double-lined, including 4 in IC 2602 and 1 in IC 2391, while 6 are single-lined, including 1 in IC 2602 and 5 in IC 2391. Our prescription also identifies the known IC 2391 binary star, L37, discussed in Section 3.1.1. We confirm for the first time that L37 is a double-lined spectroscopic binary by obtaining multi-epoch CHIRON spectra, as shown in Figure 3.15 for the lithium 6708 Å line, in slicer mode ($R \sim$ 79,000 over 59 spectral orders) and fitting the orbit using the IDL code, *rvfit* (Iglesias-Marzoa et al. 2015; see Chapter 5 for additional details). Two lithium absorption features contributed by the two members of the binary can be observed in the spectra as they dance about the rest wavelength of lithium over time. These binaries are all marked in Tables 3.4 and 3.5. The stars we do not flag as candidate spectroscopic binaries are used to estimate the cluster's radial velocities and dispersions in Chapter 4.

3.4 Confirmation of New Candidate Members

We use the presence of lithium absorption or Hα emission to help confirm membership for candidate cluster members. We observed 20 stars in IC 2602, including 14 new candidate members and 6 known members. We also observed 18 stars in IC 2391, including 12 new candidate members and 6 known members. We find that 19 of 20 IC 2602 stars show lithium absorption while 1 of them, ALN 3, does not. Moreover, 12 of 20 IC 2602 stars show Hα emission and 11 IC 2602 stars show both lithium absorption and Hα emission. Furthermore, we find that all 18 IC 2391 stars show lithium absorption while 5 of 18 show Hα emission.

The double-lined spectroscopic binary, ALN 3, is the star without detectable lithium absorption noted above. As shown in Table 3.4, this candidate cluster member of IC 2602 has a highly discrepant radial velocity, -26.69 km/s, that is the only negative value in the cluster. While this new candidate cluster member of IC 2602 shows Hα emission, a known youth indicator (Barrado Y Navascués et al. 2000; Casey et al. 2016; Gutiérrez Albarrán et al. 2020), such emission can also be produced by close-interacting field binaries (Vesper & Honeycutt 1993; Wevers et al. 2016) and other sources as described in Section 3.2.1. Given the estimated spectral type derived for this star as described in Section 3.1.1, the estimated lithium equivalent width is 0.02 Å compared with other stars of similar spectral type. If this star is a binary and the ratio of flux contributed by each member of the binary is equal, then the absorption would be reduced by half, placing this star's equivalent width below the detection limit of 0.01 Å . Therefore, because it is possible that ALN 3 has weak lithium absorption diluted by the flux of a companion, we regard the membership of ALN 3 to IC 2602 to be uncertain.

Based on consistent distances, sky positions, proper motions, and the presence of lithium absorption or Hα emission, we conclude that 19 of 20 IC 2602 and 18 IC 2391 candidate members are bona-fide cluster members. In combination with previously known members,

133 (29%) of IC 2602 and 164 (47%) of IC 2391 are spectroscopically confirmed members. Measurements are listed and duplicity is indicated for these stars in Tables 3.4 and 3.5.

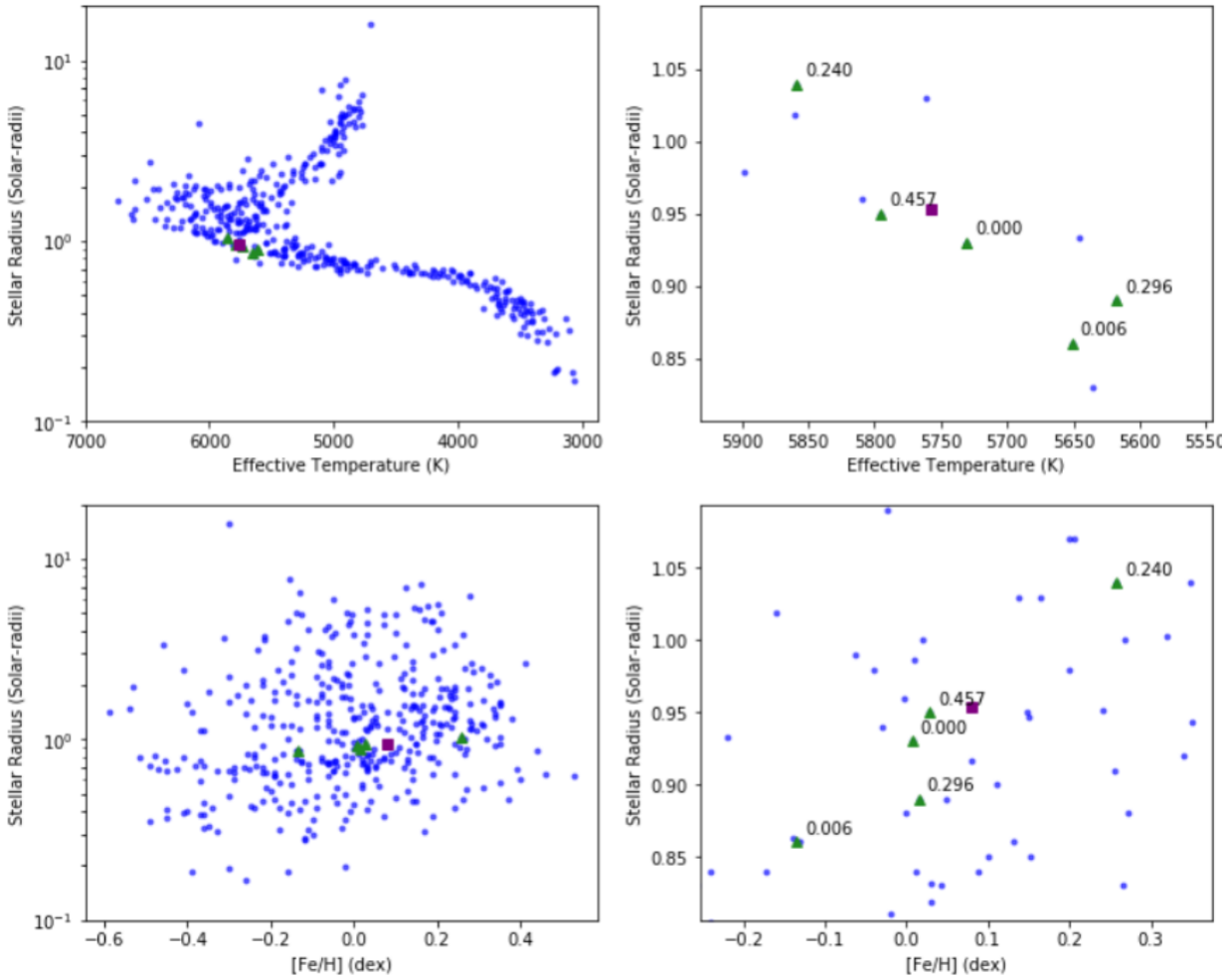

Figure 3.12 Shown are stellar properties of a known IC 2391 cluster member, VXR 22A, derived using Empirical SpecMatch (Yee et al. 2017), which makes use of a library of high-resolution standard stellar spectra to interpolate stellar parameters based on input spectra. The top row and bottom row show, respectively, how temperature and metallicity are determined, first zoomed out and then in. The 5 stellar spectra (green triangles) most similar to the input spectrum are used to infer the most likely parameters (purple square). The derived parameters for VXR 22A from Empirical SpecMatch are in agreement with values from the spectral synthesis code MOOG: Teff = 5757 K, Radius = 0.95 solar, log(g) = 4.52 dex, [Fe/H] = 0.10 dex, and Mass = 1.02 solar (De Silva et al. 2013). The weights assigned to the 5 reference stars are indicated with the numbers in the right panels.

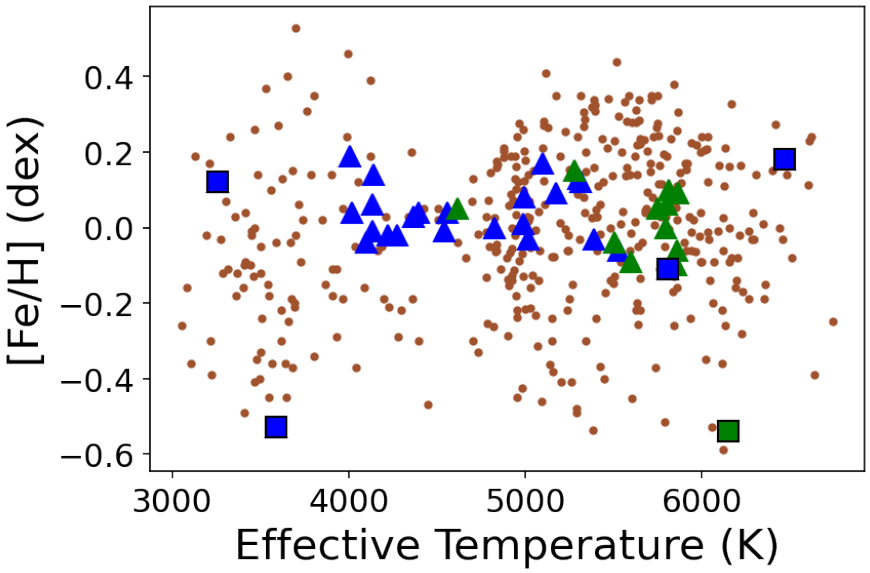

Figure 3.13 Metallicity is plotted against effective temperature for the 393 spectral standards (dwarf and subdwarf stars with 3<log(g)<5) used in the Empirical SpecMatch spectral library (brown points). Previously known members and new candidate members observed in this study are colored green and blue, respectively. Stars are marked as squares if they are candidate double-lined spectroscopic binaries (see Section 3.3) and triangles if they are not.

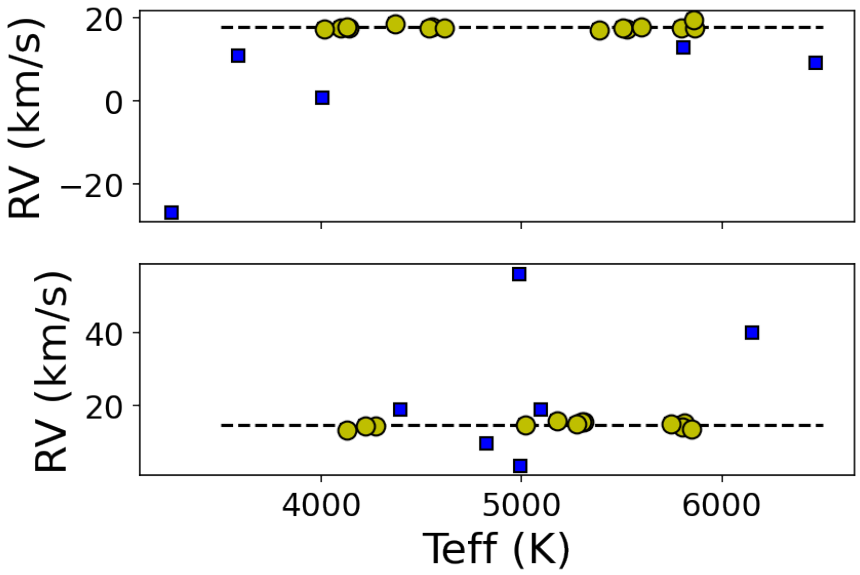

Figure 3.14 Distribution of RVs for spectroscopically observed stars in IC 2602 (*top panel*) and IC 2391 (*bottom panel*) as a function of effective temperature. Candidate binary stars (blue squares) are identified by iterative fits to the mean RVs (dotted black lines) of the ensembles; yellow circles are not candidate binaries.

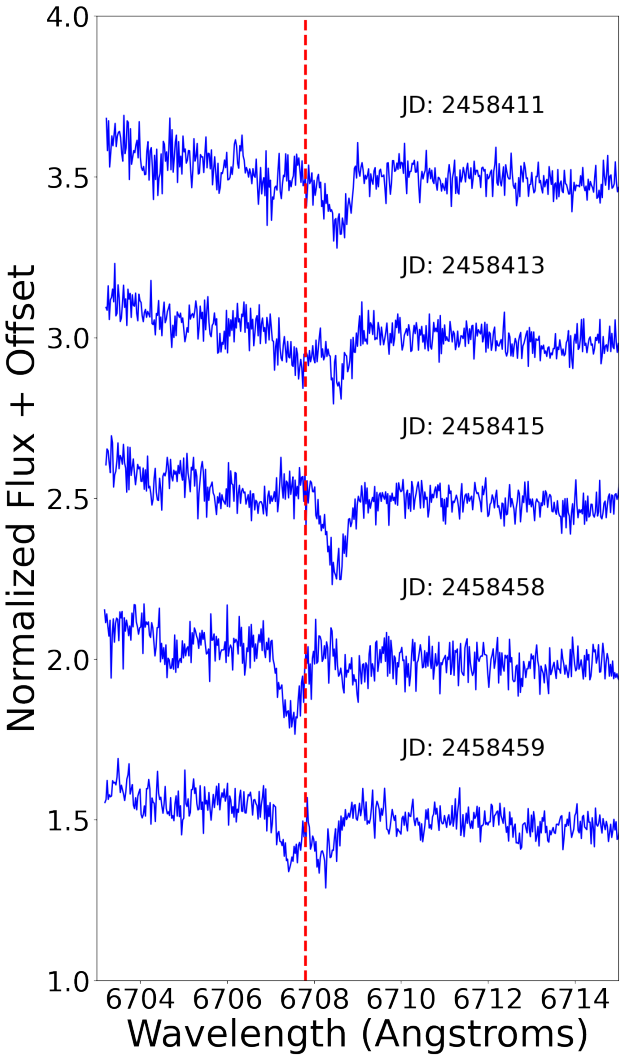

Figure 3.15 Multi-epoch CHIRON spectra in slicer mode ($R \sim 79{,}000$) are shown for known IC 2391 star, L37. The mid-observation Julian Date (JD) is shown for each epoch. The laboratory wavelength of lithium is highlighted by the dotted red line. These observations reveal that L37 is a double-lined spectroscopic binary.

Table 3.4: Measurements for 26 new candidate members of IC 2602 and IC 2391

Identifier		Measurements from CHIRON spectra				Stellar Parameters from SpecMatch		
Internal	2MASS	RV (km/s)	$v \sin i$ (km/s)	EW[Li] (Å)	EW[Hα] (Å)	Teff (K)	log(g) (dex)	[Fe/H] (dex)
IC 2602								
ALN 1	10420316-6520590	17.37±0.12	7.6±0.8	0.16±0.01	0.76±0.02	5527±110	4.53±0.12	-0.06±0.09
ALN 2	10414173-6222205	17.06±0.19	23.4±2.2	0.35±0.02	0.02±0.01	5385±110	4.50±0.12	-0.03±0.09
ALN 3[c]	10411756-6526576	-26.69±0.20	17.4±5.6	<0.01±0.01	-0.02±0.01	3257±70	4.86±0.12	0.12±0.09
ALN 4	10384893-6330430	17.69±0.12	4.6±1.8	0.05±0.01	0.72±0.03	4556±110	4.60±0.12	0.04±0.09
ALN 5[a,c]	10385502-6257272	10.88±0.21	19.6±6.4	0.02±0.01	-0.24±0.02	3586±70	4.83±0.12	-0.53±0.09
ALN 6[c]	10591218-6438089	9.28±0.21	23.3±6.6	0.02±0.01	-0.11±0.01	6465±110	3.86±0.12	0.18±0.09
ALN 7	10322955-6506403	17.47±0.17	13.6±1.3	0.31±0.02	-0.03±0.01	4537±110	4.61±0.12	-0.01±0.09
ALN 8	10482786-6554502	17.44±0.16	9.2±1.8	0.22±0.03	-0.26±0.02	4098±70	4.68±0.12	-0.04±0.09
ALN 9	10200052-6217465	18.61±0.15	7.7±1.6	0.10±0.01	-0.25±0.02	4367±70	4.65±0.12	0.03±0.09
ALN 10[b]	10280304-6316132	0.68±0.18	26.0±4.2	0.09±0.01	-0.63±0.02	4006±70	4.67±0.12	0.19±0.09
ALN 11	10521914-6558069	17.55±0.15	7.4±1.5	0.16±0.02	-0.70±0.02	4138±70	4.66±0.12	0.14±0.09
ALN 12[a,c]	10521708-6502488	12.78±0.13	20.0±5.6	0.10±0.03	-1.30±0.05	5804±110	4.28±0.12	-0.11±0.09
ALN 13	10353048-6218367	17.40±0.16	8.2±1.8	0.20±0.02	-0.85±0.02	4017±70	4.69±0.12	0.04±0.09

Table 3.4: Measurements for 26 new candidate members of IC 2602 and IC 2391

Identifier		Measurements from CHIRON spectra				Stellar Parameters from SpecMatch		
Internal	2MASS	RV (km/s)	$v \sin i$ (km/s)	EW[Li] (Å)	EW[Hα] (Å)	Teff (K)	log(g) (dex)	[Fe/H] (dex)
ALN 14	10315315-6234333	17.79±0.17	13.0±1.3	0.34±0.02	-0.66±0.02	4131±70	4.67±0.12	-0.01±0.09
IC 2391								
NTC 1	08202510-5340306	15.95±0.12	4.6±2.0	0.22±0.01	-0.22±0.02	5175±110	4.51±0.12	0.09±0.09
NTC 2	08320021-5539048	14.43±0.16	9.5±1.0	0.19±0.02	-0.41±0.02	4272±70	4.66±0.12	-0.02±0.09
NTC 3[b]	08365944-5219251	19.08±0.14	7.0±1.6	0.02±0.01	0.55±0.03	4395±70	4.64±0.12	0.04±0.09
NTC 4	08372464-5254109	14.67±0.16	7.9±1.2	0.04±0.01	-0.54±0.02	4222±70	4.66±0.12	-0.02±0.09
NTC 5	08383609-5206388	13.34±0.21	27.2±3.9	0.02±0.01	-0.23±0.01	4131±70	4.67±0.12	0.06±0.09
NTC 6	08433845-5130289	15.76±0.11	7.2±0.7	0.15±0.01	0.72±0.02	5310±110	4.48±0.12	0.12±0.09
NTC 7	08433893-5130249	15.73±0.11	5.8±2.3	0.20±0.01	0.67±0.02	5298±110	4.47±0.12	0.13±0.09
NTC 8[b]	08443450-5255325	18.88±0.09	5.1±1.4	0.02±0.01	0.82±0.02	5097±110	4.54±0.12	0.17±0.09
NTC 9[a,b]	08473860-5216099	9.80±0.13	9.3±1.0	0.03±0.01	0.33±0.01	4823±110	4.46±0.12	0.00±0.09
NTC 10[b]	08583097-5040359	3.77±0.11	7.0±1.0	0.04±0.01	0.76±0.02	4993±110	4.52±0.12	0.08±0.09
NTC 11[a]	08583180-5040360	14.81±0.11	8.3±1.3	0.05±0.01	0.77±0.02	5018±110	4.55±0.12	-0.03±0.09
NTC 12[b]	08593213-5106511	55.92±0.12	4.6±1.9	0.07±0.01	0.93±0.02	4987±110	4.53±0.12	0.01±0.09

Note. — New candidate binaries are indicated as [a]photometric, [b]single-lined spectroscopic, or [c]double-lined spectroscopic. Stars flagged as candidate double-lined spectroscopic binaries have biased equivalent widths and SpecMatch properties so those measurements are suspect in the table.

Table 3.5: Measurements for 12 known members of IC 2602 and IC 2391

Name	Measurements from CHIRON spectra						Stellar Parameters from SpecMatch			
	RV (km/s)	RV Lit. (km/s)	$v \sin i$ (km/s)	$v \sin i$ Lit. (km/s)	EW[Li] (Å)	EW[Hα] (Å)	Teff (K)	Teff Lit. (K)	log(g) (dex)	[Fe/H] (dex)
IC 2602										
W79	17.53±0.11	17.4(R18)	7.8±1.0	8(M09)	0.13±0.01	0.83±0.02	5505±110	5500(M09)	4.52±0.12	-0.04±0.09
R1	17.90±0.11	18(M09)	8.4±0.9	<10(R01)	0.19±0.01	0.60±0.02	5596±110	5320(M09)	4.53±0.12	-0.09±0.09
R10	17.61±0.16	19(M09)	14.9±1.2	14(M09)	0.23±0.02	-0.08±0.01	4614±110	4520(M09)	4.60±0.12	0.05±0.09
R66	17.64±0.13	17.4(R18)	12.0±0.9	12(S97)	0.21±0.01	0.62±0.02	5795±110	5792(R18)	4.47±0.12	0.00±0.09
R70	17.43±0.11	17.4(R18)	10.8±1.1	11(S97)	0.13±0.01	0.88±0.01	5862±110	5854(R18)	4.51±0.12	0.09±0.09
SR3	19.40±0.13	15.3(Me09)	13.2±1.2	14.7(Me09)	0.20±0.01	0.89±0.01	5860±110	N/A	4.41±0.12	-0.06±0.09
IC 2391										
VXR16A	15.49±0.19	15.5(S97)	20.8±1.9	20.7(Me09)	0.36±0.02	-0.12±0.01	5810±110	5130(M09)	4.51±0.12	0.10±0.09
VXR22A	14.26±0.11	14.0(D13)	8.4±0.6	8(M09)	0.24±0.01	0.35±0.01	5800±110	5700(D13)	4.52±0.12	0.06±0.09
VXR70	13.83±0.16	13.8(D13)	15.9±0.8	16(M09)	0.20±0.01	0.59±0.02	5850±110	5819(R18)	4.42±0.12	-0.10±0.09
PMM4362	15.14±0.10	15.11(Pl07)	9.2±0.6	9.0(Me09)	0.20±0.01	0.91±0.01	5746±110	5740(M09)	4.52±0.12	0.05±0.09
SHJM6	15.20±0.13	15.2(D13)	10.9±0.8	10(M09)	0.23±0.01	0.33±0.01	5276±110	5210(M09)	4.48±0.12	0.15±0.09
L37[a,c]	39.81±0.13	31.69(Me09)	11.0±1.4	11.8(Me09)	0.07±0.00	0.64±0.01	6150±110	5900(M09)	4.09±0.12	-0.54±0.09

Note. — Known binaries are indicated as [a]photometric, [b]single-lined spectroscopic, or [c]double-lined spectroscopic. Stars flagged as known double-lined spectroscopic binaries have biased equivalent widths and SpecMatch properties so those measurements are suspect in the table. The

references are as follows: D13 = De Silva et al. 2013, M09 = Marsden et al. 2009 Me09 = Mermilliod et al. 2009, Pl07 = Platais et al. 2007, R01 = Randich et al. 2001, R18 = Randich et al. 2018, S97 = Stauffer et al. 1997.

CHAPTER 4

ENSEMBLE CLUSTER PROPERTIES OF IC 2602 AND IC 2391

We use the newly assembled measurements from Chapters 2 and 3 to determine ensemble cluster properties for IC 2602 and IC 2391. Cluster properties based on *Gaia* DR2 positions and space motions are described in Section 4.1, while those ensemble properties determined from spectroscopic analyses are discussed in Section 4.2. In Table 4.1, we report all ensemble cluster property values and associated uncertainties in the 2nd column. We also compute standard deviations, for comparison with mean individual uncertainties for each ensemble parameter, in the 3rd column.

4.1 Ensemble Astrometric & Kinematic Properties

In Chapter 2, we identified 451 candidate cluster members of IC 2602 and 350 candidate cluster members of IC 2391, based on precise astrometric and kinematic information from *Gaia* DR2 (Gaia Collaboration et al. 2018). We use the data for these candidate members to calculate the mean sky positions of right ascension (RA) and declination (DEC) for the two clusters. We find that IC 2602 has central positions at RA=160.524±0.004 and DEC=-64.387±0.004 degrees, while IC 2391 has central positions at RA=130.276±0.005 and DEC=-52.923±0.005 degrees. Here, the errors represent uncertainties in the mean values.

Using the *Gaia* DR2 data, we also estimate mean parallaxes and proper motions for cluster stars. We illustrate the distributions of these properties as histograms in Figure 4.1, which highlights that the majority of stars in each cluster span well-constrained ranges of parallax and proper motion values. Aside from ensemble values we calculate directly from

the *Gaia* DR2 database, we additionally report mean cluster distances and estimated cluster ages obtained from indirect approaches.

While it may be tempting to estimate distances to each star by simply inverting the parallaxes reported by *Gaia* DR2, reliable distances cannot be inferred this way for most stars because of the nonlinearity of the transformation and the positivity constraint of distance (Lindegren et al. 2012; Luri et al. 2018). Because the only consistent and physically meaningful way to infer distances and their uncertainties is through a probabilistic analysis, as described by Bailer-Jones (2015), we compute mean cluster distances using the distances calculated by Bailer-Jones et al. (2018) with the exponentially decreasing space density prior.

We find that candidate members of IC 2602 have an average distance of 151.58 pc, with an uncertainty in the mean of ∼1.8 pc and a standard deviation of 3.90 pc that is 2.1 times larger than the average distance uncertainty. Candidate members of IC 2391 have an average distance of 150.44 pc, with an uncertainty in the mean of ∼1.8 pc and a standard deviation of 4.99 pc that is 2.7 times larger than the average distance uncertainty. This implies that the observed spread in distances in the cluster are real and not artifacts of measurement errors.

For completeness, we also list cluster ages for IC 2602 and IC 2391 in Table 4.1 from Bravi et al. (2018). The values reported here were originally determined by Randich et al. (2018), who estimated the ages of the clusters by modeling the Lithium Depletion Boundary (LDB) and using isochrones. The LDB ages are adopted by Randich et al. (2018) and Bravi et al. (2018) because they are far less model-dependent than isochronal ages (Soderblom et al. 2010, 2014). These LDB cluster ages are in excellent agreement with previous estimates in the literature as reported by Dobbie et al. (2010) for IC 2602 and Barrado y Navascues et al. (2004). The reported uncertainties are derived from the PROSECCO model (Tognelli et al. 2015a, b) used by Randich et al. (2018) to fit the LDB.

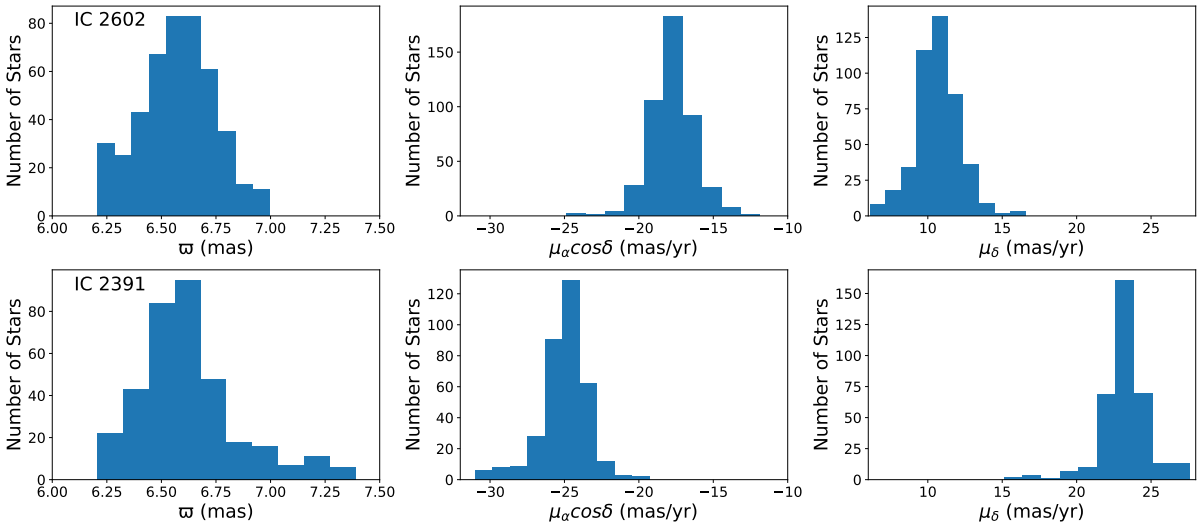

Figure 4.1 For all 451 members of IC 2602 (*top panels*) and all 350 members of IC 2391 (*bottom panels*), histograms of parallax (*left panels*), proper motion in right ascension (*center panels*), and proper motion in declination (*right panels*) are shown. These ensemble values are discussed in Section 4.1.

4.2 Ensemble Spectroscopic Properties

In Chapter 3, we used CHIRON spectra and Empirical SpecMatch (Yee et al. 2017) to measure signatures of youth and determine stellar properties for 38 stars observed in IC 2602 and IC 2391. In Table 4.1, we report two of these stellar properties, radial velocity (RV) and metallicity ([Fe/H]) values, because they are most relevant for assessing cluster membership. In order to not bias mean values for the clusters, we exclude candidate spectroscopic binaries from the average cluster RVs and double-lined binaries from the average [Fe/H]. Candidate spectroscopic binary stars are identified according to the prescription in Chapter 3.

In total, 15 IC 2602 and 12 IC 2391 stars are used to estimate mean RVs while 16 IC 2602 and 17 IC 2391 stars are used to estimate mean metallicities. We illustrate the distributions of these spectroscopic properties as histograms in Figure 4.2, which highlights that the majority of observed stars in each cluster cover a small range of RV and [Fe/H] values. Our measured ensemble values for RV and [Fe/H] for IC 2602 and IC 2391 agree with literature values to

within the uncertainties of previous estimates, as reported by Randich et al. (2001), Platais et al. (2007), and Marsden et al. (2009).

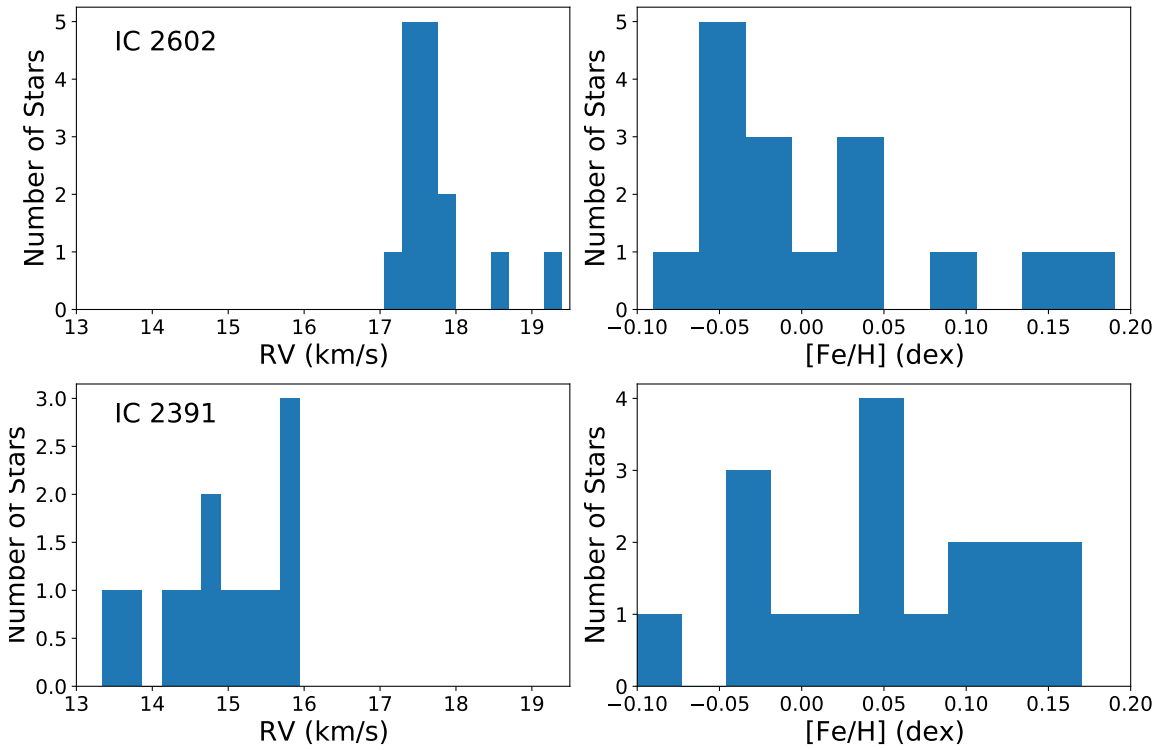

Figure 4.2 Histograms of radial velocity (*left panels*) and metallicity (*right panels*) for IC 2602 (*top panels*) and IC 2391 (*bottom panels*) are shown. Binaries are excluded as described in Chapter 3. The mean ensemble values are discussed in Section 4.2.

We find that IC 2602 members have a mean RV of 17.73 km/s with an uncertainty in the mean of 0.04 km/s and a standard deviation of 0.56 km/s that is 3.9 times larger than the average RV uncertainty. We also determine that IC 2391 members have a mean RV of 14.88 km/s with an uncertainty in the mean of 0.04 km/s and a standard deviation of 0.78 km/s that is 5.6 times larger than the average RV uncertainty. Given that the standard deviation of RVs is ∼0.8 km/s in IC 2391 and ∼0.6 km/s in IC 2602, we confirm that the standard deviations in these clusters is < 1 km/s (Stauffer et al. 1997).

For the spectroscopic cluster properties we measure, Table 4.1 reveals that standard deviations of RVs are larger than both ensemble and mean individual uncertainties, which again suggests that the observed spread in cluster properties is real and not an artifact of

measurement errors. This is not the case for [Fe/H] because the standard deviation is smaller than the mean individual uncertainty. This is promising and expected because the chemical abundances between stars in an open cluster is expected to be very similar.

Moreover, as Figures 4.1 and 4.2 reveal, IC 2602 and IC 2391 are unlikely to be associated despite having similar sky positions, metallicities, and distances from Earth. While the mean proper motions in right ascension and declination are -17.740 and 10.669 mas/yr for IC 2602, they are -25.005 and 23.236 mas/yr for IC 2391. The different kinematics between clusters confirm that the clusters have different origins.

Table 4.1. Summary of Ensemble Cluster Properties

Property	**Value**	**Std. Dev.**	**Nstars**
IC 2602			
Center RA (deg)	160.524±0.004	$3.585(52\sigma_{mn})$	451
Center DEC (deg)	-64.387±0.004	$1.231(18\sigma_{mn})$	451
Avg. ϖ (mas)	6.576±0.004	$0.170(2.2\sigma_{mn})$	451
Avg. $\mu_\alpha \cos\delta$ (mas/yr)	-17.740±0.009	$1.528(11\sigma_{mn})$	451
Avg. μ_δ (mas/yr)	10.669±0.008	$1.530(12\sigma_{mn})$	451
Avg. Distance (pc)	$151.58^{+1.87}_{-1.80}$	$3.90(2.1\sigma_{mn})$	451
Age (Myr)	$43.7^{+4.3}_{-3.9}(B18)$		
Avg. RV (km/s)	17.73±0.04	$0.56(3.9\sigma_{mn})$	15
Avg. [Fe/H] (dex)	0.02±0.02	$0.07(0.8\sigma_{mn})$	16
IC 2391			
Center RA (deg)	130.276±0.005	$1.630(24\sigma_{mn})$	350
Center DEC (deg)	-52.923±0.005	$1.763(23\sigma_{mn})$	350
Avg. ϖ (mas)	6.628±0.005	$0.228(2.9\sigma_{mn})$	350
Avg. $\mu_\alpha \cos\delta$ (mas/yr)	-25.005±0.010	$1.590(10\sigma_{mn})$	350
Avg. μ_δ (mas/yr)	23.236±0.011	$1.609(10\sigma_{mn})$	350
Avg. Distance (pc)	$150.44^{+1.86}_{-1.79}$	$4.99(2.7\sigma_{mn})$	350
Age (Myr)	$51.3^{+5.0}_{-4.5}(B18)$		
Avg. RV (km/s)	14.88±0.04	$0.78(5.6\sigma_{mn})$	12
Avg. [Fe/H] (dex)	0.05±0.02	$0.07(0.8\sigma_{mn})$	17

Note. — Ensemble cluster property values and uncertainties are listed in Column 2 while standard deviations are compared with mean individual uncertainties (σ_{mn}) in Column 3. The number of stars used to determine these values (Nstars) is listed in Column 4. Here, the reference B18 refers to Bravi et al. (2018).

CHAPTER 5

MONITORING RADIAL VELOCITIES OF YOUNG SUNS IN IC 2602, IC 2391, AND TUCANA-HOROLOGIUM

Thus far, previous chapters have discussed an effort to map out the stellar populations of open clusters IC 2602 and IC 2391. This has involved identifying candidate cluster members from *Gaia* DR2 data (Chapter 2), confirming a subsample of newly identified members as bona-fide cluster members with spectroscopy (Chapter 3), and describing the ensemble properties that arise from the new data (Chapter 4). Here, we now discuss an independent, high-precision, radial velocity (RV) monitoring project to potentially identify new candidate hot Jupiter planets and directly measure the magnitude of stellar jitter at the critical transitional age of $\sim$ 50 Myr, as detailed in Chapter 1. The stars monitored include a subsample of stars from the IC 2602 and IC 2391 open clusters, as well as stars in the Tucana-Horologium (Tuc-Hor) moving group.

We discuss the stellar sample in Section 5.1, the observations in Section 5.2, the calculated stellar parameters in Section 5.3, and the techniques used to distinguish between stellar activity and the reflex motion caused by a companion in Section 5.4.

5.1 Sample Selection

Due to their young ages, the stellar populations of IC 2602, IC 2391, and Tucana-Horologium have received meager attention in planet-detection surveys using the RV technique. However, NASA's *TESS* mission has revealed transiting worlds among them, including two in IC 2602

(Nardiello et al. 2020; Bouma et al. 2020) and one in Tucana-Horologium (Newton et al. 2019; Montet et al. 2020; Zhou et al. 2020).

The 44 Myr and 51 Myr open clusters, IC 2602 and IC 2391, are ideal targets for our RV survey because, as noted in Chapter 1, they are among the youngest, closest ($\sim$ 150 pc; Bravi et al. 2018), richest (400-500 members; see Chapter 2), open clusters with solar metallicity (0.00$\pm$0.01 and 0.06$\pm$0.06, respectively; Randich et al. 2001, 2002; Spina et al. 2017). Tucana-Horologium members represent an ideal sample for extending our survey because they have approximately the same age ($\sim$ 40-45 Myr; Kraus et al. 2014; Bell et al. 2015) and solar metallicity (-0.03$\pm$0.05; Almeida et al. 2009), and make up one of the largest young stellar populations within 100 pc. Sources of membership for IC 2602 and IC 2391 are drawn from the lists assembled by Barnes et al. (1999), Barrado y Navascues et al. (1999), Randich et al. (2001), Dodd et al. (2004), Platais et al. (2007), Marsden et al. (2009), and Mermilliod et al. (2009). All are confirmed as members following the methodology used in Chapter 2. Membership and rotation periods for Tucana-Horologium stars originate from the lists of Zuckerman & Song (2004), Torres et al. (2008), and Messina et al. (2011).

Sun-like stars are preferred in large-scale RV surveys over later-type stars given their higher hot Jupiter occurrence rate (Wright et al. 2012; Kovacs et al. 2013). Early-type stars are typically avoided in these surveys because their optical spectra present fewer spectral lines and generally present higher projected rotation velocities ($v \sin i$) than Sun-like stars (Grandjean et al. 2021). To optimize our likelihood of detecting exoplanets, we focus on Sun-like single stars with spectral types that range from F5 to K0. At a spectral type of K0, stars in IC 2602 and IC 2391 have V magnitudes of $\sim$ 12, and we set this as the magnitude limit for our survey. For precise monitoring of RVs, we select against stars with rapid rotation. For stars with rotation periods available in the literature, we select those with periods greater than $\sim$ 3 days. Otherwise, we choose stars with $v \sin i$ values less than 30 km/s, similar to the cutoff adopted by Quinn et al. (2014). By imposing these cuts, we arrive at a sample of 29 stars, including 10 in IC 2602, 10 in IC 2391, and 9 in Tucana-Horologium. 17 stars in

this sample have measured rotation periods, and all stars have measured $v \sin i$ values. The stellar samples are listed in Table 5.1.

5.2 Observations and Observing Cadence

Similar to the observing program we describe in Chapter 3, we observe each star in our sample with an integration time of 1200 s using the CHIRON spectrograph (Tokovinin et al. 2013; L. Paredes et al. 2021). We obtain a thorium-argon lamp spectrum following the observation of a science target for wavelength-calibration. To achieve the highest possible precision, spectra are obtained in slicer mode, which covers 4500-8900 Å over 59 spectral orders and yields a resolving power of 79,000. We note that this is a different setup than the observations described in Chapter 3; those were obtained in fiber mode, which yields a resolving power of 27,000. To assist with our spectroscopic analyses, we also observed a set of 7 spectral standards, ranging in spectral type from F6 to K2. These stars all have known RVs, $v \sin i$ values, and stellar properties (as assembled by Yep et al. 2021). This sample of standard stars is listed in Table 5.2. The spectra are reduced, extracted, and normalized in identical fashion to that described in Chapter 3.

For our monitoring program, we obtained a minimum of 7 observations for each star, depending upon the availability of telescope time and targets. Similar to the distributed observing campaign of the N2K consortium (Fischer et al. 2004) and nearby cluster surveys (Quinn et al. 2012, 2014), we observe most stars several times over 1-3 weeks to place constraints on any short-period gas giant planets. For most stars in the sample, however, we were able to obtain several additional observations to improve detection limits. Stars were targeted specifically because they showed evidence of RV variations at the few 100 m/s level in initial data analyses (consistent with that expected for a hot Jupiter companion). Unfortunately, not all observations obtained were of sufficient quality to be useful. The queue scheduling format of CHIRON observations sometimes yields low signal-to-noise ratio (SNR) spectra that are of insufficient quality for precise RV analysis. From a total of 339 slicer

observations, a total of 15 observations (4 %) were not useful. This translated to 2 stars having only 6 observations.

For each star, the total number of observations (Tobs), the number of useful observations (Uobs), and the number of rejected observations (Robs) are listed in Table 5.1. The distribution of useful observations for stars in our sample is presented in Figure 5.1 for IC 2602, IC 2391, Tucana-Horologium, and the complete set. These observations are broadly distributed between 6 and 20, and the mean number of observations per star is 11.

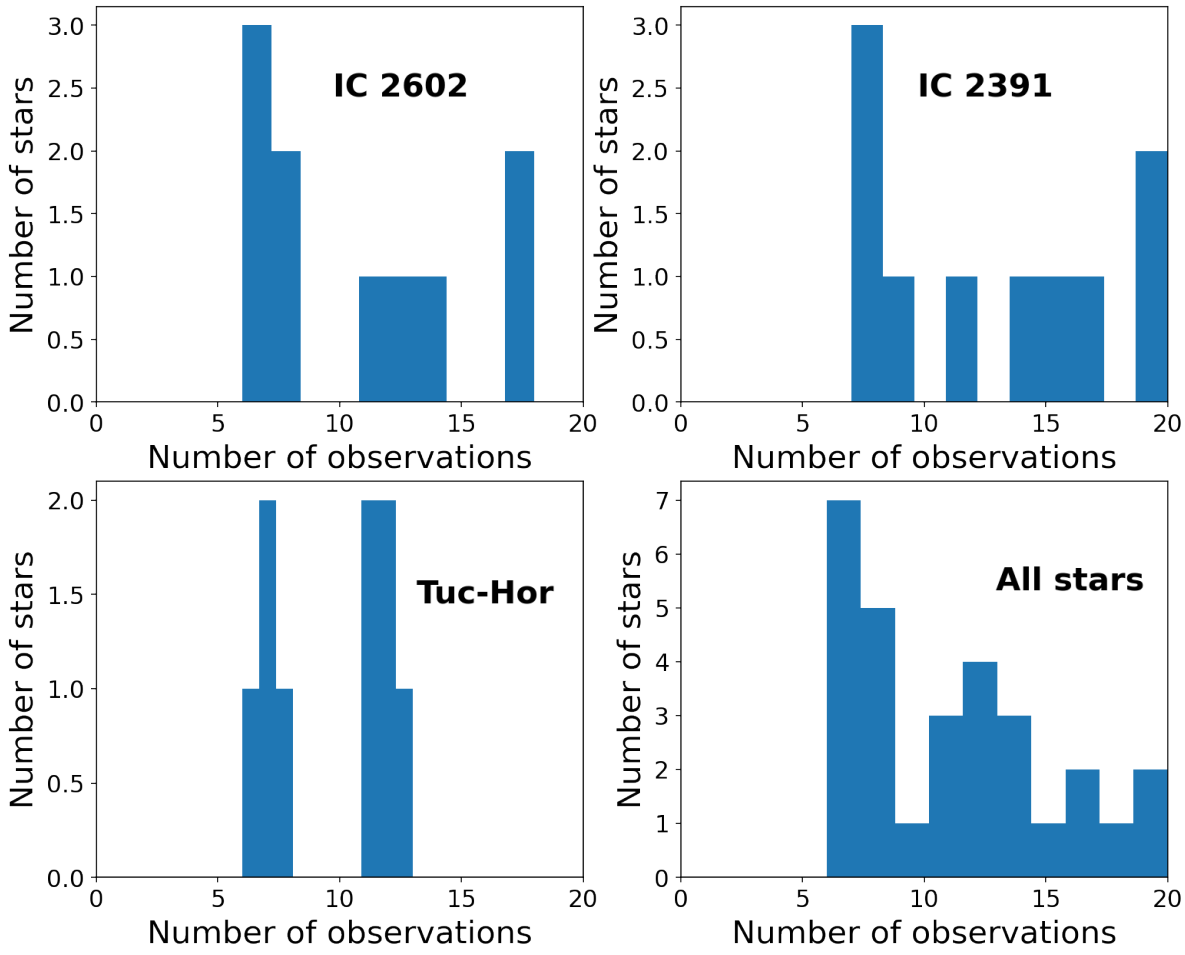

Figure 5.1 Histograms of useful observations (Uobs in Table 5.1) are plotted for IC 2602 (top left panel), IC 2391 (top right panel), Tucana-Horologium (lower left panel) and the complete set of 29 stars (lower right panel). These observations are discussed in Section 5.2.

Table 5.1: Monitoring Observations for Stars in IC 2602, IC 2391, and Tucana-Horologium

Name	RA (h:m:s)	DEC (d:m:s)	V (mag)	Tobs	Uobs	Robs	Date	SNR	Standard	Rot (days)	SpT
IC2602											
B134	10:45:29.05	-64:25:10.6	11.9	8	8	0	21-01-18	37	HD115617	6.8(B99)	G5(M09)
R1	10:28:32.40	-63:44:32.0	11.6	13	12	1	20-12-12	25	HD10700		
R14	10:33:38.91	-64:46:29.3	11.7	8	7	1	20-12-16	22	HD26965		
R42B	10:39:39.08	-65:20:35.0	11.3	14	14	0	21-04-13	28	HD115617		G5(Me09)
R45	10:39:59.19	-63:15:00.9	10.6	17	17	0	22-02-11	41	HD59967		
R66	10:44:06.45	-63:59:32.4	11.1	12	11	1	21-01-18	29	HD59967	3.3(B99)	G4(M09)
R70	10:44:23.03	-64:15:29.2	10.9	7	6	1	19-07-04	34	HD4391	4.3(B99)	G0(M09)
SR3	10:43:16.85	-64:24:11.8	10.8	19	18	1	21-04-29	36	HD59967		
TYC8964171	10:28:08.50	-64:30:13.2	10.6	7	7	0	21-04-28	38	HD115617	3.0(B20)	G0/F9(B20)
W79	10:42:08.93	-64:46:24.6	11.6	9	8	1	21-04-13	23	HD10700	6.2(B99)	G(M09)
IC2391											
PMM665	08:37:51.55	-53:45:32.3	11.4	8	8	0	20-11-17	24	HD10700		G8(D13)
PMM756	08:43:00.08	-53:53:59.0	11.1	15	15	0	21-04-13	32	HD10700	3.15(D16)	G9(D16)
PMM2012	08:43:58.39	-53:33:28.9	11.7	17	17	0	22-02-07	26	HD30652		K0(D13)
PMM3359	08:36:54.78	-53:08:26.2	11.5	8	8	0	20-11-04	22	HD10700	3.84(D13)	
PMM4280	08:34:20.43	-52:50:07.0	10.3	9	9	0	20-11-14	45	HD115617		G5(D13)
PMM4362	08:38:26.16	-52:56:21.9	11.0	14	14	0	21-04-28	32	HD59967	3.93(D13)	
PMM5884	08:44:25.13	-52:42:22.1	11.5	8	7	1	20-11-15	23	HD10700	3.23(D13)	G9(D13)

Table 5.1: Monitoring Observations for Stars in IC 2602, IC 2391, and Tucana-Horologium

Name	RA (h:m:s)	DEC (d:m:s)	V (mag)	Tobs	Uobs	Robs	Date	SNR	Standard	Rot (days)	SpT
SHJM6	08:39:56.15	-52:57:30.0	11.9	19	19	0	19-11-27	19	HD26965	3.86(D13)	K0(D13)
VXR22A	08:40:48.13	-53:37:35.4	11.1	21	20	1	20-11-04	30	HD115617		G6(D13)
VXR70	08:44:07.42	-52:52:50.7	10.8	14	12	2	20-11-30	37	HD59967	2.67(D13)	G3(D13)
Tuc-Hor											
HD1466	00:18:25.69	-63:28:43.9	7.5	7	7	0	20-10-29	164	HD4391		F8V(T06)
HD222259A	23:39:41.00	-69:11:35.1	8.5	14	13	1	19-07-04	99	HD115617	2.85(M10)	G6V(T08)
HD222259B	23:39:41.07	-69:11:29.5	9.8	12	11	1	19-08-04	76	HD22049		K3V(T08)
HIP490	00:05:54.15	-41:45:16.2	7.5	7	6	1	19-09-19	130	HD4391		G0V(T06)
HIP1113	00:13:53.33	-74:40:54.6	8.7	8	7	1	19-07-05	85	HD10700	3.67(D16)	G8V(D16)
HIP6485	01:23:22.27	-57:28:55.3	8.5	12	12	0	20-10-29	90	HD115617	3.59(M10)	G7V(T06)
HIP9141	01:57:50.12	-21:53:56.8	8.1	12	12	0	19-07-05	123	HD59967	3.05(D16)	G4V(D16)
HIP21632	04:38:45.26	-27:01:56.5	8.5	12	11	1	19-09-21	91	HD59967	4.25(M10)	G3V(T06)
HIP105388	21:20:52.81	-53:01:24.9	8.7	8	8	0	21-04-14	98	HD115617	3.43 (D16)	G7V(D16)

Note. — Description of Column Headings: The Common Name (Name), Right-Ascension (RA), Declination (DEC), V-magnitude (V), Total Number of Observations (Tobs), Number of Useful Observations (Uobs), Number of Rejected Observations (Robs), Date of the Epoch with the Highest-SNR Spectrum (Date), SNR of the Spectrum with the Highest SNR (SNR), Comparison CHIRON Standard Star (Standard), Measured Rotation Period from the Literature (Rot), and the Measured Spectral Type from the Literature (SpT). The references are as follows: B99 = Barnes et al. (1999), M09 = Marsden et al. (2009), Me09 = Mermilliod et al. (2009), B20 = Bouma et al.

(2020), D13 = De Silva et al. (2013), D16 = Distefano et al. (2016), T06 = Torres et al. (2006), M10 = Messina et al. (2010), and T08 = Torres et al. (2008).

Table 5.2: CHIRON Slicer Standards

Spectral Type	Name	RA (h m s)	DEC (d m s)	V	RV (km/s)	vsini (km/s)	Date Observed	Exposure Time (s)
F6	HD30652	04 04 50.41	+06 06 40.6	3.19	24.11(Md10)	16.8(M14)	19-02-15	600
G3	HD4391	00 00 45.59	-47 47 07.1	5.80	-11.01(G18)	5(S09)	18-11-01	300
G3	HD59967	07 07 42.51	-37 37 21.7	6.64	9.37(G18)	3.4(S09)	20-02-08	800
G7	HD115617	13 13 24.31	-18 18 40.3	4.74	-7.85(N02)	3.9(A12)	19-08-27	120
G8.5	HD10700	01 01 04.08	-15 15 14.9	3.50	-16.619(N02)	3.26(M10)	18-07-28	60
K0	HD26965	04 04 16.32	-07 07 10.3	4.43	-42.331(N02)	0.5(M14)	20-02-07	70
K2	HD22049	03 03 55.84	-09 09 29.7	3.73	16.332(N02)	2.4(M14)	18-10-22	19

Note. — CHIRON slicer standard star observations used to determine radial and projected rotational velocities, as well as line bisector spans, for stars observed in the monitoring program (see Table 5.1) are shown. The references are as follows: Md10 = Maldonado et al. (2010), M14 = Marsden et al. (2014), G18 = Gaia Collaboration et al. (2018), S09 = Schroder et al. (2009), Nidever et al. (2002), A12 = Ammler-Von Eiff et al. (2012), and M10 = Martinez-Arnaiz et al. (2010).

5.3 Stellar Fundamental Parameters

We measure absolute radial velocities and projected rotational velocities for the stars in our sample, following a prescription similar to the one described in Chapter 3. For this monitoring survey, we match each observed star with one CHIRON slicer-mode standard (listed in Table 5.1) during cross-correlation analysis. Once weighted-mean RV and $v \sin i$ values, weighted by the RV uncertainties of the spectral orders, are obtained for an epoch, absolute RV and $v \sin i$ values are determined by taking the average of those values across epochs, respectively. The corresponding uncertainties for these absolute RV and $v \sin i$ values are set to the standard deviation of values across epochs. This differs from the setup in Chapter 3, which computes the absolute RV and $v \sin i$ from a single epoch by taking the average of RV and $v \sin i$ values calculated with three CHIRON fiber-mode standards for comparison.

We also determine effective temperatures, metallicities, and surface gravities using Empirical SpecMatch (Yee et al. 2017), in the same way we do in Chapter 3 with one caveat. Because multiple observation are available for each star in our monitoring campaign, we use the spectrum with the highest signal-to-noise ratio (SNR) value available for each star. We determine SNR values at 5500 Å using the prescription in Chapter 3. We list the highest SNR values and their associated epochs of observation for each star in Table 5.1.

The stellar parameters we determine for each star are presented in Table 5.3. Our measured $v \sin i$ values are less than 30 km/s, consistent with the modest rotation we require for the monitoring project. The distribution of effective temperatures, which range from $\sim$ 4800-6500 K, are consistent with the expectation for Sun-like stars with FGK spectral types (Pecaut & Mamajek 2013). The distribution of surface gravities, which range from $\sim$ 4.2-4.6, is fairly typical of dwarf stars on the main-sequence (da Silva et al. 2015). The metallicities we measure for our sample stars also appear to be approximately solar ([Fe/H] = 0.00); only 3 stars have metallicity absolute values greater than 0.15.

In Table 5.3, we compare our results with those we assemble from the literature. We report literature values of RV and $v \sin i$ for all 29 stars, effective temperature for 27 stars, surface gravity for 13 stars, and metallicity for 15 stars in our sample. Our measured values agree well with literature values, thereby confirming the reliability of our techniques. We find that the mean difference is less than 1 km/s for both RV and $v \sin i$ in 25 of 29 stars, less than 100 K for effective temperature in 24 of 27 stars, less than 0.1 dex for surface gravity in 10 of 13 stars, and less than 0.1 dex for metallicity in 12 of 15 stars.

In Table 5.4, we compare the stellar parameter results between fiber mode and slicer mode for the 9 known cluster members of IC 2602 and IC 2391 in our monitoring program that are also observed in fiber mode for the spectroscopic survey discussed in Chapter 3. We find that all values of RV and $v \sin i$ agree within 0.2 and 1.5 km/s, respectively. We note, however, that uncertainties are limited by the uncertainty of standards for absolute RV and $v \sin i$ values. Excluding the IC 2391 star, SHJM6, all values of effective temperature, surface gravity, and metallicity agree within 100 K, 0.07 dex, and 0.15 dex, respectively.

Table 5.3: Measured stellar parameters for IC 2602, IC 2391, and Tucana-Horologium

Name	RV (km/s)	RV Lit (km/s)	vsini (km/s)	vsini Lit (km/s)	Teff (K)	Teff Lit (K)	log(g) (dex)	log(g) Lit (dex)	[Fe/H] (dex)	[Fe/H] Lit (dex)
IC 2602										
B134	20.81±0.07	20.81(Me09)	9.1±0.1	8.4(Me09)	4874±110		4.48±0.12		0.10±0.09	
R1	17.81±0.20	18(M09)	7.0±0.4	<10(R01)	5557±110	5320(M09)	4.49±0.12	4.50(DR09)	0.06±0.09	0.01(Bo18)
R14	17.34±0.25	16(M09)	12.6±0.5	11(M09)	5448±110	5410(M09)	4.49±0.12	4.50(DR09)	0.01±0.09	0.00(DR09)
R42B	17.82±0.14	18.1(Me09)	10.1±0.3	9.7(Me09)	6232±110		4.26±0.12		-0.05±0.09	-0.15(Bo18)
R45	17.75±0.17	18(M09)	13.1±0.4	14(M09)	5911±110	5960(M09)	4.44±0.12		0.07±0.09	
R66	17.60±0.24	17.4(R18)	12.1±0.3	12(S97)	5811±110	5792(R18)	4.48±0.12		0.03±0.09	
R70	17.29±0.08	17.4(R18)	10.4±0.3	11(S97)	5845±110	5854(R18)	4.45±0.12		0.04±0.09	
SR3	19.60±0.13	15.3(Me09)	13.0±0.4	14.7(Me09)	5886±110		4.41±0.12		-0.01±0.09	
TYC8964171	17.98±0.33	17.45(G18)	15.4±0.4	16.2(B20)	5798±110	6047(B20)	4.36±0.12	4.467(B20)	-0.06±0.09	-0.069(B20)
W79	17.55±0.07	17.4(R18)	6.7±0.4	8(M09)	5503±110	5500(M09)	4.53±0.12		-0.17±0.09	
IC 2391										
PMM665	14.54±0.13	14.6(D13)	7.88±0.3	7.47(D13)	5613±110	5550(D13)	4.53±0.12	4.53(D13)	-0.02±0.09	-0.07(D13)
PMM756	16.09±0.36	12.15(D13)	15.3±0.8	16.5(D13)	5878±110	5357(D13)	4.49±0.12		0.02±0.09	
PMM2012	14.37±0.39	13.9(D13)	12.9±1.0	17.4(D13)	5398±110	5080(D13)	4.52±0.12		-0.03±0.09	
PMM3359	14.68±0.11	14.7(D13)	7.9±0.3	7.88(D13)	5650±110	5380(D13)	4.51±0.12	4.5(D13)	0.04±0.09	0.00(D13)
PMM4280	12.20±0.12	18.68(D13)	14.6±0.6	16(D13)	6080±110	5729(D13)	4.21±0.12		0.05±0.09	
PMM4362	15.16±0.05	15.11(Pl07)	8.6±0.1	8.61(D13)	5824±110	5740(M09)	4.47±0.12	4.45(DR09)	0.04±0.09	0.00(DR09)
PMM5884	14.50±0.41	14.49(D13)	14.5±0.8	13.9(D13)	5569±110	5257(D13)	4.53±0.12		-0.13±0.09	

Table 5.3: Measured stellar parameters for IC 2602, IC 2391, and Tucana-Horologium

Name	RV (km/s)	RV Lit (km/s)	vsini (km/s)	vsini Lit (km/s)	Teff (K)	Teff Lit (K)	log(g) (dex)	log(g) Lit (dex)	[Fe/H] (dex)	[Fe/H] Lit (dex)
SHJM6	15.28±0.21	15.2(D13)	11.8±0.8	10(M09)	6523±110	5210(M09)	4.15±0.12		-0.32±0.09	
VXR22A	14.12±0.17	14.0(D13)	7.1±0.3	8(M09)	5916±110	5700(D13)	4.49±0.12	4.3(D13)	0.14±0.09	-0.07(D13)
VXR70	14.01±0.29	13.8(D13)	15.5±0.6	16(M09)	5788±110	5819(R18)	4.35±0.12		-0.07±0.09	
Tuc-Hor										
HD1466	6.84±0.39	6.40(G06)	19.8±1.1	21(T06)	6153±110	6135(L18)	4.24±0.12	4.39(L18)	0.07±0.09	-0.06(L18)
HD222259A	7.97±0.55	8.0(T06)	16.5±0.9	18.3(T06)	5802±110	5414(C11)	4.51±0.12		0.09±0.09	-0.02(Bo18)
HD222259B	6.27±0.51	6.1(T06)	12.5±0.7	14.6(T06)	5854±110		4.50±0.12		0.14±0.09	
HIP490	1.82±0.08	1.70(V05)	13.5±0.1	15(T06)	5966±110	5977(L18)	4.36±0.12	4.42(L18)	-0.07±0.09	-0.06(Bo18)
HIP1113	9.37±0.16	9.393(S18)	7.6±0.8	7.3(T06)	5633±110	5581(St20)	4.52±0.12	4.50(L18)	0.03±0.09	0.00(L18)
HIP6485	9.29±0.19	9.141(S18)	13.5±0.5	13.8(T06)	5749±110	5675(C20)	4.53±0.12	4.515(C20)	0.03±0.09	-0.063(C20)
HIP9141	6.50±0.23	6.8(T06)	14.1±0.3	13.46(W07)	5915±110	5899(F14)	4.49±0.12	4.48(B16)	0.10±0.09	0.06(B16)
HIP21632	19.23±0.40	18.8(T06)	20.5±0.8	17.53(M10)	6016±110		4.44±0.12		0.16±0.09	
HIP105388	-1.29±0.28	-1.31(St20)	14.2±0.8	14.7(St20)	5819±110	5902(H20)	4.50±0.12	4.50(C19)	0.15±0.09	0.17(St20)

Note. — Measured stellar properties are presented for the 29 stars observed in our monitoring campaign. These properties include radial velocity (RV), projected rotational velocity (vsini), effective temperature (Teff), surface gravity (log(g)), and metallicity ([Fe/H]). Our measured values are compared with corresponding values we assemble from the literature, if available (RV Lit, vsini Lit, Teff Lit, log(g) Lit, [Fe/H] Lit). The references for stellar parameter values reported from the literature are as follows: Me09 = Mermilliod et al. 2009, M09 = Marsden et al. 2009, R01 = Randich et al. 2001, DR09 = D'Orazi & Randich 2009, Bo18 = Bochanski et al. 2018, R18 = Randich et al. 2018, S97 = Stauffer et al. 1997, G18 = Gaia Collaboration et al. 2018, B20 = Bouma et al. 2020, D13

= De Silva et al. 2013, Pl07 = Platais et al. 2007, G06 = Gontcharov et al. 2006, T06 = Torres et al. 2006, L18 = Luck et al. 2018, C11 = Casagrande et al. 2011, V05 = Valenti & Fischer 2005, S18 = Soabiran et al. 2018, St20 = Steinmetz et al. 2020, C20 = Casali et al. 2020, W07 = White et al. 2007, F14 = Franchini et al. 2014, B16 = Brewer et al. 2016, M10 = Messina et al. 2010, H20 = Hojjatpanah et al. 2020, C19 = Chavero et al. 2019.

Table 5.4: Comparison of SpecMatch Properties: Slicer-mode versus Fiber-mode

Name	Slicer RV (km/s)	Fiber RV (km/s)	Slicer vsini (km/s)	Fiber vsini (km/s)	Slicer Teff (K)	Fiber Teff (K)	Slicer log(g) (dex)	Fiber log(g) (dex)	Slicer [Fe/H] (dex)	Fiber [Fe/H] (dex)
IC 2602										
W79	17.55±0.07	17.53±0.11	6.7±0.4	7.8±1.0	5503±110	5505±110	4.53±0.12	4.52±0.12	-0.17±0.09	-0.04±0.09
R1	17.81±0.20	17.90±0.11	7.0±0.4	8.4±0.9	5557±110	5596±110	4.49±0.12	4.53±0.12	0.06±0.09	-0.09±0.09
R66	17.60±0.24	17.64±0.13	12.1±0.3	12.0±0.9	5811±110	5795±110	4.48±0.12	4.47±0.12	0.03±0.09	0.00±0.09
R70	17.29±0.08	17.43±0.11	10.4±0.3	10.8±1.1	5845±110	5862±110	4.45±0.12	4.51±0.12	0.04±0.09	0.09±0.09
SR3	19.60±0.13	19.40±0.13	13.0±0.4	13.2±1.2	5886±110	5860±110	4.41±0.12	4.41±0.12	-0.01±0.09	-0.06±0.09
IC 2391										
VXR22A	14.12±0.17	14.26±0.11	7.1±0.3	8.4±0.6	5916±110	5800±110	4.49±0.12	4.52±0.12	0.14±0.09	0.06±0.09
VXR70	14.01±0.29	13.83±0.16	15.5±0.6	15.9±0.8	5788±110	5850±110	4.35±0.12	4.42±0.12	-0.07±0.09	-0.10±0.09
PMM4362	15.16±0.05	15.14±0.10	8.6±0.1	9.2±0.6	5824±110	5746±110	4.47±0.12	4.52±0.12	0.04±0.09	0.05±0.09
SHJM6	15.28±0.21	15.20±0.13	11.8±0.8	10.9±0.8	6523±110	5276±110	4.15±0.12	4.48±0.12	-0.32±0.09	0.15±0.09

5.4 Identifying Candidate Planets in the Presence of Active Stars

As discussed in Chapter 1, one of the big challenges in detecting exoplanets orbiting young, Sun-like stars is that the stars are magnetically active. The stellar activity of these stars manifests as radial velocity variability that can mask or even mimic planetary RV signals (Queloz et al. 2001; Figueira et al. 2010). The need for techniques to reliably disentangle this stellar RV "jitter" from reflex motion due to a companion has become increasingly urgent in the era of extreme-precision spectrographs (Zhao et al. 2022). With sub-meter-per-second RV precision, photospheric velocities from stellar variability and activity features are the dominant source of RV scatter. While a wide host of techniques have been developed over the past two decades, such as Gaussian process (GP) models, most of them require large datasets and would not be appropriate for measuring the stellar jitter in our sample stars, which receive an average of 11 observations each. Given the length of our exposures and the time-scales over which we observe the stars in our sample, the most significant source of stellar jitter is likely to be star spots (Haywood et al. 2015). A long-standing and successful way of identifying apparent RV variations caused by cool star spots is line bisector measurements (Torres et al. 2004).

We demonstrate the RV precision of CHIRON in Section 5.4.1, discuss our line bisector measurements in Section 5.4.2, describe our prescription for assessing the correlation between RVs and bisector spans in Section 5.4.3, and explain how candidate hot Jupiters can be identified from our RV measurements in Section 5.4.4.

5.4.1 Demonstrated RV Precision of 7.5 m/s

When a companion orbits a star, it induces a radial velocity variation that can potentially be identified, depending on the inclination of the orbit, from the periodic Doppler shifting of spectral lines. To identify such Doppler shifts for a star, we first determine the RV at every epoch of observation relative to a comparison standard using the cross-correlation analysis

discussed in Chapter 3 and Section 5.3. For precise monitoring of RVs, we calculate the weighted-mean RV, weighted by the individual uncertainties per epoch, and subtract this value from the relative RVs we measure for each epoch such that the new mean of these shifted relative RVs becomes zero. This helps us to measure the dispersion of RVs and assess the possible origins of observed RV variations. To measure the dispersion of RVs for a star, we calculate the mean absolute deviation (MAD) of RVs, which is more robust to outlier RVs than standard deviations; this is similar to the prescription applied by Paredes et al. (2021).

We test the precision of our prescription by running our analysis code for 36 CHIRON slicer-mode spectra of the bright (V = 5.72), inactive, K4 field star, HIP 73184. All spectra were obtained on the same night, and span $\sim$ 5 hours. We use the spectrum obtained for this star with the highest SNR value as the comparison standard for our cross-correlation analysis. For each epoch, we determine the weighted-mean RV uncertainty, weighted by RV uncertainties measured across epochs, using the prescription of Butler et al. (1996) as discussed in Chapter 3. We find that the RV uncertainty per epoch is less than 3.5 m/s for this star. To test the stability of the CHIRON spectrograph, we calculate the MAD of RVs for all 36 observations (see Figure 5.2) and find that to be 7.5 m/s. This is consistent with the predicted stability ($\sim$ 7 m/s) of the ThAr lamp (Tokovinin et al. 2013). While our analysis technique is developed independently from that of Paredes et al. (2021), our MAD values are similar for the same set of observations (7.5 m/s versus 10.9 m/s reported in their study), further confirming the stability of the instrument and achievable RV precision. Moreover, Paredes et al. (2021) reports MAD values for stars over months and years that range from 8-15 m/s, which suggests that the CHIRON instrument has high long-term stability of similar precision. According to Figure 5 of Paredes et al. (2021), MAD values can reach $\sim$ 20 m/s for V $\sim$ 11. While this precision is insufficient to detect Earth-like exoplanets, it is ideal for detecting short-period gas giant planets that can produce RV variations on the order of several 100 m/s. We present our results and RV curve for HIP 73184 in Figure 5.2.

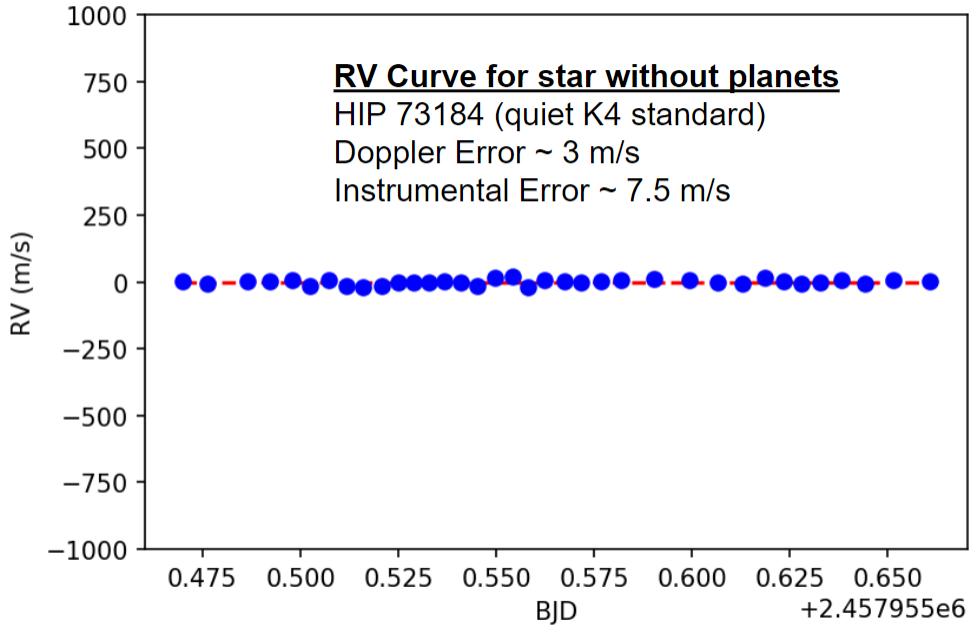

Figure 5.2 Shown are relative RVs measured from 36 CHIRON spectra on July 20, 2017 for HIP 073184, a quiet K4 standard star. Here, the error bars are smaller than the data points. The dispersion is 7.5 m/s, consistent with the predictions of Tokovinin et al. (2013) and Paredes et al. (2021).

Similarly, we measure the MAD of RVs for the stars in our monitoring program and present these results in Table 5.5. The results are illustrated in Figure 5.3 as a functions of projected rotational velocity. The MAD values range from 43 m/s to 379 m/s. Only 5 of the 29 stars in this sample have MAD values less than 100 m/s. Accounting for individual RV uncertainties per epoch, which range from 5.7 to 8 m/s (compared with 3.5 m/s measured for HIP 73184), and the instrumental RV uncertainty, measured to be $\sim$ 7.5 m/s, we can confidently assert that these apparent RV variations are not an artifact of measurement errors. Instead, they must either be a product of intrinsic stellar jitter or companions.

In order to diagnose the origin of these RV variations, we plot the MAD values against our measured $v \sin i$ values for these 29 young stars in Figure 5.3. Because faster-rotating stars are known to be more active, a correlation between RV dispersion and $v \sin i$ suggests that the RV dispersion is a product of stellar jitter for most stars. While the scatter appears to be large, a quadratic function (indicated with the green dashed line) can be fit to the

points on the plot. This is reasonable given that the hot Jupiter occurrence rate in open clusters is estimated to be $\sim 1\%$ (e.g. Quinn et al. 2016), so we should expect that most of the observed RV variations are induced by stellar jitter.

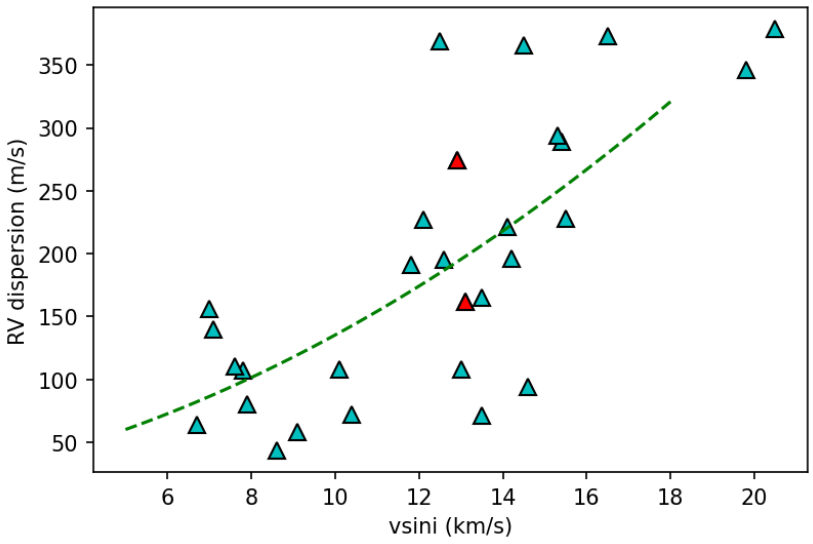

Figure 5.3 Measured RV dispersion (MAD) and $v \sin i$ values are plotted for the 29 stars in our monitoring program, shown as cyan triangles. The two stars marked red are identified as potential planet hosts in Section 6.1. We fit the points on this plot with a quadratic polynomial, shown as a green dashed line.

5.4.2 Line Bisector Spans

Like companions, star spots can produce apparent Doppler shifts in the absorption lines of stellar spectra by making their shapes asymmetric (Zhao et al. 2022). The cartoon shown in Figure 5.4 illustrates how this occurs. As a star rotates, the side of the star rotating toward the observatory appears blue-shifted while the side rotating away appears red-shifted. For a featureless star, the same amount of flux comes from both sides, so these effects cancel out and absorption lines appear symmetric. Star spots, which have a lower temperatures than the rest of the star, break this balance because they suppress flux on the side of the star in which they are found (Saar & Donahue 1997; Meunier et al. 2010). They locally modify absorption and emission processes and produce asymmetry in the integrated spectral line profiles that vary with stellar rotation as they rotate in and out of view. These line-shape changes can be

mistaken for true center-of-mass shifts in RV analyses and can even masquerade as periodic, false planet signals (Rajpaul et al. 2016). Because orbiting companions do not induce changes to the shapes of stellar spectral lines, apparent RV variations are likely a product of stellar jitter if they are correlated with line-shape variations.

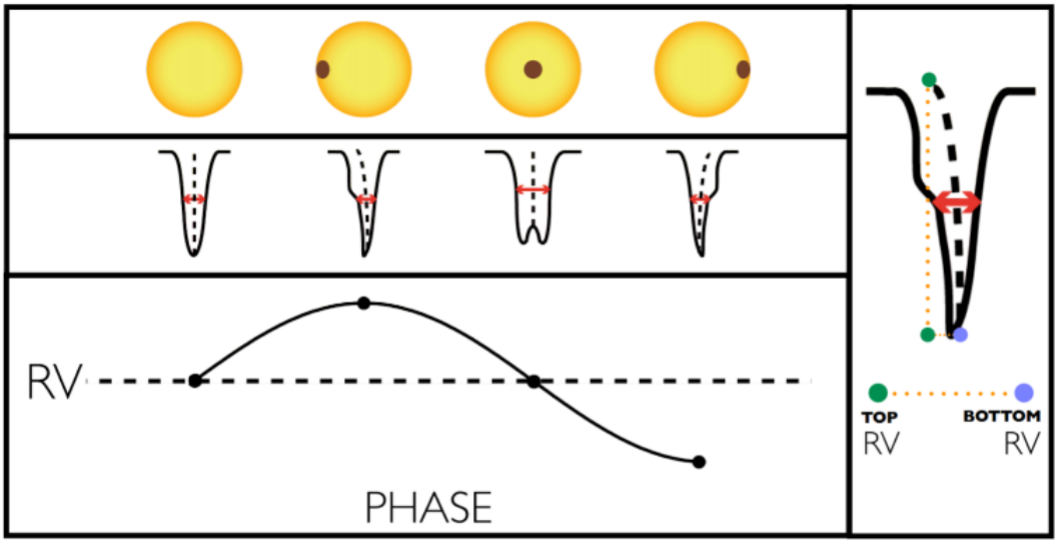

Figure 5.4 As a star spot rotates into and out of view (upper left panel), the shape of the absorption lines in the spectrum of the star is distorted (middle left panel), producing a false RV modulation that may be mistaken for a companion (lower left panel). The presence of star spots thus causes distortions in the spectral lines, which can be identified by measuring the variations in line bisector spans (right panel; e.g. Torres et al. 2004). Bisector spans are determined by subtracting the RV at the top point of the bisector from the bottom. This figure is from Haywood et al. (2015).

To quantify these line-shape variations, we measure the changes in line bisectors. Instead of monitoring the line bisector asymmetries of every absorption line in our spectra individually, we monitor the line bisectors of cross-correlation functions (CCF). The CCF can be thought of as an inverted average of all line shapes in a spectrum and is therefore only sensitive to line-shape changes that appear in most lines (Zhao et al. 2022). To quantify the line bisector shape, we measure line bisector spans, following the prescription of Toner & Gray (1988). The line bisector span is defined to be the difference in velocity between a point near the top of the bisector and a point near the bottom. This well-known diagnostic of stellar activity is

frequently used to rule out candidate planets orbiting active stars (e.g. Queloz et al. 2001; Povich et al. 2001).

Our prescription for measuring line bisector spans is shown in Figure 5.5. To measure the line bisector span of one epoch for one star, we first determine the CCF for each spectral order. We limit the CCF coefficients to range between 65% and 85% of the maximum CCF coefficient (typically ~ 1). Next, we fit the right wing of the CCF profile using a 3rd order polynomial, and use this polynomial to interpolate RVs of points on the right wing for the CCF coefficients of points on the left wing (typically ~ 12 points). We then construct a line bisector for each spectral order by computing the midpoints of horizontal line segments bounded by the CCF line profile. Finally, we determine the line bisector span by subtracting the velocity at the top of the bisector from the velocity at the bottom. For each epoch, we determine the mean line bisector span across the 12 spectral orders weighted by the RV uncertainty.

We use the same RV standard that we used to test our RV precision to test the precision with which our line bisector spans can be measured. Based on the same 36 spectra of HIP 73184 obtained on a single night, we measure 432 line bisector spans in total. The MAD of line bisector spans across epochs was ~ 7 m/s.

We measure the MAD of line bisector spans for the stars in our monitoring program and present these results in Table 5.5. The MAD values range from 21 m/s to 116 m/s. MAD values do not appear to be correlated with spectral order numbers. An example of this is shown in Figure 5.6. Only 1 star in IC 2391, SHJM6, of the 29 in this sample has a MAD value greater than 100 m/s. Given that the lowest dispersion in spans measured for the young stars is three times greater than the precision (~ 7 m/s), it appears that these stars experience absorption line distortions, likely caused by star spots.

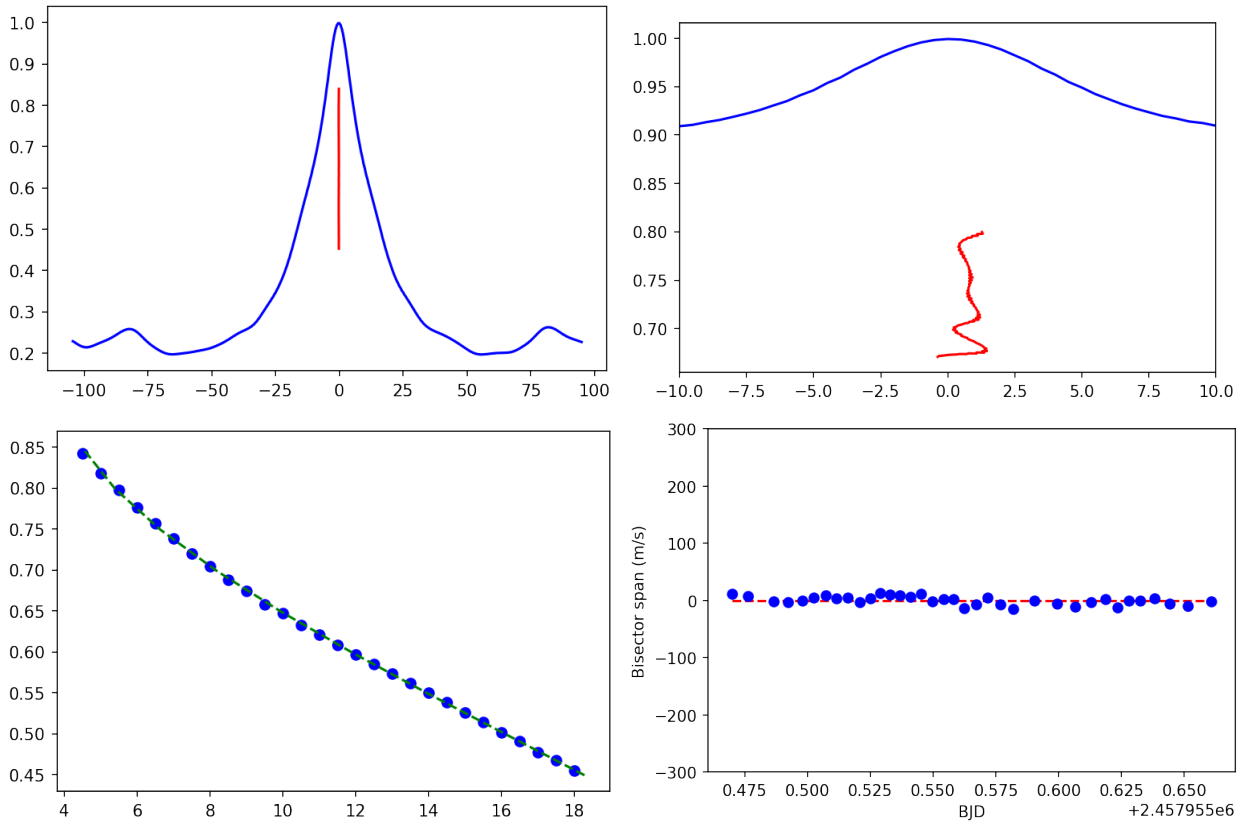

Figure 5.5 The line bisector of the CCF for one spectral order of one epoch of HIP 73184 is presented (top left panel). Because the shape of the line bisector, shown as a red line, is difficult to see by eye, we zoom in and show an example of a line bisector shape (top right panel). We derive line bisector shapes by fitting a polynomial to the right wing of the CCF profile (bottom left panel) and determining the RVs of points on the right wing at CCF values for points on the left wing. We test the precision of our prescription by monitoring the line bisector spans for 36 epochs of HIP 73184 (bottom right panel). We achieve a precision of $\sim$ 7 m/s.

5.4.3 Assessing the Correlation of RVs and Bisector Spans

If a star's line bisector span variations are correlated with its RV variations, then the RV variations are likely dominated by stellar activity because orbiting companions do not change the shapes of stellar absorption lines. We therefore search for a correlation between RV variations and line bisector span variations for every star monitored. To quantify this correlation for the stars we analyze in our sample, we use the *spearmanr*() SciPy Python function (Zwillinger & Kwoska 2000), which calculates the Spearman rank-order correlation

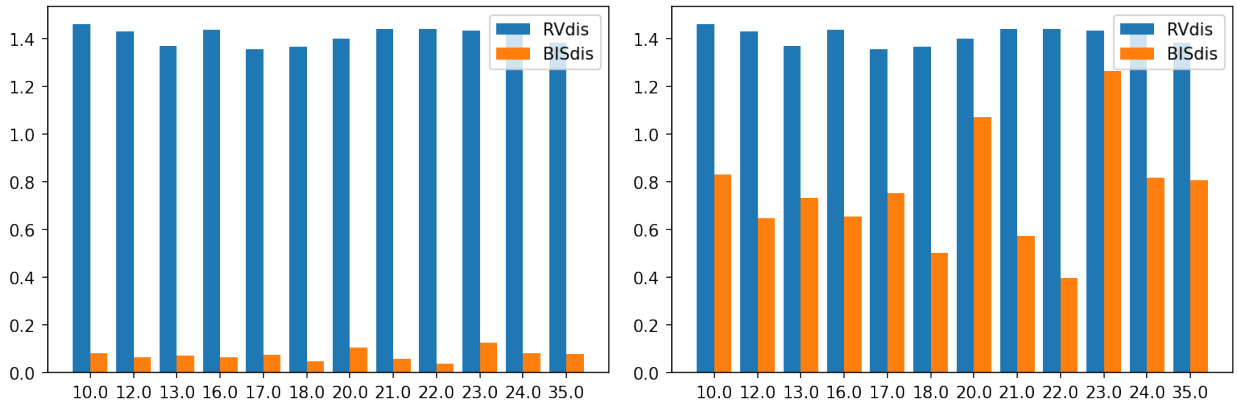

Figure 5.6 Mean absolute deviation values for radial velocities (RVdisp) and line bisector spans (BISdisp) are plotted in m/s as a function of spectral order for the 17 observations obtained for the IC 2602 star, R45. The left panel shows the true measured values for the bisector span variations while the right panel shows the original bisector span dispersion values per order multiplied by 10.

coefficient (SpCoeff; Figueira et al. 2014, Oshagh et al. 2017). While the Pearson correlation coefficient sees considerable usage in the literature as well (Basturk et al. 2011; Cabrera et al. 2017), the Spearman coefficient does not assume a linear relationship or a Gaussian distribution of variables, making it a more robust test of correlation. Instead of calculating the covariance and standard deviation on the samples themselves, the Spearman coefficient calculates these statistics from the relative rank of values on each sample. Like other correlation coefficients, the Spearman coefficient varies between -1 and +1 with 0 implying no correlation. Correlations of -1 or +1 imply an exact monotonic relationship. To help interpret these coefficients, the code also computes the p-value, that is the probability of having a larger or equal correlation coefficient under the hypothesis that the data pairs are uncorrelated (our null hypothesis); small p-values imply that the data are more likely correlated.

For the 29 stars in our monitoring program, we present the distribution of Spearman rank-order correlation coefficients and p-values in Figure 5.7. The Spearman coefficients range from $\sim$ 0.2 to 1.0 and the p-values range from $\sim$ 0.0 to 0.6. Most stars ($\sim$ 70%) in our sample have correlation coefficients greater than 0.7 and p-values less than 0.05, which suggests that line bisector spans and RVs are strongly correlated for those stars. We determine that

the RVs and bisector spans for a star are correlated if the p-value for that star is less than 0.05, similar to the prescription of Oshagh et al. (2017), because the probability that the correlation is observed by chance is less than 5%. While stars with a p-value less than 0.05 may still host companions, it is unlikely, to at least a 95% confidence level, that a planet is causing the observed RV variations. Instead, stellar activity is likely the cause and we identify these stars as "stellar activity" candidates. Only 9 of the stars in our sample have p-values > 0.05 and they range from 0.066 to 0.589, which correspond to an ~ 7 to 59% chance that the observed correlation is observed by coincidence. While the RV variations of these stars may also be correlated with bisector spans, additional observations are needed to rule out companions or stellar jitter. While we identify these stars as "ambiguous RV variables", we note that 7 of these 9 stars have fewer than 8 observations per star. Therefore, the p-value is likely biased by the low number of available observations. We list the slope of RV versus bisector span, Spearman rank-order correlation coefficient, p-value, and identification of the star as either a stellar activity candidate or ambiguous RV variable in Table 5.5 for all 29 stars in our sample.

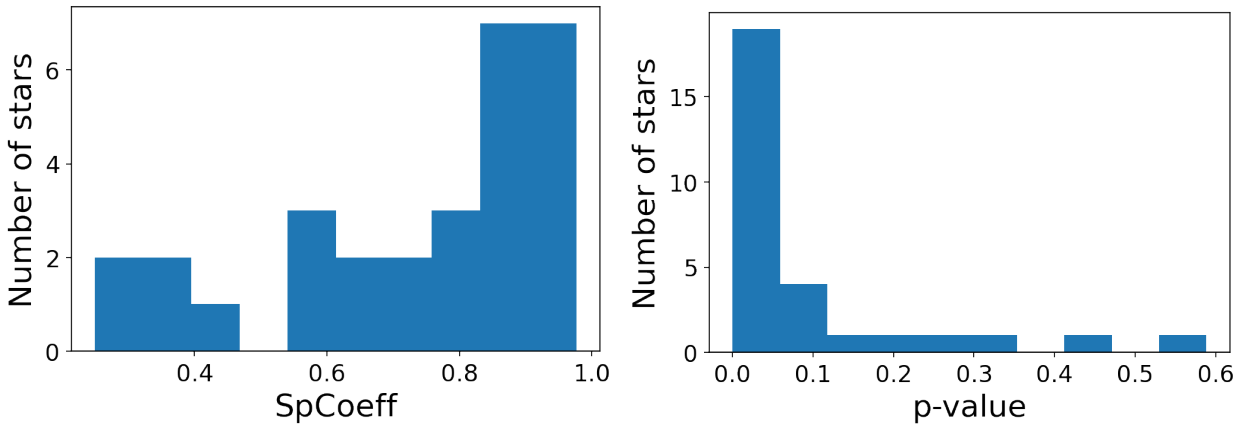

Figure 5.7 Histograms of the Spearman rank-order correlation coefficient (SpCoeff) and p-value are presented for all 29 stars in the monitoring program in the left panel and right panel, respectively. These distributions are discussed in more detail in Section 5.4.3.

5.4.4 Fitting orbits using rvfit

In order to help explain the large (> 100 m/s) RV variations observed for the majority of stars in our sample, we consider the possible orbital properties of companions that could reproduce the observed MAD values. To this end, we fit simple Keplerian models to the observed RVs of our stars using the IDL code written by Iglesias-Marzoa et al. (2015). This code, known as *rvfit*, uses an Adaptive Simulated Annealing (ASA) algorithm (Ingber et al. 1996) to compute six Keplerian parameters from a model: the orbital period P, the time of periastron passage T_P, the eccentricity e, the argument of the periastron ω, the systemic velocity γ, and the semi-amplitude of the radial velocity K_1. The name of this heuristic algorithm originates from annealing in metallurgy, a technique involving heating and cooling of a material to alter its physical properties. In practice, simulated annealing algorithms gradually minimize an objective function, called "temperature". At each time step, the algorithm randomly selects a solution close to the current one, measures its quality, and moves to it based on the temperature-dependent probabilities of selecting better or worse solutions. The *rvfit* code minimizes the χ^2 function when fitting Keplerian orbits (Iglesias-Marzoa et al. 2015).

Given the limited sampling for our young stars, we simplify the fit by assuming circular orbits; fixing the eccentricity to zero also fixes ω to 90 degrees. Newton et al. (2019) applies the same constraint for determining the orbital properties of a giant short-period exoplanet in Tucana-Horologium. We note that most hot Jupiter planets are expected have tidally circularized orbits (Crouzet et al. 2020; Fortney et al. 2021). We also limit the orbital period of our fit to range between 0.7 and 10 days. We note that while hot Jupiter planets typically have orbital periods that range from 1 to 10 days, and most have periods of 2 to 3 days (Figuera et al. 2010), the shortest-period hot Jupiter known has an orbital period of 0.77 days (McCormac et al. 2020). Given that hot Jupiters can generate RV semi-amplitudes on the order of a few hundred meters per second, the semi-amplitude of the orbit can be used to help infer if the origin of observed RV variations is hot Jupiter-like. For reference, a Jupiter-mass planet on an edge-on, circular orbit around a solar-mass star with an orbital period of 3 days

would generate a semi-amplitude of $\sim$ 140 m/s (Blake et al. 2007). In Figure 5.8, we show an example of *rvfit* being used to fit an initial non-precessing Keplerian RV curve to the RVs of the IC 2391 star, VXR22A. The estimated orbital period and semi-amplitude derived from the initial observations for this star are 2.0 days and 309 m/s, respectively.

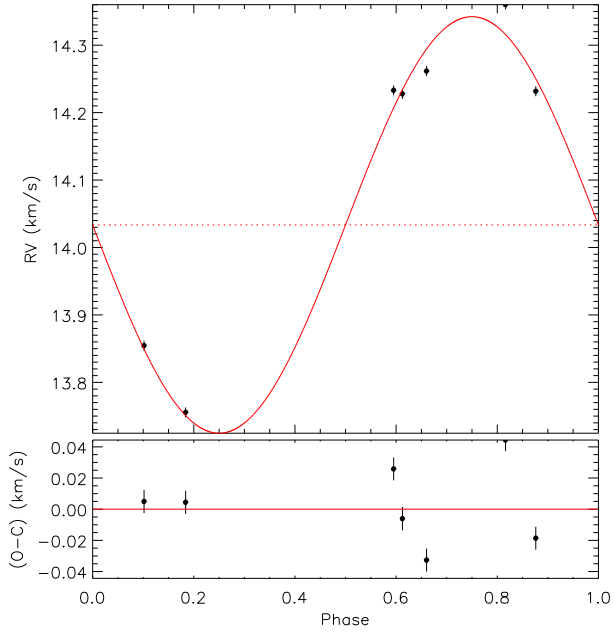

Figure 5.8 A best-fit orbit is derived for the IC 2391 star, VXR22A, using the code, *rvfit*. Based on the first set of 7 observations for this star, a period of 2.0 days and a semi-amplitude of 309 m/s is yielded for an eccentricity fixed to zero.

5.5 Two interesting candidate planet-hosts

We can use the analysis techniques of Section 5.4 to help distinguish between stars that host hot Jupiter planets and stars whose apparent reflex motions are caused by stellar jitter. In Figure 5.9, the MAD values of RV and bisector span are plotted for all 29 stars in our monitoring project. Surprisingly, most of the stars appear to follow a linear relationship, especially at lower MAD values of bisector span. Such a linear correlation implies that many of the stars in our sample have RV variations that are produced by stellar jitter. However,

stars with a low dispersion of bisector span but a high dispersion of RV may be promising exoplanet hosts. Two stars have RV variations above this empirical relation, suggesting they have RV variations larger than that expected by star spots alone. These stars are the IC 2391 member, PMM2012, and the IC 2602 member, R45. For a dispersion of bisector spans less than 40 m/s, these stars show a dispersion of RVs greater than 100 m/s.

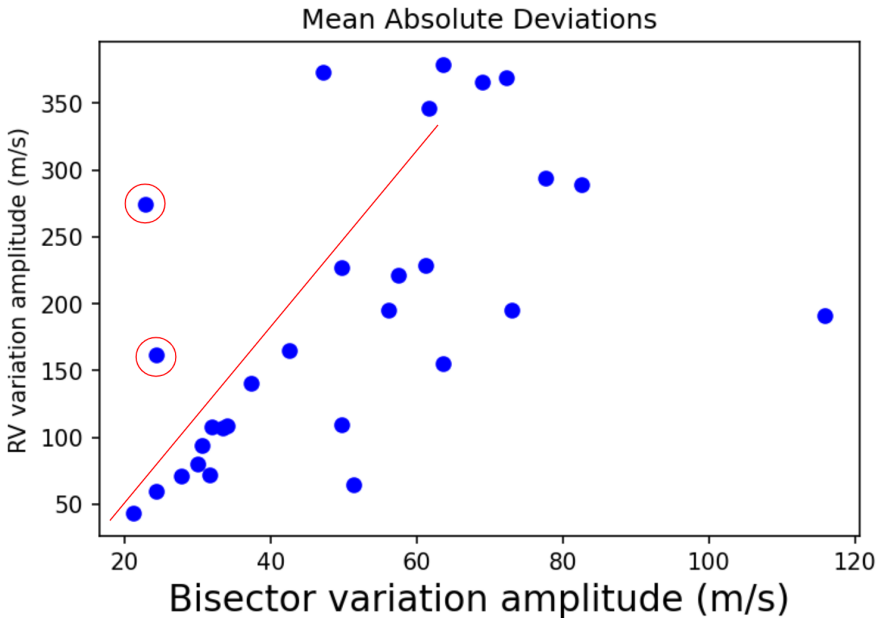

Figure 5.9 Mean absolute deviations of RVs and bisectors are plotted for all 29 stars in our sample. A linear trend is shown as a red line and the two stars of interest, PMM2012 and R45, are circled in red.

Table 5.5: Measurements of variation in RVs and bisector spans for 29 stars in monitoring survey

Name	Std (m/s)	RV disp (m/s)	BIS disp (m/s)	Slope	SpCoef	p-value	Planets?	Nobs	Baseline (days)
IC 2602									
B134	73	58	24	2.1	0.857	6.5e-3	S	8	86
R1	197	156	63	1.5	0.853	4.2e-4	S	7	70
								12	604
R14	247	195	73	2.1	0.821	2.3e-2	S	7	13
R42B	142	108	32	3.1	0.877	3.8e-5	S	7	18
								14	129
R45	170	162	24	4.3	0.777	2.4e-4	S	8	117
								17	425
R66	235	227	50	3.9	0.809	2.6e-3	S	5	26
								11	2565
R70	77	72	32	0.9	0.371	4.7e-1	P	6	47
SR3	131	108	34	2.4	0.709	9.9e-4	S	5	79
								11	638
								18	741

Table 5.5: Measurements of variation in RVs and bisector spans for 29 stars in monitoring survey

Name	Std (m/s)	RV disp (m/s)	BIS disp (m/s)	Slope	SpCoef	p-value	Planets?	Nobs	Baseline (days)
TYC8964171	334	289	83	2.4	0.714	7.1e-2	KP	7	6
W79	69	64	51	0.9	0.857	6.5e-3	S	8	723
IC 2391									
PMM665	135	107	33	2.9	0.905	2.0e-3	S	8	185
PMM756	361	294	79	3.1	0.571	2.6e-2	S	8	32
								15	164
PMM2012	387	274	23	6.5	0.691	2.1e-3	S	8	184
								17	467
PMM3359	108	80	30	2.6	0.571	1.4e-1	P	8	184
PMM4280	125	94	31	2.7	0.617	7.7e-2	P	9	187
PMM4362	51	43	21	0.8	0.345	2.3e-1	P	7	407
								14	930
PMM5884	408	366	68	5.0	0.679	9.4e-2	P	7	33
SHJM6	214	191	116	0.2	0.254	2.9e-1	P	7	404
								12	752

Table 5.5: Measurements of variation in RVs and bisector spans for 29 stars in monitoring survey

Name	Std (m/s)	RV disp (m/s)	BIS disp (m/s)	Slope	SpCoef	p-value	Planets?	Nobs	Baseline (days)
								19	927
VXR22A	168	140	37	3.0	0.842	3.2e-6	S	7	236
								13	757
								20	928
VXR70	294	228	61	3.5	0.881	1.5e-4	S	6	420
Tuc-Hor									
HD1466	390	346	62	4.5	0.893	6.8e-3	S	7	12
HD222259A	552	373	47	3.9	0.819	6.2e-4	KS	8	33
								13	495
HD222259B	508	369	72	2.0	0.573	6.6e-2	P	6	33
								11	494
HIP490	79	71	28	2.5	0.943	4.8e-3	S	6	13
HIP1113	158	110	50	0.6	0.250	5.9e-1	P	7	70
HIP6485	192	165	43	3.7	0.944	3.9e-6	S	7	10
								12	421

Table 5.5: Measurements of variation in RVs and bisector spans for 29 stars in monitoring survey

Name	Std (m/s)	RV disp (m/s)	BIS disp (m/s)	Slope	SpCoef	p-value	Planets?	Nobs	Baseline (days)
HIP9141	230	221	58	3.3	0.916	2.8e-5	S	7	77
								12	490
HIP21632	404	379	64	5.2	0.964	1.9e-6	S	7	12
								11	417
HIP105388	283	196	56	3.8	0.976	3.3e-5	S	8	684
								12	778

Note. — Name, standard deviation (Std) of RV, mean absolute deviation of RV (RV disp), mean absolute deviation of line bisector spans (BIS disp), calculated slope of linear relationship of RV versus bisector span (Slope), Spearman's rank-order correlation coefficient (SpCoef), probability of null hypothesis (p-value), candidate identification (Planets?) for stellar-activity (S) and ambiguous RV variables (P) as well as stars with known exoplanet detections in the literature (K), number of observations in total per set (Nobs), and baseline of observations including all previous sets (Baseline).

CHAPTER 6

CANDIDATE HOT JUPITER PLANETS AND STELLAR JITTER

In this chapter, we discuss the candidate planet-hosts and stellar-activity candidates we identified in Chapter 5, and then we determine the stellar jitter and discuss the planet-detection prospects in IC 2602, IC 2391, and Tucana-Horologium.

6.1 Revisiting the interesting candidate planet hosts

At the end of Chapter 5, we identified two interesting candidate exoplanet-host stars, PMM 2012 and R45, based on their large dispersion of RVs compared with their small dispersion of line bisector spans. Moreover, the stars showed much larger-than-average slopes (> 4) in plots of line bisector versus RV. To confirm or refute the periodic RV trends observed, follow-up observations were observed.

6.1.1 Follow-up observations of PMM2012

The IC 2391 star, PMM2012, has received two sets of observations, including follow-up, in CHIRON slicer-mode, as shown in Table 5.5, that are separated by ~ 1 year apart. The first set includes 8 observations over 184 days. As can be inferred from visual inspection of the RV curve shown in Figure 6.1, the 7 initial observations of this set were conducted within 3 weeks. Fitting an orbit to this RV curve, as shown in Figure 6.2, yields a periodic RV variation of 3.6 days with a semi-amplitude of 603 m/s. Including the second set of follow-up observations, the temporal baseline increases to 467 days and a total set of 17 observations is produced.

The updated fit to the orbit, shown in Figure 6.2, reveals a drastically reduced period of 1.8 days and a semi-amplitude of 427 m/s. Thus, the previous orbit was not confirmed.

Assessing the correlation between RVs and line bisector spans using all 17 epochs, shown in Figure 6.1, a Spearman's rank-order correlation coefficient of 0.691 is obtained with a corresponding p-value of 0.002. This implies that the probability of observing this correlation by pure coincidence is less than 0.2%, making stellar activity the likely cause of the star's RV variations. However, we additionally note that we calculated a correlation coefficient of 0.405 and a p-value of 0.320 (not tabulated) for this star during the first set of observations, which made this a compelling candidate planet host. Moreover, the slope of RV versus bisector span is 6.5 for PMM2012, the highest in the sample. While this star may still host planets, the follow-up observations and resulting p-values reveal that a planet is not likely causing the observed RV variations. Instead, stellar jitter is likely the cause, and so we list this as a "stellar activity" candidate in Table 5.5.

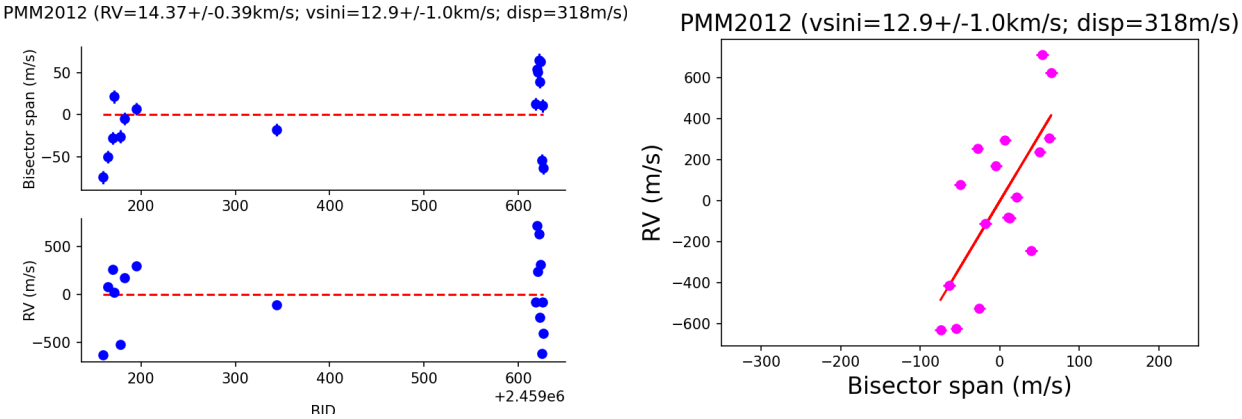

Figure 6.1 Measured line bisector spans and RVs are plotted, respectively, against barycentric Julian dates for the 17 observations of the IC 2391 star, PMM2012, in the left panel. The observations after day 600 are the follow-up data. The correlation between RVs and spans for the observed epochs of this star can be seen in the right panel.

6.1.2 Follow-up observations of R45

Like PMM2012, the IC 2602 star, R45, has received two sets of observations including follow-up, as shown in Table 5.5, that are separated by $\sim$ 1 year apart. The first set includes

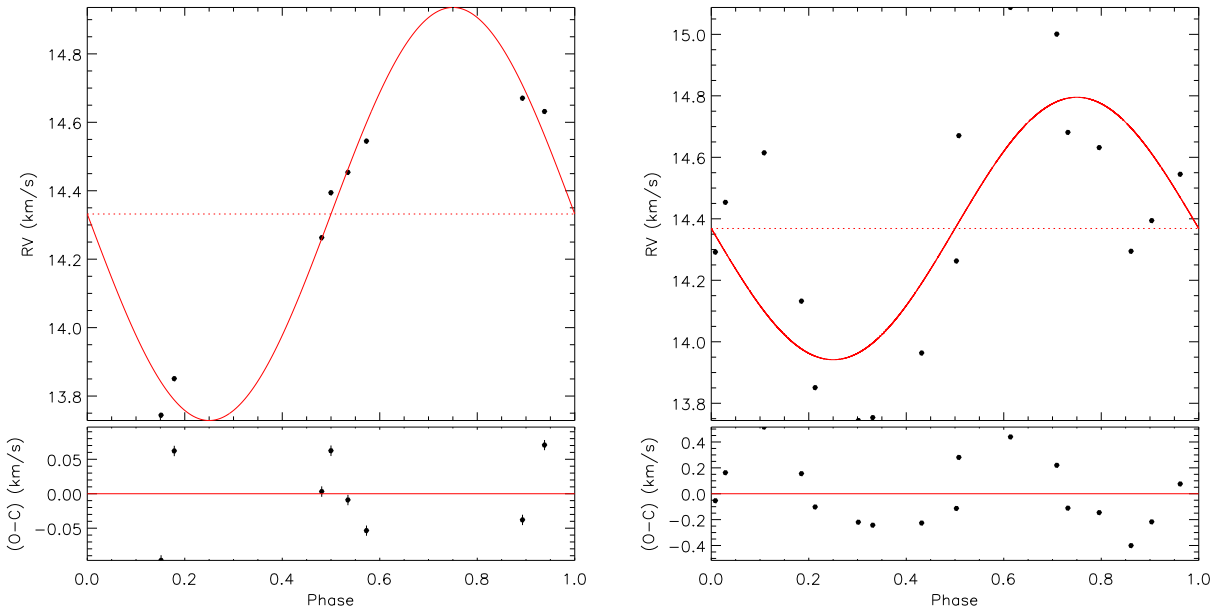

Figure 6.2 Best-fit orbits are derived for the IC 2391 star, PMM2012, using the code, *rvfit*, as discussed in Chapter 5. Possible orbits are fit to the first set of 8 observations in the left panel, yielding a period of 3.6 days and a semi-amplitude of 603 m/s for an eccentricity fixed to zero. The fit to the final set of 17 observations is also shown in the right panel, revealing far greater scatter than in the left panel. From the final fit, we arrive at an orbital period of 1.8 days and a semi-amplitude of 427 m/s. Based on the residuals shown, there does appear to be a periodic RV signal in the data, but jitter is likely the cause.

8 observations over 117 days and, as can be inferred from visual inspection of the RV curve in Figure 6.3, the 7 initial observations were conducted within 3 weeks. Fitting an orbit to this RV curve, as shown in Figure 6.4, yields a periodic RV variation of 4.0 days with a semi-amplitude of 358 m/s. Including the second set of follow-up observations, the temporal baseline increases to 425 days and a total set of 17 observations is produced. The updated fit to the orbit, shown in Figure 6.4, reveals a drastically reduced period of 2.9 days and a semi-amplitude of 195 m/s. As was the case with PMM2012, the orbit derived from the first set of observations was not confirmed.

Assessing the correlation between RVs and line bisector spans in the final set shown in Figure 6.3, a Spearman's rank-order correlation coefficient of 0.777 is obtained with a corresponding p-value of 2.4e-4. This implies that the probability of observing this correlation

by pure chance is very unlikely, again making stellar activity the likely cause of the star's observed RV variations. While the correlation coefficient for the first set of observations for this star suggested that the RVs and spans are correlated, the slope of the correlation is still quite high at 4.3. As with PMM2012, we list R45 as a stellar activity candidate in Table 5.5.

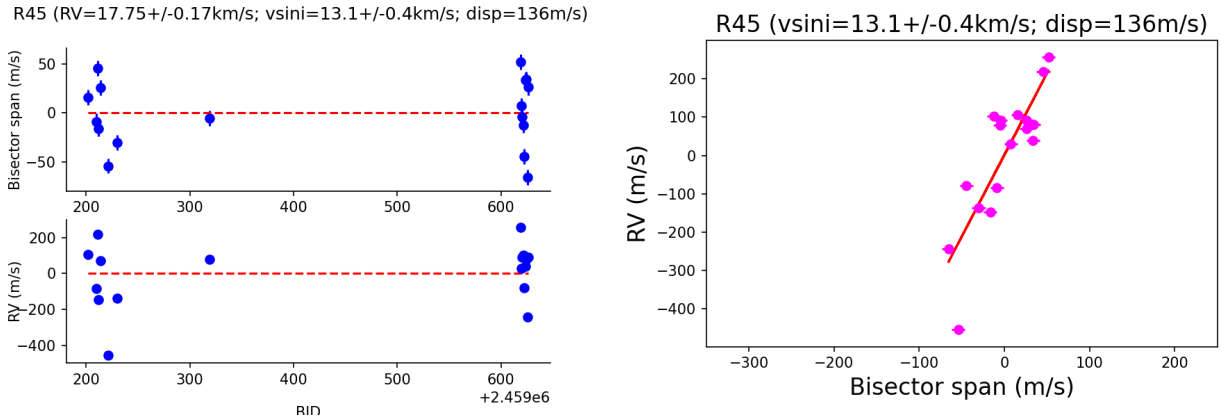

Figure 6.3 Measured line bisector spans and RVs are plotted, respectively, against barycentric Julian dates for the 17 observations of the IC 2602 star, R45, in the left panel. The observations after day 600 are the follow-up data. The correlation between RVs and spans for the observed epochs of this star can be seen in the right panel.

6.2 Ambiguous RV Variables for Follow-up

While the two interesting candidate planet-hosts from Section 6.1 appear to be likely stellar-activity candidates based on results from follow-up observations, we now discuss the stars in our sample for which the probability is less than 95% that an apparent correlation between RVs and bisector spans is real. Of the 29 stars in our sample, 9 fulfill this criterion with a p-value greater than 0.05, including 1 star from IC 2602, 5 stars from IC 2391, and 3 stars from Tucana-Horologium. These stars are R70, PMM3359, PMM4280, PMM4362, PMM5884, SHJM6, HD222259B, HIP1113, and TYC8964171. As discussed in Chapter 5, the p-values for these stars range from 0.066 to 0.589, which correspond to an $\sim$ 7 to 59% chance that the observed correlations are not real. Most of these stars have only received one set of observations, being observed fewer than 10 times. Thus, many of them may appear to be planet candidates but could possibly be ruled out with additional follow-up observations,

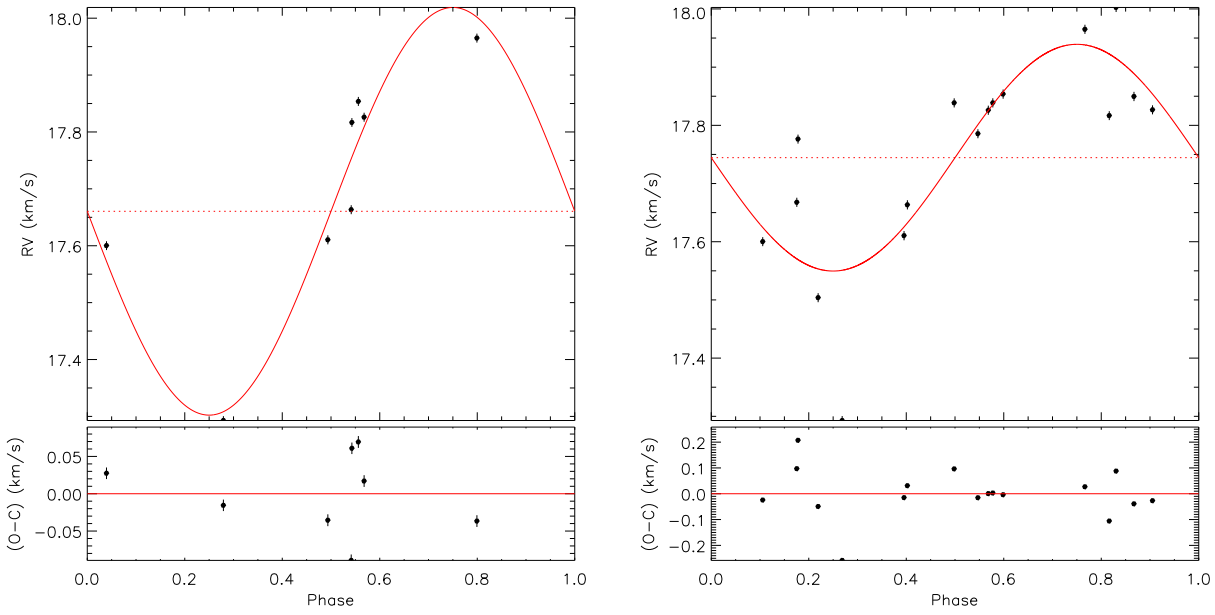

Figure 6.4 Best-fit orbits are derived for the IC 2602 star, R45, using the code, *rvfit*, as discussed in Chapter 5. Possible orbits are fit to the first set of 8 observations in the left panel, yielding a period of 4.0 days and a semi-amplitude of 358 m/s for an eccentricity fixed to zero. The fit to the final set of 17 observations is also shown in the right panel, revealing greater scatter than in the left panel. From the final fit, we arrive at an orbital period of 2.9 days and a semi-amplitude of 195 m/s, but jitter is likely the cause.

similar to the cases of PMM2012 and R45 discussed in Section 6.1. Plots of line bisector span versus RV are shown for the 6 stars that did not receive follow-up observations in Figure 6.5.

However, 3 of these 9 stars have received follow-up observations, separated from their initial sets of observations by $\sim$ 1 year. These stars have received between 11 and 19 observations in total. These stars include the 2 IC 2391 stars, PMM4362 and SHJM6, and the Tucana-Horologium star, HD222259B. As shown in Table 5.5, PMM4362 received two sets of observations, an initial set of 7 over a baseline of 407 days and a final follow-up set to reach 14 over a total baseline of 930 days. As visual inspection of Figure 6.6 reveals, the slope is 0.8 and the correlation is weak with a correlation coefficient of 0.345 and a p-value of 0.227. Thus, the 95% confidence level to assert that the RVs and spans of this star are correlated is not reached. By fitting an orbit to this star's final set of RVs while fixing the eccentricity to zero, we calculate a period of 3.4 days and a K-amplitude of 64 m/s. Given

that most hot Jupiters produce semi-amplitudes of approximately 100 m/s (Fortney et al. 2021) and we measure a mean absolute deviation of RVs for this star of about 43 m/s, we express skepticism that this target represents a hot Jupiter planet.

The other IC 2391 star with RV variations that do not correlate with bisector spans, SHJM6, received three sets of observations resulting in a total of 19 observations with a total baseline of 927 days. Examining the relationship between RVs and bisector spans, shown in Figure 6.7, we find that the slope is 0.2, the lowest slope in our survey sample. As shown in Table 5.5, SHJM6 also possesses a correlation coefficient of 0.254 and a p-value of 0.293, the second lowest values of correlation, right below those of another ambiguous RV variable in our sample, HIP1113. Fitting an orbit to the RVs of SHJM6, we find a period of 3.8 days and a semi-amplitude of 218 m/s. Given that we measure a similarly large RV dispersion of 191 m/s, a hot Jupiter planet may very well be the cause of the observed RV variations for this star. However, as the orbit-fit in Figure 6.7 reveals, there is considerable uncertainty and scatter about the best-fit orbit. While the correlation between RVs and spans is poor for this star, more sophisticated modeling techniques may be necessary to disentangle any possible planetary RV signals that may be present.

6.2.1 The interesting candidate planet-host of Tucana-Horologium

The Tucana-Horologium member, HD222259B, is an interesting star because it is part of a known binary with another star in our sample, HD222259A. A planet with mass intermediate between that of Neptune and Saturn was discovered orbiting the primary of this multiple-star system with an orbital period of 8 days and inducing an RV semi-amplitude of 100 m/s (Newton et al. 2019). Unfortunately, we do not retrieve the exoplanet RV signal for the known planet-host, HD222259A, which received 13 observations in total (see Figure 6.8). Moreover, we observe a high level of correlation between the RVs and line bisectors measured for HD222259A based on a correlation coefficient of 0.819 and a p-value of 6.2e-4. We conclude that there may be no planet.

We observed HD222259B in two sets, resulting in a total of 11 observations over a baseline of 494 days. As shown in Table 5.5, we find that a companion with an orbital period of 6.9 days and a K-amplitude of 725 m/s could produce the RV dispersion observed for this star, which we measure to be 369 m/s. While the correlation coefficient is 0.573 and the p-value is 0.066, which indicates that the RVs and spans for this star may not be correlated, visual inspection of Figure 6.9 suggests that one data point with an RV of $\sim$ 1 km/s above the mean RV for this star may be impacting our interpretation of this result. The other points in the plot of RV versus bisector span appear to visually follow a clear linear trend between -200 and 150 m/s so we express doubt that a planetary RV signal has been retrieved. While we cannot rule out that data point, the origin is uncertain and additional observations are needed. We speculate that this point may result from the primary in the binary, HD222259A, since that star has also shown some unusually large $>$ 1 km/s RV variations. Given the close separation between the primary and secondary ($\sim$ 6 mas) in the sky, it is conceivable that another star besides the target was observed and the single errant point can be excluded. Thus, it appears that the RV variations in both stars observed in this monitoring program are more likely to be the product of stellar jitter rather than companions.

6.3 Candidate Stellar-Activity stars

As discussed in Chapter 5, we identified stars in our sample as "stellar-activity candidates" and "ambiguous RV variables" based on whether their p-value was less than or greater than 0.05, respectively. By this diagnostic of correlation between RVs and bisector spans, we identified 20 stellar-activity candidates and 9 ambiguous RV variables. Of the 20 stellar-activity candidates marked in Table 5.5, 8 stars are from IC 2602, 5 stars are from IC 2391, and 7 stars are from Tucana-Horologium. 13 of these 20 stars have follow-up observations, and have received between 11 and 20 observations per star in total. Similar to the case of PMM2012 discussed in Section 6.1, initial analyses revealed them to be compelling targets for follow-up with hot Jupiter-like RV variations but later analyses revealed them to each have

an RV dispersion that was most likely produced by stellar jitter. Despite the higher p-values of ambiguous RV variables we mark in Table 5.5, the discussion in Section 6.2 reveals that we are unable to rule out stellar jitter as the cause of their observed RV variations for any of them. Consequently, we will use the full set of 29 stars to measure the magnitude of stellar jitter at the age of ∼50 Myr for IC 2602, IC 2391, and Tucana-Horologium.

6.4 Stellar Jitter at ∼50 Myr

The measured dispersion of RVs (typically > 100 m/s) for the 29 stars observed in our monitoring campaign are much larger than the individual RV uncertainties per epoch (∼ 5-8 m/s) and the instrumental RV uncertainty of CHIRON in slicer mode (∼ 7.5 m/s).

To compare with values of stellar jitter in the literature, we measure the RV stellar dispersion, σ_{RV}, for each star as a simple standard deviation of RVs across epochs, following the prescription of Luhn et al. (2020), where N is the total number of velocities for the given star and $\overline{RV}$ is the mean RV of the star:

$$\sigma_{RV} \simeq \sqrt{\frac{1}{N-1}\sum(RV - \overline{RV})^2} \tag{6.1}$$

We report these standard deviations for each star in Table 5.5. We do not use a true root-mean-square (RMS) in this case because the zero-point for each RV time series is arbitrary and so it is necessary to subtract off the mean rather than simply taking the square root of the sum of squared residuals. Past works, such as those of Wright (2005), find the "jitter" by subtracting the mean reported instrumental uncertainty, σ_{instr} from the RMS term (σ_{RV}) in quadrature. Because we have well-characterized individual measurement (σ_{int}) and instrumental (σ_{CHIRON}) errors (Paredes et al. 2021), we determine the stellar jitter ($\sigma_\star$) for a star in our sample, following the prescription given by Quinn et al. (2016):

$$\sigma_\star = \sqrt{\sigma_{RV}^2 - \sigma_{int}^2 - \sigma_{CHIRON}^2} \tag{6.2}$$

We determine the stellar jitter for a stellar population by taking the average of stellar jitter values for members of that population. We determine the uncertainty in this mean by taking the standard deviation of these values. For IC 2602, we find that, based on 10 stars, the mean RV jitter is 168 m/s, the standard deviation is 83 m/s, and the median is 156 m/s. For IC 2391, we find that, based on 10 stars, the mean RV jitter is 225 m/s, the standard deviation is 123 m/s, and the median is 191 m/s. For Tucana-Horologium, we find that, based on 9 stars, the mean RV jitter is 311 m/s, the standard deviation is 153 m/s, and the median is 283 m/s. We present these results in Table 6.1. We find that at $\sim$ 50 Myr, based on all 29 stars in our sample, the mean RV jitter is 237 m/s, the standard deviation is 126 m/s, and the median is 214 m/s.

In Table 6.1, we assemble the stellar jitter measurements available in the literature to-date for other nearby clusters and moving groups. These measurements are taken from the works of Lagrange et al. (2013), Cabrera Salazar (2017), Paulson & Yelda (2006), Quinn et al. (2012,2014), and Takarada et al. (2020). The reported uncertainties are standard deviations of RV dispersion across the number of stars used to determine the RV jitter. As expected from initial studies, such as those of Paulson & Yelda (2006), of stars younger than $\sim$ 300 Myr, the jitter at $\sim$ 50 Myr is larger and more dispersed than at older ages. We illustrate this in Figure 6.10. Our measurements of stellar jitter are larger than previous estimates, but previous estimates typically relied on fewer stars and selected stars with slower $v \sin i$ values (Paulson & Yelda 2006).

6.4.1 Prospects of planet detection at $\sim$ 50 Myr

Given that we measure the mean RV jitter at $\sim$ 50 Myr to be 237 m/s, most hot Jupiter planets (with typical semi-amplitudes of $\sim$ 100 m/s) will be masked by the RV scatter caused by stellar jitter. Using the equation for semi-amplitude given by Cumming et al. (1999), assuming a circular orbit and a solar-mass host star, this amplitude is similar to a 2

Jupiter-mass companion in a 3 day orbit or a 3 Jupiter-mass companion in a 10 day orbit ($\sim$ 280 m/s in both cases).

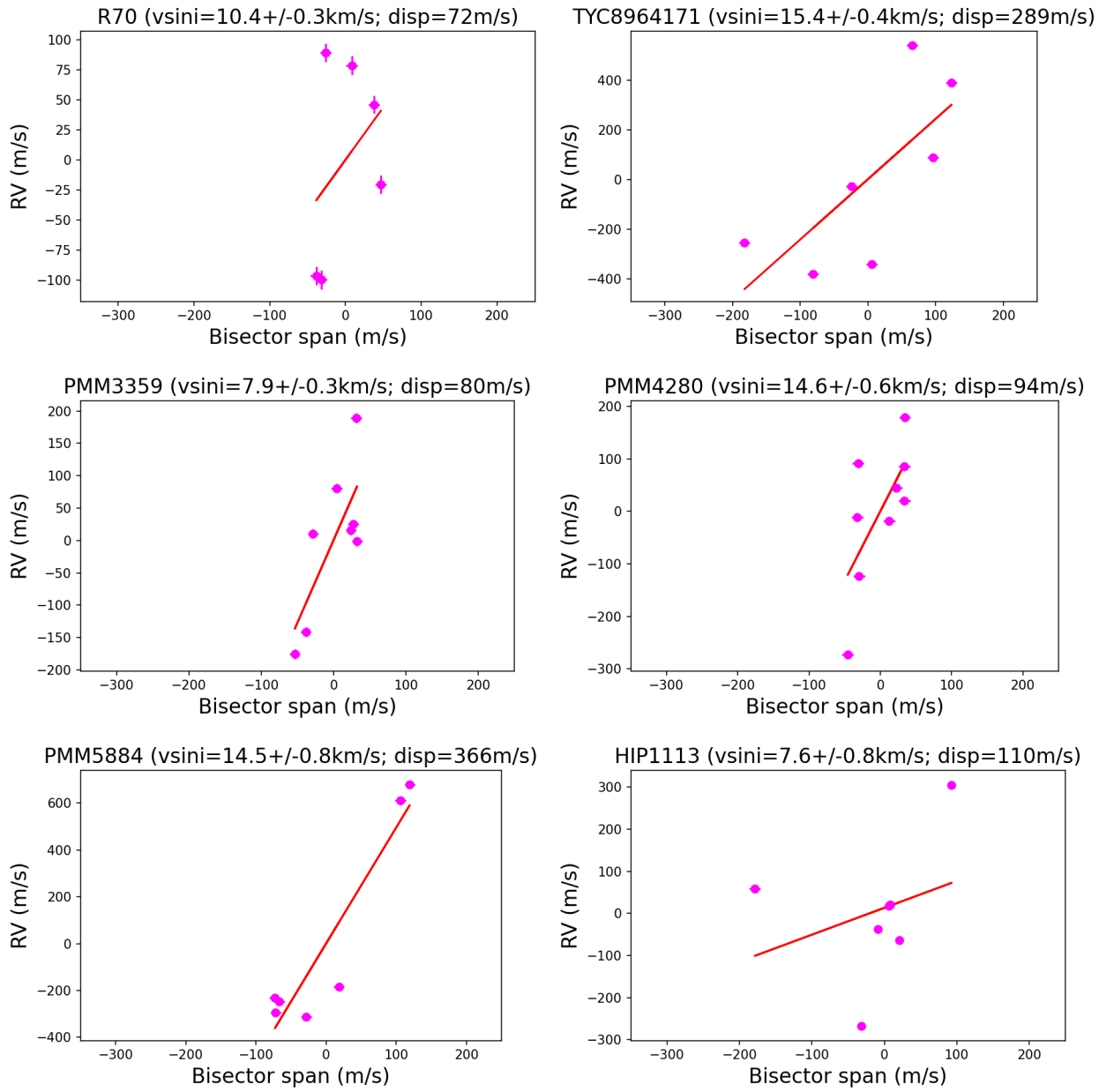

Figure 6.5 Radial velocities are plotted against line bisector spans across epochs for each of the 6 stars that appear to have RVs and spans that are uncorrelated. These stars require additional follow-up to confirm if they may host any hot Jupiter planets.

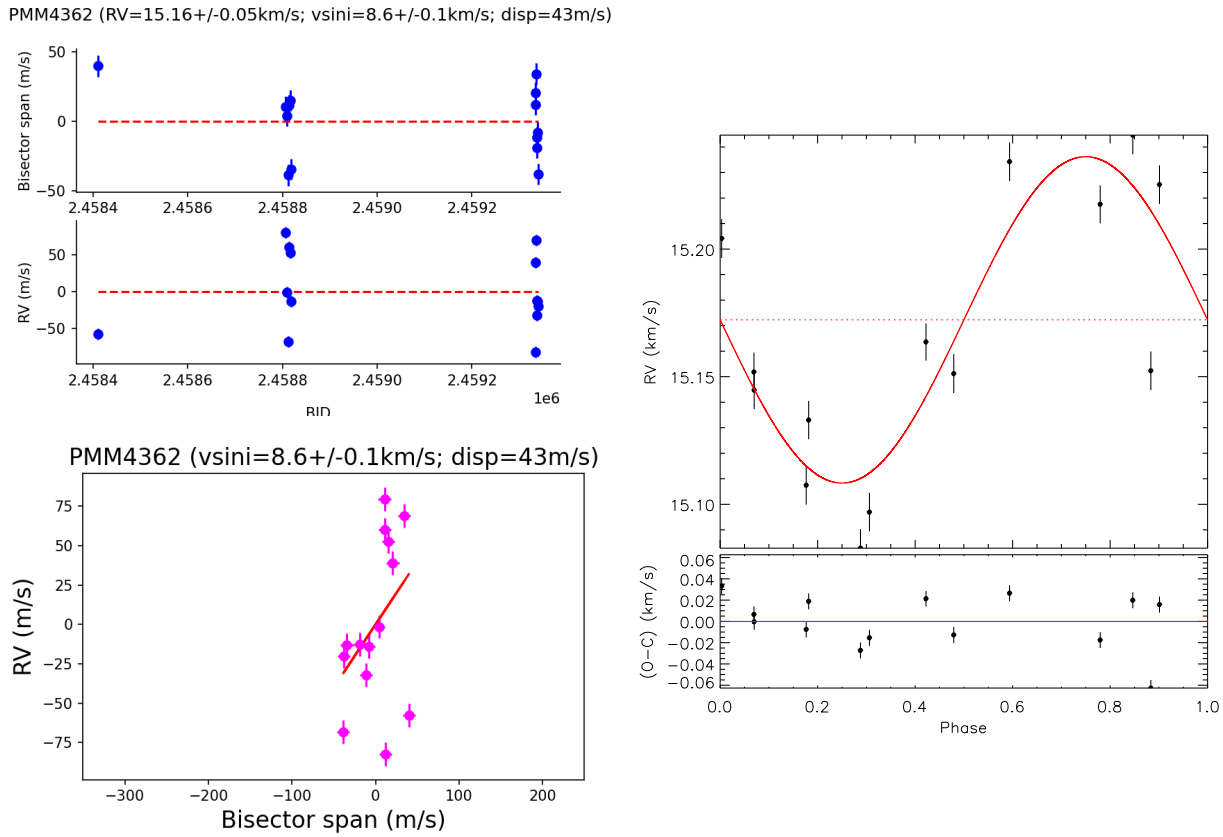

Figure 6.6 Measured line bisector spans and RVs are plotted, respectively, against barycentric Julian dates for the 14 observations of the IC 2391 star, PMM4362, in the top left panel. The observations after day 2.4592e6 are the follow-up data. The correlation between RVs and spans for the observed epochs of this star can be seen in the bottom left panel. In the right panel, a best-fit orbit is derived for this star using the code, *rvfit*, as discussed in Chapter 5. Based on the fit, the observed RV variations for this star could be explained by a companion with an orbital period of 3.4 days and a semi-amplitude of 64 m/s.

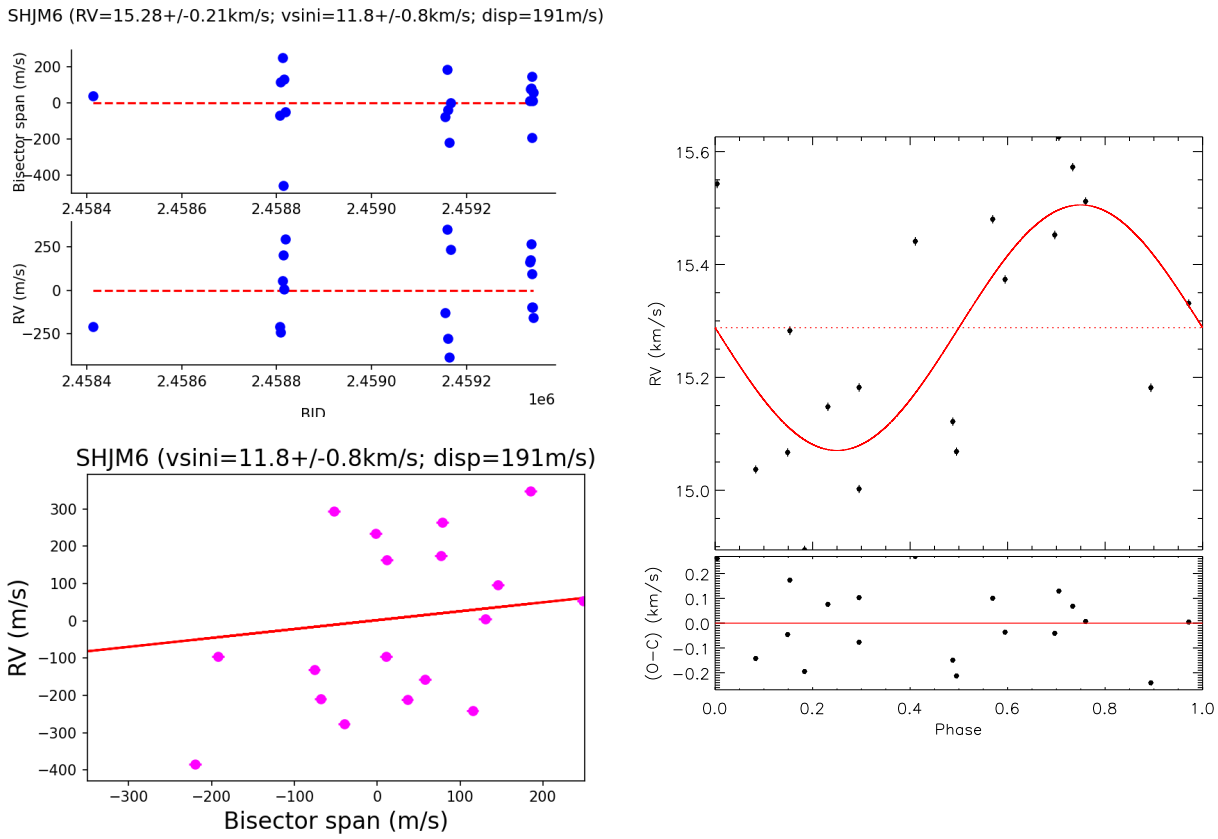

Figure 6.7 Measured line bisector spans and RVs are plotted, respectively, against barycentric Julian dates for the 19 observations of the IC 2391 star, SHJM6, in the top left panel. The observations between days 2.4590e6 and 2.4592e6 are the first set of follow-up data, and the observations after day 2.4592e6 are the second set of follow-up data. The correlation between RVs and spans for the observed epochs of this star can be seen in the bottom left panel. In the right panel, a best-fit orbit is derived for this star using the code, *rvfit*, as discussed in Chapter 5. Based on the fit, the observed RV variations for this star could be explained by a companion with an orbital period of 3.8 days and a semi-amplitude of 218 m/s.

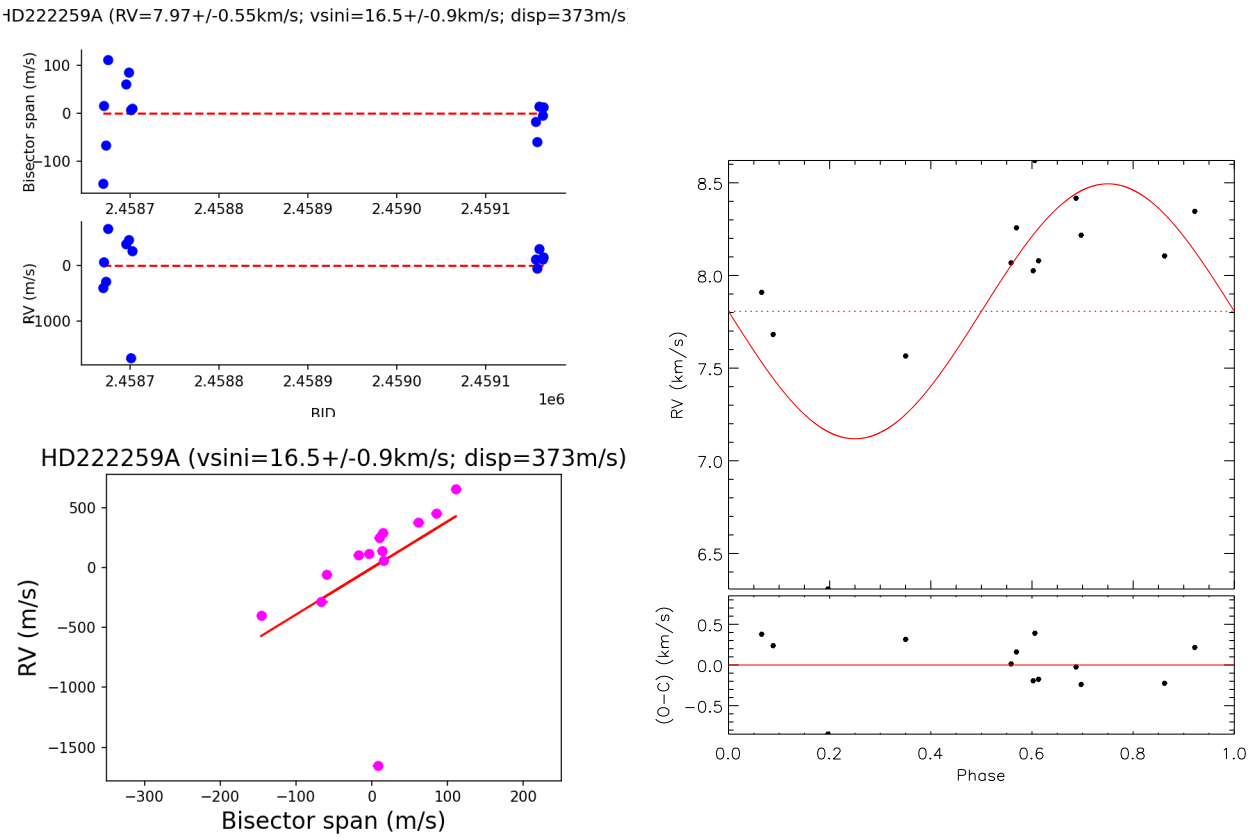

Figure 6.8 Measured line bisector spans and RVs are plotted, respectively, against barycentric Julian dates for the 11 observations of the Tucana-Horologium star, HD222259A, in the top left panel. The observations after day 2.4591e6 are the follow-up data. The correlation between RVs and spans for the observed epochs of this star can be seen in the bottom left panel. In the right panel, a best-fit orbit is derived for this star using the code, *rvfit*, as discussed in Chapter 5. Based on the fit, the observed RV variations for this star could be explained by a companion with an orbital period of 3.9 days and a semi-amplitude of 688 m/s.

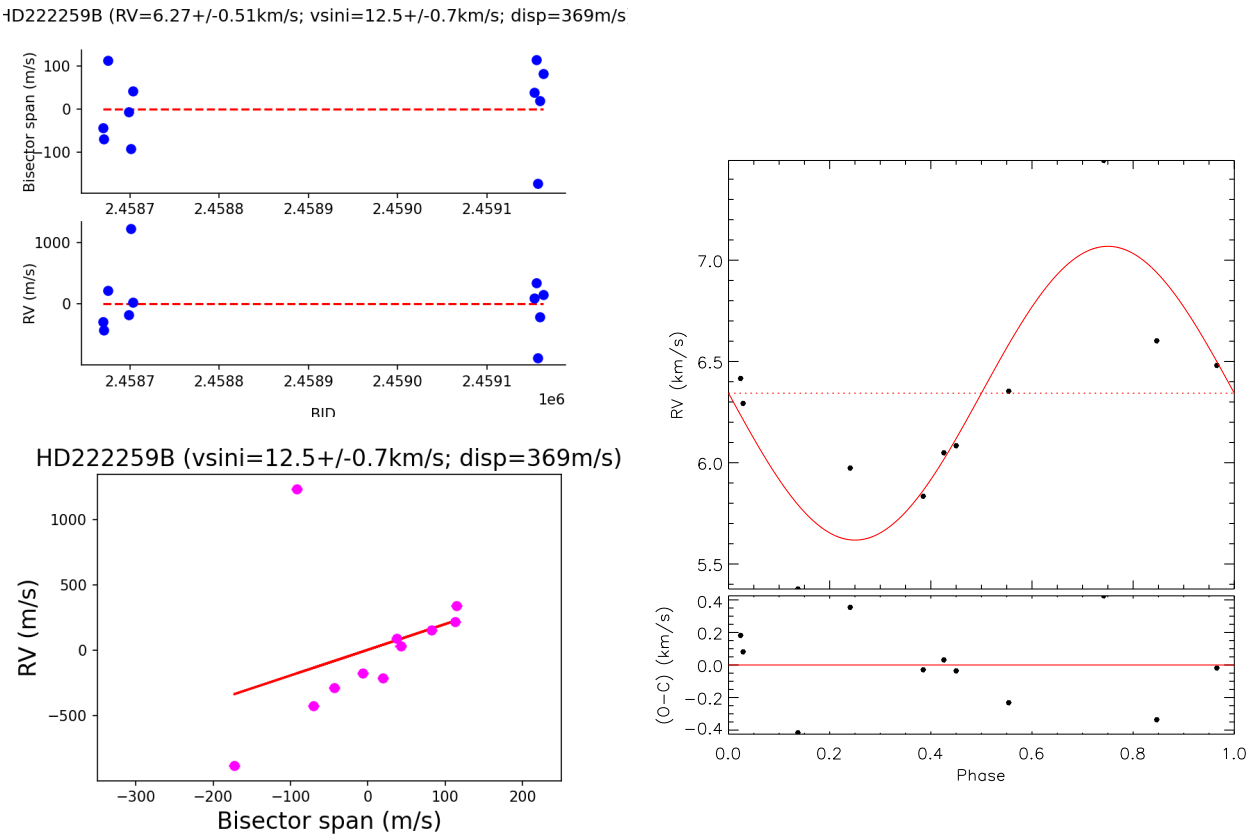

Figure 6.9 Measured line bisector spans and RVs are plotted, respectively, against barycentric Julian dates for the 11 observations of the Tucana-Horologium star, HD222259B, in the top left panel. The observations after day 2.4591e6 are the follow-up data. The correlation between RVs and spans for the observed epochs of this star can be seen in the bottom left panel. In the right panel, a best-fit orbit is derived for this star using the code, *rvfit*, as discussed in Chapter 5. Based on the fit, the observed RV variations for this star could be explained by a companion with an orbital period of 6.9 days and a semi-amplitude of 725 m/s.

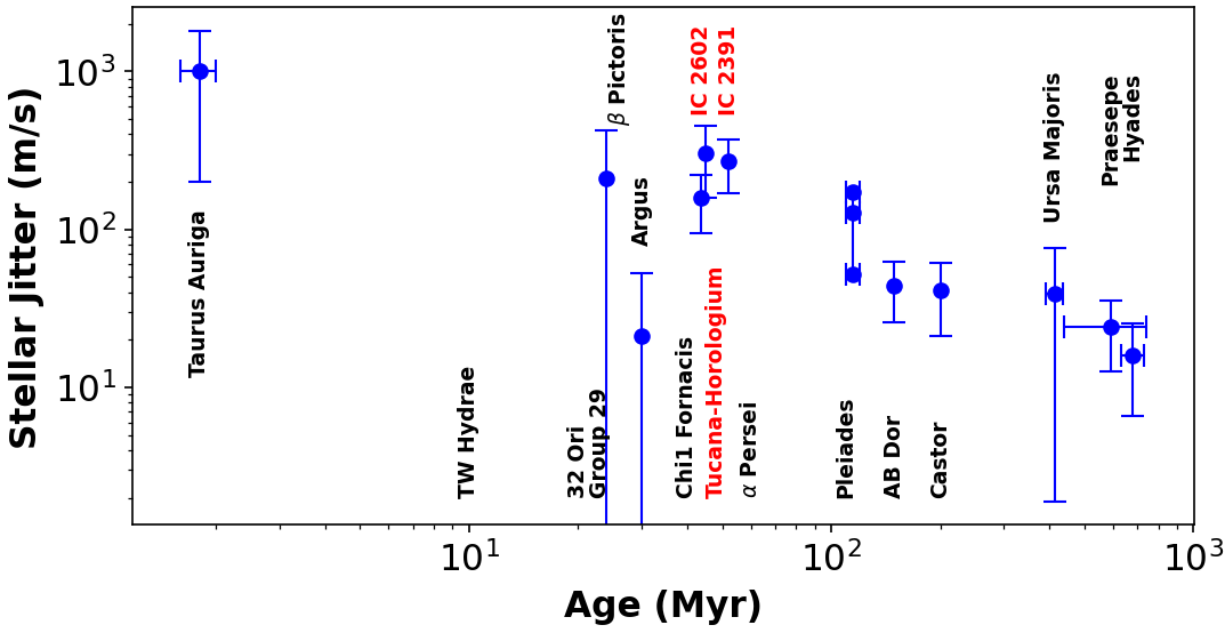

Figure 6.10 Stellar jitter measurements are plotted as a function of age for nearby open clusters and moving groups. The error bars are standard deviations of these jitter values. The names of the stellar populations studied in this dissertation are colored red.

Table 6.1: Jitter in young stellar populations

Name	Age (Myr)	Ref	Jitter (m/s)	Ref	Nstars
IC 2602	44	B18	168±83	this study	10
IC 2391	51	B18	225±123	this study	10
Tuc-Hor	40	K14	311±153	this study	9
Beta Pic	24	B15	211±211	L13	2
Argus	30	D13	21±32	L13	2
AB Dor	149	B15	44±18	C17	6
Castor	200	B98	41±20	PY06	7
Ursa Major	500	K03	37±39	PY06	9
Praesepe	578	D11	24±11	Q12	46
Hyades	750	BH15	22±12	Q14	16
Pleaides	115	D15	52-173	T20	30

Note. — Stellar Jitter values are presented for young stellar populations. References are as follows: B18 = Bravi et al. (2018); K14 = Kraus et al. (2014); B15 = Bell et al. (2015); D13 = De Silva et al. (2013); B98 = Barrado y Navascues (1998); K03 = King et al. (2003); D11 = Delorme et al. (2011); BH15 = Brandt Huang (2015); D15 = Dahm et al. (2015); L13 =

Lagrange et al. (2013), C17 = Cabrera Salazar (2017), PY06= Paulson & Yelda (2006), Q12,Q14 = Quinn et al. (2012,2014), and T20 = Takarada et al. (2020).

CHAPTER 7

CONCLUSIONS

In this dissertation, we present results from two main spectroscopic projects. In the first project, described in Chapters 2, 3, and 4, we map out the stellar populations of the young open clusters, IC 2602 and IC 2391. In the second project, described in Chapters 5 and 6, we monitor the RVs of Sun-like stars in IC 2602, IC 2391, and Tucana-Horologium to directly measure the stellar jitter at $\sim$ 50 Myr and potentially identify new exoplanet hosts. The main results of the first project are summarized in Section 7.1 and the main results of the second project are summarized in Section 7.2.

7.1 Summary of Spectroscopic Survey for New Candidate Members

We use *Gaia* DR2 positions, space motions, and photometry to map out the stellar populations of IC 2602 and IC 2391. Using the CHIRON spectrograph in fiber mode and Empirical SpecMatch, we determine stellar properties and measure signatures of youth for 38 stars. On the basis of this analysis, we obtain the following main results:

- We refine the single-star main sequences of IC 2602 (451 stars) and IC 2391 (350 stars). We find a large population of new candidate cluster members (331 stars in IC 2602, 198 stars in IC 2391), never reported before in the literature. The refined membership lists are useful for calibrating models of stellar evolution, planet formation and migration.

- We identify new candidate photometric (4 stars) and spectroscopic (10 stars) binaries; 6 of the latter are single-lined while 4 are double-lined. These findings can be used to

improve binary fraction estimates in these clusters. If follow-up observations reveal them to be eclipsing binaries as well, the data can be used to improve stellar evolution models and relations.

- We determine radial and projected rotational velocities, equivalent widths of lithium and Hα, effective temperatures, surface gravities, and metallicities for all 38 stars observed. We confirm that 13 IC 2602 and 12 IC 2391 new candidate members are *bona-fide* cluster members. This increases the spectroscopically confirmed stellar populations of these clusters (120 stars in IC 2602; 152 stars in IC 2391) by 12% and 8% respectively.

7.2 Summary of Monitoring Project to measure Stellar Jitter at $\sim$ 50 Myr

Using the CHIRON spectrograph in slicer mode, we monitor the precise RVs and line bisector spans of 29 slowly-rotating Sun-like stars in IC 2602, IC 2391, and Tucana-Horologium. Using CHIRON spectra and Empirical SpecMatch, we also determine stellar properties for the 29 stars in our sample. On the basis of this analysis, we obtain the following main results:

- We directly measure the stellar jitter at $\sim$ 50 Myr using 10 stars in IC 2602, 10 stars in IC 2391, and 9 stars in Tucana-Horologium. We measure the mean RV jitter of these stellar populations to be 168, 225, and 311 m/s, respectively. Using all 29 stars in our sample, we measure a mean stellar jitter of 237 m/s. This high stellar jitter is expected to mask most hot Jupiters with masses less than twice that of Jupiter.

- The measured stellar jitter values at $\sim$ 50 Myr fill out a gap in our knowledge of the magnitude and age-dependence of stellar jitter in the range of 10-100 Myr. Our results reveal that stellar jitter decreases linearly with age on a log-log plot.

- We identify an empirical relation between the dispersion of RVs and the dispersion of bisector spans. We find that candidate planet-hosts can be identified as points above this relation given their large variations in RV but their comparatively small

variations in bisector span. We identify 2 such candidate planet-hosts, PMM2012 and R45, based on 8 observations for each. However, it is difficult to confidently identify planet candidates based on line bisector analyses alone for stars with fewer than 10 observations. Follow-up observations for these stars suggest that the observed RV variations are most likely caused by stellar jitter.

- Based on Spearman rank-order correlation coefficients and associated p-values ($p > 0.05$) for the relationship between line bisector spans and RVs, 9 of the 29 stars in our sample have RV variations of ambiguous origin. We are unable to rule out stellar jitter as the cause of their observed RV variations.

- We demonstrate an instrumental RV precision of 7.5 m/s using the CHIRON spectrograph in slicer mode at $V \sim 8$. This precision declines to approximately 20 m/s at $V \sim 11$.

BIBLIOGRAPHY

Abt, H. A. & Morgan, W. W. 1972, ApJ, 174, L131. doi:10.1086/180965

Ammler-von Eiff M., Reiners A., 2012, A&A, 542, A116. doi:10.1051/0004-6361/201118724

Andrew S., Penoyre Z., Belokurov V., Evans N. W., Oh S., 2022, arXiv, arXiv:2206.04392

Anger S., Rizzuto A., Kraus A., 2020, AAS

Bailer-Jones C. A. L., 2015, PASP, 127, 994. doi:10.1086/683116

Bailer-Jones, C. A. L., Rybizki, J., Fouesneau, M., et al. 2018, AJ, 156, 58. doi:10.3847/1538-3881/aacb21

Bae J., Zhu Z., Baruteau C., Benisty M., Dullemond C. P., Facchini S., Isella A., et al., 2019, ApJL, 884, L41. doi:10.3847/2041-8213/ab46b0

Bailey J. I., Mateo M., White R. J., Shectman S. A., Crane J. D., Olszewski E. W., 2016, AJ, 152, 9. doi:10.3847/0004-6256/152/1/9

Baraffe, I., Homeier, D., Allard, F., et al. 2015, A&A, 577, A42. doi:10.1051/0004-6361/201425481

Baraffe I., Pratt J., Goffrey T., Constantino T., Folini D., Popov M. V., Walder R., et al., 2017, ApJL, 845, L6. doi:10.3847/2041-8213/aa82ff

Baratella M., D'Orazi V., Carraro G., Desidera S., Randich S., Magrini L., Adibekyan V., et al., 2020, A&A, 634, A34. doi:10.1051/0004-6361/201937055

Barnes S. A., Sofia S., Prosser C. F., Stauffer J. R., 1999, ApJ, 516, 263. doi:10.1086/307091

Barnes S. A., 2007, ApJ, 669, 1167. doi:10.1086/519295

Barrado y Navascues D., 1998, A&A, 339, 831

Barrado y Navascués D., Stauffer J. R., Patten B. M., 1999, ApJL, 522, L53. doi:10.1086/312212

Barrado Y Navascués, D., Stauffer, J. R., & Patten, B. M. 2000, Stellar Clusters and Associations: Convection, Rotation, and Dynamos, 198, 269

Barrado y Navascués, D., Stauffer, J. R., Briceño, C., et al. 2001, ApJS, 134, 103. doi:10.1086/320359

Barrado y Navascués, D., Stauffer, J. R., & Jayawardhana, R. 2004, ApJ, 614, 386. doi:10.1086/423485

Barragán O., Aigrain S., Kubyshkina D., Gandolfi D., Livingston J., Fridlund M. C. V., Fossati L., et al., 2019, MNRAS, 490, 698. doi:10.1093/mnras/stz2569

Baruteau C., Bai X., Mordasini C., Mollière P., 2016, SSRv, 205, 77. doi:10.1007/s11214-016-0258-z

Baştürk Ö., Dall T. H., Collet R., Lo Curto G., Selam S. O., 2011, A&A, 535, A17. doi:10.1051/0004-6361/201117740

Bell C. P. M., Mamajek E. E., Naylor T., 2015, MNRAS, 454, 593. doi:10.1093/mnras/stv1981

Bergeron P., Dufour P., Fontaine G., Coutu S., Blouin S., Genest-Beaulieu C., Bédard A., et al., 2019, ApJ, 876, 67. doi:10.3847/1538-4357/ab153a

Bildsten L., Brown E. F., Matzner C. D., Ushomirsky G., 1997, ApJ, 482, 442. doi:10.1086/304151

Binks A. S., Jeffries R. D., 2014, MNRAS, 438, L11. doi:10.1093/mnrasl/slt141

Blake C. H., Charbonneau D., White R. J., Marley M. S., Saumon D., 2007, ApJ, 666, 1198. doi:10.1086/520124

Bochanski J. J., Faherty J. K., Gagné J., Nelson O., Coker K., Smithka I., Desir D., et al., 2018, AJ, 155, 149. doi:10.3847/1538-3881/aaaebe

Bodenheimer P., 1965, ApJ, 142, 451. doi:10.1086/148310

Boss A. P., 1997, Sci, 276, 1836. doi:10.1126/science.276.5320.1836

Boudreault, S. & Bailer-Jones, C. A. L. 2009, ApJ, 706, 1484. doi:10.1088/0004-637X/706/2/1484

Bouma L. G., Hartman J. D., Brahm R., Evans P., Collins K. A., Zhou G., Sarkis P., et al., 2020, AJ, 160, 239. doi:10.3847/1538-3881/abb9ab

Braes, L. L. E. 1962, , 16, 297

Brandt, T. D. & Huang, C. X. 2015, ApJ, 807, 24. doi:10.1088/0004-637X/807/1/24

Brault J. W., Mueller E. A., 1975, SoPh, 41, 43. doi:10.1007/BF00152954

Bravi, L., Zari, E., Sacco, G. G., et al. 2018, A&A, 615, A37. doi:10.1051/0004-6361/201832645

Briceno, C., Calvet, N., Hernandez, J., et al. 2018, arXiv:1805.01008

Brewer J. M., Fischer D. A., Valenti J. A., Piskunov N., 2016, ApJS, 225, 32. doi:10.3847/0067-0049/225/2/32

Buscombe, W. 1965, MNRAS, 129, 411. doi:10.1093/mnras/129.6.411

Butler, R. P., Marcy, G. W., Williams, E., et al. 1996, PASP, 108, 500. doi:10.1086/133755

Cabrera Salazar, N. E., 2017, Dissertation, Georgia State University. doi:10.57709/9558001

Cantat-Gaudin, T., Jordi, C., Vallenari, A., et al. 2018, A&A, 618, A93. doi:10.1051/0004-6361/201833476

Cantat-Gaudin T., Krone-Martins A., Sedaghat N., Farahi A., de Souza R. S., Skalidis R., Malz A. I., et al., 2019, A&A, 624, A126. doi:10.1051/0004-6361/201834453

Cantat-Gaudin T., Anders F., Castro-Ginard A., Jordi C., Romero-Gómez M., Soubiran C., Casamiquela L., et al., 2020, A&A, 640, A1. doi:10.1051/0004-6361/202038192

Cantat-Gaudin T., Anders F., 2020, A&A, 633, A99. doi:10.1051/0004-6361/201936691

Cantat-Gaudin T., 2022, Univ, 8, 111. doi:10.3390/universe8020111

Carmichael T. W., Quinn S. N., Mustill A. J., Huang C., Zhou G., Persson C. M., Nielsen L. D., et al., 2020, AJ, 160, 53. doi:10.3847/1538-3881/ab9b84

Carpenter J. M., Mamajek E. E., Hillenbrand L. A., Meyer M. R., 2006, ApJL, 651, L49. doi:10.1086/509121

Carrasco J. M., Catalán S., Jordi C., Tremblay P.-E., Napiwotzki R., Luri X., Robin A. C., et al., 2014, A&A, 565, A11. doi:10.1051/0004-6361/201220596

Casagrande L., Schönrich R., Asplund M., Cassisi S., Ramírez I., Meléndez J., Bensby T., et al., 2011, A&A, 530, A138. doi:10.1051/0004-6361/201016276

Casali G., Spina L., Magrini L., Karakas A. I., Kobayashi C., Casey A. R., Feltzing S., et al., 2020, A&A, 639, A127. doi:10.1051/0004-6361/202038055

Casey, A. R., Ruchti, G., Masseron, T., et al. 2016, MNRAS, 461, 3336. doi:10.1093/mnras/stw1512

Castro-Ginard A., Jordi C., Luri X., Julbe F., Morvan M., Balaguer-Núñez L., Cantat-Gaudin T., 2018, A&A, 618, A59. doi:10.1051/0004-6361/201833390

Castro-Ginard A., Jordi C., Luri X., Cantat-Gaudin T., Balaguer-Núñez L., 2019, A&A, 627, A35. doi:10.1051/0004-6361/201935531

Castro-Ginard A., Jordi C., Luri X., Álvarez Cid-Fuentes J., Casamiquela L., Anders F., Cantat-Gaudin T., et al., 2020, A&A, 635, A45. doi:10.1051/0004-6361/201937386

Cayrel, R. 1988, The Impact of Very High S/N Spectroscopy on Stellar Physics, 132, 345

Chabrier G., Johansen A., Janson M., Rafikov R., 2014, prpl.conf, 619. doi:10.2458/azu_uapress_9780816531240-ch027

Chavero C., de la Reza R., Ghezzi L., Llorente de Andrés F., Pereira C. B., Giuppone C., Pinzón G., 2019, MNRAS, 487, 3162. doi:10.1093/mnras/stz1496

Chen X., Bourke T. L., Launhardt R., Henning T., 2008, ApJL, 686, L107. doi:10.1086/593033

Chereul E., Crézé M., Bienaymé O., 1999, A&AS, 135, 5. doi:10.1051/aas:1999160

Constantino T., Baraffe I., Goffrey T., Pratt J., Guillet T., Vlaykov D. G., Amard L., 2021, A&A, 654, A146. doi:10.1051/0004-6361/202141402

Conti P. S., Leep E. M., 1974, ApJ, 193, 113. doi:10.1086/153135

Crockett C. J., Mahmud N. I., Prato L., Johns-Krull C. M., Jaffe D. T., Hartigan P. M., Beichman C. A., 2012, ApJ, 761, 164. doi:10.1088/0004-637X/761/2/164

Crouzet N., Healy B. F., Hébrard G., McCullough P. R., Long D., Montañés-Rodríguez P., Ribas I., et al., 2020, AJ, 159, 44. doi:10.3847/1538-3881/ab5b1

Cumming A., Marcy G. W., Butler R. P., 1999, ApJ, 526, 890. doi:10.1086/308020

Cummings, J. D., Deliyannis, C. P., Maderak, R. M., et al. 2017, AJ, 153, 128. doi:10.3847/1538-3881/aa5b86

Czesla S., Schröter S., Schneider C. P., Huber K. F., Pfeifer F., Andreasen D. T., Zechmeister M., 2019, ascl.soft. ascl:1906.010

da Silva R., Milone A. de C., Rocha-Pinto H. J., 2015, A&A, 580, A24. doi:10.1051/0004-6361/201525770

Dahm S. E., 2015, ApJ, 813, 108. doi:10.1088/0004-637X/813/2/108

David T. J., Conroy K. E., Hillenbrand L. A., Stassun K. G., Stauffer J., Rebull L. M., Cody A. M., et al., 2016, AJ, 151, 112. doi:10.3847/0004-6256/151/5/112

David T. J., Hillenbrand L. A., Petigura E. A., Carpenter J. M., Crossfield I. J. M., Hinkley S., Ciardi D. R., et al., 2016, Natur, 534, 658. doi:10.1038/nature18293

David T. J., Cody A. M., Hedges C. L., Mamajek E. E., Hillenbrand L. A., Ciardi D. R., Beichman C. A., et al., 2019, AJ, 158, 79. doi:10.3847/1538-3881/ab290f

D'Orazi, V. & Randich, S. 2009, A&A, 501, 553. doi:10.1051/0004-6361/200811587

D'Orazi, V., De Silva, G. M., & Melo, C. F. H. 2017, A&A, 598, A86. doi:10.1051/0004-6361/201629888

De Silva, G. M., D'Orazi, V., Melo, C., et al. 2013, MNRAS, 431, 1005. doi:10.1093/mnras/stt153

Deliyannis, C. P., Pinsonneault, M. H., & Duncan, D. K. 1993, ApJ, 414, 740. doi:10.1086/173120

Deliyannis, C. P., Anthony-Twarog, B. J., Lee-Brown, D. B., et al. 2019, AJ, 158, 163. doi:10.3847/1538-3881/ab3fad

Delorme P., Collier Cameron A., Hebb L., Rostron J., Lister T. A., Norton A. J., Pollacco D., et al., 2011, MNRAS, 413, 2218. doi:10.1111/j.1365-2966.2011.18299.x

Desort M., Lagrange A.-M., Galland F., Udry S., Mayor M., 2007, A&A, 473, 983. doi:10.1051/0004-6361:20078144

Distefano E., Lanzafame A. C., Lanza A. F., Messina S., Spada F., 2016, A&A, 591, A43. doi:10.1051/0004-6361/201527698

Dobbie, P. D., Lodieu, N., & Sharp, R. G. 2010, MNRAS, 409, 1002. doi:10.1111/j.1365-2966.2010.17355.x

Dodd, R. J. 2004, MNRAS, 355, 959. doi:10.1111/j.1365-2966.2004.08378.x

Donati J.-F., Yu L., Moutou C., Cameron A. C., Malo L., Grankin K., Hébrard E., et al., 2017, MNRAS, 465, 3343. doi:10.1093/mnras/stw2904

Donor J., Frinchaboy P. M., Cunha K., O'Connell J. E., Allende Prieto C., Almeida A., Anders F., et al., 2020, AJ, 159, 199. doi:10.3847/1538-3881/ab77bc

Dreyer J. L. E., 1888, MmRAS, 49, 1

Drimmel, R., Bucciarelli, B., & Inno, L. 2019, Research Notes of the American Astronomical Society, 3, 79. doi:10.3847/2515-5172/ab2632

Dufour P., Blouin S., Coutu S., Fortin-Archambault M., Thibeault C., Bergeron P., Fontaine G., 2017, ASPC, 509, 3

Durisen R. H., Boss A. P., Mayer L., Nelson A. F., Quinn T., Rice W. K. M., 2007, prpl.conf, 607

Dutra C. M., Bica E., 2001, A&A, 376, 434. doi:10.1051/0004-6361:20010978

Eastman, J., Gaudi, B. S., & Agol, E. 2013, PASP, 125, 83. doi:10.1086/669497

Ebbets D., 1982, ApJS, 48, 399. doi:10.1086/190783

Eggen, O. J. 1975, PASP, 87, 37. doi:10.1086/129722

Eggen, O. J. 1983a, MNRAS, 204, 377. doi:10.1093/mnras/204.2.377

Eggen, O. J. 1983b, MNRAS, 204, 391. doi:10.1093/mnras/204.2.391

Eggen, O. J. 1991, AJ, 102, 2028. doi:10.1086/116025

Eggleton P. P., Kiseleva L. G., Hut P., 1998, ApJ, 499, 853. doi:10.1086/305670

Esplin, T. L. & Luhman, K. L. 2019, AJ, 158, 54. doi:10.3847/1538-3881/ab2594

Fabrycky D., Tremaine S., 2007, ApJ, 669, 1298. doi:10.1086/521702

Feinstein, A. 1961, PASP, 73, 410. doi:10.1086/127722

Figueira P., Marmier M., Bonfils X., di Folco E., Udry S., Santos N. C., Lovis C., et al., 2010, A&A, 513, L8. doi:10.1051/0004-6361/201014323

Figueira P., Oshagh M., Adibekyan V. Z., Santos N. C., 2014, A&A, 572, A51. doi:10.1051/0004-6361/201424902

Fischer D. A., Laughlin G., Butler R. P., Marcy G. W., Johnson J., Henry G., Valenti J., et al., 2004, arXiv, astro-ph/0409107

Foster, D. C., Byrne, P. B., Hawley, S. L., et al. 1997, A&AS, 126, 81. doi:10.1051/aas:1997251

Fortney J. J., Lodders K., Marley M. S., Freedman R. S., 2008, ApJ, 678, 1419. doi:10.1086/528370

Fortney J. J., Dawson R. I., Komacek T. D., 2021, JGRE, 126, e06629. doi:10.1029/2020JE006629

Franchini M., Morossi C., di Marcantonio P., Malagnini M. L., Chavez M., 2014, MNRAS, 442, 220. doi:10.1093/mnras/stu873

Froebrich D., Scholz A., Raftery C. L., 2007, MNRAS, 374, 399. doi:10.1111/j.1365-2966.2006.11148.x

Fujii M. S., Hori Y., 2019, A&A, 624, A110. doi:10.1051/0004-6361/201834677

Furlan E., Howell S. B., 2020, ApJ, 898, 47. doi:10.3847/1538-4357/ab9c9c

Gagné, J., Mamajek, E. E., Malo, L., et al. 2018, ApJ, 856, 23. doi:10.3847/1538-4357/aaae09

Gaia Collaboration, Prusti T., de Bruijne J. H. J., Brown A. G. A., Vallenari A., Babusiaux C., Bailer-Jones C. A. L., et al., 2016, A&A, 595, A1. doi:10.1051/0004-6361/201629272

Gaia Collaboration, Brown A. G. A., Vallenari A., Prusti T., de Bruijne J. H. J., Mignard F., Drimmel R., et al., 2016, A&A, 595, A2. doi:10.1051/0004-6361/201629512

Gaia Collaboration, van Leeuwen F., Vallenari A., Jordi C., Lindegren L., Bastian U., Prusti T., et al., 2017, A&A, 601, A19. doi:10.1051/0004-6361/201730552

Gaia Collaboration, Babusiaux, C., van Leeuwen, F., et al. 2018, A&A, 616, A10. doi:10.1051/0004-6361/201832843

Gaia Collaboration, 2022, yCat, I/355

Gaidos, E., Mann, A. W., Rizzuto, A., et al. 2017, MNRAS, 464, 850. doi:10.1093/mnras/stw2345

Gontcharov G. A., 2006, AstL, 32, 759. doi:10.1134/S1063773706110065

Grandjean A., Lagrange A.-M., Meunier N., Rubini P., Desidera S., Galland F., Borgniet S., et al., 2021, A&A, 650, A39. doi:10.1051/0004-6361/202039672

Gray, D. F. 1976, A Wiley-Science Publication, New York: Wiley, 1976

Gray, D. F. 1992, Camb. Astrophys. Ser., Vol. 20,

Gray D. F., 1994, PASP, 106, 1248. doi:10.1086/133502

Gutiérrez Albarrán, M. L., Montes, D., Gómez Garrido, M., et al. 2020, A&A, 643, A71. doi:10.1051/0004-6361/202037620

Gray D. F., 1996, IAUS, 176, 227

Hayes, C. R. & Friel, E. D. 2014, AJ, 147, 69. doi:10.1088/0004-6256/147/4/69

Haywood R. D., 2015, PhDT. doi:10.5281/zenodo.35161

Herbig G. H., 1985, ApJ, 289, 269. doi:10.1086/162887

Høg E., Fabricius C., Makarov V. V., Urban S., Corbin T., Wycoff G., Bastian U., et al., 2000, A&A, 355, L27

Hojjatpanah S., Oshagh M., Figueira P., Santos N. C., Amazo-Gómez E. M., Sousa S. G., Adibekyan V., et al., 2020, A&A, 639, A35. doi:10.1051/0004-6361/202038035

Howard A. W., Johnson J. A., Marcy G. W., Fischer D. A., Wright J. T., Bernat D., Henry G. W., et al., 2010, ApJ, 721, 1467. doi:10.1088/0004-637X/721/2/1467

Howell S. B., Sobeck C., Haas M., Still M., Barclay T., Mullally F., Troeltzsch J., et al., 2014, PASP, 126, 398. doi:10.1086/676406

Hubrig S., Briquet M., Morel T., Schöller M., González J. F., De Cat P., 2008, A&A, 488, 287. doi:10.1051/0004-6361:200809972

Hunt E. L., Reffert S., 2021, A&A, 646, A104. doi:10.1051/0004-6361/202039341

Iglesias-Marzoa R., López-Morales M., Jesús Arévalo Morales M., 2015, PASP, 127, 567. doi:10.1086/682056

James, H., 2022, AJ, in prep.

James D. J., Jardine M. M., Jeffries R. D., Randich S., Collier Cameron A., Ferreira M., 2000, MNRAS, 318, 1217. doi:10.1046/j.1365-8711.2000.03838.x

Jeffries R. D., 2014, EAS, 65, 289. doi:10.1051/eas/1465008

Johns-Krull C. M., McLane J. N., Prato L., Crockett C. J., Jaffe D. T., Hartigan P. M., Beichman C. A., et al., 2016, ApJ, 826, 206. doi:10.3847/0004-637X/826/2/206

Jones, J., White, R. J., Boyajian, T., et al. 2015, ApJ, 813, 58. doi:10.1088/0004-637X/813/1/58

Jurić M., Tremaine S., 2008, ApJ, 686, 603. doi:10.1086/590047

Kharchenko N. V., Piskunov A. E., Schilbach E., Röser S., Scholz R.-D., 2013, A&A, 558, A53. doi:10.1051/0004-6361/201322302

Kim J. S., Walter F. M., Wolk S. J., 2005, AJ, 129, 1564. doi:10.1086/428002

King J. R., Villarreal A. R., Soderblom D. R., Gulliver A. F., Adelman S. J., 2003, AJ, 125, 1980. doi:10.1086/368241

Kovács G., Hodgkin S., Sipőcz B., Pinfield D., Barrado D., Birkby J., Cappetta M., et al., 2013, EPJWC, 47, 01002. doi:10.1051/epjconf/20134701002

Kozai Y., 1962, AJ, 67, 591. doi:10.1086/108790

Kraus A. L., Shkolnik E. L., Allers K. N., Liu M. C., 2014, AJ, 147, 146. doi:10.1088/0004-6256/147/6/146

Lada, C. J. & Lada, E. A. 2003, ARA&A, 41, 57. doi:10.1146/annurev.astro.41.011802.094844

Lagrange A.-M., Meunier N., Chauvin G., Sterzik M., Galland F., Lo Curto G., Rameau J., et al., 2013, A&A, 559, A83. doi:10.1051/0004-6361/201220770

Lamers H. J. G. L. M., Leitherer C., 1993, ApJ, 412, 771. doi:10.1086/172960

Leitherer C., 1988, ApJ, 326, 356. doi:10.1086/166097

Levato H., 1974, PASP, 86, 940. doi:10.1086/129701

Levato, H., Garcia, B., Lousto, C., et al. 1988, AP&SS, 146, 361. doi:10.1007/BF00637586

Libralato M., Nardiello D., Bedin L. R., Borsato L., Granata V., Malavolta L., Piotto G., et al., 2016, MNRAS, 463, 1780. doi:10.1093/mnras/stw1932

Lidov M. L., 1962, P&SS, 9, 719. doi:10.1016/0032-0633(62)90129-0

Lin D. N. C., Bodenheimer P., Richardson D. C., 1996, Natur, 380, 606. doi:10.1038/380606a0

Lindegren L., Lammers U., Hobbs D., O'Mullane W., Bastian U., Hernández J., 2012, A&A, 538, A78. doi:10.1051/0004-6361/201117905

Lindegren, L., Hernández, J., Bombrun, A., et al. 2018, A&A, 616, A2. doi:10.1051/0004-6361/201832727

Ingber, L., 1996, Lester Ingber Papers 96as, Lester Ingber.

Liu L., Pang X., 2019, ApJS, 245, 32. doi:10.3847/1538-4365/ab530a

Livingston J. H., Dai F., Hirano T., Gandolfi D., Nowak G., Endl M., Velasco S., et al., 2018, AJ, 155, 115. doi:10.3847/1538-3881/aaa841

Livingston J. H., Dai F., Hirano T., Gandolfi D., Trani A. A., Nowak G., Cochran W. D., et al., 2019, MNRAS, 484, 8. doi:10.1093/mnras/sty3464

Lodieu, N., Pérez-Garrido, A., Smart, R. L., et al. 2019, A&A, 628, A66. doi:10.1051/0004-6361/201935533

López-Santiago J., Montes D., Gálvez-Ortiz M. C., Crespo-Chacón I., Martínez-Arnáiz R. M., Fernández-Figueroa M. J., de Castro E., et al., 2010, A&A, 514, A97. doi:10.1051/0004-6361/200913437

Luck R. E., 2018, AJ, 155, 111. doi:10.3847/1538-3881/aaa9b5

Luhman, K. L. & Esplin, T. L. 2020, AJ, 160, 44. doi:10.3847/1538-3881/ab9599

Luhn J. K., Wright J. T., Howard A. W., Isaacson H., 2020, AJ, 159, 235. doi:10.3847/1538-3881/ab855a

Luri X., Brown A. G. A., Sarro L. M., Arenou F., Bailer-Jones C. A. L., Castro-Ginard A., de Bruijne J., et al., 2018, A&A, 616, A9. doi:10.1051/0004-6361/201832964

Lyngå, G. 1962, Arkiv for Astronomi, 3, 65

Lyra W., Porto de Mello G. F., 2005, A&A, 431, 329. doi:10.1051/0004-6361:20040249

Maitzen H. M., Schneider H., Weiss W. W., 1988, A&AS, 75, 391

Maldonado J., Martínez-Arnáiz R. M., Eiroa C., Montes D., Montesinos B., 2010, A&A, 521, A12. doi:10.1051/0004-6361/201014948

Mann A. W., Gaidos E., Mace G. N., Johnson M. C., Bowler B. P., LaCourse D., Jacobs T. L., et al., 2016, ApJ, 818, 46. doi:10.3847/0004-637X/818/1/46

Mann A. W., Newton E. R., Rizzuto A. C., Irwin J., Feiden G. A., Gaidos E., Mace G. N., et al., 2016, AJ, 152, 61. doi:10.3847/0004-6256/152/3/61

Mann, A. W., Gaidos, E., Vanderburg, A., et al. 2017, AJ, 153, 64. doi:10.1088/1361-6528/aa5276

Marino A., Micela G., Peres G., Sciortino S., 2003, A&A, 407, L63. doi:10.1051/0004-6361:20031053

Marsden S. C., Waite I. A., Carter B. D., Donati J.-F., 2004, AN, 325, 246. doi:10.1002/asna.200310217

Marsden S. C., Waite I. A., Carter B. D., Donati J.-F., 2005, MNRAS, 359, 711. doi:10.1111/j.1365-2966.2005.08946.x

Marsden, S. C., Carter, B. D., & Donati, J.-F. 2009, MNRAS, 399, 888. doi:10.1111/j.1365-2966.2009.15319.x

Marsden S. C., Petit P., Jeffers S. V., Morin J., Fares R., Reiners A., do Nascimento J.-D., et al., 2014, MNRAS, 444, 3517. doi:10.1093/mnras/stu1663

Martínez-Arnáiz R., Maldonado J., Montes D., Eiroa C., Montesinos B., Ribas I., Solano E., 2010, ASSP, 14, 423. doi:10.1007/978-3-642-11250-8_110

Marzari F., Nagasawa M., 2020, MNRAS, 493, 427. doi:10.1093/mnras/staa271

McCormac J., Gillen E., Jackman J. A. G., Brown D. J. A., Bayliss D., Wheatley P. J., Anderson D. R., et al., 2020, MNRAS, 493, 126. doi:10.1093/mnras/staa115

Megessier C., Hensberge H., 1983, A&AS, 54, 483

Meibom S., Torres G., Fressin F., Latham D. W., Rowe J. F., Ciardi D. R., Bryson S. T., et al., 2013, Natur, 499, 55. doi:10.1038/nature12279

Mercer A., Stamatellos D., 2020, A&A, 633, A116. doi:10.1051/0004-6361/201936954

Merle, T., Van Eck, S., Jorissen, A., et al. 2017, A&A, 608, A95. doi:10.1051/0004-6361/201730442

Mermilliod J.-C., 1995, ASSL, 203, 127. doi:10.1007/978-94-011-0397-8_12

Mermilliod, J.-C., Mayor, M., & Udry, S. 2009, A&A, 498, 949. doi:10.1051/0004-6361/200810244

Messina S., Rodonò M., Guinan E. F., 2001, A&A, 366, 215. doi:10.1051/0004-6361:20000201

Messina, S., Pizzolato, N., Guinan, E. F., et al. 2003, A&A, 410, 671. doi:10.1051/0004-6361:20031203

Messina S., Desidera S., Turatto M., Lanzafame A. C., Guinan E. F., 2010, A&A, 520, A15. doi:10.1051/0004-6361/200913644

Messina S., Desidera S., Lanzafame A. C., Turatto M., Guinan E. F., 2011, A&A, 532, A10. doi:10.1051/0004-6361/201016116

Meunier N., Desort M., Lagrange A.-M., 2010, A&A, 512, A39. doi:10.1051/0004-6361/200913551

Montet B. T., Feinstein A. D., Luger R., Bedell M. E., Gully-Santiago M. A., Teske J. K., Wang S. X., et al., 2020, AJ, 159, 112. doi:10.3847/1538-3881/ab6d6d

Moulds V. E., Watson C. A., Bonfils X., Littlefair S. P., Simpson E. K., 2013, MNRAS, 430, 1709. doi:10.1093/mnras/sts709

Naoz S., 2016, ARA&A, 54, 441. doi:10.1146/annurev-astro-081915-023315

Nardiello D., Piotto G., Deleuil M., Malavolta L., Montalto M., Bedin L. R., Borsato L., et al., 2020, MNRAS, 495, 4924. doi:10.1093/mnras/staa1465

Nazé Y., Rauw G., 2008, A&A, 490, 801. doi:10.1051/0004-6361:200810364

Newton E. R., Mann A. W., Tofflemire B. M., Pearce L., Rizzuto A. C., Vanderburg A., Martinez R. A., et al., 2019, ApJL, 880, L17. doi:10.3847/2041-8213/ab2988

Newville, M., Stensitzki, T., Allen, D. B., et al. 2014, Zenodo

Nidever D. L., Marcy G. W., Butler R. P., Fischer D. A., Vogt S. S., 2002, ApJS, 141, 503. doi:10.1086/340570

Nielsen L. D., Bouchy F., Turner O., Giles H., Suárez Mascareño A., Lovis C., Marmier M., et al., 2019, A&A, 623, A100. doi:10.1051/0004-6361/201834577

Noyes R. W., Hartmann L. W., Baliunas S. L., Duncan D. K., Vaughan A. H., 1984, ApJ, 279, 763. doi:10.1086/161945

Ochsenbein, F., Bauer, P., & Marcout, J. 2000, A&AS, 143, 23. doi:10.1051/aas:2000169

Oshagh M., Santos N. C., Figueira P., Barros S. C. C., Donati J.-F., Adibekyan V., Faria J. P., et al., 2017, A&A, 606, A107. doi:10.1051/0004-6361/201731139

Paredes L. A., Henry T. J., Quinn S. N., Gies D. R., Hinojosa-Goñi R., James H.-S., Jao W.-C., et al., 2021, AJ, 162, 176. doi:10.3847/1538-3881/ac082a

Paulson D. B., Cochran W. D., Hatzes A. P., 2004, AJ, 127, 3579. doi:10.1086/420710

Paulson, D. B. & Yelda, S. 2006, PASP, 118, 706. doi:10.1086/504115

Pecaut, M. J. & Mamajek, E. E. 2013, ApJS, 208, 9. doi:10.1088/0067-0049/208/1/9

Penoyre Z., Belokurov V., Evans N. W., 2022, MNRAS, 513, 5270. doi:10.1093/mnras/stac1147

Pepper J., Gillen E., Parviainen H., Hillenbrand L. A., Cody A. M., Aigrain S., Stauffer J., et al., 2017, AJ, 153, 177. doi:10.3847/1538-3881/aa62ab

Perri F., Cameron A. G. W., 1974, Icar, 22, 416. doi:10.1016/0019-1035(74)90074-8

Persson C. M., Fridlund M., Barragán O., Dai F., Gandolfi D., Hatzes A. P., Hirano T., et al., 2018, A&A, 618, A33. doi:10.1051/0004-6361/201832867

Pettersson B., 1987, A&AS, 70, 69

Pinsonneault M., 1997, ARA&A, 35, 557. doi:10.1146/annurev.astro.35.1.557

Piskunov N. E., Valenti J. A., 2002, A&A, 385, 1095. doi:10.1051/0004-6361:20020175

Pizzolato N., Maggio A., Micela G., Sciortino S., Ventura P., 2003, A&A, 397, 147. doi:10.1051/0004-6361:20021560

Platais I., 1988, NInfo, 65, 119

Platais, I., Melo, C., Mermilliod, J.-C., et al. 2007, A&A, 461, 509. doi:10.1051/0004-6361:20065756

Pöhnl H., Maitzen H. M., Paunzen E., 2003, A&A, 402, 247. doi:10.1051/0004-6361:20030266

Pollack J. B., Hubickyj O., Bodenheimer P., Lissauer J. J., Podolak M., Greenzweig Y., 1996, Icar, 124, 62. doi:10.1006/icar.1996.0190

Povich M. S., Giampapa M. S., Valenti J. A., Tilleman T., Barden S., Deming D., Livingston W. C., et al., 2001, AJ, 121, 1136. doi:10.1086/318745

Puls J., Kudritzki R.-P., Herrero A., Pauldrach A. W. A., Haser S. M., Lennon D. J., Gabler R., et al., 1996, A&A, 305, 171

Queloz D., Henry G. W., Sivan J. P., Baliunas S. L., Beuzit J. L., Donahue R. A., Mayor M., et al., 2001, A&A, 379, 279. doi:10.1051/0004-6361:20011308

Quinn S. N., White R. J., Latham D. W., Buchhave L. A., Cantrell J. R., Dahm S. E., Fűrész G., et al., 2012, ApJL, 756, L33. doi:10.1088/2041-8205/756/2/L33

Quinn S. N., White R. J., Latham D. W., Buchhave L. A., Torres G., Stefanik R. P., Berlind P., et al., 2014, ApJ, 787, 27. doi:10.1088/0004-637X/787/1/27

Quinn, S. N. & White, R. J. 2016, ApJ, 833, 173. doi:10.3847/1538-4357/833/2/173

Ragusa, E., Rosotti, G., Teyssandier, J., et al. 2018, MNRAS, 474, 4460. doi:10.1093/mnras/stx3094

Rajpaul V., Aigrain S., Roberts S., 2016, MNRAS, 456, L6. doi:10.1093/mnrasl/slv164

Randich, S., Aharpour, N., Pallavicini, R., et al. 1997, A&A, 323, 86

Randich, S., Pallavicini, R., Meola, G., et al. 2001, A&A, 372, 862. doi:10.1051/0004-6361:20010339

Randich, S., Primas, F., Pasquini, L., et al. 2002, A&A, 387, 222. doi:10.1051/0004-6361:20020355

Randich, S., Bragaglia, A., Pastori, L., et al. 2005, The Messenger, 121, 18

Randich, S., Tognelli, E., Jackson, R., et al. 2018, A&A, 612, A99. doi:10.1051/0004-6361/201731738

Rasio F. A., Ford E. B., 1996, Sci, 274, 954. doi:10.1126/science.274.5289.954

Richer, H. B., Caiazzo, I., Du, H., et al. 2021, ApJ, 912, 165. doi:10.3847/1538-4357/abdeb7

Ricker G. R., Winn J. N., Vanderspek R., Latham D. W., Bakos G. Á., Bean J. L., Berta-Thompson Z. K., et al., 2014, SPIE, 9143, 914320. doi:10.1117/12.2063489

Riedel A. R., Alam M. K., Rice E. L., Cruz K. L., Henry T. J., 2017, ApJ, 840, 87. doi:10.3847/1538-4357/840/2/87

Rolleston, W. R. J. & Byrne, P. B. 1997, A&AS, 126, 357. doi:10.1051/aas:1997270

Saar S. H., Donahue R. A., 1997, ApJ, 485, 319. doi:10.1086/304392

Schröder C., Reiners A., Schmitt J. H. M. M., 2009, A&A, 493, 1099. doi:10.1051/0004-6361:200810377

Sestito P., Randich S., 2005, A&A, 442, 615. doi:10.1051/0004-6361:20053482

Shara M. M., Hurley J. R., Mardling R. A., 2016, ApJ, 816, 59. doi:10.3847/0004-637X/816/2/59

Siegler N., Muzerolle J., Young E. T., Rieke G. H., Mamajek E. E., Trilling D. E., Gorlova N., et al., 2007, ApJ, 654, 580. doi:10.1086/509042

Sim G., Lee S. H., Ann H. B., Kim S., 2019, JKAS, 52, 145. doi:10.5303/JKAS.2019.52.5.145

Simon, T. & Patten, B. M. 1998, PASP, 110, 283. doi:10.1086/316131

Skumanich A., 1972, ApJ, 171, 565. doi:10.1086/151310

Smiljanic R., Randich S., Pasquini L., 2011, A&A, 535, A75. doi:10.1051/0004-6361/201117157

Soderblom D. R., 2010, ARA&A, 48, 581. doi:10.1146/annurev-astro-081309-130806

Soderblom D. R., Hillenbrand L. A., Jeffries R. D., Mamajek E. E., Naylor T., 2014, prpl.conf, 219. doi:10.2458/azu_uapress_9780816531240-ch010

Sousa S. G., Alapini A., Israelian G., Santos N. C., 2010, A&A, 512, A13. doi:10.1051/0004-6361/200913388

Somers G., Pinsonneault M. H., 2014, ApJ, 790, 72. doi:10.1088/0004-637X/790/1/72

Soto M. G., Jenkins J. S., 2018, A&A, 615, A76. doi:10.1051/0004-6361/201731533

Soubiran C., Cantat-Gaudin T., Romero-Gómez M., Casamiquela L., Jordi C., Vallenari A., Antoja T., et al., 2018, A&A, 619, A155. doi:10.1051/0004-6361/201834020

Spiegel D. S., Burrows A., 2012, ApJ, 745, 174. doi:10.1088/0004-637X/745/2/174

Spina, L., Randich, S., Magrini, L., et al. 2017, A&A, 601, A70. doi:10.1051/0004-6361/201630078

Stahl O., Kaufer A., Rivinius T., Szeifert T., Wolf B., Gaeng T., Gummersbach C. A., et al., 1996, A&A, 312, 539

Stauffer J., Hartmann L. W., Jones B. F., McNamara B. R., 1989, ApJ, 342, 285. doi:10.1086/167592

Stauffer, J. R., Hartmann, L. W., Prosser, C. F., et al. 1997, ApJ, 479, 776. doi:10.1086/303930

Steinmetz M., Guiglion G., McMillan P. J., Matijevič G., Enke H., Kordopatis G., Zwitter T., et al., 2020, AJ, 160, 83. doi:10.3847/1538-3881/ab9ab8

Takarada T., Sato B., Omiya M., Hori Y., Fujii M. S., 2020, PASJ, 72, 104. doi:10.1093/pasj/psaa105

Thaller M. L., 1997, ApJ, 487, 380. doi:10.1086/304615

Thao P. C., Mann A. W., Johnson M. C., Newton E. R., Guo X., Kain I. J., Rizzuto A. C., et al., 2020, AJ, 159, 32. doi:10.3847/1538-3881/ab579b

Tognelli E., Degl'Innocenti S., Marcucci L. E., Prada Moroni P. G., 2015, PhLB, 742, 189. doi:10.1016/j.physletb.2015.01.033

Tognelli E., Degl'Innocenti S., Prada Moroni P. G., 2015, MmSAI, 86, 356

Tokovinin, A., Fischer, D. A., Bonati, M., et al. 2013, PASP, 125, 1336. doi:10.1086/674012

Toner C. G., Gray D. F., 1988, ApJ, 334, 1008. doi:10.1086/166893

Torres C. A. O., da Silva L., Quast G. R., de la Reza R., Jilinski E., 2000, AJ, 120, 1410. doi:10.1086/301539

Torres C. A. O., Quast G. R., da Silva L., de La Reza R., Melo C. H. F., Sterzik M., 2006, A&A, 460, 695. doi:10.1051/0004-6361:20065602

Torres, C. A. O., Quast, G. R., Melo, C. H. F., et al. 2008, Handbook of Star Forming Regions, Volume II, 757

Torres G., Konacki M., Sasselov D. D., Jha S., 2004, ApJ, 614, 979. doi:10.1086/423734

Tschäpe R., Rüdiger G., 2001, A&A, 377, 84. doi:10.1051/0004-6361:20010482

Valenti J. A., Fischer D. A., 2005, ApJS, 159, 141. doi:10.1086/430500

Vesper, D. N. & Honeycutt, R. K. 1993, PASP, 105, 731. doi:10.1086/133224

Viana Almeida P., Santos N. C., Melo C., Ammler-von Eiff M., Torres C. A. O., Quast G. R., Gameiro J. F., et al., 2009, A&A, 501, 965. doi:10.1051/0004-6361/200811194

Vincke K., Pfalzner S., 2018, ApJ, 868, 1. doi:10.3847/1538-4357/aae7d1

Weidenschilling S. J., Marzari F., 1996, Natur, 384, 619. doi:10.1038/384619a0

Wenger, M., Ochsenbein, F., Egret, D., et al. 2000, A&AS, 143, 9. doi:10.1051/aas:2000332

Wevers, T., Hodgkin, S. T., Jonker, P. G., et al. 2016, MNRAS, 458, 4530. doi:10.1093/mnras/stw643

White, R. J., Gabor, J. M., & Hillenbrand, L. A. 2007, AJ, 133, 2524. doi:10.1086/514336

White R. J., Basri G., 2003, ApJ, 582, 1109. doi:10.1086/344673

White R. J., Hillenbrand L. A., 2005, ApJL, 621, L65. doi:10.1086/428752

Whiteoak, J. B. 1961, MNRAS, 123, 245. doi:10.1093/mnras/123.3.245

Winn J. N., Fabrycky D. C., 2015, ARA&A, 53, 409. doi:10.1146/annurev-astro-082214-122246

Wright J. T., 2005, PASP, 117, 657. doi:10.1086/430369

Wright, J. T. & Eastman, J. D. 2014, PASP, 126, 838. doi:10.1086/678541

Wright J. T., Marcy G. W., Howard A. W., Johnson J. A., Morton T. D., Fischer D. A., 2012, ApJ, 753, 160. doi:10.1088/0004-637X/753/2/160

Wu Y., Murray N., 2003, ApJ, 589, 605. doi:10.1086/374598

Wu Y., Lithwick Y., 2011, ApJ, 735, 109. doi:10.1088/0004-637X/735/2/109

Wu, Z.-Y., Zhou, X., Ma, J., et al. 2009, MNRAS, 399, 2146. doi:10.1111/j.1365-2966.2009.15416.x

Yee, S. W., Petigura, E. A., & von Braun, K. 2017, ApJ, 836, 77. doi:10.3847/1538-4357/836/1/77

Yen S. X., Reffert S., Schilbach E., Röser S., Kharchenko N. V., Piskunov A. E., 2018, A&A, 615, A12. doi:10.1051/0004-6361/201731905

Yep, A. C., 2021, Dissertation, Georgia State University. doi:10.57709/23991663

Yep A. C., White R. J., 2022, MNRAS, 511, 4500. doi:10.1093/mnras/stab3725

Zhao L. L., Fischer D. A., Ford E. B., Wise A., Cretignier M., Aigrain S., Barragan O., et al., 2022, AJ, 163, 171. doi:10.3847/1538-3881/ac5176

Zhou G., Winn J. N., Newton E. R., Quinn S. N., Rodriguez J. E., Mann A. W., Rizzuto A. C., et al., 2020, ApJL, 892, L21. doi:10.3847/2041-8213/ab7d3c

Zhou G., Quinn S. N., Irwin J., Huang C. X., Collins K. A., Bouma L. G., Khan L., et al., 2021, AJ, 161, 2. doi:10.3847/1538-3881/abba22

Zuckerman B., Webb R. A., 2000, ApJ, 535, 959. doi:10.1086/308897

Zuckerman B., Song I., 2004, ARA&A, 42, 685. doi:10.1146/annurev.astro.42.053102.134111

Zuckerman, B., Klein, B., & Kastner, J. 2019, ApJ, 887, 87. doi:10.3847/1538-4357/ab45ea

Zwillinger, D. and Kokoska, S. (2000). CRC Standard Probability and Statistics Tables and Formulae. Chapman Hall: New York. 2000. Section 14.7

APPENDIX A

REFINED MEMBERSHIP LISTS

Table A.1: Refined Membership List of IC 2391

2MASS	RA (deg)	RA_{err} (deg)	DEC (deg)	DEC_{err} (deg)	Plx (mas)	Plx_{err} (mas)	pmRA (mas/yr)	$pmRA_{err}$ (mas/yr)	pmDEC (mas)	$pmDEC_{err}$ (mas/yr)	G (mag)	BP-RP (mag)
08422538-5306501	130.61	0.18	-53.11	0.24	7.11	0.23	-24.58	0.38	22.77	0.46	4.78	-0.24
08392384-5326230	129.85	0.12	-53.44	0.14	6.53	0.14	-25.79	0.31	21.19	0.32	5.42	-0.21
08395759-5303170	129.99	0.19	-53.05	0.23	6.76	0.21	-25.43	0.39	22.32	0.4	5.14	-0.2
08401759-5255190	130.07	0.34	-52.92	0.39	6.59	0.41	-30.56	0.78	21.43	0.76	3.47	-0.19
08401745-5300554	130.07	0.08	-53.02	0.09	6.46	0.09	-24.79	0.17	23.08	0.16	5.52	-0.18
08480022-5251006	132	0.04	-52.85	0.04	6.44	0.04	-24.95	0.07	23.27	0.07	6.25	-0.12
08384480-5305253	129.69	0.11	-53.09	0.12	6.98	0.12	-23.63	0.26	23.09	0.23	6.42	-0.11
08395937-5315393	130	0.05	-53.26	0.07	6.51	0.05	-23.66	0.11	23.62	0.13	7.2	-0.01
08404853-5248071	130.2	0.11	-52.8	0.13	6.67	0.12	-24.52	0.24	23.02	0.25	7.25	0
08420996-5258038	130.54	0.03	-52.97	0.04	6.63	0.04	-25.69	0.07	23.53	0.08	7.36	0.02
08232798-4536430	125.87	0.03	-45.61	0.04	6.56	0.04	-21.55	0.07	22.53	0.07	7.71	0.08
08371059-5315334	129.29	0.11	-53.26	0.12	6.6	0.13	-21.5	0.24	19.84	0.26	7.81	0.1
08293527-5525009	127.4	0.04	-55.42	0.05	7.16	0.04	-25.28	0.1	26.58	0.1	7.67	0.1
08382390-5343184	129.6	0.03	-53.72	0.03	6.77	0.04	-24.07	0.08	24.41	0.06	7.63	0.1
08430347-5304406	130.76	0.03	-53.08	0.03	6.45	0.03	-25.75	0.05	27.59	0.06	7.64	0.11
08433284-5200137	130.89	0.06	-52	0.07	6.41	0.07	-25.42	0.13	25.56	0.12	7.85	0.14
08391654-5218499	129.82	0.04	-52.31	0.04	6.67	0.04	-23.85	0.09	22.43	0.09	8.43	0.29
08400164-5242126	130.01	0.03	-52.7	0.03	6.64	0.03	-24.57	0.06	23.38	0.05	8.47	0.34
08395854-5303025	129.99	0.04	-53.05	0.04	6.61	0.04	-25.3	0.07	24.69	0.07	8.62	0.39

Table A.1: Refined Membership List of IC 2391

2MASS	RA (deg)	RA_{err} (deg)	DEC (deg)	DEC_{err} (deg)	Plx (mas)	Plx_{err} (mas)	pmRA (mas/yr)	$pmRA_{err}$ (mas/yr)	pmDEC (mas)	$pmDEC_{err}$ (mas/yr)	G (mag)	BP-RP (mag)
	127.84	0.13	-52.66	0.12	6.94	0.14	-26.78	0.27	15.91	0.28	18.14	0.44
08312173-4726369	127.84	0.03	-47.44	0.04	7.23	0.04	-25.23	0.08	24.47	0.06	8.63	0.48
08394304-5257510	129.93	0.02	-52.96	0.03	6.64	0.03	-25.44	0.05	22.48	0.05	8.99	0.52
08431790-5236112	130.82	0.02	-52.6	0.03	6.52	0.03	-24.65	0.05	22.76	0.05	9.03	0.54
	129.43	0.28	-46.08	0.3	7.3	0.34	-30.27	0.64	27.61	0.6	19.62	0.57
08421822-5354082	130.58	0.03	-53.9	0.03	6.64	0.04	-24.63	0.06	23.31	0.06	9.26	0.58
08562408-5419213	134.1	0.02	-54.32	0.02	7.05	0.02	-28.2	0.04	23.62	0.04	9.22	0.58
08362476-5015198	129.1	0.02	-50.26	0.03	6.53	0.03	-23.55	0.05	22.48	0.06	9.35	0.59
08412275-5338092	130.34	0.02	-53.64	0.02	6.53	0.02	-24.91	0.04	23.2	0.05	9.4	0.6
08374705-5252123	129.45	0.02	-52.87	0.02	6.53	0.02	-21.62	0.05	22.01	0.04	9.54	0.61
08385984-5301263	129.75	0.05	-53.02	0.06	6.84	0.06	-19.29	0.1	24.9	0.09	9.52	0.61
08200366-5355181	125.02	0.02	-53.92	0.03	7.09	0.03	-23.82	0.05	27.38	0.05	9.28	0.61
08435230-5313598	130.97	0.02	-53.23	0.02	6.64	0.03	-25.69	0.05	22.68	0.05	9.61	0.64
08421230-5306038	130.55	0.03	-53.1	0.04	6.6	0.03	-22.73	0.06	21.79	0.08	9.5	0.64
08410997-5254105	130.29	0.02	-52.9	0.03	6.58	0.03	-25.68	0.05	22.85	0.06	9.71	0.65
08453913-5225595	131.41	0.03	-52.43	0.03	6.54	0.03	-25.96	0.06	21.08	0.05	9.76	0.67
08411261-5715431	130.3	0.02	-57.26	0.03	7.35	0.02	-26.17	0.05	24.15	0.05	9.51	0.68
08280114-4841022	127	0.03	-48.68	0.02	6.75	0.03	-23.53	0.05	23.85	0.05	9.97	0.71
08395544-5121562	129.98	0.02	-51.37	0.03	6.54	0.03	-24.62	0.05	22.37	0.05	10.08	0.71

Table A.1: Refined Membership List of IC 2391

2MASS	RA (deg)	RA_{err} (deg)	DEC (deg)	DEC_{err} (deg)	Plx (mas)	Plx_{err} (mas)	pmRA (mas/yr)	$pmRA_{err}$ (mas/yr)	pmDEC (mas)	$pmDEC_{err}$ (mas/yr)	G (mag)	BP-RP (mag)
08362426-5401056	129.1	0.02	-54.02	0.02	6.47	0.02	-23.69	0.04	23.38	0.05	10.04	0.73
08342051-5250049	128.59	0.02	-52.83	0.03	6.49	0.03	-19.54	0.05	20.23	0.05	10.16	0.75
08424659-5301013	130.69	0.03	-53.02	0.03	6.38	0.03	-25.7	0.06	22.61	0.06	10.22	0.76
08284563-5205267	127.19	0.02	-52.09	0.02	6.42	0.02	-23.03	0.04	23.05	0.04	10.31	0.77
08454794-5325507	131.45	0.02	-53.43	0.02	6.71	0.03	-26.09	0.05	23.48	0.05	10.1	0.77
08461527-5345225	131.56	0.02	-53.76	0.02	6.65	0.03	-24.66	0.05	22.92	0.04	10.23	0.78
08410126-5431022	130.26	0.02	-54.52	0.02	6.89	0.02	-26.66	0.04	24.64	0.04	10.33	0.79
08400624-5338069	130.03	0.02	-53.64	0.02	6.29	0.02	-23.66	0.05	21.4	0.04	10.3	0.79
08561078-4929266	134.04	0.04	-49.49	0.04	7.16	0.05	-25.46	0.08	18.67	0.08	10.12	0.79
08440521-5253171	131.02	0.03	-52.89	0.03	6.54	0.03	-22.78	0.07	22	0.07	10.62	0.84
08393882-5310072	129.91	0.05	-53.17	0.06	6.65	0.06	-24.6	0.11	24.28	0.11	9.77	0.85
08382290-5256480	129.6	0.02	-52.95	0.02	6.66	0.02	-25.24	0.05	24.23	0.04	10.78	0.85
08385566-5257517	129.73	0.02	-52.96	0.03	6.53	0.03	-24.18	0.05	23.23	0.04	10.13	0.86
08404910-5337453	130.2	0.02	-53.63	0.02	6.71	0.02	-24.04	0.04	23.8	0.04	10.86	0.9
08430040-5354076	130.75	0.03	-53.9	0.03	6.38	0.03	-23.29	0.06	22.85	0.06	10.88	0.91
08390282-5242384	129.76	0.02	-52.71	0.02	6.5	0.02	-23.71	0.05	23.82	0.05	10.69	0.93
08570063-4523310	134.25	0.02	-45.39	0.04	6.57	0.03	-30.03	0.05	25.4	0.06	10.99	0.93
08375156-5345458	129.46	0.02	-53.76	0.02	6.68	0.02	-24.73	0.04	23.76	0.04	11.24	0.94
08255549-4733175	126.48	0.02	-47.55	0.03	6.66	0.03	-22.94	0.05	23.31	0.05	11.07	0.96

Table A.1: Refined Membership List of IC 2391

2MASS	RA (deg)	RA_{err} (deg)	DEC (deg)	DEC_{err} (deg)	Plx (mas)	Plx_{err} (mas)	pmRA (mas/yr)	$pmRA_{err}$ (mas/yr)	pmDEC (mas)	$pmDEC_{err}$ (mas/yr)	G (mag)	BP-RP (mag)
08365498-5308342	129.23	0.02	-53.14	0.02	6.71	0.02	-23.96	0.05	23.78	0.04	11.33	0.97
08442615-5242323	131.11	0.02	-52.71	0.02	6.58	0.03	-24.87	0.05	23.38	0.04	11.3	0.98
08433845-5130289	130.91	0.03	-51.51	0.04	6.54	0.05	-25.61	0.06	23.41	0.06	11.49	1.01
08421476-5256024	130.56	0.03	-52.93	0.03	6.59	0.03	-24.68	0.07	23.39	0.07	10.48	1.03
08435902-5333436	131	0.02	-53.56	0.02	6.7	0.03	-25.95	0.05	24	0.05	11.57	1.05
08401624-5256292	130.07	0.02	-52.94	0.03	6.54	0.03	-23.22	0.04	23.23	0.04	11.58	1.07
08395305-5257569	129.97	0.02	-52.97	0.02	6.56	0.02	-24.35	0.04	23.9	0.04	11.66	1.07
08435681-5241056	130.99	0.08	-52.68	0.08	6.68	0.09	-22.95	0.16	22.84	0.14	11.32	1.09
08443450-5255325	131.14	0.02	-52.93	0.02	6.44	0.02	-29.63	0.05	19.01	0.04	11.6	1.09
08375557-5257109	129.48	0.04	-52.95	0.04	6.62	0.05	-28.79	0.09	27.04	0.08	11.33	1.1
08593213-5106511	134.88	0.02	-51.11	0.02	6.21	0.02	-22.33	0.05	26.05	0.05	11.89	1.11
08583097-5040359	134.63	0.02	-50.68	0.03	7.23	0.03	-24.62	0.05	17.47	0.05	11.77	1.15
08432928-5241284	130.87	0.02	-52.69	0.02	6.61	0.03	-24.58	0.05	19.76	0.05	11.57	1.15
08462946-5256474	131.62	0.02	-52.95	0.02	6.78	0.03	-26.23	0.06	23.79	0.04	11.62	1.16
08341306-5258200	128.55	0.02	-52.97	0.02	6.7	0.02	-24.41	0.04	24.29	0.04	11.85	1.18
08341815-5215576	128.58	0.02	-52.27	0.02	6.44	0.02	-23.47	0.04	23.07	0.04	12.01	1.19
08202510-5340306	125.1	0.02	-53.68	0.02	6.51	0.02	-30.7	0.04	20.58	0.05	12.03	1.19
08441019-5343337	131.04	0.02	-53.73	0.03	6.68	0.03	-25.05	0.05	23.87	0.05	11.94	1.19
08583180-5040360	134.63	0.02	-50.68	0.02	7.19	0.03	-24.08	0.05	17.15	0.05	11.34	1.2

Table A.1: Refined Membership List of IC 2391

2MASS	RA (deg)	RA_{err} (deg)	DEC (deg)	DEC_{err} (deg)	Plx (mas)	Plx_{err} (mas)	pmRA (mas/yr)	$pmRA_{err}$ (mas/yr)	pmDEC (mas)	$pmDEC_{err}$ (mas/yr)	G (mag)	BP-RP (mag)
08473426-5429009	131.89	0.02	-54.48	0.02	6.55	0.02	-25.28	0.05	23.66	0.04	11.94	1.21
08350120-5214014	128.75	0.02	-52.23	0.02	6.83	0.02	-24.52	0.04	24.36	0.04	11.9	1.21
08433893-5130249	130.91	0.03	-51.51	0.04	6.5	0.04	-23.05	0.06	21.81	0.06	12.03	1.25
08354369-5321202	128.93	0.25	-53.36	0.27	6.34	0.28	-24.26	0.53	23.51	0.5	11.92	1.26
08473860-5216099	131.91	0.07	-52.27	0.08	6.95	0.09	-25.41	0.16	24.42	0.18	11.67	1.32
08392258-5355056	129.84	0.04	-53.92	0.05	6.48	0.05	-24.45	0.1	23.44	0.11	12.23	1.33
08452692-5252020	131.36	0.02	-52.87	0.02	6.65	0.02	-25.58	0.05	23.42	0.04	12.4	1.34
08354551-5315242	128.94	0.02	-53.26	0.02	6.54	0.02	-24.65	0.04	23.58	0.04	12.17	1.35
08412588-5322415	130.36	0.02	-53.38	0.02	6.65	0.03	-25.04	0.05	25.06	0.04	12.17	1.36
08375623-5257055	129.48	0.03	-52.95	0.03	6.66	0.03	-23.73	0.05	23.74	0.05	12.56	1.43
08365944-5219251	129.25	0.02	-52.32	0.03	6.31	0.03	-29.72	0.05	26.39	0.05	12.87	1.43
08383609-5206388	129.65	0.03	-52.11	0.02	6.63	0.03	-24.97	0.05	23.59	0.04	12.54	1.45
08320021-5539048	128	0.02	-55.65	0.02	6.92	0.02	-24.71	0.05	25.72	0.04	12.55	1.45
08415784-5252139	130.49	0.02	-52.87	0.03	6.58	0.03	-25.73	0.05	22.7	0.05	12.84	1.56
08372464-5254109	129.35	0.02	-52.9	0.02	6.54	0.02	-23.94	0.05	22.51	0.05	12.89	1.57
08401829-5330288	130.08	0.02	-53.51	0.02	6.6	0.02	-23.75	0.04	22.46	0.04	12.87	1.57
08294327-5105176	127.43	0.02	-51.09	0.01	6.56	0.02	-28.73	0.03	25.05	0.03	13.43	1.6
08413966-5259340	130.42	0.02	-52.99	0.03	6.58	0.03	-24.12	0.05	20.11	0.05	12.84	1.69
08434685-5250521	130.95	0.01	-52.85	0.01	6.59	0.02	-25.03	0.03	23.39	0.03	13.45	1.83

Table A.1: Refined Membership List of IC 2391

2MASS	RA (deg)	RA_{err} (deg)	DEC (deg)	DEC_{err} (deg)	Plx (mas)	Plx_{err} (mas)	pmRA (mas/yr)	$pmRA_{err}$ (mas/yr)	pmDEC (mas)	$pmDEC_{err}$ (mas/yr)	G (mag)	BP-RP (mag)
08432785-5257358	130.87	0.01	-52.96	0.01	6.61	0.01	-24.2	0.03	24.35	0.03	13.34	1.83
08493665-5254187	132.4	0.01	-52.91	0.02	6.36	0.02	-25.25	0.03	21.32	0.03	13.55	1.83
08371520-5320183	129.31	0.01	-53.34	0.01	6.58	0.01	-24.02	0.03	23.07	0.03	13.46	1.84
08370225-5246594	129.26	0.01	-52.78	0.01	6.55	0.01	-23.26	0.03	23.7	0.03	13.63	1.92
08344639-5327447	128.69	0.02	-53.46	0.02	6.5	0.02	-23.94	0.03	23.74	0.03	13.7	1.92
08423068-5257345	130.63	0.02	-52.96	0.02	6.59	0.02	-24.92	0.03	22.86	0.03	13.63	1.93
08395291-4957445	129.97	0.02	-49.96	0.02	6.62	0.02	-24.54	0.03	21.93	0.03	13.63	1.93
08502511-5308188	132.6	0.02	-53.14	0.02	6.5	0.02	-26.29	0.03	22.32	0.03	13.74	1.97
08392711-5352150	129.86	0.07	-53.87	0.08	7.01	0.08	-26.85	0.16	23.18	0.16	13.15	1.99
08385874-5319126	129.74	0.02	-53.32	0.02	6.6	0.02	-24.9	0.04	23	0.04	13.07	2.01
08520573-5113458	133.02	0.02	-51.23	0.02	6.31	0.03	-24.42	0.05	21	0.04	14.08	2.09
08401055-5309537	130.04	0.05	-53.16	0.06	6.29	0.06	-25.82	0.11	23.91	0.1	13.9	2.1
08395367-5318036	129.97	0.02	-53.3	0.02	6.57	0.02	-24.78	0.04	23.41	0.03	14.11	2.1
08421855-5301569	130.58	0.02	-53.03	0.03	6.56	0.02	-23.47	0.04	23.34	0.05	13.16	2.11
	130.87	0.04	-52.96	0.04	6.66	0.04	-26.48	0.09	22.77	0.09	13.69	2.18
08424099-5330359	130.67	0.02	-53.51	0.03	6.54	0.03	-24.13	0.05	23.69	0.06	14.34	2.26
08442025-5217087	131.08	0.24	-52.29	0.21	6.93	0.23	-26.39	0.52	22.97	0.42	14.33	2.28
08405752-5238207	130.24	0.02	-52.64	0.03	6.59	0.03	-25.24	0.06	23.57	0.06	14.37	2.28
08443068-5428556	131.13	0.02	-54.48	0.02	6.68	0.03	-29.68	0.05	23.86	0.05	13.8	2.28

Table A.1: Refined Membership List of IC 2391

2MASS	RA (deg)	RA_{err} (deg)	DEC (deg)	DEC_{err} (deg)	Plx (mas)	Plx_{err} (mas)	pmRA (mas/yr)	$pmRA_{err}$ (mas/yr)	pmDEC (mas)	$pmDEC_{err}$ (mas/yr)	G (mag)	BP-RP (mag)
08454418-5315116	131.43	0.02	-53.25	0.03	7.03	0.03	-26.93	0.05	24.29	0.05	14.31	2.3
08421130-5210232	130.55	0.04	-52.17	0.05	6.57	0.04	-25.18	0.08	23.15	0.09	13.76	2.33
08420879-5244496	130.54	0.03	-52.75	0.03	6.62	0.03	-24.9	0.07	23.01	0.06	14.06	2.34
08520865-5905038	133.04	0.03	-59.08	0.04	6.5	0.03	-25.97	0.07	23.41	0.08	14.66	2.35
08411411-5240213	130.31	0.04	-52.67	0.04	6.53	0.04	-24.27	0.1	23.75	0.09	14.68	2.4
08470861-5219587	131.79	0.03	-52.33	0.03	6.53	0.04	-25.14	0.06	22.95	0.06	14.73	2.41
08415154-5320597	130.46	0.03	-53.35	0.04	6.48	0.04	-24.58	0.07	23.3	0.07	14.71	2.45
08383911-5045113	129.66	0.06	-50.75	0.07	6.32	0.07	-24.17	0.13	15.12	0.14	14.82	2.46
08431058-5250135	130.79	0.08	-52.84	0.09	6.29	0.09	-24.89	0.19	25.24	0.17	14.6	2.47
08400821-5317408	130.03	0.03	-53.29	0.03	6.64	0.03	-24.77	0.07	24.08	0.06	14.87	2.5
08404808-5247302	130.2	0.04	-52.79	0.04	6.56	0.04	-24.26	0.09	23.07	0.09	14.88	2.5
08523295-5247230	133.14	0.03	-52.79	0.04	6.49	0.04	-25.94	0.08	21.95	0.06	14.87	2.5
08422615-5218516	130.61	0.04	-52.31	0.04	6.43	0.04	-24.1	0.08	22.04	0.08	14.97	2.53
08342872-4918278	128.62	0.03	-49.31	0.03	7.03	0.04	-26.53	0.07	23.65	0.06	14.81	2.53
08420492-5253539	130.52	0.04	-52.9	0.04	6.51	0.04	-24.44	0.08	23.37	0.08	14.83	2.53
08410820-5238056	130.28	0.03	-52.63	0.04	6.63	0.04	-25.58	0.08	24.05	0.08	15.1	2.59
08222743-5221351	125.61	0.04	-52.36	0.04	7.39	0.04	-24.09	0.08	27.58	0.07	14.87	2.6
08411014-5239211	130.29	0.04	-52.66	0.04	6.61	0.04	-25.16	0.09	23.51	0.1	15.17	2.64
08434574-5504409	130.94	0.05	-55.08	0.04	7.04	0.05	-27.61	0.1	25.35	0.08	14.88	2.65

Table A.1: Refined Membership List of IC 2391

2MASS	RA (deg)	RA_{err} (deg)	DEC (deg)	DEC_{err} (deg)	Plx (mas)	Plx_{err} (mas)	pmRA (mas/yr)	$pmRA_{err}$ (mas/yr)	pmDEC (mas)	$pmDEC_{err}$ (mas/yr)	G (mag)	BP-RP (mag)
08395349-5150452	129.97	0.08	-51.85	0.08	6.98	0.09	-26.37	0.17	24.36	0.17	16.48	2.66
08372893-4753243	129.37	0.04	-47.89	0.04	6.78	0.05	-23.5	0.08	22.49	0.08	15.25	2.67
08485107-5705449	132.21	0.03	-57.1	0.04	6.4	0.04	-25.56	0.08	22.67	0.08	15.32	2.67
08333581-5309499	128.4	0.04	-53.16	0.04	6.3	0.04	-23.3	0.08	23.67	0.07	15.39	2.67
	129.37	0.04	-47.89	0.04	6.65	0.05	-25.38	0.09	22.05	0.08	15.36	2.67
08403783-4724369	130.16	0.07	-47.41	0.07	6.9	0.08	-25.07	0.14	23.31	0.15	16.81	2.68
08371818-5255568	129.33	0.11	-52.93	0.13	6.5	0.13	-24.49	0.28	22.99	0.31	17.82	2.68
08562998-5242456	134.12	0.05	-52.71	0.05	6.6	0.06	-26.09	0.1	21.96	0.1	15.55	2.69
08422316-5341188	130.6	0.04	-53.69	0.05	6.55	0.05	-25.28	0.08	22.42	0.09	15.29	2.7
08433373-5313588	130.89	0.04	-53.23	0.04	6.61	0.04	-25.62	0.08	23.36	0.07	15.39	2.7
08394100-5211432	129.92	0.04	-52.2	0.05	6.49	0.05	-24.89	0.1	23.8	0.09	15.44	2.72
08404513-5248521	130.19	0.04	-52.81	0.04	6.4	0.05	-23.97	0.1	22.53	0.08	15.18	2.74
08544504-5512477	133.69	0.05	-55.21	0.05	6.77	0.06	-26.47	0.11	22.98	0.1	14.59	2.74
08484576-5319039	132.19	0.08	-53.32	0.08	6.43	0.08	-25.94	0.18	22.85	0.14	16.05	2.75
08393791-5300033	129.91	0.04	-53	0.05	6.63	0.05	-25.01	0.09	22.3	0.08	15.51	2.75
08262640-5445046	126.61	0.05	-54.75	0.05	6.48	0.05	-27.59	0.11	22.25	0.09	15.98	2.75
08354363-5158066	128.93	0.09	-51.97	0.1	6.38	0.1	-26.54	0.19	24.49	0.17	14.89	2.75
08513515-5729004	132.9	0.05	-57.48	0.05	7.08	0.05	-27.53	0.11	24.57	0.09	15.7	2.76
08392716-5309519	129.86	0.05	-53.16	0.04	6.59	0.05	-25.84	0.1	24.35	0.08	15.48	2.76

Table A.1: Refined Membership List of IC 2391

2MASS	RA (deg)	RA_{err} (deg)	DEC (deg)	DEC_{err} (deg)	Plx (mas)	Plx_{err} (mas)	pmRA (mas/yr)	$pmRA_{err}$ (mas/yr)	pmDEC (mas)	$pmDEC_{err}$ (mas/yr)	G (mag)	BP-RP (mag)
08293908-5305406	127.41	0.04	-53.09	0.04	6.63	0.05	-23.46	0.1	24.34	0.09	15.59	2.76
08403748-5307427	130.16	0.04	-53.13	0.05	6.55	0.05	-25.79	0.1	23.17	0.09	15.75	2.77
08383261-5256067	129.64	0.06	-52.94	0.07	6.23	0.07	-24.74	0.13	23.07	0.12	15.72	2.77
08332808-5229553	128.37	0.1	-52.5	0.11	6.63	0.11	-23.75	0.21	23.88	0.21	14.83	2.77
08392481-5332074	129.85	0.05	-53.54	0.05	6.61	0.05	-24.3	0.11	22.49	0.1	15.66	2.78
08441257-5337343	131.05	0.04	-53.63	0.05	6.63	0.05	-25.49	0.1	23.68	0.09	15.47	2.78
08243544-5051263	126.15	0.04	-50.86	0.05	6.87	0.05	-23.77	0.09	25.33	0.1	15.48	2.78
08392749-5334527	129.86	0.09	-53.58	0.11	6.41	0.11	-22.52	0.22	23.06	0.25	17.65	2.78
08350067-5529555	128.75	0.06	-55.5	0.07	7.08	0.07	-25.8	0.13	26.11	0.12	15.82	2.79
08385874-5301247	129.74	0.05	-53.02	0.06	6.46	0.07	-24.75	0.11	22.56	0.11	15.83	2.79
08413718-5212438	130.4	0.05	-52.21	0.06	6.65	0.06	-26.04	0.11	23.36	0.1	15.83	2.79
08365358-5250316	129.22	0.05	-52.84	0.06	6.31	0.06	-24.02	0.11	22.89	0.11	15.95	2.79
08484790-5252221	132.2	0.06	-52.87	0.07	6.59	0.07	-25.8	0.14	22.62	0.14	15.35	2.79
08510948-5218314	132.79	0.05	-52.31	0.05	6.35	0.06	-24.38	0.1	21.97	0.09	16.2	2.8
08525486-5308285	133.23	0.05	-53.14	0.06	6.61	0.06	-27.17	0.12	22.65	0.1	15.59	2.8
08425869-5305541	130.74	0.04	-53.1	0.04	6.75	0.04	-25.17	0.08	22.9	0.09	14.98	2.8
08492069-5411520	132.34	0.05	-54.2	0.05	6.47	0.06	-25.5	0.1	22.78	0.1	15.79	2.8
08372091-5152040	129.34	0.05	-51.87	0.05	6.66	0.06	-24.24	0.12	24	0.09	15.68	2.81
08411447-5343133	130.31	0.05	-53.72	0.06	6.61	0.06	-25.29	0.13	22.68	0.14	15.72	2.81

Table A.1: Refined Membership List of IC 2391

2MASS	RA (deg)	RA_{err} (deg)	DEC (deg)	DEC_{err} (deg)	Plx (mas)	Plx_{err} (mas)	pmRA (mas/yr)	$pmRA_{err}$ (mas/yr)	pmDEC (mas)	$pmDEC_{err}$ (mas/yr)	G (mag)	BP-RP (mag)
08231926-5346508	125.83	0.05	-53.78	0.04	6.38	0.05	-30.99	0.11	20.18	0.09	15.74	2.82
08350713-5304252	128.78	0.04	-53.07	0.06	6.53	0.05	-23.44	0.1	23.92	0.11	15.57	2.82
08314956-5245237	127.96	0.05	-52.76	0.05	6.69	0.05	-27.76	0.1	19.55	0.09	16.25	2.82
08365607-5231215	129.23	0.04	-52.52	0.05	6.39	0.05	-23.56	0.1	22.76	0.13	16.09	2.82
08310255-5629557	127.76	0.04	-56.5	0.05	6.39	0.04	-23.03	0.09	24.43	0.09	15.48	2.83
08355198-5352054	128.97	0.05	-53.87	0.06	6.46	0.05	-23.63	0.1	24.23	0.11	15.66	2.83
08475573-5445223	131.98	0.05	-54.76	0.05	6.92	0.06	-26.41	0.11	24.36	0.1	15.81	2.83
08380122-5232017	129.5	0.04	-52.53	0.04	6.73	0.05	-24.78	0.1	23.78	0.08	15.7	2.83
08413909-5309238	130.41	0.05	-53.16	0.06	6.86	0.06	-25.68	0.11	23.88	0.12	15.76	2.84
08491222-5327527	132.3	0.06	-53.46	0.07	6.81	0.07	-27.19	0.13	23.55	0.13	15.81	2.84
08415356-5257556	130.47	0.06	-52.97	0.08	6.54	0.07	-24.7	0.13	22.9	0.16	15.81	2.84
08245466-5735470	126.23	0.04	-57.6	0.05	7.26	0.05	-22.45	0.1	17.15	0.11	16.08	2.85
08343289-5352417	128.64	0.04	-53.88	0.05	6.2	0.05	-22.31	0.11	22.87	0.1	16.05	2.87
08453518-5459180	131.4	0.05	-54.99	0.06	6.89	0.06	-26.14	0.11	24.59	0.13	15.93	2.87
08471230-5051317	131.8	0.05	-50.86	0.06	6.77	0.06	-26.1	0.1	22.28	0.1	16.25	2.88
08354341-5220168	128.93	0.05	-52.34	0.07	6.64	0.07	-24.39	0.13	23.2	0.14	16.22	2.89
08502358-5336596	132.6	0.12	-53.62	0.14	6.68	0.12	-26.99	0.26	23.61	0.28	18.08	2.89
08394652-5219162	129.94	0.05	-52.32	0.06	6.65	0.06	-24.22	0.12	23.52	0.13	16.31	2.9
08390567-5321446	129.77	0.05	-53.36	0.06	6.72	0.06	-25.22	0.12	23.52	0.1	15.79	2.9

Table A.1: Refined Membership List of IC 2391

2MASS	RA (deg)	RA_{err} (deg)	DEC (deg)	DEC_{err} (deg)	Plx (mas)	Plx_{err} (mas)	pmRA (mas/yr)	$pmRA_{err}$ (mas/yr)	pmDEC (mas)	$pmDEC_{err}$ (mas/yr)	G (mag)	BP-RP (mag)
08464263-5508129	131.68	0.06	-55.14	0.06	6.85	0.06	-26.38	0.13	23.65	0.12	15.09	2.9
	132.19	0.06	-53.32	0.07	6.5	0.07	-25.68	0.14	22.06	0.12	16.03	2.9
08430352-5326571	130.76	0.07	-53.45	0.08	6.33	0.08	-25.22	0.16	22.56	0.18	16.79	2.92
08474672-5147396	131.94	0.05	-51.79	0.06	6.75	0.06	-26.46	0.11	23.05	0.1	15.91	2.92
08471290-5150300	131.8	0.06	-51.84	0.07	6.71	0.08	-25.56	0.14	22.9	0.16	16.51	2.92
08452471-5301227	131.35	0.06	-53.02	0.06	6.63	0.07	-24.55	0.14	22.98	0.12	16.44	2.93
08453846-5453327	131.41	0.06	-54.89	0.08	6.45	0.07	-24.17	0.13	22.99	0.15	16.54	2.93
08274484-5319217	126.94	0.06	-53.32	0.06	6.53	0.06	-22.74	0.14	24.16	0.13	16.29	2.94
08343096-5602569	128.63	0.05	-56.05	0.05	7.18	0.05	-26.13	0.11	26.07	0.09	15.71	2.94
08492254-5257411	132.34	0.04	-52.96	0.05	6.47	0.05	-25.98	0.09	22.05	0.11	16.06	2.95
08542939-5206159	133.62	0.05	-52.1	0.06	6.74	0.07	-26.22	0.12	22.54	0.14	16.14	2.97
08415765-5331090	130.49	0.06	-53.52	0.09	6.65	0.08	-24.91	0.14	23.81	0.19	16.46	2.98
08392784-5232586	129.87	0.05	-52.55	0.05	6.54	0.06	-24.07	0.13	22.42	0.11	16.58	2.98
08424846-5303184	130.7	0.06	-53.06	0.07	6.39	0.07	-24.87	0.14	23.15	0.16	16.76	2.98
08483385-5327456	132.14	0.05	-53.46	0.06	6.75	0.06	-26.6	0.11	23.89	0.1	16	3
08530884-5337231	133.29	0.06	-53.62	0.05	6.51	0.06	-26.03	0.13	22.5	0.1	16.18	3
08520910-5514253	133.04	0.07	-55.24	0.09	6.4	0.09	-26.5	0.17	22.95	0.19	16.04	3
08414722-5233175	130.45	0.06	-52.55	0.07	6.64	0.07	-24.92	0.14	22.01	0.16	16.31	3
08344264-5317025	128.68	0.05	-53.28	0.06	6.71	0.06	-23.81	0.12	24.17	0.15	16.02	3

Table A.1: Refined Membership List of IC 2391

2MASS	RA (deg)	RA_{err} (deg)	DEC (deg)	DEC_{err} (deg)	Plx (mas)	Plx_{err} (mas)	pmRA (mas/yr)	$pmRA_{err}$ (mas/yr)	pmDEC (mas)	$pmDEC_{err}$ (mas/yr)	G (mag)	BP-RP (mag)
08401809-5148109	130.08	0.09	-51.8	0.11	6.7	0.1	-24.34	0.18	22.05	0.21	15.82	3.01
08371520-5324130	129.31	0.07	-53.4	0.07	7.01	0.07	-25.47	0.15	25.26	0.14	16.77	3.01
08352178-5219410	128.84	0.07	-52.33	0.08	6.56	0.08	-23.78	0.15	23.58	0.19	16.57	3.01
08451667-4757453	131.32	0.07	-47.96	0.07	6.42	0.08	-24.19	0.15	21.05	0.13	17	3.01
08351153-5327129	128.8	0.06	-53.45	0.08	6.49	0.07	-23.9	0.13	24.39	0.15	16.27	3.01
08404989-5430219	130.21	0.05	-54.51	0.06	6.99	0.06	-26.53	0.12	24.75	0.1	16.32	3.02
08371285-5419367	129.3	0.07	-54.33	0.08	6.67	0.08	-24.49	0.16	24.14	0.16	16.65	3.02
08383696-5252424	129.65	0.07	-52.88	0.07	6.44	0.08	-23.09	0.17	23.46	0.15	16.97	3.03
08532403-5344060	133.35	0.05	-53.73	0.05	6.43	0.05	-25.85	0.11	21.9	0.09	15.59	3.03
08310632-5337250	127.78	0.08	-53.62	0.07	7.01	0.08	-30.45	0.18	21.18	0.15	17.18	3.04
08410847-5544371	130.29	0.1	-55.74	0.11	6.33	0.12	-25.37	0.26	24.93	0.26	17.77	3.05
08433841-5250551	130.91	0.07	-52.85	0.07	6.5	0.08	-24.9	0.16	22.72	0.14	16.49	3.05
08360063-4600437	129	0.08	-46.01	0.1	6.51	0.1	-28.55	0.18	26.46	0.2	16.91	3.06
08341816-5238452	128.58	0.06	-52.65	0.08	6.47	0.07	-23.21	0.13	23.16	0.16	16.73	3.06
08424726-5309229	130.7	0.12	-53.16	0.15	6.56	0.16	-25.11	0.33	23.63	0.33	17.93	3.06
08433935-5307556	130.91	0.05	-53.13	0.06	6.3	0.06	-24.17	0.11	23.91	0.14	16.31	3.07
08260487-4841236	126.52	0.06	-48.69	0.07	6.7	0.07	-22.92	0.14	23.89	0.12	15.71	3.07
08455376-5310055	131.47	0.06	-53.17	0.07	6.59	0.08	-25.35	0.15	23.31	0.16	16.71	3.08
08453190-5207592	131.38	0.14	-52.13	0.15	6.71	0.16	-24.82	0.29	22.84	0.29	18.25	3.08

Table A.1: Refined Membership List of IC 2391

2MASS	RA (deg)	RA_{err} (deg)	DEC (deg)	DEC_{err} (deg)	Plx (mas)	Plx_{err} (mas)	pmRA (mas/yr)	$pmRA_{err}$ (mas/yr)	pmDEC (mas)	$pmDEC_{err}$ (mas/yr)	G (mag)	BP-RP (mag)
08384728-5244326	129.7	0.14	-52.74	0.13	6.28	0.14	-23.95	0.32	23.42	0.29	18.47	3.08
08404175-5308348	130.17	0.08	-53.14	0.09	6.56	0.09	-24.04	0.19	23.52	0.2	17.16	3.08
08472257-5132535	131.84	0.24	-51.55	0.28	6.51	0.29	-29.7	0.56	17.08	0.64	16.84	3.09
08394843-5313583	129.95	0.07	-53.23	0.08	6.71	0.09	-24.77	0.16	24.09	0.14	16.84	3.09
08352798-5240319	128.87	0.06	-52.68	0.07	6.61	0.07	-23.13	0.15	22.71	0.15	16.58	3.1
08391040-5436118	129.79	0.07	-54.6	0.07	6.71	0.07	-25.22	0.16	24.02	0.15	16.87	3.11
08340352-5225103	128.51	0.08	-52.42	0.1	6.77	0.09	-24.13	0.2	23.99	0.23	17.02	3.11
08375686-5255547	129.49	0.06	-52.93	0.06	6.62	0.07	-25.01	0.15	24	0.13	16.37	3.11
08404439-5307000	130.18	0.24	-53.12	0.25	6.48	0.29	-24.61	0.61	21.88	0.49	19.23	3.11
08404704-5248310	130.2	0.09	-52.81	0.09	6.4	0.1	-24.28	0.22	23.82	0.22	17.29	3.11
08425983-5305070	130.75	0.13	-53.09	0.17	6.22	0.16	-23.89	0.31	22.88	0.39	18.34	3.12
08451883-5259257	131.33	0.07	-52.99	0.08	6.43	0.08	-25.14	0.16	22.56	0.16	16.96	3.13
08413595-5309268	130.4	0.05	-53.16	0.07	6.57	0.07	-24.61	0.14	22.86	0.16	16.68	3.13
08435941-5202192	131	0.07	-52.04	0.08	6.52	0.08	-25.12	0.17	22.08	0.16	17.03	3.13
08415135-5249079	130.46	0.07	-52.82	0.09	6.28	0.09	-23.72	0.18	22.83	0.21	16.95	3.13
08305460-5035377	127.73	0.07	-50.59	0.08	6.51	0.08	-23.05	0.14	22.7	0.16	16.71	3.14
08481211-5419348	132.05	0.07	-54.33	0.07	6.32	0.08	-24.8	0.15	22.99	0.13	15.92	3.14
08320809-5311055	128.03	0.11	-53.18	0.12	6.85	0.13	-23.73	0.23	24.26	0.24	17.94	3.15
08440464-5300016	131.02	0.06	-53	0.07	6.58	0.07	-24.32	0.16	23.64	0.16	16.91	3.15

Table A.1: Refined Membership List of IC 2391

2MASS	RA (deg)	RA_{err} (deg)	DEC (deg)	DEC_{err} (deg)	Plx (mas)	Plx_{err} (mas)	pmRA (mas/yr)	$pmRA_{err}$ (mas/yr)	pmDEC (mas)	$pmDEC_{err}$ (mas/yr)	G (mag)	BP-RP (mag)
08445554-5246418	131.23	0.06	-52.78	0.07	6.92	0.07	-24.98	0.14	23.76	0.14	16.69	3.15
08364573-5311330	129.19	0.07	-53.19	0.08	6.42	0.08	-23.59	0.15	24.57	0.17	17.11	3.15
08371605-5221396	129.32	0.06	-52.36	0.07	6.58	0.07	-24.33	0.15	23.27	0.14	16.88	3.16
08402789-5341365	130.12	0.06	-53.69	0.06	6.72	0.06	-24.65	0.15	24.08	0.13	16.96	3.16
08394056-5306074	129.92	0.09	-53.1	0.11	6.49	0.11	-24.71	0.21	24.13	0.25	17.57	3.16
08404828-5220294	130.2	0.06	-52.34	0.07	6.5	0.07	-24.38	0.13	22.82	0.15	16.7	3.16
08383657-5011516	129.65	0.06	-50.2	0.07	6.64	0.08	-23.94	0.15	22.28	0.16	16.77	3.17
08342721-5212483	128.61	0.06	-52.21	0.07	6.68	0.07	-24.15	0.15	24.17	0.14	16.64	3.17
08412915-5316223	130.37	0.07	-53.27	0.09	6.62	0.09	-24.84	0.19	22.4	0.2	17.17	3.17
08381883-5058073	129.58	0.07	-50.97	0.07	7.37	0.08	-27.33	0.16	25.07	0.15	16.48	3.17
08420631-5200062	130.53	0.09	-52	0.12	6.73	0.12	-25.83	0.2	23.14	0.29	17.68	3.18
08380059-5506206	129.5	0.06	-55.11	0.07	6.51	0.07	-23.58	0.15	24.96	0.15	16.1	3.18
08431548-5238493	130.81	0.06	-52.65	0.08	6.58	0.08	-25.26	0.14	23.01	0.15	16.13	3.18
08410809-5358445	130.28	0.07	-53.98	0.09	6.45	0.08	-24.94	0.15	22.72	0.18	16.96	3.19
08404084-5313317	130.17	0.09	-53.23	0.11	6.37	0.12	-24.98	0.28	22.85	0.22	17.1	3.19
08240751-4845349	126.03	0.1	-48.76	0.14	6.44	0.14	-21.9	0.24	22.58	0.26	17.72	3.19
08403030-5311308	130.13	0.09	-53.19	0.1	6.47	0.1	-24.51	0.22	23.19	0.23	17.45	3.19
08401609-5325476	130.07	0.07	-53.43	0.09	6.37	0.09	-24.21	0.16	23.41	0.2	17.16	3.21
08503837-4909072	132.66	0.08	-49.15	0.07	6.66	0.08	-24.27	0.16	21.13	0.15	16.29	3.21

Table A.1: Refined Membership List of IC 2391

2MASS	RA (deg)	RA_{err} (deg)	DEC (deg)	DEC_{err} (deg)	Plx (mas)	Plx_{err} (mas)	pmRA (mas/yr)	$pmRA_{err}$ (mas/yr)	pmDEC (mas)	$pmDEC_{err}$ (mas/yr)	G (mag)	BP-RP (mag)
08423215-5351398	130.63	0.07	-53.86	0.08	6.38	0.08	-25.23	0.15	22.77	0.17	17.1	3.21
08374058-5345579	129.42	0.08	-53.77	0.09	6.8	0.09	-24.16	0.18	24.61	0.19	17.3	3.21
08424903-5252157	130.7	0.06	-52.87	0.07	6.42	0.08	-25.68	0.15	23.77	0.15	15.99	3.21
08285672-4816195	127.24	0.12	-48.27	0.13	6.66	0.14	-22.04	0.26	23.03	0.28	17.86	3.22
08441929-5209384	131.08	0.08	-52.16	0.08	6.67	0.09	-24.99	0.16	22.59	0.16	17	3.22
08362092-5240120	129.09	0.08	-52.67	0.1	6.35	0.1	-23.87	0.22	23.57	0.19	16.46	3.23
08415490-5449131	130.48	0.05	-54.82	0.05	6.86	0.06	-26.66	0.11	24.55	0.1	15.94	3.23
08434102-5110565	130.92	0.08	-51.18	0.09	6.59	0.1	-25.68	0.18	22.36	0.18	17.53	3.23
08421152-5155140	130.55	0.08	-51.92	0.09	6.62	0.1	-24.45	0.18	24.62	0.19	17.22	3.23
08430678-5315450	130.78	0.1	-53.26	0.1	6.31	0.11	-24.26	0.24	23.33	0.22	17.31	3.23
08434809-5332567	130.95	0.08	-53.55	0.1	6.63	0.1	-25.91	0.2	24.03	0.22	17.28	3.23
08413471-5554255	130.39	0.05	-55.91	0.06	7.24	0.06	-27.48	0.13	25.36	0.12	16.56	3.24
08412598-5326349	130.36	0.08	-53.44	0.08	6.49	0.09	-23.79	0.17	22.11	0.16	16.66	3.25
08475640-5229210	131.98	0.1	-52.49	0.11	6.72	0.12	-26.2	0.23	22.1	0.25	17.68	3.26
08475929-5327406	132	0.07	-53.46	0.08	6.62	0.09	-25.75	0.16	21.8	0.15	16.93	3.26
08404046-5322507	130.17	0.08	-53.38	0.09	6.55	0.09	-24.92	0.18	23.48	0.19	17.14	3.27
08413679-5356019	130.4	0.1	-53.93	0.1	6.71	0.11	-25.4	0.22	24.38	0.2	16.51	3.27
08405301-5223001	130.22	0.08	-52.38	0.1	6.45	0.09	-24.19	0.17	22.35	0.22	17.38	3.27
08450191-5333282	131.26	0.09	-53.56	0.11	6.73	0.12	-24.8	0.23	22.38	0.23	17.76	3.28

Table A.1: Refined Membership List of IC 2391

2MASS	RA (deg)	RA$_{err}$ (deg)	DEC (deg)	DEC$_{err}$ (deg)	Plx (mas)	Plx$_{err}$ (mas)	pmRA (mas/yr)	pmRA$_{err}$ (mas/yr)	pmDEC (mas)	pmDEC$_{err}$ (mas/yr)	G (mag)	BP-RP (mag)
08410885-5248386	130.29	0.07	-52.81	0.08	6.46	0.08	-23.79	0.16	23.26	0.18	16.86	3.28
08360225-5237159	129.01	0.07	-52.62	0.09	6.43	0.09	-24.18	0.17	24.37	0.21	17.16	3.28
08381187-5222510	129.55	0.11	-52.38	0.12	6.5	0.14	-24.95	0.27	23.41	0.29	18.23	3.28
08400954-5337498	130.04	0.1	-53.63	0.11	6.61	0.11	-24.56	0.23	23.2	0.27	17.98	3.28
08411247-5438286	130.3	0.06	-54.64	0.08	6.86	0.08	-25.33	0.14	24.34	0.15	16.41	3.29
08532096-5306267	133.34	0.09	-53.11	0.09	6.72	0.11	-26.15	0.21	21.65	0.18	17.56	3.3
08454560-5312378	131.44	0.12	-53.21	0.13	6.49	0.15	-25.08	0.27	23.07	0.26	18.03	3.3
08432375-5314159	130.85	0.18	-53.24	0.19	6.68	0.2	-24.47	0.4	23.63	0.4	18.73	3.31
08382430-5315047	129.6	0.07	-53.25	0.07	6.55	0.07	-24.65	0.15	23.09	0.14	16.89	3.31
08454259-5259286	131.43	0.1	-52.99	0.11	6.25	0.12	-25.68	0.24	22.25	0.24	17.94	3.32
08375918-5321554	129.5	0.12	-53.37	0.13	6.52	0.14	-23.32	0.28	23.61	0.29	17.95	3.32
08504797-5428285	132.7	0.09	-54.47	0.11	6.29	0.11	-25	0.22	22.72	0.23	17.36	3.33
08411237-5309100	130.3	0.11	-53.15	0.12	6.4	0.13	-23.87	0.27	23.15	0.3	17.79	3.33
08372434-5316494	129.35	0.14	-53.28	0.16	6.36	0.17	-24.14	0.3	23.62	0.38	18.21	3.33
08524693-5212501	133.2	0.13	-52.21	0.13	6.59	0.14	-26.98	0.3	22.39	0.28	18.1	3.33
08352155-5424552	128.84	0.07	-54.42	0.08	6.4	0.08	-23.79	0.17	23.86	0.16	16.51	3.33
08382711-5325105	129.61	0.07	-53.42	0.08	6.72	0.08	-25.36	0.17	24.84	0.17	17.31	3.35
08391095-5401011	129.8	0.1	-54.02	0.12	6.72	0.11	-23.69	0.22	23.8	0.24	17.4	3.35
08424578-5250065	130.69	0.25	-52.84	0.31	6.48	0.31	-23.75	0.55	23.03	0.59	18.99	3.35

Table A.1: Refined Membership List of IC 2391

2MASS	RA (deg)	RA_{err} (deg)	DEC (deg)	DEC_{err} (deg)	Plx (mas)	Plx_{err} (mas)	pmRA (mas/yr)	$pmRA_{err}$ (mas/yr)	pmDEC (mas)	$pmDEC_{err}$ (mas/yr)	G (mag)	BP-RP (mag)
08322976-5545212	128.12	0.1	-55.76	0.11	7.29	0.11	-26.72	0.22	27.6	0.2	17.76	3.36
08384226-5230371	129.68	0.07	-52.51	0.08	6.72	0.08	-25.05	0.15	23.86	0.18	17.26	3.37
08420134-5244422	130.51	0.09	-52.74	0.1	6.59	0.11	-24.35	0.21	23.41	0.23	17	3.37
08405520-5234499	130.23	0.07	-52.58	0.09	6.55	0.09	-25.62	0.18	23.53	0.2	17.02	3.38
08500234-5221238	132.51	0.13	-52.36	0.13	6.66	0.15	-25.09	0.28	21.56	0.24	17.93	3.39
08401000-5235115	130.04	0.07	-52.59	0.08	6.44	0.08	-24.52	0.18	23.47	0.16	16.74	3.39
08393118-5430504	129.88	0.11	-54.51	0.13	6.79	0.12	-25.22	0.24	24.57	0.25	17.87	3.39
08515384-5821566	132.97	0.07	-58.37	0.08	7.24	0.08	-28.86	0.15	25.53	0.18	16.48	3.4
08462628-5301534	131.61	0.13	-53.03	0.14	6.85	0.15	-24.24	0.3	23.18	0.27	18.14	3.41
08455439-4938400	131.48	0.08	-49.64	0.08	6.97	0.09	-24.89	0.17	22.21	0.15	17.27	3.41
08423185-4931198	130.63	0.06	-49.52	0.07	7.08	0.08	-26.44	0.13	23.86	0.13	16.99	3.41
08402769-5230007	130.12	0.08	-52.5	0.09	6.29	0.09	-23.55	0.18	22.17	0.2	17.28	3.42
08372520-5231159	129.35	0.12	-52.52	0.12	7.02	0.13	-25.53	0.27	24.42	0.28	18.06	3.43
08260871-4822281	126.54	0.11	-48.37	0.13	6.79	0.13	-23.41	0.25	24.32	0.25	17.74	3.43
08343253-5252050	128.64	0.13	-52.87	0.16	6.31	0.15	-22.76	0.29	23.23	0.36	18.16	3.44
08483562-5153275	132.15	0.11	-51.89	0.12	6.76	0.14	-25.75	0.26	22.53	0.26	18	3.46
08270150-5455438	126.76	0.12	-54.93	0.12	6.99	0.14	-25.61	0.24	27.32	0.2	17.95	3.47
08364036-5321300	129.17	0.11	-53.36	0.13	6.57	0.13	-23.78	0.25	23.42	0.32	18.13	3.48
08472808-5328411	131.87	0.19	-53.48	0.2	6.76	0.23	-26.15	0.42	22.43	0.4	18.83	3.48

Table A.1: Refined Membership List of IC 2391

2MASS	RA (deg)	RA_{err} (deg)	DEC (deg)	DEC_{err} (deg)	Plx (mas)	Plx_{err} (mas)	pmRA (mas/yr)	$pmRA_{err}$ (mas/yr)	pmDEC (mas)	$pmDEC_{err}$ (mas/yr)	G (mag)	BP-RP (mag)
08443421-5308321	131.14	0.18	-53.14	0.19	7.22	0.2	-29.15	0.41	26.77	0.4	18.72	3.48
08431512-5258228	130.81	0.13	-52.97	0.15	6.72	0.16	-24.45	0.33	23.76	0.34	17.6	3.48
08544460-5454503	133.69	0.16	-54.91	0.18	6.48	0.18	-26.44	0.36	21.39	0.36	18.14	3.49
08423002-5421174	130.62	0.14	-54.35	0.16	6.47	0.16	-24	0.34	22.38	0.32	18.2	3.49
08401447-5838109	130.06	0.17	-58.64	0.18	7.35	0.19	-27.16	0.39	27.25	0.38	18.36	3.5
08352160-5342051	128.84	0.15	-53.7	0.21	6.63	0.19	-24.3	0.36	24.9	0.54	18.51	3.5
08401477-5327362	130.06	0.13	-53.46	0.14	6.7	0.15	-23.6	0.27	23.16	0.27	18.08	3.55
08423486-5228561	130.65	0.23	-52.48	0.29	6.69	0.28	-24.07	0.54	23.43	0.61	18.96	3.55
08574836-5941234	134.45	0.18	-59.69	0.18	6.37	0.19	-25.55	0.38	22.31	0.34	18.55	3.55
08480858-5305372	132.04	0.09	-53.09	0.1	6.48	0.11	-25.21	0.22	23.14	0.21	17.59	3.56
08590302-5221535	134.76	0.16	-52.36	0.17	6.48	0.19	-27.28	0.34	22.1	0.3	17.51	3.57
08432174-5200544	130.84	0.11	-52.02	0.13	6.81	0.13	-25.6	0.24	23.61	0.24	18.08	3.58
08412877-5121114	130.37	0.14	-51.35	0.18	6.39	0.17	-25.75	0.29	22.05	0.38	18.34	3.61
08460200-5152444	131.51	0.17	-51.88	0.19	6.64	0.2	-24.36	0.36	21.97	0.39	18.52	3.62
08321518-5344422	128.06	0.17	-53.74	0.18	6.32	0.19	-22.74	0.37	23.13	0.39	18.35	3.64
08354209-5401227	128.93	0.17	-54.02	0.24	6.59	0.2	-28.04	0.42	26.89	0.71	18.62	3.71
08345831-5232131	128.74	0.21	-52.54	0.25	6.73	0.24	-24.22	0.46	22.58	0.59	18.85	3.72
08415898-5312368	130.5	0.13	-53.21	0.17	6.72	0.17	-24.73	0.34	23.35	0.44	18.25	3.74
08470344-5246523	131.76	0.11	-52.78	0.11	6.53	0.13	-25.77	0.25	22.1	0.25	17.96	3.78

Table A.1: Refined Membership List of IC 2391

2MASS	RA (deg)	RA_{err} (deg)	DEC (deg)	DEC_{err} (deg)	Plx (mas)	Plx_{err} (mas)	pmRA (mas/yr)	$pmRA_{err}$ (mas/yr)	pmDEC (mas)	$pmDEC_{err}$ (mas/yr)	G (mag)	BP-RP (mag)
08421871-5239398	130.58	0.22	-52.66	0.31	6.46	0.27	-25.55	0.5	23.53	0.79	19.02	3.83
08503994-5449203	132.67	0.12	-54.82	0.13	7.19	0.14	-28.03	0.3	24.74	0.28	18.13	3.92
08440210-5244107	131.01	0.25	-52.74	0.27	6.39	0.29	-23.69	0.51	24.49	0.57	18.89	3.93
08452888-5347108	131.37	0.17	-53.79	0.19	6.92	0.19	-26.92	0.36	24.79	0.36	18.24	3.96
08392711-5352150	129.75	0.1	-53.02	0.09	6.66	0.09	-25.81	0.21	26.11	0.14	12.83	nan
	129.86	0.06	-53.87	0.04	6.7	0.05	-22.24	0.15	22.56	0.08	13.96	nan
08393692-5805092	129.9	0.13	-58.09	0.11	6.87	0.11	-24.86	0.27	19.1	0.2	16.99	nan
08520910-5514253	133.04	0.18	-55.24	0.23	6.52	0.19	-23.33	0.41	19.2	0.61	17.63	nan

Note. — The complete table of 350 candidate cluster members of IC 2391 identified using the prescription of Chapter 2 is provided. Here, the astrometric and photometric parameter values are concatenated to two decimal places.

Table A.2: Refined Membership List of IC 2602

2MASS	RA (deg)	RA_{err} (deg)	DEC (deg)	DEC_{err} (deg)	Plx (mas)	Plx_{err} (mas)	pmRA (mas/yr)	$pmRA_{err}$ (mas/yr)	pmDEC (mas)	$pmDEC_{err}$ (mas/yr)	G (mag)	BP-RP (mag)
10465124-6423005	161.71	0.18	-64.38	0.16	6.34	32.8	-18.92	0.33	9.45	0.3	4.78	-0.22
10401142-6506006	160.05	0.1	-65.1	0.1	6.49	56.38	-19.31	0.2	9.56	0.19	5.45	-0.2
10440694-6357400	161.03	0.28	-63.96	0.52	6.81	14.69	-15.03	0.45	11.41	0.56	4.72	-0.19
10461656-6430526	161.57	0.1	-64.51	0.09	6.41	60.2	-16.19	0.2	10.85	0.18	5.28	-0.13
10462961-6415475	161.62	0.15	-64.26	0.15	6.76	38.7	-17.9	0.29	9.54	0.27	5.17	-0.1
10392283-6406423	159.84	0.04	-64.11	0.04	6.33	140.22	-16.88	0.09	9.93	0.08	6.3	-0.09
10043407-6438518	151.14	0.03	-64.65	0.03	6.47	195.3	-14.11	0.05	13.18	0.05	6.89	-0.08
10381755-6502310	159.57	0.04	-65.04	0.04	6.48	138.77	-17.5	0.07	11.54	0.07	6.7	-0.07
10410641-6428278	160.28	0.03	-64.47	0.03	6.49	190.05	-17.21	0.07	10.67	0.06	6.69	-0.05
10264443-6421062	156.68	0.04	-64.35	0.03	6.43	173.15	-15.76	0.07	11.77	0.06	7.4	0
10385139-6429522	159.71	0.07	-64.5	0.07	6.73	84.36	-16.29	0.15	6.8	0.13	7.15	0
10422517-6423559	160.6	0.04	-64.4	0.04	6.44	146.1	-17.49	0.08	11.07	0.07	7.24	0
10413515-6406229	160.4	0.04	-64.11	0.04	6.48	150.47	-17.41	0.08	10.21	0.07	7.14	0.01
11044995-6436566	166.21	0.04	-64.62	0.04	6.61	152.12	-19.59	0.07	9.15	0.07	7.21	0.02
10475352-6415461	161.97	0.25	-64.26	0.26	6.46	22.57	-23.53	0.47	11.13	0.47	6.43	0.03
10261363-6317549	156.56	0.1	-63.3	0.1	6.75	61	-15.72	0.2	6.39	0.19	7.03	0.03
10423841-6440406	160.66	0.04	-64.68	0.03	6.65	159.47	-17.53	0.07	10.98	0.07	7.56	0.04
10390248-6458297	159.76	0.03	-64.97	0.03	6.47	185.38	-16.84	0.06	10.69	0.06	7.55	0.04
10432947-6404065	160.87	0.03	-64.07	0.03	6.57	193.09	-18.32	0.06	10.13	0.06	7.57	0.06

Table A.2: Refined Membership List of IC 2602

2MASS	RA (deg)	RA_{err} (deg)	DEC (deg)	DEC_{err} (deg)	Plx (mas)	Plx_{err} (mas)	pmRA (mas/yr)	$pmRA_{err}$ (mas/yr)	pmDEC (mas)	$pmDEC_{err}$ (mas/yr)	G (mag)	BP-RP (mag)
10345648-6408023	158.74	0.03	-64.13	0.03	6.57	201.45	-16.41	0.05	11.67	0.05	7.45	0.06
10201885-6603491	155.08	0.02	-66.06	0.03	6.71	215.05	-16.32	0.05	13.88	0.05	7.51	0.08
11015473-6600445	165.48	0.04	-66.01	0.03	6.46	159.53	-18.79	0.07	9.89	0.06	7.49	0.09
10460993-6435440	161.54	0.03	-64.6	0.03	6.52	211.52	-17.94	0.05	10.7	0.05	7.82	0.13
10504602-6428460	162.69	0.04	-64.48	0.04	6.51	138.97	-18.32	0.08	9.55	0.08	7.71	0.16
10470917-6415529	161.79	0.04	-64.26	0.03	6.55	164.97	-15.49	0.07	7	0.06	7.82	0.18
10484197-6349587	162.17	0.03	-63.83	0.03	6.54	206.78	-18.53	0.06	9.65	0.06	8.17	0.2
10453396-6442138	161.39	0.03	-64.7	0.03	6.53	201.32	-18.72	0.06	10.14	0.05	8.09	0.21
10214068-6606455	155.42	0.03	-66.11	0.03	6.83	197.39	-17.02	0.06	11.94	0.05	8.21	0.26
10273023-6331238	156.88	0.03	-63.52	0.03	6.78	181.93	-19.85	0.06	7.24	0.06	8.28	0.28
	159.71	0.06	-64.5	0.03	6.26	122.14	-14.86	0.09	9.62	0.05	8.75	0.3
10392498-6346411	159.85	0.03	-63.78	0.03	6.58	183.87	-17.39	0.06	10.12	0.06	8.21	0.3
11195476-6345010	169.98	0.03	-63.75	0.03	6.67	207.36	-20.46	0.05	7.57	0.05	8.66	0.4
10134595-6353597	153.44	0.03	-63.9	0.03	6.46	190.94	-15.36	0.06	12.03	0.06	8.69	0.4
10292597-6552329	157.36	0.02	-65.88	0.03	6.45	233.92	-16.18	0.05	12.34	0.05	8.8	0.45
10090825-6547538	152.28	0.02	-65.8	0.03	6.36	211.98	-13.93	0.05	13.55	0.05	9.02	0.54
10542828-6358215	163.62	0.03	-63.97	0.02	6.67	214.81	-18.95	0.05	9.55	0.05	8.96	0.54
10314490-6329220	157.94	0.02	-63.49	0.02	6.62	289.03	-17.15	0.04	10.64	0.04	9.12	0.57
10393069-6504598	159.88	0.03	-65.08	0.03	6.56	211.23	-15.81	0.05	10.74	0.05	9.22	0.57

Table A.2: Refined Membership List of IC 2602

2MASS	RA (deg)	RA_{err} (deg)	DEC (deg)	DEC_{err} (deg)	Plx (mas)	Plx_{err} (mas)	pmRA (mas/yr)	$pmRA_{err}$ (mas/yr)	pmDEC (mas)	$pmDEC_{err}$ (mas/yr)	G (mag)	BP-RP (mag)
11024504-6329404	165.69	0.03	-63.49	0.03	6.76	224.53	-19.97	0.05	8.68	0.05	9.14	0.6
10452826-6413449	161.37	0.06	-64.23	0.06	6.43	88.1	-18.21	0.11	10.42	0.11	9.04	0.61
10113980-6313270	152.92	0.03	-63.22	0.03	6.62	222.44	-14.75	0.06	11.83	0.07	9.47	0.62
10310749-6410551	157.78	0.03	-64.18	0.03	6.62	213.14	-16.54	0.06	11.08	0.05	9.45	0.63
10285377-6109494	157.22	0.03	-61.16	0.03	6.72	208.42	-17.48	0.06	9.78	0.05	9.51	0.64
10462879-6407577	161.62	0.03	-64.13	0.03	6.59	206.98	-17.37	0.05	10.22	0.05	9.76	0.68
10393158-6505008	159.88	0.03	-65.08	0.03	6.58	178.24	-20.27	0.07	10.66	0.06	9.91	0.74
10300911-6631335	157.54	0.04	-66.53	0.03	6.85	178.48	-17.34	0.08	14.43	0.06	10.1	0.74
10572258-6416344	164.34	0.03	-64.28	0.03	6.79	207.37	-18.4	0.06	9.3	0.05	10.09	0.76
10315410-6348520	157.98	0.02	-63.81	0.02	6.66	268.76	-17.22	0.04	11.72	0.04	10.25	0.78
10561156-6448017	164.05	0.04	-64.8	0.06	6.62	86.44	-19.43	0.12	9.41	0.1	10.35	0.78
10311728-6729287	157.82	0.02	-67.49	0.02	6.34	255.3	-11.88	0.04	12.04	0.04	10.66	0.8
10280898-6430189	157.04	0.02	-64.51	0.02	6.99	310.84	-18.02	0.04	11.31	0.04	10.36	0.81
10381765-6408064	159.57	0.02	-64.14	0.02	6.54	300.94	-16.98	0.04	10.77	0.04	10.44	0.82
10510611-6236331	162.78	0.02	-62.61	0.02	6.34	270.37	-17.99	0.04	8.45	0.04	10.68	0.83
10400003-6315110	160	0.05	-63.25	0.04	6.62	139.64	-18.03	0.09	10.43	0.06	10.57	0.83
10431570-6423542	160.82	0.04	-64.4	0.04	6.62	121.05	-16.17	0.08	10.61	0.07	10.56	0.84
10442256-6415301	161.09	0.02	-64.26	0.03	6.71	195.62	-17.3	0.05	10.71	0.05	10.75	0.86
10461483-6402580	161.56	0.02	-64.05	0.02	6.68	247.55	-18.03	0.05	10.02	0.04	10.55	0.86

Table A.2: Refined Membership List of IC 2602

2MASS	RA (deg)	RA_{err} (deg)	DEC (deg)	DEC_{err} (deg)	Plx (mas)	Plx_{err} (mas)	pmRA (mas/yr)	$pmRA_{err}$ (mas/yr)	pmDEC (mas)	$pmDEC_{err}$ (mas/yr)	G (mag)	BP-RP (mag)
10424152-6421043	160.67	0.06	-64.35	0.06	6.21	81.85	-17.13	0.11	11	0.11	10.4	0.87
10244513-6501562	156.19	0.02	-65.03	0.02	6.76	323.87	-19.38	0.04	8.66	0.04	10.76	0.88
10445962-6502190	161.25	0.03	-65.04	0.03	6.39	224.34	-17.63	0.05	9.82	0.05	10.68	0.89
10572548-6414590	164.36	0.02	-64.25	0.02	6.61	270.56	-19.2	0.04	10.68	0.04	10.85	0.9
10440681-6359351	161.03	0.02	-63.99	0.02	6.65	262.73	-17.86	0.05	11.46	0.04	10.88	0.9
10463300-6527183	161.64	0.02	-65.46	0.02	6.58	267.96	-18.14	0.04	11.35	0.04	10.78	0.91
11075601-6202529	166.98	0.03	-62.05	0.02	6.23	181.28	-18.69	0.05	6.78	0.04	10.85	0.91
10430024-6530178	160.75	0.02	-65.5	0.02	6.5	278.03	-17.52	0.04	10.66	0.04	11.03	0.93
	161.39	0.08	-64.7	0.1	6.51	68.37	-17.76	0.17	10.45	0.19	15.12	0.93
10393995-6520563	159.92	0.02	-65.35	0.02	6.44	217.94	-17.22	0.05	11.38	0.04	11.23	0.96
10214368-6214330	155.43	0.03	-62.24	0.02	6.54	248.1	-16.21	0.05	11.16	0.04	11.19	0.97
10420316-6520590	160.51	0.02	-65.35	0.02	6.34	239.95	-17.02	0.05	10.01	0.04	11.35	0.98
10055446-6625573	151.48	0.02	-66.43	0.02	6.99	284.59	-15.14	0.05	15.72	0.04	11.15	0.98
10420707-6446078	160.53	0.02	-64.77	0.02	6.63	238.92	-17.82	0.05	11.09	0.05	11.32	1
10283121-6344155	157.13	0.02	-63.74	0.02	6.68	311.05	-17.05	0.04	11.35	0.04	11.24	1.01
10452374-6146304	161.35	0.02	-61.78	0.03	6.82	246.31	-19.29	0.05	9.83	0.05	11.27	1.03
10342989-6235572	158.62	0.13	-62.6	0.12	6.77	47.99	-16.1	0.25	11.07	0.25	10.3	1.04
10494839-6446284	162.45	0.02	-64.77	0.02	6.51	273.45	-18.15	0.04	9.63	0.04	11.36	1.05
10293275-6349156	157.39	0.02	-63.82	0.02	6.73	295.78	-16.57	0.04	11.62	0.04	11.24	1.07

Table A.2: Refined Membership List of IC 2602

2MASS	RA (deg)	RA_{err} (deg)	DEC (deg)	DEC_{err} (deg)	Plx (mas)	Plx_{err} (mas)	pmRA (mas/yr)	$pmRA_{err}$ (mas/yr)	pmDEC (mas)	$pmDEC_{err}$ (mas/yr)	G (mag)	BP-RP (mag)
10333968-6446522	158.42	0.02	-64.78	0.02	6.67	310.64	-16.87	0.04	12.51	0.04	11.51	1.08
10414173-6222205	160.42	0.02	-62.37	0.02	6.27	253	-16.78	0.04	9.01	0.04	11.59	1.11
10541737-6440512	163.57	0.02	-64.68	0.03	6.62	257.09	-18.31	0.04	10.21	0.05	11.51	1.11
10334180-6413457	158.42	0.13	-64.23	0.13	6.74	41.33	-19.27	0.25	9.4	0.22	11.38	1.12
10425611-6355510	160.73	0.03	-63.93	0.03	6.6	205.84	-17.22	0.06	11.63	0.06	11.6	1.13
10395596-6359300	159.98	0.02	-63.99	0.02	6.65	288.07	-17.02	0.04	10.58	0.04	11.75	1.19
10544998-6526458	163.71	0.02	-65.45	0.02	6.5	261.33	-18.91	0.04	9.25	0.04	11.75	1.24
10384893-6330430	159.7	0.02	-63.51	0.02	6.53	273.86	-17.59	0.04	10.25	0.04	12.35	1.33
10363796-6447538	159.16	0.02	-64.8	0.02	6.62	286.25	-17.58	0.04	10.3	0.04	12.33	1.34
10591218-6438089	164.8	0.02	-64.64	0.02	6.21	233.44	-17.46	0.04	8.89	0.04	12.37	1.35
10322955-6506403	158.12	0.02	-65.11	0.02	6.28	254.43	-15.99	0.04	11.34	0.04	12.38	1.37
10411756-6526576	160.32	0.02	-65.45	0.03	6.33	255.64	-17.57	0.05	11.82	0.05	12.23	1.42
10465180-6334157	161.72	0.02	-63.57	0.02	6.8	261.95	-19.33	0.05	10.37	0.04	12.57	1.49
10463531-6403445	161.65	0.02	-64.06	0.02	6.61	248.46	-18.73	0.05	10.68	0.04	12.27	1.49
10495685-6348191	162.49	0.02	-63.81	0.03	6.48	243.01	-16.21	0.04	7.55	0.05	12.52	1.5
10482786-6554502	162.12	0.02	-65.91	0.02	6.5	283.96	-17.5	0.04	10.52	0.04	12.67	1.52
10200052-6217465	155	0.02	-62.3	0.02	6.58	255.96	-16.71	0.05	9.86	0.05	12.71	1.53
10280304-6316132	157.01	0.05	-63.27	0.05	6.5	111.71	-14.2	0.1	12.7	0.1	12.7	1.56
10353048-6218367	158.88	0.02	-62.31	0.02	6.52	247.58	-17.08	0.04	9.81	0.04	12.87	1.57

Table A.2: Refined Membership List of IC 2602

2MASS	RA (deg)	RA_{err} (deg)	DEC (deg)	DEC_{err} (deg)	Plx (mas)	Plx_{err} (mas)	pmRA (mas/yr)	$pmRA_{err}$ (mas/yr)	pmDEC (mas)	$pmDEC_{err}$ (mas/yr)	G (mag)	BP-RP (mag)
10521914-6558069	163.08	0.02	-65.97	0.02	6.68	268.08	-18.8	0.04	11.19	0.04	12.83	1.59
10385502-6257272	159.73	0.04	-62.96	0.05	6.48	116.8	-17.4	0.09	9.53	0.1	12.24	1.6
10315315-6234333	157.97	0.02	-62.58	0.02	6.79	303.15	-17.78	0.04	10.23	0.04	12.86	1.64
10305781-6208487	157.74	0.01	-62.15	0.01	6.26	408.2	-15.9	0.03	9.92	0.03	13.13	1.65
10482539-6422439	162.11	0.01	-64.38	0.01	6.55	410.79	-18.24	0.03	10.93	0.02	13.06	1.65
10414524-6428036	160.44	0.01	-64.47	0.02	6.63	430.55	-17.5	0.03	9.69	0.03	13.15	1.71
11010020-6458369	165.25	0.02	-64.98	0.02	6.55	248.95	-19.14	0.04	8.35	0.04	12.96	1.72
10451855-6332265	161.33	0.01	-63.54	0.01	6.71	420.21	-18.66	0.03	11.22	0.03	13.42	1.82
10521708-6502488	163.07	0.05	-65.05	0.05	6.55	119.53	-19.02	0.1	10.02	0.09	12.7	1.85
10345408-6408451	158.73	0.02	-64.15	0.01	6.49	348.21	-17.02	0.03	11.39	0.03	13.44	1.88
10405563-6543082	160.23	0.02	-65.72	0.02	6.68	274.95	-17.17	0.04	7.93	0.04	13.21	1.88
10362643-6500165	159.11	0.01	-65	0.01	6.6	401.86	-17.93	0.03	11.68	0.03	13.66	1.94
10354744-6418449	158.95	0.02	-64.31	0.02	6.32	361.67	-16.42	0.03	11.15	0.03	13.74	1.95
10344080-6340139	158.67	0.03	-63.67	0.03	6.45	175.98	-17.41	0.06	11.14	0.06	13.45	1.95
10261431-6555371	156.56	0.02	-65.93	0.02	6.41	342.91	-16.23	0.03	11.96	0.03	13.92	2.04
10403019-6442168	160.13	0.02	-64.7	0.02	6.53	311.02	-17.72	0.03	10.59	0.03	13.89	2.08
10374942-6400505	159.46	0.02	-64.01	0.02	6.55	309.11	-17.14	0.04	10.85	0.03	14.02	2.12
10483151-6406465	162.13	0.02	-64.11	0.01	6.65	379.66	-17.6	0.03	10.58	0.03	13.94	2.14
10435316-6452006	160.97	0.02	-64.87	0.02	6.56	293.29	-17.18	0.04	10.86	0.04	14.12	2.15

Table A.2: Refined Membership List of IC 2602

2MASS	RA (deg)	RA$_{err}$ (deg)	DEC (deg)	DEC$_{err}$ (deg)	Plx (mas)	Plx$_{err}$ (mas)	pmRA (mas/yr)	pmRA$_{err}$ (mas/yr)	pmDEC (mas)	pmDEC$_{err}$ (mas/yr)	G (mag)	BP-RP (mag)
10395540-6336200	159.98	0.02	-63.61	0.02	6.57	274.7	-18.27	0.04	10.75	0.04	14.13	2.19
11000028-6433385	165	0.02	-64.56	0.02	6.25	256.88	-18.16	0.04	8.13	0.04	14.39	2.2
10361824-6414564	159.08	0.02	-64.25	0.02	6.6	291.89	-17.31	0.04	10.82	0.03	14.11	2.2
10440998-6414507	161.04	0.02	-64.25	0.02	6.59	233.66	-17.96	0.04	11.37	0.04	14.12	2.21
10393483-6608093	159.89	0.02	-66.14	0.02	6.59	259.1	-17.36	0.04	11.97	0.04	14.23	2.22
10502229-6601199	162.59	0.03	-66.02	0.03	6.41	224.85	-18.13	0.06	10.43	0.06	14.36	2.27
10444188-6555303	161.17	0.02	-65.93	0.03	6.87	228.94	-18.97	0.05	11.48	0.04	14.24	2.27
10420333-6521048	160.51	0.03	-65.35	0.03	6.27	201.27	-17.26	0.05	9.92	0.05	14.44	2.28
10261504-6317264	156.56	0.02	-63.29	0.03	6.71	226.39	-20.26	0.05	7.65	0.05	14.15	2.3
10543009-6400065	163.63	0.03	-64	0.02	6.75	223.28	-19.02	0.05	10.09	0.04	14.29	2.31
10454079-6516024	161.42	0.03	-65.27	0.02	6.54	237.21	-18.3	0.05	10.81	0.04	14.41	2.32
10482670-6245213	162.11	0.03	-62.76	0.03	6.71	203.15	-18.66	0.05	10	0.05	14.45	2.34
10595477-6515081	164.98	0.04	-65.25	0.03	6.69	176.84	-17.94	0.07	9.83	0.06	14.34	2.35
11071615-6239420	166.82	0.03	-62.66	0.02	6.33	202.65	-19.21	0.05	7.89	0.05	14.72	2.35
10365921-6458527	159.25	0.03	-64.98	0.03	6.24	202.94	-16.11	0.05	10.93	0.05	14.67	2.39
10451972-6507040	161.33	0.08	-65.12	0.08	6.43	70.99	-17.67	0.17	8.29	0.15	13.78	2.4
11020821-6442052	165.53	0.03	-64.7	0.04	6.5	151.83	-18.44	0.07	8.53	0.06	14.58	2.4
10521828-6410522	163.08	0.03	-64.18	0.03	6.54	186.28	-18.91	0.06	10.54	0.06	14.82	2.4
10390342-6236426	159.76	0.04	-62.61	0.03	6.72	182.37	-17.84	0.07	10.56	0.06	14.67	2.41

Table A.2: Refined Membership List of IC 2602

2MASS	RA (deg)	RA_{err} (deg)	DEC (deg)	DEC_{err} (deg)	Plx (mas)	Plx_{err} (mas)	pmRA (mas/yr)	$pmRA_{err}$ (mas/yr)	pmDEC (mas)	$pmDEC_{err}$ (mas/yr)	G (mag)	BP-RP (mag)
10343570-6127527	158.65	0.07	-61.46	0.07	6.82	85.47	-19.57	0.12	12.9	0.12	13.84	2.42
11050000-6542414	166.25	0.03	-65.71	0.03	6.38	194.34	-18.45	0.06	9.44	0.06	14.71	2.45
10444285-6350437	161.18	0.03	-63.85	0.03	6.88	180.68	-19.27	0.06	10.05	0.06	14.81	2.46
10391363-6440562	159.81	0.03	-64.68	0.03	6.72	221.93	-17.23	0.05	11.07	0.04	14.64	2.46
10581674-6431416	164.57	0.03	-64.53	0.03	6.75	181.46	-19.58	0.06	10.15	0.05	14.76	2.5
10425056-6421533	160.71	0.05	-64.36	0.06	6.62	106.37	-17.52	0.1	11.35	0.12	15.83	2.51
10322621-6406114	158.11	0.18	-64.1	0.18	6.44	30.31	-17.07	0.34	10.6	0.32	18.63	2.53
10410006-6420006	160.25	0.03	-64.33	0.04	6.66	190.46	-17.86	0.06	13.43	0.07	14.23	2.53
10540761-6544558	163.53	0.03	-65.75	0.03	6.56	183	-18.69	0.06	10.26	0.06	14.93	2.55
10525873-6402049	163.24	0.03	-64.03	0.03	6.59	174	-18.29	0.07	10.08	0.06	14.99	2.55
10301236-6417458	157.55	0.03	-64.3	0.03	6.7	197.9	-16.9	0.06	11.95	0.06	14.9	2.55
10392000-6438588	159.83	0.03	-64.65	0.03	6.37	194.11	-16.51	0.06	11.07	0.05	14.89	2.55
11052538-6517056	166.36	0.03	-65.28	0.03	6.62	196.07	-19.79	0.06	9.56	0.05	14.8	2.56
10422815-6436128	160.62	0.07	-64.6	0.07	6.28	71.37	-17.53	0.14	12.36	0.14	14.5	2.56
10325373-6531315	158.22	0.03	-65.53	0.04	6.68	167.12	-17.22	0.07	12.27	0.07	14.94	2.57
10454181-6207111	161.42	0.19	-62.12	0.19	6.53	28.68	-18.04	0.4	9.26	0.35	14.19	2.58
	161.69	0.12	-64.13	0.14	6.67	46.82	-18.85	0.32	9.77	0.32	17.05	2.58
10540239-6547452	163.51	0.03	-65.8	0.03	6.55	180.39	-18.43	0.07	9.57	0.06	14.92	2.59
10521366-6605064	163.06	0.06	-66.09	0.05	6.26	99.65	-14.12	0.11	13.42	0.09	16.53	2.6

Table A.2: Refined Membership List of IC 2602

2MASS	RA (deg)	RA_{err} (deg)	DEC (deg)	DEC_{err} (deg)	Plx (mas)	Plx_{err} (mas)	pmRA (mas/yr)	$pmRA_{err}$ (mas/yr)	pmDEC (mas)	$pmDEC_{err}$ (mas/yr)	G (mag)	BP-RP (mag)
11052996-6341294	166.37	0.03	-63.69	0.03	6.37	164.65	-18.8	0.07	8.65	0.06	15.02	2.61
10373120-6514074	159.38	0.22	-65.24	0.21	6.46	25.59	-18.4	0.43	10.72	0.34	18.63	2.61
10445710-6524562	161.24	0.03	-65.42	0.03	6.51	174.37	-18.6	0.07	9.48	0.06	14.79	2.61
11003192-6344044	165.13	0.04	-63.73	0.03	6.56	167.35	-19.26	0.07	9.23	0.06	14.99	2.62
10444598-6554260	161.19	0.03	-65.91	0.04	6.91	163.63	-18.75	0.06	11.91	0.07	14.9	2.64
10411914-6544389	160.33	0.04	-65.74	0.04	6.74	164.84	-17.39	0.07	11.16	0.07	15.02	2.64
10480930-6425415	162.04	0.05	-64.43	0.04	6.54	133.67	-17.93	0.09	10.31	0.08	15.15	2.65
10432300-6429120	160.85	0.03	-64.49	0.04	6.66	154.86	-19.12	0.07	11.15	0.07	15.16	2.65
10331666-6503548	158.32	0.04	-65.07	0.04	6.64	155.27	-17.85	0.08	9.74	0.08	14.58	2.65
10314603-6545281	157.94	0.03	-65.76	0.03	6.62	191.43	-16.6	0.06	12.38	0.06	15.18	2.66
11153615-6513588	168.9	0.04	-65.23	0.03	6.54	149.19	-20.12	0.08	8.61	0.06	15.16	2.67
10361023-6359502	159.04	0.04	-64	0.04	6.71	151.79	-17.51	0.07	10.41	0.07	14.97	2.67
10532609-6403084	163.36	0.03	-64.05	0.03	6.57	171.63	-18.39	0.07	9.69	0.06	15.22	2.67
10345586-6407385	158.73	0.04	-64.13	0.04	6.59	149.93	-17.5	0.07	12	0.07	14.39	2.68
10283209-6707534	157.13	0.04	-67.13	0.04	6.74	160.03	-19.21	0.07	9.25	0.07	15	2.68
10245249-6344547	156.22	0.05	-63.75	0.06	6.56	98.92	-15.82	0.1	12.65	0.09	15.13	2.68
	164.98	0.07	-65.25	0.06	6.26	83.21	-20.71	0.15	9.71	0.11	15.2	2.68
10073313-6246547	151.89	0.04	-62.78	0.04	6.68	147.34	-15.52	0.08	12.75	0.08	15.07	2.69
10423472-6449491	160.64	0.04	-64.83	0.04	6.5	136.16	-16.81	0.08	11.2	0.08	15.46	2.69

Table A.2: Refined Membership List of IC 2602

2MASS	RA (deg)	RA_{err} (deg)	DEC (deg)	DEC_{err} (deg)	Plx (mas)	Plx_{err} (mas)	pmRA (mas/yr)	$pmRA_{err}$ (mas/yr)	pmDEC (mas)	$pmDEC_{err}$ (mas/yr)	G (mag)	BP-RP (mag)
10502171-6331129	162.59	0.07	-63.52	0.06	6.54	76.11	-18.7	0.14	10.44	0.12	14.77	2.7
10471900-6400463	161.83	0.04	-64.01	0.04	6.21	126.49	-17.11	0.08	9.52	0.08	15.39	2.7
10381300-6541455	159.55	0.06	-65.7	0.04	6.25	121.48	-16.88	0.11	10.33	0.09	15.26	2.7
10440829-6442183	161.03	0.05	-64.7	0.06	6.77	110.59	-15.36	0.1	10.08	0.1	14.76	2.7
10435896-6425565	161	0.04	-64.43	0.04	6.69	124.79	-17.73	0.09	11.83	0.08	15.57	2.7
10482690-6555347	162.11	0.04	-65.93	0.03	6.54	159.67	-17.56	0.07	10.96	0.06	15.14	2.7
11001712-6411317	165.07	0.04	-64.19	0.04	6.31	133.61	-18.25	0.09	9.02	0.07	15.49	2.72
10305415-6432454	157.73	0.04	-64.55	0.05	6.61	129.55	-16.53	0.09	11.71	0.09	15.24	2.72
10434454-6407064	160.94	0.05	-64.12	0.05	6.6	117.69	-18.95	0.09	10.06	0.09	15.38	2.72
10544640-6552393	163.69	0.04	-65.88	0.04	6.37	148.51	-17.77	0.08	9.06	0.08	15.41	2.73
10540731-6338199	163.53	0.22	-63.64	0.25	6.42	23.46	-19.33	0.47	8.08	0.44	19.13	2.73
10422712-6421401	160.61	0.08	-64.36	0.08	6.41	68.54	-17.18	0.16	12.33	0.14	16.64	2.74
10391157-6604546	159.8	0.04	-66.08	0.04	6.24	126.74	-16.73	0.08	10.57	0.08	15.37	2.74
	160.07	0.04	-63.9	0.04	6.69	131.16	-18.07	0.09	10.62	0.09	15.42	2.75
10243021-6519104	156.13	0.05	-65.32	0.04	6.79	149.7	-17.15	0.09	13.3	0.08	14.86	2.76
10553742-6344167	163.91	0.04	-63.74	0.04	6.53	145.25	-19.12	0.07	9.03	0.07	15.47	2.76
10472668-6357591	161.86	0.05	-63.97	0.04	6.53	124.05	-17.38	0.09	10.51	0.08	15.51	2.77
10361534-6346599	159.06	0.04	-63.78	0.04	6.78	122.78	-17.39	0.09	10.97	0.08	15.74	2.78
10451852-6426535	161.33	0.05	-64.45	0.05	6.7	117.15	-17.09	0.1	11.42	0.09	15.44	2.78

Table A.2: Refined Membership List of IC 2602

2MASS	RA (deg)	RA_{err} (deg)	DEC (deg)	DEC_{err} (deg)	Plx (mas)	Plx_{err} (mas)	pmRA (mas/yr)	$pmRA_{err}$ (mas/yr)	pmDEC (mas)	$pmDEC_{err}$ (mas/yr)	G (mag)	BP-RP (mag)
11070411-6103484	166.77	0.04	-61.06	0.04	6.47	121.06	-20	0.08	6.98	0.06	15.5	2.78
10281501-6609508	157.06	0.05	-66.16	0.05	6.44	120.58	-16.06	0.09	11.19	0.1	15.52	2.79
10585180-6412414	164.72	0.04	-64.21	0.04	6.6	146.31	-19.2	0.08	9.8	0.06	15.31	2.79
10453580-6341437	161.4	0.04	-63.7	0.04	6.4	126.76	-17.8	0.08	10.88	0.08	15.39	2.79
10114164-6311428	152.92	0.05	-63.2	0.06	6.86	110.5	-18.43	0.13	8.55	0.13	15.36	2.79
11123326-6420264	168.14	0.05	-64.34	0.05	6.7	111.35	-19.8	0.1	8.78	0.09	15.41	2.8
10080169-6330084	152.01	0.05	-63.5	0.05	6.4	122.33	-14.97	0.11	12.57	0.1	15.53	2.8
10401598-6353470	160.07	0.04	-63.9	0.04	6.68	161.23	-17.53	0.07	11.12	0.07	15.32	2.8
10351553-6544398	158.81	0.04	-65.74	0.04	6.51	128.2	-17.46	0.08	11.65	0.07	15.31	2.8
10342900-6503493	158.62	0.06	-65.06	0.06	6.65	102.95	-18.81	0.12	12.66	0.12	14.99	2.8
10353245-6519358	158.88	0.05	-65.33	0.05	6.48	120.61	-16.45	0.1	11.41	0.09	15.61	2.81
10531380-6457255	163.31	0.05	-64.96	0.05	6.81	119.98	-18.71	0.09	10.05	0.09	15.55	2.82
10354349-6450089	158.93	0.06	-64.84	0.07	6.4	84.19	-15.74	0.14	10.38	0.12	15.89	2.82
10284313-6429316	157.18	0.26	-64.49	0.26	6.71	21.7	-17.3	0.54	13.12	0.47	19.32	2.83
10350009-6505465	158.75	0.05	-65.1	0.04	6.75	129.05	-17.27	0.09	12.71	0.09	15.63	2.83
10442121-6430060	161.09	0.04	-64.5	0.05	6.75	123.82	-17.9	0.09	12.06	0.09	15.72	2.84
11124386-6533482	168.18	0.05	-65.56	0.05	6.8	106.74	-19.49	0.1	9.03	0.09	15.86	2.84
10312716-6419465	157.86	0.04	-64.33	0.05	6.93	136.96	-20.66	0.09	7.71	0.09	15.54	2.84
11143077-6605223	168.63	0.04	-66.09	0.04	6.68	138.16	-20.7	0.09	9.23	0.08	15.57	2.84

Table A.2: Refined Membership List of IC 2602

2MASS	RA (deg)	RA$_{err}$ (deg)	DEC (deg)	DEC$_{err}$ (deg)	Plx (mas)	Plx$_{err}$ (mas)	pmRA (mas/yr)	pmRA$_{err}$ (mas/yr)	pmDEC (mas)	pmDEC$_{err}$ (mas/yr)	G (mag)	BP-RP (mag)
10384099-6450185	159.67	0.04	-64.84	0.05	6.48	118.75	-16.42	0.09	11.35	0.08	15.72	2.84
10325497-6139544	158.23	0.05	-61.67	0.05	6.66	103.64	-18.08	0.1	10.47	0.1	15.79	2.85
10533217-6525230	163.38	0.05	-65.42	0.05	6.59	112.07	-18.52	0.11	10.79	0.09	16.1	2.85
10351999-6404020	158.83	0.05	-64.07	0.05	6.37	100.65	-17.29	0.1	10.27	0.1	15.92	2.86
10371076-6535383	159.29	0.06	-65.59	0.07	6.46	93.69	-17.2	0.12	11.13	0.12	15.79	2.87
10580521-6625081	164.52	0.05	-66.42	0.05	6.36	118.36	-18.05	0.09	9.53	0.09	15.77	2.87
10395531-6520361	159.98	0.04	-65.34	0.04	6.65	135.5	-17.38	0.08	12	0.07	15.76	2.87
10541075-6438294	163.54	0.05	-64.64	0.06	6.51	109.42	-17.99	0.1	10.36	0.11	15.73	2.87
10295071-6352525	157.46	0.05	-63.88	0.05	6.68	120.29	-17.21	0.1	10.33	0.1	15.38	2.87
10390735-6416543	159.78	0.05	-64.28	0.04	6.67	138.18	-17.42	0.09	10.77	0.08	16.04	2.88
10275679-6429392	156.99	0.05	-64.49	0.05	6.43	113.64	-16.05	0.1	11.98	0.1	15.96	2.88
10452557-6419430	161.36	0.06	-64.33	0.06	6.59	97.11	-18.33	0.12	10.22	0.11	16.3	2.88
10583367-6454524	164.64	0.05	-64.91	0.04	6.89	128.32	-19.76	0.1	11.05	0.08	15.76	2.88
10350707-6505354	158.78	0.05	-65.09	0.05	6.41	114.88	-16.55	0.1	11.07	0.1	16.08	2.88
10014112-6216185	150.42	0.05	-62.27	0.05	6.82	129.84	-14.74	0.1	13.61	0.09	15.8	2.88
10280398-6256164	157.02	0.11	-62.94	0.11	6.5	49.77	-18.42	0.2	11.05	0.2	17.53	2.88
10593784-6541375	164.91	0.1	-65.69	0.1	6.22	51.69	-19.02	0.23	9.6	0.2	16.75	2.89
	155.07	0.16	-67.27	0.15	6.77	35.4	-15.91	0.32	16.42	0.28	16.94	2.89
10340239-6523485	158.51	0.04	-65.4	0.04	6.67	135.49	-16.84	0.09	11.31	0.08	16.03	2.89

Table A.2: Refined Membership List of IC 2602

2MASS	RA (deg)	RA$_{err}$ (deg)	DEC (deg)	DEC$_{err}$ (deg)	Plx (mas)	Plx$_{err}$ (mas)	pmRA (mas/yr)	pmRA$_{err}$ (mas/yr)	pmDEC (mas)	pmDEC$_{err}$ (mas/yr)	G (mag)	BP-RP (mag)
10324556-6220430	158.19	0.05	-62.35	0.04	6.63	118.5	-17.54	0.09	10.46	0.08	16	2.89
11101587-6419229	167.57	0.04	-64.32	0.04	6.65	136.03	-20.46	0.08	8.3	0.07	15.42	2.89
10525366-6538290	163.22	0.05	-65.64	0.04	6.74	129.06	-18.44	0.11	10.97	0.09	15.81	2.9
10381331-6541341	159.56	0.05	-65.69	0.05	6.27	114.84	-16.7	0.11	10.46	0.1	15.91	2.9
10414862-6317541	160.45	0.05	-63.3	0.06	6.8	99.3	-18.56	0.1	11.23	0.1	15.73	2.91
10032709-6342293	150.86	0.09	-63.71	0.11	6.77	64.57	-14.48	0.21	14.17	0.23	16.56	2.91
10291767-6400158	157.32	0.03	-64	0.04	6.42	167.45	-16.44	0.07	11.54	0.07	15.4	2.91
10383621-6437051	159.65	0.06	-64.62	0.06	6.33	86.86	-16.9	0.13	10.87	0.11	16.35	2.91
10394576-6308472	159.94	0.05	-63.15	0.05	6.56	113.2	-17.54	0.1	10.76	0.09	15.82	2.91
10464405-6424503	161.68	0.07	-64.41	0.06	6.69	87.64	-17.21	0.15	9.74	0.13	16.52	2.91
	160.64	0.14	-64.83	0.15	6.81	40.87	-16.65	0.27	11.53	0.28	18.43	2.91
10461303-6426078	161.55	0.06	-64.44	0.05	6.57	100.26	-18.57	0.11	10.96	0.1	16.32	2.92
10213006-6344101	155.38	0.05	-63.74	0.05	6.64	112.93	-16.16	0.11	11.56	0.1	15.99	2.92
	162.11	0.05	-62.76	0.06	6.63	96.3	-18.35	0.11	9.53	0.11	16.23	2.93
	161.33	0.05	-65.12	0.04	6.76	127.04	-16.91	0.11	10.65	0.09	16.25	2.94
11103267-6409200	167.64	0.04	-64.16	0.04	6.56	130.1	-20.17	0.09	9.05	0.08	16.01	2.94
10394941-6444249	159.96	0.05	-64.74	0.05	6.68	128.7	-16.63	0.09	11.48	0.08	15.5	2.94
10454151-6444220	161.42	0.05	-64.74	0.05	6.76	128.44	-17.93	0.1	11.29	0.09	16.15	2.94
10263132-6454504	156.63	0.06	-64.91	0.05	6.55	105.63	-17.03	0.11	12.72	0.09	14.87	2.94

Table A.2: Refined Membership List of IC 2602

2MASS	RA (deg)	RA_{err} (deg)	DEC (deg)	DEC_{err} (deg)	Plx (mas)	Plx_{err} (mas)	pmRA (mas/yr)	$pmRA_{err}$ (mas/yr)	pmDEC (mas)	$pmDEC_{err}$ (mas/yr)	G (mag)	BP-RP (mag)
10302380-6704377	157.6	0.12	-67.08	0.1	6.38	51.24	-18.71	0.22	8.53	0.19	18.21	2.94
10454415-6715044	161.43	0.05	-67.25	0.05	6.6	111.3	-18.07	0.1	13.07	0.09	16.19	2.95
10501130-6434402	162.55	0.04	-64.58	0.04	6.66	131.7	-18.09	0.09	10.98	0.08	16.05	2.95
	158.32	0.06	-65.07	0.06	6.45	90.08	-16.57	0.13	11.93	0.13	16.23	2.95
10522767-6245414	163.12	0.06	-62.76	0.05	6.41	109.86	-17.16	0.11	9.53	0.1	15.85	2.95
10581393-6531154	164.56	0.05	-65.52	0.05	6.49	103.8	-18.68	0.11	9.61	0.09	16.12	2.95
10261293-6126108	156.55	0.06	-61.44	0.06	6.74	97.95	-17.77	0.13	10.62	0.12	16.18	2.96
10140045-6351570	153.5	0.06	-63.87	0.07	6.4	78.23	-15.14	0.12	12.58	0.11	16.18	2.96
10484604-6357575	162.19	0.14	-63.97	0.12	6.28	42.37	-18.42	0.28	9.83	0.25	18.56	2.96
10264862-6537088	156.7	0.23	-65.62	0.19	6.68	34.01	-16.83	0.42	12.64	0.38	18.69	2.97
10425245-6417006	160.72	0.11	-64.28	0.1	6.65	53.83	-17.29	0.25	10.94	0.2	17.42	2.97
10500464-6505291	162.52	0.08	-65.09	0.08	6.59	66.16	-18.08	0.18	10.93	0.15	17.17	2.97
10373190-6258326	159.38	0.07	-62.98	0.07	6.72	85.82	-18.16	0.17	11.02	0.13	16.44	2.97
10451506-6448219	161.31	0.06	-64.81	0.06	6.44	93.08	-17.64	0.13	9.73	0.11	16.13	2.97
10283496-6150440	157.15	0.07	-61.85	0.07	6.34	78.47	-16.25	0.17	9.04	0.14	17.05	2.97
11003603-6315553	165.15	0.05	-63.27	0.05	6.3	113.07	-17.9	0.1	8.51	0.09	16.25	2.97
10352814-6601420	158.87	0.06	-66.03	0.06	6.62	92.05	-17.19	0.14	12.51	0.12	16.23	2.98
10502773-6716081	162.62	0.06	-67.27	0.06	6.65	101	-18.65	0.12	13.26	0.11	15.77	2.98
10344230-6327096	158.68	0.08	-63.45	0.08	6.55	68.27	-16.77	0.18	10.18	0.17	17.16	2.98

Table A.2: Refined Membership List of IC 2602

2MASS	RA (deg)	RA_{err} (deg)	DEC (deg)	DEC_{err} (deg)	Plx (mas)	Plx_{err} (mas)	pmRA (mas/yr)	$pmRA_{err}$ (mas/yr)	pmDEC (mas)	$pmDEC_{err}$ (mas/yr)	G (mag)	BP-RP (mag)
10314120-6353098	157.92	0.05	-63.89	0.06	6.45	99.42	-15.9	0.12	10.44	0.11	16.41	2.98
10471136-6133518	161.8	0.22	-61.56	0.22	6.62	26.18	-17.17	0.41	7.27	0.37	18.84	2.98
11055482-6313165	166.48	0.07	-63.22	0.06	6.37	76.85	-18.35	0.16	7.72	0.12	16.4	2.98
10371463-6727090	159.31	0.09	-67.45	0.1	6.52	61.63	-19.35	0.19	12.78	0.18	15.65	2.99
11110208-6558531	167.76	0.05	-65.98	0.04	6.51	118.38	-19.36	0.11	9.21	0.08	15.98	2.99
11005298-6343223	165.22	0.11	-63.72	0.11	6.49	51.97	-19.6	0.24	9.68	0.21	17.8	2.99
10433908-6504373	160.91	0.25	-65.08	0.21	6.98	28.24	-16.47	0.48	13.16	0.41	15.79	3
10433908-6504373	160.91	0.11	-65.08	0.07	6.75	75.92	-17.62	0.2	11.28	0.14	15.9	3
10423714-6453308	160.65	0.06	-64.89	0.06	6.72	94.86	-18.16	0.14	11.73	0.12	16.45	3
11020181-6437457	165.51	0.05	-64.63	0.05	6.31	96.15	-17.53	0.11	9.1	0.1	16.45	3
11163615-6459533	169.15	0.05	-65	0.05	6.97	119.66	-21.56	0.1	10.15	0.09	15.88	3.01
10150647-6655424	153.78	0.07	-66.93	0.07	6.55	84.75	-24.75	0.15	15.2	0.12	16.27	3.01
10422122-6521080	160.59	0.06	-65.35	0.06	6.63	96.81	-17.74	0.11	11.25	0.1	16.26	3.01
11195363-6420078	169.97	0.07	-64.34	0.06	6.55	89.07	-20.03	0.14	7.41	0.11	17	3.02
10305370-6318097	157.72	0.06	-63.3	0.06	6.42	88.69	-16.13	0.13	10.7	0.12	15.39	3.02
10443488-6432138	161.15	0.06	-64.54	0.07	6.76	88.79	-18.89	0.16	11.39	0.14	16.56	3.02
10581113-6542506	164.55	0.05	-65.71	0.05	6.49	93.99	-18.1	0.11	10.28	0.09	15.6	3.03
10434875-6346480	160.95	0.05	-63.78	0.06	6.5	101.82	-18.34	0.1	10.6	0.1	16.12	3.03
10295456-6225326	157.48	0.24	-62.43	0.28	6.32	22.9	-17.75	0.52	10.25	0.51	18.98	3.03

Table A.2: Refined Membership List of IC 2602

2MASS	RA (deg)	RA_{err} (deg)	DEC (deg)	DEC_{err} (deg)	Plx (mas)	Plx_{err} (mas)	pmRA (mas/yr)	$pmRA_{err}$ (mas/yr)	pmDEC (mas)	$pmDEC_{err}$ (mas/yr)	G (mag)	BP-RP (mag)
11115915-6143503	168	0.07	-61.73	0.06	6.33	81.81	-19.54	0.16	6.1	0.11	16.51	3.03
10415295-6350173	160.47	0.08	-63.84	0.07	6.44	76.87	-18.18	0.16	10.95	0.14	16.66	3.03
10275640-6429415	156.98	0.05	-64.49	0.05	6.81	114.07	-15.94	0.11	12.36	0.1	16.06	3.04
10533773-6355143	163.41	0.06	-63.92	0.06	6.64	98.05	-18.43	0.12	9.66	0.1	16.3	3.04
10571536-6524337	164.31	0.07	-65.41	0.05	6.33	89.76	-17.88	0.14	9.25	0.1	16.5	3.04
10471744-6343293	161.82	0.06	-63.72	0.06	6.45	90.15	-17.73	0.13	9.9	0.12	16.5	3.05
11131190-6348416	168.3	0.06	-63.81	0.06	6.71	91.38	-19.34	0.14	8.31	0.12	16.45	3.06
10335199-6411256	158.47	0.08	-64.19	0.07	6.68	77.64	-17.03	0.17	11.89	0.14	16.3	3.06
10464783-6415458	161.7	0.08	-64.26	0.08	6.59	72.32	-17.55	0.19	10.43	0.16	16.81	3.06
10112676-6548060	152.86	0.06	-65.8	0.06	6.7	98.61	-15.22	0.12	14.56	0.11	16.3	3.06
11061789-6138241	166.57	0.14	-61.64	0.13	6.58	41.37	-19.82	0.26	7.3	0.24	18.22	3.07
10420419-6404236	160.52	0.07	-64.07	0.07	6.68	85.2	-18.23	0.17	11.83	0.14	16.84	3.07
10250889-6320398	156.29	0.06	-63.34	0.06	6.95	97.92	-17.92	0.14	12.43	0.13	16.48	3.07
10380912-6632446	159.54	0.05	-66.55	0.05	6.66	109.15	-17.33	0.1	11.37	0.09	16.41	3.07
10552783-6243189	163.87	0.17	-62.72	0.15	6.21	32.45	-18.75	0.33	9.23	0.29	15.85	3.07
10435021-6445021	160.96	0.06	-64.75	0.06	6.71	98.88	-17.31	0.12	12.04	0.12	15.95	3.08
10222805-6400544	155.62	0.08	-64.02	0.08	6.39	66.39	-15.8	0.15	12.01	0.14	16.72	3.08
10281886-6431375	157.08	0.06	-64.53	0.05	6.65	109.09	-15.99	0.11	12.2	0.1	16.49	3.08
10400504-6711220	160.02	0.07	-67.19	0.06	6.82	99.13	-18.33	0.13	12.72	0.11	16.45	3.08

Table A.2: Refined Membership List of IC 2602

2MASS	RA (deg)	RA_{err} (deg)	DEC (deg)	DEC_{err} (deg)	Plx (mas)	Plx_{err} (mas)	pmRA (mas/yr)	$pmRA_{err}$ (mas/yr)	pmDEC (mas)	$pmDEC_{err}$ (mas/yr)	G (mag)	BP-RP (mag)
11012991-6519587	165.37	0.07	-65.33	0.06	6.55	89.39	-19.27	0.13	10.36	0.12	15.94	3.08
10134614-6331024	153.44	0.17	-63.52	0.13	6.83	42.22	-13.31	0.43	13.17	0.28	16.65	3.09
10473791-6433384	161.91	0.11	-64.56	0.1	6.4	52.63	-17.59	0.25	10.89	0.2	17.78	3.09
10413118-6401026	160.38	0.32	-64.02	0.29	6.77	19.54	-19.1	0.74	9.55	0.59	19.51	3.1
10282993-6301020	157.12	0.08	-63.02	0.08	6.34	59.26	-16.63	0.17	11.12	0.15	17.12	3.1
10454983-6129572	161.46	0.06	-61.5	0.06	6.79	89.81	-19.18	0.12	9.66	0.11	16.25	3.1
10521046-6406499	163.04	0.06	-64.11	0.07	6.86	90.51	-19.96	0.14	9.53	0.13	16.43	3.1
10430236-6402132	160.76	0.1	-64.04	0.11	6.35	54.37	-17.46	0.22	10.14	0.2	17.68	3.1
10304621-6602449	157.69	0.06	-66.05	0.06	6.42	90.54	-15.78	0.12	13.3	0.12	15.81	3.11
10330537-6302274	158.27	0.08	-63.04	0.08	6.24	73.59	-16.17	0.18	10.52	0.16	16.4	3.11
10431363-6407459	160.81	0.08	-64.13	0.08	6.47	71.08	-17.84	0.16	11.63	0.14	16.57	3.11
	158.23	0.08	-61.66	0.08	6.69	67.88	-18.18	0.16	10.71	0.15	17.1	3.11
10440257-6332392	161.01	0.17	-63.54	0.18	6.4	31.44	-17.83	0.35	9.55	0.32	18.86	3.11
10395458-6701241	159.98	0.06	-67.02	0.06	6.33	90.83	-17.33	0.12	11.27	0.1	15.73	3.11
10561234-6348497	164.05	0.05	-63.81	0.06	6.55	98.54	-19.49	0.11	9.56	0.11	16.65	3.11
10434648-6410335	160.94	0.08	-64.18	0.08	6.43	66.22	-16.42	0.17	10.65	0.15	17.16	3.11
10400698-6519287	160.03	0.06	-65.32	0.06	6.67	96.03	-16.34	0.11	11.14	0.1	15.71	3.11
10200137-6217440	155.01	0.06	-62.3	0.06	6.83	97.93	-15.9	0.14	12.79	0.13	16.27	3.12
10354626-6602438	158.94	0.07	-66.05	0.07	6.56	82.7	-16.28	0.15	11.74	0.13	16.88	3.12

Table A.2: Refined Membership List of IC 2602

2MASS	RA (deg)	RA_{err} (deg)	DEC (deg)	DEC_{err} (deg)	Plx (mas)	Plx_{err} (mas)	pmRA (mas/yr)	$pmRA_{err}$ (mas/yr)	pmDEC (mas)	$pmDEC_{err}$ (mas/yr)	G (mag)	BP-RP (mag)
10591584-6427365	164.82	0.06	-64.46	0.06	6.51	84.53	-18.79	0.14	9.66	0.11	16.57	3.12
10543581-6532341	163.65	0.07	-65.54	0.06	6.58	80.38	-18.38	0.15	10.03	0.12	17.02	3.13
10504919-6430374	162.7	0.07	-64.51	0.07	6.63	82.36	-18.47	0.15	9.54	0.13	16.83	3.13
10465071-6334167	161.71	0.06	-63.57	0.06	6.81	92.54	-19.17	0.15	10.99	0.13	16.64	3.13
10420463-6434373	160.52	0.07	-64.58	0.08	6.49	75.56	-17.64	0.16	11.52	0.15	16.73	3.13
10020110-6139047	150.5	0.1	-61.65	0.09	6.55	62.19	-13.88	0.22	12.1	0.17	17.33	3.14
10572138-6424170	164.34	0.12	-64.4	0.11	6.51	49.3	-18.68	0.26	9.22	0.24	17.92	3.14
10214522-6500507	155.44	0.07	-65.01	0.07	6.66	78.91	-16.79	0.15	12.61	0.16	16.93	3.14
10315993-6231446	158	0.06	-62.53	0.06	6.52	85.28	-16.88	0.14	10.67	0.13	16.55	3.14
10484994-6412485	162.21	0.07	-64.21	0.06	6.56	89.77	-18.8	0.16	9.95	0.12	16.98	3.15
10291833-6404005	157.33	0.05	-64.07	0.06	6.43	93.64	-16.38	0.11	10.96	0.11	16.46	3.15
10375465-6408565	159.48	0.07	-64.15	0.06	6.53	88.03	-16.78	0.15	11.57	0.13	16.45	3.15
10512011-6556283	162.83	0.05	-65.94	0.06	7	115.36	-19.65	0.1	12.32	0.12	15.62	3.15
11140710-6551165	168.53	0.07	-65.85	0.07	6.64	78.94	-21.04	0.14	9.53	0.12	15.92	3.15
11022452-6510226	165.6	0.08	-65.17	0.07	6.77	75.01	-19.52	0.16	10.17	0.13	17.07	3.16
10424044-6255262	160.67	0.22	-62.92	0.23	6.64	25.38	-20.81	0.46	7.33	0.45	18.21	3.16
10242047-6224260	156.09	0.06	-62.41	0.06	6.39	85.29	-15.71	0.15	10.69	0.13	16.59	3.16
10315675-6627570	157.99	0.08	-66.47	0.09	6.36	69.33	-17.15	0.15	12.16	0.15	16.36	3.16
11072959-6554557	166.87	0.07	-65.92	0.07	6.72	74.93	-20.33	0.16	10.29	0.13	16.7	3.17

Table A.2: Refined Membership List of IC 2602

2MASS	RA (deg)	RA$_{err}$ (deg)	DEC (deg)	DEC$_{err}$ (deg)	Plx (mas)	Plx$_{err}$ (mas)	pmRA (mas/yr)	pmRA$_{err}$ (mas/yr)	pmDEC (mas)	pmDEC$_{err}$ (mas/yr)	G (mag)	BP-RP (mag)
10332668-6359511	158.36	0.07	-64	0.08	6.6	70.79	-18	0.16	11.87	0.15	16.95	3.17
10385973-6556256	159.75	0.08	-65.94	0.08	6.62	75.44	-17.9	0.18	12	0.15	16.79	3.17
10475986-6345278	162	0.06	-63.76	0.07	6.47	80.25	-18.37	0.15	9.63	0.15	16.87	3.17
10271883-6216439	156.83	0.15	-62.28	0.14	6.52	39.9	-15.87	0.34	9.43	0.29	16.38	3.18
11044915-6516024	166.2	0.06	-65.27	0.05	6.57	99.34	-19.42	0.15	10.1	0.1	16.47	3.18
10490032-6342079	162.25	0.08	-63.7	0.09	6.36	62.91	-18.44	0.17	10.08	0.16	17.19	3.18
10320703-6445068	158.03	0.07	-64.75	0.07	6.76	84.2	-17.59	0.14	12.35	0.14	17.02	3.19
10033350-6101416	150.89	0.06	-61.03	0.06	6.64	103.3	-14.52	0.13	12.11	0.13	16.19	3.19
10430890-6356228	160.79	0.08	-63.94	0.08	6.43	71.56	-17.99	0.18	10.1	0.15	17.47	3.19
10233117-6304167	155.88	0.08	-63.07	0.08	6.54	72.2	-15.82	0.17	11.83	0.16	16.69	3.19
10523282-6520242	163.14	0.06	-65.34	0.06	6.48	91.16	-18.95	0.13	10.88	0.11	16.58	3.19
10554986-6643332	163.96	0.09	-66.73	0.08	6.63	73.01	-18.82	0.21	12.13	0.16	16.97	3.19
10401542-6426214	160.06	0.12	-64.44	0.1	6.64	53.17	-17.73	0.25	10.55	0.19	17.9	3.21
11013591-6508315	165.4	0.09	-65.14	0.09	6.51	55.64	-18.86	0.2	10.01	0.17	17.54	3.21
11091591-6527549	167.32	0.08	-65.47	0.07	6.27	69.01	-19.1	0.15	8.66	0.12	17.13	3.21
10234096-6519244	155.92	0.09	-65.32	0.08	6.78	76.49	-16.46	0.21	12.54	0.18	17.02	3.21
10485165-6357419	162.22	0.08	-63.96	0.07	6.37	67.27	-18.27	0.19	9.72	0.14	17	3.21
11012768-6301203	165.37	0.07	-63.02	0.06	6.51	87.82	-19.64	0.13	8.34	0.11	17.06	3.23
11135267-6332275	168.47	0.07	-63.54	0.06	6.9	79.2	-20.86	0.16	9.39	0.12	16.64	3.23

Table A.2: Refined Membership List of IC 2602

2MASS	RA (deg)	RA$_{err}$ (deg)	DEC (deg)	DEC$_{err}$ (deg)	Plx (mas)	Plx$_{err}$ (mas)	pmRA (mas/yr)	pmRA$_{err}$ (mas/yr)	pmDEC (mas)	pmDEC$_{err}$ (mas/yr)	G (mag)	BP-RP (mag)
10523707-6447171	163.15	0.1	-64.79	0.09	6.54	54.34	-18.14	0.19	11.29	0.18	17.08	3.24
10454358-6715041	161.43	0.06	-67.25	0.05	6.64	99.36	-17.76	0.11	14.19	0.1	16.18	3.24
10433330-6434337	160.89	0.1	-64.58	0.1	6.65	52.74	-17.78	0.23	9.76	0.2	17.54	3.25
10505091-6339278	162.71	0.13	-63.66	0.11	6.45	43.08	-17.45	0.25	9.19	0.22	17.92	3.25
10471204-6514341	161.8	0.1	-65.24	0.09	6.33	58.47	-16.91	0.2	9.85	0.17	17.21	3.25
10400705-6542072	160.03	0.12	-65.7	0.12	6.76	53.1	-17.12	0.23	11.18	0.23	17.9	3.25
10332852-6416405	158.37	0.09	-64.28	0.09	6.54	58.81	-16.57	0.18	10.84	0.17	17.09	3.25
10491050-6540213	162.29	0.07	-65.67	0.07	6.68	80.43	-18.68	0.14	10.52	0.12	16.71	3.25
10421649-6340062	160.57	0.08	-63.67	0.08	6.51	74.69	-16.76	0.18	9.87	0.16	17.24	3.26
10490699-6403035	162.28	0.21	-64.05	0.19	6.51	28.75	-18.06	0.42	10.78	0.37	18.99	3.26
10442445-6226283	161.1	0.08	-62.44	0.07	6.25	69.58	-17.76	0.15	9.78	0.14	17.13	3.27
10270680-6323004	156.78	0.08	-63.38	0.08	6.75	68.85	-19.08	0.16	6.68	0.16	16.58	3.27
10470526-6403518	161.77	0.09	-64.06	0.08	6.52	64.65	-19.05	0.17	11.32	0.15	17.1	3.28
10344480-6425339	158.69	0.08	-64.43	0.08	6.59	73.7	-16.8	0.17	11.3	0.15	17.35	3.28
10285665-6411459	157.24	0.13	-64.2	0.11	6.66	49.92	-16.39	0.26	11.84	0.22	17.76	3.28
10454214-6513459	161.43	0.13	-65.23	0.11	6.53	47.56	-17.12	0.24	11.1	0.19	17.96	3.28
10485725-6441293	162.24	0.05	-64.69	0.05	6.65	107.84	-19.36	0.11	9.63	0.1	16.15	3.28
10421085-6539131	160.55	0.08	-65.65	0.07	6.72	79.9	-17.62	0.16	10.79	0.14	17.31	3.29
10105325-6109301	152.72	0.09	-61.16	0.09	6.91	66.83	-14.74	0.18	12.04	0.17	17.37	3.29

Table A.2: Refined Membership List of IC 2602

2MASS	RA (deg)	RA_{err} (deg)	DEC (deg)	DEC_{err} (deg)	Plx (mas)	Plx_{err} (mas)	pmRA (mas/yr)	$pmRA_{err}$ (mas/yr)	pmDEC (mas)	$pmDEC_{err}$ (mas/yr)	G (mag)	BP-RP (mag)
10575510-6635573	164.48	0.08	-66.6	0.07	6.72	80.04	-19.33	0.2	11.52	0.16	17.21	3.3
10164737-6250255	154.2	0.1	-62.84	0.09	6.66	58.71	-15.23	0.21	12.37	0.18	17.48	3.3
10262384-6343244	156.6	0.18	-63.72	0.18	6.22	28.84	-15.18	0.4	14.18	0.4	18.66	3.3
10401486-6426196	160.06	0.06	-64.44	0.06	6.52	92.51	-18.07	0.14	10.74	0.11	16.54	3.31
10454174-6444037	161.42	0.16	-64.73	0.17	6.48	37.89	-20.05	0.34	11.86	0.32	18.4	3.31
10562467-6407105	164.1	0.09	-64.12	0.09	6.55	62.15	-18.94	0.18	9.79	0.16	17.62	3.31
10504475-6410220	162.69	0.1	-64.17	0.09	6.59	59.58	-18.15	0.24	10.49	0.19	17.57	3.31
	163.53	0.06	-65.04	0.06	6.46	91.43	-18.18	0.15	10.26	0.12	16.95	3.33
10244657-6147030	156.19	0.08	-61.78	0.1	6.61	67.03	-16.5	0.17	11.16	0.2	17.27	3.34
10412390-6443564	160.35	0.06	-64.73	0.06	6.49	84.98	-16.98	0.14	10.51	0.13	16.48	3.34
10385682-6209043	159.74	0.2	-62.15	0.19	6.59	29.47	-18.26	0.39	9.91	0.35	18.75	3.35
11035004-6355338	165.96	0.07	-63.93	0.07	6.77	80.63	-20.16	0.15	9.27	0.14	16.5	3.35
10133276-6128099	153.39	0.1	-61.47	0.11	6.4	54.95	-15.31	0.25	11.5	0.23	17.54	3.35
10485574-6420396	162.23	0.27	-64.34	0.24	6.66	21.32	-19.38	0.52	9.79	0.43	18.9	3.35
10345544-6436000	158.73	0.11	-64.6	0.11	6.54	52.48	-16.67	0.25	10.56	0.23	17.65	3.36
11044884-6354295	166.2	0.09	-63.91	0.13	6.26	51.32	-19.34	0.2	7.88	0.23	17.77	3.36
10043794-6529245	151.16	0.08	-65.49	0.08	6.9	79.34	-16.53	0.15	14.43	0.15	17.22	3.36
10260120-6535329	156.5	0.13	-65.59	0.13	6.45	45.1	-14.52	0.29	11.36	0.27	17.67	3.36
10402617-6344389	160.11	0.09	-63.74	0.08	6.62	64.05	-16.79	0.17	10.82	0.15	17.28	3.36

Table A.2: Refined Membership List of IC 2602

2MASS	RA (deg)	RA$_{err}$ (deg)	DEC (deg)	DEC$_{err}$ (deg)	Plx (mas)	Plx$_{err}$ (mas)	pmRA (mas/yr)	pmRA$_{err}$ (mas/yr)	pmDEC (mas)	pmDEC$_{err}$ (mas/yr)	G (mag)	BP-RP (mag)
10445665-6211348	161.24	0.09	-62.19	0.09	6.56	60.99	-17.56	0.18	10.23	0.17	17.73	3.37
10370082-6622025	159.25	0.06	-66.37	0.06	6.66	92.9	-17.29	0.13	12.37	0.12	16.59	3.37
10243854-6433463	156.16	0.08	-64.56	0.09	6.71	75.74	-16.29	0.16	12.92	0.16	17.29	3.37
10503493-6715290	162.65	0.09	-67.26	0.07	6.63	80.36	-19.14	0.17	12.72	0.14	16.57	3.38
10240293-6214327	156.01	0.12	-62.24	0.12	6.69	45.66	-15.96	0.25	11.37	0.23	17.37	3.38
10405026-6453128	160.21	0.07	-64.89	0.09	6.49	63.43	-17.91	0.17	11.76	0.16	17.22	3.4
10594225-6502235	164.93	0.07	-65.04	0.07	6.23	74.3	-19.11	0.17	9.41	0.14	16.96	3.41
10485007-6431147	162.21	0.18	-64.52	0.16	6.52	33.37	-18.65	0.36	9.85	0.31	18.5	3.41
10233785-6446395	155.91	0.09	-64.78	0.08	6.42	71.24	-14.99	0.19	11.22	0.17	17.38	3.41
10504531-6608220	162.69	0.13	-66.14	0.12	6.54	47.43	-17.6	0.25	11.37	0.22	17.83	3.42
11192523-6512261	169.85	0.12	-65.21	0.11	6.9	54.86	-21.07	0.23	7.95	0.2	17.72	3.42
10355559-6328199	158.98	0.08	-63.47	0.08	6.68	72.4	-17.82	0.18	9.63	0.18	17.1	3.43
10412422-6353527	160.35	0.09	-63.9	0.09	6.95	68.34	-18.89	0.19	10.67	0.16	17.46	3.43
11003036-6633257	165.13	0.22	-66.56	0.19	6.68	29.21	-19.15	0.58	7.4	0.38	17.22	3.44
11011257-6527482	165.3	0.16	-65.46	0.13	6.79	42.73	-20.09	0.44	10.48	0.33	17.54	3.44
10334762-6642566	158.45	0.1	-66.72	0.09	6.64	63.6	-17.65	0.19	13.18	0.16	16.83	3.44
10481641-6629481	162.07	0.11	-66.5	0.12	6.72	55.77	-17.9	0.29	11.29	0.22	17.53	3.45
10513834-6501522	162.91	0.11	-65.03	0.1	6.23	47.45	-17.17	0.23	10.61	0.19	17.36	3.46
10285361-6111496	157.22	0.08	-61.2	0.08	6.73	66.9	-18.93	0.18	9.25	0.15	17.04	3.47

Table A.2: Refined Membership List of IC 2602

2MASS	RA (deg)	RA_{err} (deg)	DEC (deg)	DEC_{err} (deg)	Plx (mas)	Plx_{err} (mas)	pmRA (mas/yr)	$pmRA_{err}$ (mas/yr)	pmDEC (mas)	$pmDEC_{err}$ (mas/yr)	G (mag)	BP-RP (mag)
10052122-6410072	151.34	0.1	-64.17	0.1	6.33	54.7	-13.26	0.22	13.24	0.22	17.85	3.49
11135592-6700277	168.48	0.15	-67.01	0.12	6.24	40.1	-19.86	0.29	10.65	0.22	18.16	3.5
10304576-6614479	157.69	0.09	-66.25	0.08	6.66	66.89	-24.85	0.17	11.32	0.15	17.05	3.5
11111503-6438137	167.81	0.07	-64.64	0.06	6.99	87.6	-21.1	0.15	10.34	0.11	16.41	3.51
10361628-6337470	159.07	0.13	-63.63	0.12	6.89	45.91	-17.33	0.28	11.47	0.26	17.97	3.51
	155.21	0.13	-63.07	0.11	6.79	45.65	-17.04	0.28	12.08	0.24	17.77	3.54
10464732-6356089	161.7	0.11	-63.94	0.1	6.77	48.88	-18.25	0.19	11.08	0.17	17.34	3.54
11041371-6557200	166.06	0.13	-65.96	0.11	6.61	53.77	-19.35	0.26	11.17	0.2	17.78	3.56
10380139-6330029	159.51	0.11	-63.5	0.11	6.27	49.29	-15.95	0.24	10.02	0.22	17.92	3.56
10483822-6525087	162.16	0.17	-65.42	0.18	6.58	34.02	-16.61	0.31	10.69	0.3	18.19	3.59
10403748-6331496	160.16	0.11	-63.53	0.12	6.51	53.01	-17.23	0.22	10.21	0.22	18.07	3.59
	163.11	0.19	-62.76	0.2	6.21	29.03	-17.7	0.38	9.55	0.37	18.19	3.61
10485532-6428128	162.23	0.09	-64.47	0.08	6.44	63.99	-17.87	0.21	10.66	0.16	17.32	3.61
10460933-6330563	161.54	0.22	-63.52	0.22	6.67	26.97	-17.26	0.47	10.44	0.45	18.8	3.61
10391188-6456046	159.8	0.08	-64.93	0.08	6.4	64.19	-17.55	0.17	12.49	0.15	17.26	3.62
10581348-6528463	164.56	0.11	-65.48	0.09	6.47	52.47	-17.67	0.25	9.34	0.18	17.16	3.65
10154075-6255498	153.92	0.08	-62.93	0.07	6.91	75.79	-20.18	0.17	7.56	0.14	17.01	3.65
10291735-6401262	157.32	0.12	-64.02	0.11	6.61	51.99	-17.71	0.26	11.15	0.23	18.03	3.68
10374923-6505261	159.45	0.12	-65.09	0.12	6.62	46.41	-17.1	0.23	12.12	0.21	17.92	3.68

Table A.2: Refined Membership List of IC 2602

2MASS	RA (deg)	RA$_{err}$ (deg)	DEC (deg)	DEC$_{err}$ (deg)	Plx (mas)	Plx$_{err}$ (mas)	pmRA (mas/yr)	pmRA$_{err}$ (mas/yr)	pmDEC (mas)	pmDEC$_{err}$ (mas/yr)	G (mag)	BP-RP (mag)
11000150-6352390	165.01	0.1	-63.88	0.09	6.78	60.74	-20.85	0.2	9.17	0.17	17.71	3.68
10424020-6547190	160.67	0.1	-65.79	0.09	6.57	58.87	-18.88	0.2	12	0.17	17.92	3.68
10092784-6502555	152.37	0.3	-65.05	0.29	6.93	20.34	-17.1	0.66	16.57	0.62	19.37	3.75
10514483-6410121	162.94	0.12	-64.17	0.11	6.76	50.22	-19.24	0.26	8.26	0.22	17.92	3.76
10280822-6241221	157.03	0.16	-62.69	0.1	6.39	43.73	-17.6	0.33	10.02	0.2	17.03	nan
10401792-6341387	160.07	0.16	-63.69	0.09	6.67	52.03	-17.09	0.24	9.94	0.16	17.41	nan
10190890-6330343	154.79	0.2	-63.51	0.22	6.92	33.02	-14.53	0.42	13.99	0.45	18.73	nan
	152.92	0.12	-63.22	0.14	6.53	51.89	-14.97	0.33	12.74	0.38	15.32	nan
10451742-6456434	161.32	0.19	-64.95	0.19	6.55	35.71	-16.42	0.66	6.65	0.59	16.37	nan
	157.97	0.16	-62.58	0.1	6.79	43.05	-17.73	0.29	12.24	0.2	16.41	nan
10482896-6253025	162.12	0.1	-62.88	0.1	6.54	54.13	-18.08	0.22	10.22	0.19	17.13	nan
10510759-6139441	162.78	0.07	-61.66	0.08	6.76	81.55	-20.07	0.13	11.35	0.13	15.6	nan
	157.04	0.08	-64.51	0.11	6.68	67.97	-17.88	0.14	13.03	0.18	15.06	nan
	155	0.12	-62.3	0.07	6.55	69.59	-14.17	0.24	12.62	0.14	15.41	nan

Note. — The complete table of 451 candidate cluster members of IC 2602 identified using the prescription of Chapter 2 is provided. Here, the astrometric and photometric parameter values are concatenated to two decimal places.

APPENDIX B

RADIAL VELOCITIES FOR MONITORED STARS

Table B.1: Radial Velocity Measurements for all Epochs of Monitored Stars

Name	BJD	RV (km/s)	RVerr (km/s)
IC 2602			
B134	2459232.801983449	20.89669387476333	0.006980726221975846
	2459233.820696271	20.80800497500011	0.006870538990718281
	2459234.838092883	20.811894543578223	0.007060501710307819
	2459240.820917066	20.749117342927622	0.006916147731908666
	2459242.814771011	20.748674839093315	0.006884351530532589
	2459245.710370266	20.8476552380681	0.007066048817488988
	2459246.759515075	20.92151078990345	0.007076849280801808
	2459318.671432428	20.69427831520948	0.006927284123109162
R1	2458595.667912576	17.61101133980884	0.007256126312308587
	2458648.594823671	17.693314293407653	0.00718121392766544
	2458650.550380261	18.199370777583567	0.007234668148590012
	2458651.613043685	17.43993291953512	0.0073567235017441635
	2458653.572519411	17.834734393876097	0.0076918249000459136
	2458654.547165093	17.873916768496947	0.0073037432709389585
	2458665.555516865	18.078417930177757	0.0071776842731176675

Table B.1: Radial Velocity Measurements for all Epochs of Monitored Stars

Name	BJD	RV (km/s)	RVerr (km/s)
	2459195.814549819	17.84458552181306	0.00716431439348926
	2459196.809586789	17.717262398435224	0.00702979537962173
	2459197.83169805	17.856978980971135	0.007144696822694394
	2459198.81569004	17.639824060926912	0.007187701153513682
	2459199.823599086	17.895797412601887	0.007075258442651747
R14	2459195.830054192	17.39539694519526	0.007496948173506707
	2459196.825112379	17.16181391311185	0.007320844825529184
	2459197.84734792	17.278642420710597	0.007481147569748603
	2459199.838899087	17.47298895111382	0.007538322598243277
	2459200.842783796	17.838610189460915	0.007477102757297962
	2459207.828886514	17.009728550939403	0.007620003030184187
	2459208.807427889	17.231090162712952	0.007539263518157693
R42B	2459195.845563564	17.899246830028332	0.007468018223506101
	2459199.854225649	17.90474587411879	0.007466148487816981
	2459207.844393936	17.81596518714197	0.007456002018537063
	2459209.803404877	17.724915717978067	0.0075218260046701

Table B.1: Radial Velocity Measurements for all Epochs of Monitored Stars

Name	BJD	RV (km/s)	RVerr (km/s)
	2459210.842312786	17.91236032369337	0.007355059562942684
	2459211.808887294	17.878247843325816	0.007406762460100568
	2459213.836173397	17.82346996944323	0.007333405278216828
	2459317.673257668	17.505542903037636	0.00753597378394766
	2459318.640377226	17.960541096750795	0.007822399953588738
	2459320.624432255	17.800189468644945	0.00723446488920011
	2459321.748768453	18.084225826326758	0.007352837738808841
	2459322.653380923	17.788267696481764	0.00727884046815661 15
	2459323.645463038	17.712229698389788	0.00748721420108833 85
	2459324.642329305	17.604680333945034	0.00734474232574082 95
R45	2459201.824146254	17.85366346747298	0.007945263265507683
	2459209.819025402	17.663354928482526	0.007915579171613464
	2459210.857625422	17.96499560654447	0.00788408891593601
	2459211.824517268	17.600159331595275	0.007763732910294498
	2459213.851760596	17.816658614423197	0.007710253124249502
	2459220.844232709	17.292785603492554	0.0076894248659775365

Table B.1: Radial Velocity Measurements for all Epochs of Monitored Stars

Name	BJD	RV (km/s)	RVerr (km/s)
	2459229.761230194	17.610390771238627	0.007958837748420582
	2459318.655853412	17.82593918818212	0.007881250161389158
	2459618.828492086	18.002543507488184	0.007826032627386717
	2459619.819340777	17.776356541075685	0.007757766352731932
	2459620.732979016	17.8386004578366	0.007838397473994554
	2459621.784580277	17.84957881518386	0.007996773594474415
	2459622.663863782	17.667753018914595	0.007880891109474545
	2459623.723435686	17.785590664242783	0.007757761749322703
	2459624.744839689	17.82665352865667	0.0077945768896769485
	2459625.640356985	17.50385622409542	0.007798084303163126
	2459626.662255818	17.838636555895206	0.007855849387923507
R66	2458669.503249442	17.865501747951527	0.007654213607129184
	2458670.536394208	17.280173438223265	0.007679804570296152
	2458674.493975966	17.319810410815748	0.007758637763568827
	2458675.512240801	17.8811643849496	0.0076371989157867125
	2458695.495145029	17.350685344892483	0.007494524316012505

Table B.1: Radial Velocity Measurements for all Epochs of Monitored Stars

Name	BJD	RV (km/s)	RVerr (km/s)
	2459221.82618444	17.808998516255492	0.007566185457028512
	2459229.792772519	17.45681735930209	0.007664613727901818
	2459230.815350146	17.424569770713788	0.0077270729180659165
	2459232.758805542	17.834888438032657	0.007687309954502068
	2459233.804557464	17.48936068038452	0.007785282645494335
	2459234.822143139	17.835366098631688	0.007746810368564934
R70	2458650.584291445	17.273321115743478	0.007561589008764532
	2458669.522824039	17.33981123698174	0.00745533766159558
	2458670.553294651	17.197388673228517	0.007715428842979127
	2458674.510839967	17.37236603605274	0.00785162766945868 5
	2458675.534547803	17.38298021873968	0.0076521572341995674
	2458697.492060208	17.19414299307749	0.007745285602166095
SR3	2458596.708233898	19.75589293878487	0.007815180717433999
	2458669.483880816	19.365361229820437	0.007867851712625443
	2458670.517299248	19.56579217623561	0.00797256989173717
	2458674.47585768	19.59820957918733	0.00807534679391375

Table B.1: Radial Velocity Measurements for all Epochs of Monitored Stars

Name	BJD	RV (km/s)	RVerr (km/s)
	2458675.478745233	19.4889926621941	0.007845085092724212
	2459217.852071911	19.617201619658665	0.007886088712968949
	2459229.776636825	19.66867032763375	0.007961430526067036
	2459230.798757975	19.662880917256576	0.007805620978042196
	2459232.742461164	19.556483287628105	0.007833997676907182
	2459233.787942948	19.71948137364978	0.007914407516495742
	2459234.806125338	19.41334652558873	0.007950523872641413
	2459331.62096575	19.70042274652775	0.007984403493490312
	2459332.577909838	19.67918169630159	0.00799889092572759
	2459333.619857789	19.835553918768518	0.008005202234539018
	2459334.640273695	19.386346711606024	0.007964004708528484
	2459335.578345551	19.459244762070295	0.007938482422800815
	2459336.580157977	19.612569185462306	0.007927628898892501
	2459337.615292888	19.73936821724218	0.00789198050839277
TYC8964171	2459331.605427065	17.636854676842695	0.008093919028593891
	2459332.562061044	18.36938049983012	0.008061371417777307

Table B.1: Radial Velocity Measurements for all Epochs of Monitored Stars

Name	BJD	RV (km/s)	RVerr (km/s)
	2459333.60431928	18.068632733782806	0.008132260306520204
	2459334.593203634	17.59769203939026	0.007884408359241262
	2459335.562829189	17.952066157762	0.008043441167842705
	2459336.564596575	18.519206831441885	0.008119196969241849
	2459337.599567237	17.724812027325054	0.008118540476568018
W79	2458595.694827823	17.605887253956155	0.00728539624257671 35
	2458620.67042696	17.596040885150934	0.007276352192491584
	2458624.617047038	17.6304145422436	0.007275248045308052
	2458626.675424707	17.471964626371864	0.007221183833029353
	2458635.668631753	17.61816122727392	0.007136039679520211
	2458653.604437088	17.4466897531076	0.007550690265291346
	2458664.544999705	17.485542925232394	0.00713854915455276
	2459318.686882284	17.577465074309778	0.007271454225817228
IC 2391			
PMM665	2459159.838743512	14.613672003981648	0.00735689288349927 75
	2459163.832478214	14.765758788211341	0.00729716630202269

Table B.1: Radial Velocity Measurements for all Epochs of Monitored Stars

Name	BJD	RV (km/s)	RVerr (km/s)
	2459165.779497346	14.391993247408097	0.007213561819169232
	2459168.850168068	14.591172789089358	0.007311356003064752
	2459171.823050812	14.503662380077714	0.00743217265699482
	2459176.814886217	14.567339956127494	0.007361733191396032
	2459182.820862664	14.599959225454471	0.007260115414527859
	2459344.523740436	14.2986433976552	0.007414471566607001
PMM756	2459159.854046385	16.012048638393257	0.007893558582742984
	2459164.805152527	16.24098366343255	0.007809256524599707
	2459165.810812868	15.854203073015714	0.007842039219563161
	2459169.827990619	16.033234124092075	0.007858754567947766
	2459171.838547679	15.860842805097466	0.008031917126811847
	2459176.861318266	15.767169177922042	0.007831795016213387
	2459182.836646244	15.355195482749831	0.007799372300794876
	2459191.857897874	16.07820879321377	0.007820449737903757
	2459317.616148836	16.634913575746264	0.007850252677661313
	2459318.558583852	15.882056830445865	0.007867410692145613

Table B.1: Radial Velocity Measurements for all Epochs of Monitored Stars

Name	BJD	RV (km/s)	RVerr (km/s)
	2459319.538523586	16.580243316811785	0.007857920736848996
	2459320.575716713	16.700113470778145	0.007920974514604478
	2459321.601851095	15.781257957556267	0.007600270656775967
	2459322.58024653	16.427405083808978	0.007749364335924398
	2459323.596528804	16.176273442148663	0.007663746656371565
PMM2012	2459159.870116426	13.7439194165263	0.007533681309811955
	2459164.821153194	14.453586360058907	0.00755435943361202
	2459169.843841975	14.631560172865328	0.007415670527262299
	2459171.854673935	14.394062795281862	0.007647780804133111
	2459177.862570522	13.850780813714051	0.007529379470324886
	2459182.852762082	14.544900478935604	0.007436509321899536
	2459194.73568238	14.670351633520088	0.0075102332539335615
	2459343.583593978	14.262722615698332	0.00759793479438288
	2459618.616084596	14.29166000700189	0.007526660421494569
	2459619.715097807	15.087416066724021	0.007510160966341751
	2459620.613061547	14.614574111554338	0.007575265781349622

Table B.1: Radial Velocity Measurements for all Epochs of Monitored Stars

Name	BJD	RV (km/s)	RVerr (km/s)
	2459621.702763571	15.000692948511363	0.007598442376681399
	2459622.567211193	14.132127955962858	0.007723914525991336
	2459623.559432079	14.681077505218346	0.007247304261272525
	2459624.648080892	13.753321201511538	0.00729372670138991
	2459625.609936261	14.294400231591878	0.007762034213639193
	2459626.645541762	13.963442896358732	0.0075475393628501525
PMM3359	2459158.838688303	14.703764053641	0.007368640663286663
	2459163.771717611	14.694127400049823	0.007166635958650881
	2459164.789721788	14.759351767020117	0.007398224375887648
	2459167.834881012	14.677141553167951	0.007291302786924231
	2459170.775765153	14.50359013984977	0.0074226732217558145
	2459172.831989842	14.867813389459368	0.007603501647423801
	2459174.862524455	14.53733514690198	0.007510149018875008
	2459342.5696913	14.689315822240832	0.007328624012695563
PMM4280	2459155.864028025	12.287207996055354	0.008072036838672084
	2459158.822217611	12.374989150959307	0.008004948494445437

Table B.1: Radial Velocity Measurements for all Epochs of Monitored Stars

Name	BJD	RV (km/s)	RVerr (km/s)
	2459160.832135054	12.24104905500708	0.008081446360702878
	2459162.868886935	12.28166511222044	0.007977834543412235
	2459163.754898722	12.177340689967217	0.00809676720239465
	2459164.773285753	11.92320737506968	0.008103473496093597
	2459166.839291845	12.072417399200418	0.00788628088891911
	2459168.834608931	12.215868826609428	0.008026625069304476
	2459342.552974679	12.184778073894751	0.008128200633457214
PMM4362	2458410.86024155	15.107464641977144	0.007574326973595197
	2458806.861087244	15.244650649883612	0.0075141800675424366
	2458808.81542881	15.163606943761847	0.0073173044312613384
	2458811.8159144	15.096916846793006	0.007539712270879331
	2458813.835350446	15.22525735450221	0.0075134264946717
	2458816.816783587	15.21753435834713	0.007443253400666677
	2458817.800091671	15.15183184868242	0.00761999464461307
	2459333.493515733	15.204128421257407	0.007576752345143414
	2459334.459600647	15.082812429405237	0.007484373977401616

Table B.1: Radial Velocity Measurements for all Epochs of Monitored Stars

Name	BJD	RV (km/s)	RVerr (km/s)
	2459335.497914849	15.234238466109849	0.007562460609904728
	2459336.481698597	15.152309568071468	0.007596535002784022
	2459337.493236713	15.133005180460561	0.007515161915857634
	2459338.503543812	15.151189140983265	0.007643970793041477
	2459340.507958825	15.144728324342182	0.007462381413621616
PMM5884	2459165.826429084	14.180777944468456	0.007665908607993092
	2459169.859140626	14.310876606340706	0.007417849597084632
	2459179.840226476	14.247757041803881	0.0075357301600448125
	2459189.81655649	14.20007121787694	0.007419463228857339
	2459194.76702637	15.10536835263965	0.007559897973801831
	2459197.777985025	15.173566731790327	0.0076255224917447595
	2459198.800491339	14.262831874285698	0.00755150898986505
SHJM6	2458413.840293376	15.066907415543424	0.0074303853176132814
	2458806.844949021	15.068424049047723	0.0072785327470485965
	2458808.831521183	15.036777443498805	0.00716761595416626
	2458811.832021912	15.330948493091972	0.007266878380498931

Table B.1: Radial Velocity Measurements for all Epochs of Monitored Stars

Name	BJD	RV (km/s)	RVerr (km/s)
	2458813.851623543	15.480094622738283	0.007413727458642427
	2458815.823942393	15.282622089630978	0.00781364016134071
	2458817.783898301	15.572440275843437	0.007411025551054639
	2459153.875718558	15.147778242299204	0.007476635205842171
	2459158.854404625	15.626100600796834	0.007235835606630554
	2459160.847755138	15.002188440290293	0.007277238832501977
	2459163.84792056	14.894254456058631	0.007424084953204784
	2459165.79531483	15.511613845985035	0.007358880763471997
	2459333.509538419	15.440937479714659	0.007664208936431256
	2459334.475693934	15.452251283961749	0.007609375506367656
	2459335.514013851	15.542643006160596	0.007565256464413524
	2459336.497739728	15.182071510274962	0.007556764178781322
	2459337.509350741	15.37343250937647	0.007477638906558844
	2459338.519679812	15.18158413078414	0.007670002110184864
	2459340.524894609	15.121560958273278	0.007340387613993132
VXR22A	2458412.827049852	14.23300666526444	0.007350754514676554

Table B.1: Radial Velocity Measurements for all Epochs of Monitored Stars

Name	BJD	RV (km/s)	RVerr (km/s)
	2458415.829369998	13.854361168362198	0.007432071762397657
	2458416.847390694	14.227834833917447	0.007530190984871337
	2458457.843083926	13.755464814535246	0.007424811293732812
	2458458.792429019	14.261588143999864	0.007360151693112502
	2458636.467911828	14.360056115665708	0.007120697429613224
	2458648.544167506	14.231635487378934	0.007356307023646647
	2459158.869825924	14.09362073635962	0.007208954975820975
	2459160.863109969	14.11424601069647	0.007208989442708683
	2459163.863541742	14.14218281068216	0.007215387494122121
	2459166.856450553	14.067622791166189	0.0072585382224336715
	2459167.850227587	14.064139504593465	0.007325826635724284
	2459169.811658754	13.984578369145249	0.007053607105440482
	2459333.525225075	14.178608258557224	0.007372970471981871
	2459334.491439395	13.940649963778027	0.0073515518354359734
	2459335.5298968	14.37254024563435	0.007457357469289842
	2459336.513436012	13.878618261532369	0.007431047798903747

Table B.1: Radial Velocity Measurements for all Epochs of Monitored Stars

Name	BJD	RV (km/s)	RVerr (km/s)
	2459337.525077986	14.316630321522334	0.007362750145270075
	2459338.535576886	13.993126879673191	0.007517808658594149
	2459340.540536363	14.231309970346079	0.007342690975007573
VXR70	2458416.863511561	14.011967874628796	0.008068876122435554
	2458806.829276849	14.708150498568985	0.007985426227414022
	2458808.847146691	13.940504985254195	0.007843968548892884
	2458813.819500878	13.787091981335292	0.00791112514921866
	2458817.815831419	14.013815920669494	0.00798244195744745
	2458836.751041352	14.389854079025127	0.008022260287526851
	2459164.862699587	13.85021407656929	0.008007804210801111
	2459170.791239012	13.66183349922553	0.008077041592561094
	2459172.847452997	14.150934596516722	0.008134785739520155
	2459179.824677393	13.745287577824275	0.007645212017917221
	2459184.85846058	13.69883519397158	0.008105290673704234
	2459194.751253386	14.150200966283718	0.008074464383788525
Tuc-Hor			

Table B.1: Radial Velocity Measurements for all Epochs of Monitored Stars

Name	BJD	RV (km/s)	RVerr (km/s)
HD1466	2459152.626457209	6.867682113713785	0.006473911832173207
	2459154.644945678	7.412771319447156	0.006893442027766391
	2459158.621002647	6.410575560009914	0.006644456063893038
	2459160.615023861	6.328286723356751	0.006657385169233271
	2459162.58213876	7.272258733146078	0.006623877244595733
	2459163.711100935	6.5887269016920165	0.0065886456850597725
	2459164.706025452	7.033211977008737	0.00702118102394851
HD222259A	2458669.90993315	7.565240123329011	0.006555117137216724
	2458670.904402925	8.025310831062317	0.006814218004170505
	2458672.819416653	7.6813768377679486	0.007862785470932375
	2458674.859133959	8.620387309154362	0.00700781893370566
	2458695.815649665	8.345678746421678	0.007613777403019558
	2458698.832435564	8.416581799848599	0.007110349878691085
	2458700.840379772	6.308134008087789	0.0069997113403412236
	2458702.81397845	8.217156875936166	0.007139625558223229
	2459155.598900318	8.067747366429895	0.00687647720793923

Table B.1: Radial Velocity Measurements for all Epochs of Monitored Stars

Name	BJD	RV (km/s)	RVerr (km/s)
	2459157.596738847	7.90865768087151	0.006697514064304742
	2459159.582545057	8.25669039293281	0.006862388278103605
	2459163.69693586	8.07909368450565	0.006879296257156878
	2459164.679111159	8.105104299849131	0.007112570889583359
HD222259B	2458669.891723145	5.973479715442527	0.00703454978722559
	2458670.884709095	5.8343144116931605	0.007131946176023762
	2458674.878569577	6.480298932681613	0.007409212885121241
	2458698.84892762	6.083769409746697	0.00715058478520233
	2458700.856558085	7.492334282757108	0.0072231076444226276
	2458702.830208909	6.292615376070673	0.007434283447876875
	2459153.573337839	6.352909941939593	0.007252309313370541
	2459155.58691599	6.601737510548961	0.007257800043463946
	2459157.584764903	5.37643434447768	0.0071250620506039366
	2459159.570576947	6.048832154062627	0.007318712807973701
	2459163.684713169	6.4160175226591	0.007412132006104441
HIP490	2458734.798067285	1.9071655518851722	0.005700724634127017

Table B.1: Radial Velocity Measurements for all Epochs of Monitored Stars

Name	BJD	RV (km/s)	RVerr (km/s)
	2458738.761937152	1.7098303034758637	0.00611482893739558
	2458741.62364246	1.7127625615083382	0.005943486126065206
	2458744.70706929	1.8304932195260744	0.005910084671833767
	2458746.707673966	1.874907099465485	0.005651117289164539
	2458747.730174092	1.8768304875879132	0.006408113688867385
HIP1113	2458664.846625663	9.327675010283185	0.004901766127409117
	2458669.927148516	9.30094560191563	0.004612489129202292
	2458670.925087404	9.3825293965032	0.004616440695892748
	2458672.858396173	9.423187624356778	0.007459799339051025
	2458674.896707007	9.384812745136072	0.005830158644233828
	2458695.904053239	9.669775915499358	0.005505708392000886
	2458734.81162548	9.097697143191084	0.005761882407797945
HIP6485	2458738.800450215	9.291050800620756	0.006962539421237508
	2458739.704026116	9.417686516591722	0.007295754553889227
	2458741.662418069	9.392793703389136	0.006753133800651607
	2458744.788670688	9.358763433442594	0.006470817711651903

Table B.1: Radial Velocity Measurements for all Epochs of Monitored Stars

Name	BJD	RV (km/s)	RVerr (km/s)
	2458746.756998072	9.60264769302361	0.006335181520243875
	2458747.76079068	9.011011261689955	0.0068582408836259596
	2458748.733969869	9.153664798680321	0.006363435350678985
	2459151.62250581	9.150238097380042	0.006338607815866577
	2459152.657820359	9.349444239259801	0.006214852038237873
	2459154.672609066	9.103084879148208	0.006350541805830924
	2459157.672119359	9.576251364165302	0.006284868159664418
	2459159.654914845	9.014504463148848	0.00642396485585465
HIP9141	2458670.942594488	6.241154649131669	0.005754767264349161
	2458674.92997319	6.219746631415127	0.0068198232149581945
	2458741.764618848	6.691420269548752	0.0067224809097213
	2458743.843171657	6.85366078555132	0.007551586908857136
	2458745.760544223	6.262385850660991	0.007153731389181651
	2458746.775343503	6.769828494255108	0.00627942675720216
	2458747.802904984	6.606850221678002	0.0065354205322429295
	2459153.679077387	6.683374711244612	0.006260738699669935

Table B.1: Radial Velocity Measurements for all Epochs of Monitored Stars

Name	BJD	RV (km/s)	RVerr (km/s)
	2459155.678504024	6.268216909728691	0.0066717112445746985
	2459156.64671268	6.697570996395667	0.0062324154960758825
	2459158.668957599	6.369545826396767	0.00700261567685246
	2459160.669053982	6.285501442304755	0.0066123398869254784
HIP21632	2458740.886546005	18.97191346310887	0.0073643443204753
	2458742.878957323	18.811351396618804	0.007799262634039053
	2458744.865919306	19.492466533280755	0.0076496432562688475
	2458748.889772802	19.61246527195354	0.007165533727279753
	2458750.78956427	18.93681908856894	0.007298860137971926
	2458751.848961832	19.665465769021353	0.007465227416006137
	2458752.856568221	18.52108919655999	0.007560924550039535
	2459153.766750152	19.542101690914677	0.007457914702113485
	2459154.760671422	19.727376879286183	0.007235666621382045
	2459155.769941291	19.399660631084842	0.007345859950933255
	2459157.753756922	18.7953525035357	0.0073799366169025726
HIP105388	2458635.933040417	-1.2480553617219314	0.006146333929200679

Table B.1: Radial Velocity Measurements for all Epochs of Monitored Stars

Name	BJD	RV (km/s)	RVerr (km/s)
	2458637.867914083	-1.2602538400131387	0.0067700281250598245
	2458638.836355414	-1.6646584652157799	0.007368770782639803
	2458640.877482269	-1.3876184968423928	0.006831789954639539
	2458662.818206422	-1.491436174971394	0.006273755703178031
	2458664.765660189	-0.6335475254849801	0.006608480142459337
	2458667.767357247	-1.255709546262059	0.006459004560023783
	2459319.891623656	-1.4181336540554668	0.006117298499602879

Note. — Radial velocities and associated uncertainties for all epochs of the 29 stars observed in the monitoring program described in Chapters 5 and 6 are listed.